UNIVERSIDAD CARLOS III DE MADRID

THESIS

Thermo-Fluid Dynamic Evaluation of Components in Adiabatic Absorption Systems

Autora:
Geydy Gutiérrez Urueta

Director:
Pedro Acisclo Rodríguez Aumente

DEPARTAMENTO DE INGENIERÍA TÉRMICA Y DE FLUIDOS

Leganés, 2009

“THERMO-FLUID DYNAMIC EVALUATION OF COMPONENTS IN ABSORPTION SYSTEMS”

Autor: Geydy Luz GUTIÉRREZ URUETA

Director/es: Pedro Acisclo RODRÍGUEZ AUMENTE

Firma del Tribunal Calificador:

Firma

Presidente:

Vocal:

Vocal:

Vocal:

Secretario:

Calificación:

Leganés, de de 2009

To my family, especially my grandparents:
Ana
Lorenzo
Mami Olga
Papá Francisco (R.I.P)

Acknowledgment

Thanks God, always.

Infinite THANKS to my tutor, Prof. Pedro Rodriguez Aumente, for trusting me. For the great effort devoted to shaping a full investigation and for teaching me the highs and lows of the research ... Anything I write with three sentences will be little, but I express my deep admiration, esteem and respect.

Professor Antonio Lecuona: for helping me and unselfishly put his great contribution to my training as well as Jose Nogueira, for giving me his support when he could.

Manuel Santos and Carlos Cobos: For their contribution in installation and assembly of equipments and instruments. Without them, I could not have completed this work.

A also thank Prof. Felix Ziegler and Prof. Jose Miguel Corberán, for giving me the opportunity to learn with their team.

Prof. Francesco Asdrubali and Filipe Mendes for the time dedicated to evaluate this Thesis.

The Ministry of Science and Technology: for the financing granted to me by a Doctoral fellowship and the Universidad Carlos III de Madrid, the institution that welcomed me to perform my graduate studies.

To all the people who contributed to this project, with the different tasks necessary for designing and operation of the facility.

Thanks to all who have contributed to my emotional equilibrium during this time:

My friend, Maria, for everything (this means a lot!).

Mathieu Legrand, my friend since my arrival at the university, whom I admire and appreciate very much and from whom I learned much, both academically and personally. Thanks "Mary" (Maria del Carmen Rodriguez) for being my friend and colleague and for your support. Cheer up!

Juan Carlos: For all your help, for your advices. I have missed you a lot.

For so many laughs and good times, for a day to day more enjoyable and for hearing all of my sorrows: Ana (la maña), Rachel, Ruben, Rafa, Sara, Mat. Sergio, for the encouragement given sometimes.

To all of YOU, those whose presence in the hospital and at home made the impossible: made me laugh. It was the best cure. I will always remember you.

To those friends I've known in the university: Carlos Martinez, Eva, Jorge Angarita, Hugo, Eli, Alejandro, Ali, Isabel, Iliana, Orlando, Omar L., Omar H., Florina, Kenneth, Betty, Diana, Diego, Karina, Leo ... for filling my days.

Thanks to my family who always encouraged me from afar to go forward.

Juan: for these experiences in the past year.

And those with whom I have had the pleasure of sharing something in these years.

ABSTRACT

In this PhD thesis, a facility for experimental evaluation of innovative components forming part of a single effect H_20-LiBr adiabatic absorption chiller is analyzed. The adopted methodology has been mainly experimental. Plate heat exchangers functioning as generator, solution heat exchanger, condenser and subcooler have been incorporated in the design. Two adiabatic absorber configurations, droplets and liquid sheets, were tested and evaluation parameters were experimentally determined.

Overall test facility performance is analyzed in the first stage of the research. The preliminary analysis gives an idea about the operational features of the machine, which allow subsequent detailed components analysis. This analysis is oriented to the interpretation of experimental data including the particular features, in both design and operation, of the facility here presented: study of evaporators' efficiency, solution heat exchanger efficiency and thermal losses. Performance parameters, cooling capacity and *COP*, are expressed in terms of a diagnostic absorption model and compared with experimental results. The differences observed between ideal and experimental results help to validate the influence of components performances on the overall performance of the facility.

An extension of the characteristic equation method, based on the characteristic temperature difference to adiabatic absorption chillers, has been developed and applied considering the facility features. Evaporator limitations have been included in the analysis. The agreement between experimental data and the extended characteristic equation is discussed, showing a good predictive capability, even at off-design operating conditions.

The performances of two types of absorbers (liquid sheets and droplets as solution spreading mechanisms in the absorber) have been characterized in terms of heat and mass transfer. The liquid sheet configuration has shown better evaluation parameters than droplets configuration.

Single and two phase heat transfer and pressure drop in a plate heat exchanger operating as generator, has been analyzed. For the cases of subcooler and solution heat exchanger, single phase heat transfer data has been obtained. The corresponding results are analysed for each case and correlations equations have been obtained and compared with those reported in literature.

TABLE OF CONTENTS

LIST OF FIGURES

LIST OF TABLES

Chapter 1

INTRODUCTION

Index

1.1. Interest in the Subject

One aspect that accompanies the development of industrialized countries is the increased use of heating and cooling systems. The environmental impact of these systems, measured by the atmospheric ozone depletion and increased greenhouse effect, can be very important in the future, especially if the summers are warmer and the need for thermal comfort increases. These negative effects are consequence of the use of organic refrigerants and consumption of electric or mechanic energy, two necessary factors for the operation of conventional refrigeration and air conditioning systems.

An alternative to replace those refrigerants by natural substances is the use of absorption systems, whose adequacy is to use the waste heat from processes that use thermal energy produced from burning fossil fuels. This allows the use of heat that would otherwise be expelled to the atmosphere, contributing to reduce the use of conventional energy to activate the air conditioning or refrigeration equipment, more expensive and harmful to the environment.

In recent years there is an increased interest in introducing absorption systems for air conditioning and refrigeration applications. In the development of absorption refrigeration machines, the absorber design is important because of its influence on machine performance. In particular, in the development of machines condensed by air the absorber is shown as a barrier to marketing because it is larger and heavier than those condensed by liquid.

Falling film absorption is used in the majority of absorbers. This method consists of dripping the concentrated solution on tubes which are cooled by a fluid circulating through it (See Appendix A for a brief description of basic absorption cycles). In this case, absorption and cooling are generated simultaneously in the absorbing film. Another absorption method is the bubble absorption. The basis for the development of bubble absorption is the following: if the steam is divided into small bubbles and injected into concentrated solution, the interfacial area per unit volume of vapour increases and more mixing occurs at the interface liquid - vapour, yielding more compact absorbers.

Improving the processes of heat and mass transfer is the key to reduce the exchange area and size of equipment, thereby reducing its weight, volume and cost of absorption machines. In this way, the basis for the development of adiabatic absorption

is the following: if the concentrated solution is subcooled, i.e. its temperature is reduced below the equilibrium temperature at the current concentration, and then it is distributed on the refrigerant vapour into an adiabatic chamber, the refrigerant vapour is absorbed by solution drops or other method to spread the solution. Once absorption process begins, the solution is diluted and its temperature increased as a result of the transformation of vapour into liquid. Then, the processes of heat and mass transfer is separated in two different equipments: the process of solution cooling is moved out of the absorber and small dimensions heat exchangers can be used, so the heat transfer area can be reduced. When this absorption method is used, part of the solution that leaves the absorber has to be subcooled and recirculated to the absorber, with the aim of reaching the final concentration required for the diluted solution. The other part is pumped to the generator to be concentrated again.

Being so important to use of renewable energy to meet the current energy and environmental goals, the absorption systems may use them in certain cases. A very attractive application is to adapt a system for harnessing solar energy to produce cold through absorption systems. The heat obtained from this use is utilized in the generator to operate in simple cycle. The growing importance of solar energy systems makes absorption systems an alternative for use in summer for air conditioning.

Today mainly large machines are marketed; therefore it is advisable to initiate an optimization for small sizes. Research conducted in this field is necessary to contribute to improving these systems in terms of efficiency and cost - size reduction.

1.2. Financing and Operational Context

The construction and testing of an absorption machine involves the acquisition of special materials and high-precision instruments. The chemical and physical properties working fluids and their operating conditions in the cycle, force to provide suitable materials for this. Moreover, the need to obtain the lowest possible uncertainty requires that the instruments used to measure the processes are the most highly accurate, in addition to provision of infrastructure as a welding machine with high technology. This requires significant investment for the purchase of high technology components. The research is supported by the Ministry of Education, Science and Technology through the project CLIMABCAR “DEVELOPMENT OF ABSORPTION UNITS IN AUTOMOBILE AIR CONDITIONING, FOR AN ENVIRONMENTAL IMPACT REDUCTION, BY MEANS OF WASTE HEAT RECOVERY”.

The purpose of the aforementioned project, within which this thesis was partially developed, was aiming at the design and manufacturing of several prototypes of absorbers with different technology and operating principles. It also includes other critical components, some of them not available in catalogues of commercial products. The prototypes should be tested in a modular absorption machine in order to evaluate their performances and the degree of optimization achieved in each design.

This research has also acquired funds from project MINICOM: (Development of a Thermal Miniature Compressor) and TRANSMACA (Heat and Mass Transfer).

1.3. Objectives and Methodology

1.3.1. General and Specific Objectives

General Objective

To experimentally evaluate the overall and components performance of an adiabatic absorption facility, designed and built at Universidad Carlos III de Madrid, for different operating conditions.

Specific Objectives:

- Evaluate the global performance of the adiabatic absorption facility in terms of cooling capacity and *COP*.
- Develop a diagnostic thermodynamic model and compare it with experimental data in order to identify the influence of components performance on the overall performance of the facility.
- Assess the performance of specific components through a characterization process in the modular absorption facility.
- Analyze the influence of particular operating and design conditions on the cycle performance.
- Instrument and test an experimental set up for testing an adiabatic absorption cycle for different operating conditions.
- Obtain experimental results for two adiabatic absorber configurations, called droplets and fan sheets, and evaluate the results obtained in terms of performance, for size reduction purposes.
- Test the configuration of several generators.
- Characterize the single and two-phase heat transfer and pressure drop processes in a plate heat exchanger, with a Water - LiBr solution in order to estimate the single and two-phase heat transfer coefficients and Fanning friction factor.
- Develop empirical correlations for heat transfer and pressure drop calculations in plate heat exchangers.

1.3.2. Methodology

In order to achieve the above mentioned objectives, the following work was carried out:

- Familiarization with the techniques of research, consultation and implementation of sources and references. This field has been worked with bibliographic databases and interaction with the scientific expertise on issues related to the project through scientific meetings at different levels.
- Deepening on the experimental techniques in diagnostic procedures and instrumentation. The knowledge gained in this field, was put into practice for the acquisition of new instrumentation for the testing facility, from the standpoint of the objectives pursued in the project. Besides this, according to the usual methodology, a process of instrument calibration was carried out.
- Specific training in processes of heat transfer with phase-change. For this purpose a stage was conducted at Universidad Politécnica de Valencia, where an experimental work on plate heat exchangers was developed with Prof. José. M. Corberán and his team, an expert on such systems. Management of the software Engineering Equation Solver (EES) during this period was essential for data processing in the course of development of the Doctoral Thesis.
- Getting to the evaluation of performance of absorption refrigeration machines. The results of this learning process are the currently available experimental results. In this same field, another stage was carried out at Technischen Universität Berlin with Detlef Riebow, who belongs to research team directed by Prof. Felix Ziegler. This research team has a prestigious history and wide experience in the production of cold by absorption.
- Testing of an experimental facility specific for adiabatic absorbers, to be incorporated to absorption refrigeration machines: experiments were conducted in a test chamber designed and built for the characterization of the distribution units of solution. The absorber configuration based on fan sheets was tested for design purposes in this preliminary facility, before being tested in the complete adiabatic absorption test rig.
- Instrument and testing of the diagnostic adiabatic absorption cycle and adapt it for testing two adiabatic absorber configurations: droplets and fan sheets.

- Application of knowledge acquired in the previous steps for conducting experiments and evaluating performance of components, as well as for analyzing the processes of heat transfer and pressure drop in plate heat exchangers.

The study was developed in the modular absorption test facility, designed and built at the University Carlos III of Madrid, located in the Laboratory of the Department of Thermal and Fluid Engineering.

1.4. Structure of the Thesis

This PhD Thesis has been divided in 7 chapters and 2 appendixes.

This first chapter has served to highlight the need for research in the field of absorption systems and situate the work within the project of which it is part. The work purposes have been presented as well as the methodology used in the period of development of the PhD Thesis for the achievement of those purposes.

The literature review about the fields of interest of this research has been carried out in depth in Chapter 2. The state of the art regarding absorption systems and plate heat exchangers is given there in detail.

As the present study is essentially experimental, Chapter 3 is dedicated to the comprehensive description of the experimental facility utilized in the research. The measurement procedures and the uncertainty analysis are presented.

Chapter 4 deals with the experimental evaluation of the overall performance of the machine in terms of the cooling capacity and COP. In addition, the particular detailed analysis of each component is developed in order to explain their effects on the overall performance obtained: analysis on the evaporators, the solution heat exchanger, thermal losses and operational particularities observed. Also, a basic thermodynamic model including the particular features in both design and operation of the facility analyzed is presented.

In Chapter 5 cooling capacity is analyzed in terms of the characteristic temperature difference $\Delta\Delta t$, based on the work developed by Hellmann et al. (1998). The development of an extended version of the characteristic equation model, adapted to the facility features, is exposed. The adjustment of both the original and extended model to the data is also presented in this part.

The experimental results obtained from testing two adiabatic absorber configurations are shown in Chapter 6, in terms of evaluation parameters. A comparison in terms of performance and absorption efficiency is presented for free falling drops and fan sheets adiabatic absorber configurations.

Chapter 7 is aiming to study the single and two-phase heat transfer and pressure drop in the plate heat exchangers used in the experimental facility. The Wilson plot technique is applied to find the single phase heat transfer coefficients. Particular attention has been paid to the case of generator. Correlations for single-phase Fanning

friction factor and heat transfer coefficients are obtained. The subsequent procedure to estimate the two-phase heat transfer coefficients are explained and results are discussed.

Chapter 8 summarizes the most significant conclusions obtained in this Doctoral Thesis and suggest possible lines of future research.

The reader can find a specific nomenclature from Chapters 3 to 7 at the beginning of each one. At the end of each chapter the partial conclusions obtained are given.

The appendix A summarized the basics of absorption cycles. The operation, advantages and disadvantages of absorption systems and adiabatic absorption are briefly described.

The appendix B provides a description of the practical calibration procedure of instrumentation used in the simple effect absorption facility studied here, as well as the uncertainty of calculated variables.

Chapter 2

LITERATURE REVIEW

Index

2.1. Fields of research on Water-LiBr absorption systems

Theoretical and experimental investigations relating to absorption cycles include several fields or motivations. According to the common objective, these fields can be categorized as follows:

- Study of heat and mass transfer process inside the absorber.
- Design, construction and/or evaluation of new absorption prototypes.
- Development of models or calculation methods to analyze the performance of absorption cycles and machines.
- Study of the influence of operating variables over the absorption cycles.
- Study of the behaviour and properties of the fluids used in absorption process.
- Report of the combined use of renewable energies and absorption cycles.
- Monitoring of absorption systems into a real air conditioning application.

According to the objectives of the present Thesis, a more extended summary is offered below for the first four fields above listed.

- Study of heat and mass transfer process inside the absorber.

As explained in Chapter 1, there is an increased interest in introducing absorption systems for air conditioning and refrigeration applications, but the absorber is shown as a critical component because of their size and weight. This has motivated a lot of research in which the main objectives are the study and improvement of heat and mass transfer process inside the absorber. This wide classification includes both diabatic (falling film and bubble absorption) and adiabatic absorption. The basis of these absorption methods are given briefly in Appendix A. Being the last topic of special interest for this work, the literature review presented next has focused on the state of the art on adiabatic absorption.

In the literature review conducted, for the case of water-lithium bromide solution, are identified important researches on adiabatic absorption. These researches were performed, in chronological order, by Nakoryakov and Grigoreva (1977), Paniev (1983), Burdukov et al. (1989), Morioka et al. (1992), followed by Ryan (1994) and Ryan et al. (1995). State of the art, including these papers and other experimental and theoretical studies concerning adiabatic absorption, was well resumed by Venegas et al.

(2004, 2005) and Arzoz (2005). Venegas et al. (2004) carried out a numerical simulation of the simultaneous heat and mass transfer and during the absorption of ammonia vapour by a droplet of lithium nitrate-ammonia solution, considering the low-pressure and high-pressure absorbers of a double-stage absorption system. Results showed that Newman model (Newman, 1931) is adequate for predicting mass transfer during gas absorption by moving droplets with diameters smaller than 100 mm, because the internal circulation for small droplets is insignificant.

Arzoz et al. (2005) developed an experimental study of water vapour into aqueous LiBr solution, for three different arrangements. The influence of subcooling over the mass transfer coefficients and rate of absorption was studied, concluding that the specific water absorption capacity depends on the initial subcooling of the solution. They found that the required absorption chamber volume per unit cooling power is significantly smaller with falling films than with droplet or jet flows.

Further works in the field of adiabatic absorption using aqueous lithium bromide are found in the literature so far:

Warnakulasuriya and Worek (2006) developed an experimental work in order to measure the water absorption quality of a lithium-based liquid absorbent. This was carried out under different operating conditions in an adiabatic spray chamber. They specified the best nozzle types to be used in design applications, and the optimum operating conditions for those selected nozzles. The experimental results were compared with an analytical model based on existing first principal Newman model, showing good agreement.

Elperin et al. (2007) analyzed the simultaneous heat and mass transfer during droplet absorption with internal circulation, reducing the problem to numerical solution of Volterra integral equation of the second kind. It was explained that the heat released during absorption causes the increase of a droplet temperature and the equilibrium temperature increase at the gas-liquid interface. This causes a decrease of the equilibrium absorbate concentration, reduces the driving force of mass transfer during absorption. The theoretical results were compared with experimental data for water vapour absorption by falling aqueous solution of LiBr droplet with internal circulation. The comparison shows good agreement regardless of a high scatter of experimental results.

Wang et al. (2007) studied a gas-fired air-cooled double effect adiabatic absorption system, simulating its thermodynamic performance. In this case, the

influence of outdoor air temperature is relevant. The optimization design results of thermodynamic parameters for the standard design conditions are taken as a reference point. Results indicate that the reduction of the solution distribution ratio (ratio of the solution mass flow rate into the high pressure generator to total solution mass flow rate leaving the absorber) helps to obtain higher COP when outdoor air temperatures are higher than that in normal operation conditions. But it also increases risk of crystallization in the high temperature heat exchanger as the air temperature decreases. So, its control is important to ensure high efficiency and reliability of operation. It also leads to cooling capacity decrease. It was found that outdoor air temperature has a strong influence on cooling capacity and COP. In addition, the effects of air temperature on the recirculation solution flow rate are relevant.

- Design, construction and/or evaluation of new absorption machines:

A group of papers focuses on the development of new configurations to improve the heat and mass transfer process, multi-effect cycles, air cooled prototypes and even miniature systems.

Flamensbeck et al. (1998) presented a double effect absorption heat pump with water and hydroxides as working pair and an adiabatic absorber, with good results. It is worth mentioning that plate heat exchangers have been used in this machine. Compact plate heat exchangers have been suggested in this work to increase the weight-specific cooling capacity (W/kg), because of the reduction of the wall thickness.

Stitou et al. (2000) investigated the various coupling possibilities between a solid/gas chemical reaction process and a liquid/gas absorption process, for air conditioning purpose. A comparison of different configurations of this coupling was carried out considering as criteria: the specific consumption of expensive energy, the operating cost and the investment cost. This comparison enabled to highlight the most interesting systems, concluding that the development high performance triple-effect, even quadruple-effect sorption machines is conceivable.

Multi-effect absorption systems have an important role when the objective is to improve the COP and to fully use the thermal energy of high temperature heat sources. Some works are available in the literature using LiBr – water as working fluid:

Arun et al. (2001) compares series and parallel flow in a double-effect refrigeration cycle, in terms of COP and its sensitivity to temperatures and heat exchanger effectiveness, finding greater COP for parallel flow.

Kaita (2002) simulated three kinds of triple-effect absorption cycles: parallel-flow, series-flow and reverse-flow. Again, parallel-flow cycle shows the highest COP, followed by the reverse-flow II cycle. The maximum pressure and temperature in the reverse-flow cycle are lower than those of other cycles. Zhao et al (2003) simulated a new solution cycle, showing its advantages regarding to stability, temperature lift and easier operation and control. The performance enhancement of a double-effect machine is investigated by Worek et al. (2003) by adding a Vapour Recompression Absorber (an adiabatic component used to evaporate more refrigerant).The results of the simulation carried out show a significant increase of COP and cooling power by increasing both mass flow rate of refrigerant and the solution temperature entering the high stage generator.

Most recent works in this field, which uses Water-LiBr solution, can be summarized as follows:

Kim et al. (2008) presented the development of the design of a miniature absorption system, to remove heat from electronic components (To accomplish this, dual-channel evaporator, micro-channel heat/mass exchanger, and hydrophobic membrane condenser/absorber were incorporated). The performance of the components and the entire system is numerically evaluated, demonstrating its feasibility for this application.

Izquierdo et al. (2008) presented the results of an experimental study conducted in Madrid, using an air-cooled absorption chiller for air conditioning. This commercial chiller (Rotartica 045v) is based on rotary absorption technology and its performance was evaluated in terms of chilling power and the daily COP, calculated for each of the three days selected for the study. The results for the period as a whole showed that cooling power tended to decline with rising outdoor dry bulb temperatures.

- Development of models or calculation methods to analyze the performance of an absorption cycle.

In other field of investigation, various works accomplish a theoretical simulation, methods or models applied to absorption machines.

A comparison of sorption systems is presented by Pons et al. (1999) for several applications in terms of thermodynamic performance. For air-conditioning, LiBr – Water systems shows the best results, and for those water-cooled, triple effect cycles results in the highest.

With the aim of predicting the performance of absorption refrigeration systems, some works have been found in the literature. Hellman et al (1998) developed a model able to represent both the capacity and the COP of diabatic absorption chillers and heat pumps by means of simple algebraic equations. These equations are expressed as a function of the "characteristic temperature difference", which depend on heat exchanger external flow average temperatures, and a parameter representing the slope of an average solution isostere in the Dühring chart diagram. The comparison presented shows a good agreement with the numerical exact simulations. This topic will be discussed in depth in Chapter 5.

Joudi and Lafta (2001) developed a simulation in order to find the effect of several operating conditions on the functioning of each component and the whole system, with good results. Florides et al (2003) made a sensitivity analysis of several variables in the operation of the machine and a cost analysis. The relations between several operation variables, the influence of solution heat exchanger area and solution strength on the efficiency of the machine were determined.

J. Castro et al. (2008) focus on the enhancement for the design and prediction of the heat and mass exchange components of absorption chillers, considering that the most limiting factor for some facilities is the price. Recent works include the dynamic simulation model developed by Kohlenbach and Ziegler, part I (2008) and its numerical verification, part II (2008).

Thermoeconomic optimization is an important part of the amount of works about single and double effect absorption systems. Also, numerous studies have been developed for processes using ammonia as the working fluid. Although these works contain relevant information, they go out of the scope of this thesis.

- Study of the influence of operating variables over the absorption cycles.

In the last years, the influence of operating parameters (such as temperatures and flow rates) over the performance of Water-LiBr single effect absorption cycles has been extensively studied.

Martinez and Pinazo (2002) used statistical tools to measure the effect of variation of heat exchanger areas on the performance of a single effect machine. From the fact that the area and its distribution among the components of the machine determine the COP, they obtained regression models to get an improvement in the COP with a redistribution of the total heat transfer area among the heat exchangers. Subsequent to

the previous work, the same authors (2003) presented another one consisting on the use of the same statistical study to determine regression models for the performance (COP and capacity) of an absorption machine as a function of external fluid temperatures and hot water mass flow rate. A First-order model was obtained for the capacity; while a second-order model was necessary for the COP.

Soto and Pinazo (2003) presented a mathematical model for the prediction of performance of the absorber taking into account the wetting effects. Statistical study was also carried out in this study. A multi-factorial study of water vapour absorption by a falling film of LiBr over a horizontal smooth tube absorber is developed, being the response parameters the average convective heat transfer and mass transfer coefficients of the falling film, expressed as a function of the factors used in such study. They could indicate a polynomial correlation to study the most influential factors and their binary interactions. The model accurately predicts the heat load and the average convective heat transfer coefficient, but is not good at predicting the mass transfer. In a later paper, the same authors (Soto and Pinazo, 2004) compare the results for the same machine, but using an alcohol as surfactant.

Park et al. (2004) also presented performance characteristic, but focused only in the effect of cooling water temperature and flow rate on such performance and on the energy consumption. The inlet water temperature has more effect on the performance of absorption system than the cooling water flow rate. In addition, when the partial load is in determined range the required power can be reduced by decreasing the cooling water inlet temperature.

Asdrubali and Grignaffini (2005) conducted an experimental study with a water-cooled single effect absorption chiller. Besides the evaluation of parameters that caused the low COP of the machine, they simulated its operation through the change of the flow rate and the temperature of the supplying hot water. An important result was to verify the possibility to work the machine with solar collectors. Syed et al (2005) posed the performances of a water-cooled single effect absorption chiller, powered by 50 m^2 of flat plate thermal solar collectors. The machine was operated at part load along the summer of 2004 in Madrid.

In the same line that the above mentioned papers, a recent experimental work by Jahnke et al. (2005) showed a mathematical model for the response variables (*COP* and heat fluxes) as a function of several input variables, including temperatures and flow rates in external circuits. These models have been obtained using data analysis software.

Another recent work (Kaynakli and Kilic, 2007) do not use statistical methods, but a parametric thermodynamic analysis to illustrate the effect of temperatures and efficiency of heat exchangers on both the thermal loads of components and performance. The effects of solution and refrigerant heat exchangers on several parameters were compared, resulting that the influence of the first is more important.

A further experimental work presented by Aphornratana (2007) also takes as parameters: the operating temperatures, the solution circulation ratio and heat exchanger effectiveness, in order to measure its influence on the COP. Besides the effect of every parameter investigated over the performance, the importance of the solution heat exchanger and absorber effectiveness was emphasized.

- Study of the behaviour and properties of the fluids used in absorption process.

Many papers concentrate on the study of fluids used in absorption process. Water-LiBr solution is investigated in terms of its properties, offering wider ranges of parameters, by means of correlations of selected experimental data (Pátek and J. Klomfar, 2006; Kaita, 2001) or using a Gibbs energy equation (Kim and Ferreira, 2006) The interest of these studies is found in its use for new applications. An easier way to calculate those thermodynamic properties from complex differential equations is also proposed by Şencan et al. (2006). The use of surfactants is also reported by Kulankara and Herold (2002).

In addition, there is a clear effort to explore new mixtures (including or not LiBr) or new fluids in order to overcome the limitations or drawbacks imposed by the use of Water-LiBr and ammonia-water solutions. Binary, ternary and even multi-component solution have been explored, aiming at reducing crystallization risk, reducing viscosity, varying pressures in the cycle, increasing COP and capacity and even avoiding toxicity, among others. The use of additives to promote surface renovation in absorption processes has been also explored, as well as the corrosivity of the solution and its reduction caused by additives. Much work has been devoted to organic mixtures, but also to ionic solutions. The literature on solution properties, performance and experimental results is ample and too large to be described here; so, only a few references are here given. The effectiveness of these new fluids has been evaluated experimentally by Muthu et al, 2008; Yuyuan et al 2006; Yoon et al, 2005; Donate et al., 2005; Bourouis et al., 2005; Medrano et al, 2001, among others.

2.2. Single and Two Phase Heat Transfer and Pressure Drop in Plate Heat Exchangers

The works found in the literature, about heat transfer and operational aspects of Plate Heat Exchangers (PHE) can be classified in the following fields:

- Study of heat transfer coefficients and pressure drop:

The measurement of the film heat transfer coefficient and pressure drop is the general objective of the works found in this category, listed in Table 1. Inside this classification there are specific works dedicated to the study of the influence of several operating variables on them, achieved by experimentation with different fluids, for both single and two phase flow (evaporation and condensation).

For single phase flow, there are a large number of reported works and therefore many published empirical correlations are provided, based on the experimental data for the specific geometry tested, which are rarely given in detail. Previous works have summarized extensive information and literature about single phase flow (Manglik, 1996; Muley et al., 1999; Muley and Manglik, 1997; Claesson, 2005). Table 1 manifest the variety of fluids and geometries tested in some works, capturing the attempt to study the influence of geometrical parameters for different flow conditions, summarized by non-dimensional numbers (Re, Pr, μ/μ_w). The effect of geometrical variations has a big influence on the heat transfer and pressure drop, specifically the corrugation angle. So, correlations obtained are difficult to generalize. Some of them are extracted among these papers for comparison purposes, in Chapter 7.

In the case of two phase flow, various papers have reported experimental results, mainly with organic refrigerants, such as R-134, R-410 and R-22. In recent works (Garcia-C. et al., 2007; Jokar et al., 2006; Claesson, 2005) an extensive review of previous investigations and published correlations is presented. For the case of flow boiling, in the open literature it is not clear if nucleate or convective boiling is the governing mechanism on the flow boiling heat transfer coefficient and there seems to be an agreement about the relation between the boiling regime and the dependence of the heat transfer coefficients with the mass flux, heat flux and vapour quality. It is supported that if the boiling heat transfer coefficient is affected by heat flux represents a nucleative boiling regime and if the influence variable is the vapour quality it represents

convective boiling. In this sense, Thonon (1995) introduced a criterion for the transition between the nucleative boiling and convective boiling, using the product of the boiling number and the Lockhart-Martinelli parameter. The papers reviewed on Table 1 give indications of the existence of both mechanisms in the experimental results. Inside this group of papers (not listed in table 1) it is worthy to highlight the paper presented by Corberán and Gonzálvez (2002). They show the influence of operating conditions on the uncertainty in the calculation on two phase heat transfer coefficients, stressing the importance of a good estimation of the single heat transfer coefficient. Boiling of the water-ammonia mixture has been investigated by Taboas (2006) in which the estimation of a valid correlation for the plate heat exchanger functioning as generator was the principal objective.

- Visualization of flow patterns:

These papers make an effort for obtaining maps for flow patterns, the distribution of phases or flow characteristics inside the plate heat exchanger. This is achieved by the visualization of the processes. Vlasogiannis et al. (2002) present results also for heat transfer coefficients and Shiomi et al. (2004) for pressure drop.

- Study of fouling:

In general, these works focus on the investigation of the influence of geometrical and operational factors on the surface fouling in a plate heat exchanger. Particulate fouling is studied by Thonon et al (1999), Grandgeorge et al. (1998), Karabelas et al. (1997) and Bossan et al. (1995). The effects of nature and concentration of particle, mass flow rate and type of fluids, on the fouling resistance are analyzed. Among other important conclusions, they indicate the large influence of chevron angle in the fouling resistance as well as the velocity of the fluid. The higher are both parameters, the less the fouling resistance value.

Tables 1 to 3 summarize the most important information about the papers reviewed corresponding to the above mentioned fields, in descending chronological order.

	Title	Author	Working Fluids	Lenghx Width (mm)	Chevron angle (From vertical)	Process studied
Single phase flow	Heat transfer and pressure drop properties of high viscous solutions in plate heat exchangers	F.S.K. Warnakulasuriya and W.M. Worek	LZB	457x178	60º	Cooling
	Enhanced heat transfer characteristics of viscous liquid flows in a chevron plate heat exchanger	Muley A, Manglik RM, Metwally HM	Vegetal oil – Water	(55,41x5, 08)x163	30/30, 60/60, 30/60	Cooling
	Experimental Study of turbulent Flow Heat Transfer and Pressure drop in a plate Heat Exchanger with Chevron Plates	A Muley, R.M Manglik	Single phase of Water-Water	392x163	30/30, 60/60, 30/60	Cooling
	Plate heat exchangers for process industry applications: Enhanced thermal-hydraulic characteristics of chevron plates	Raj M. Manglik	Review of experimental works regarding the thermo-hydraulic performance of PHEs			
	Enhanced heat transfer characteristics of single-phase flows in a plate heat exchangers with mixed chevron plates	Muley A, Manglik RM	Vegetal oil – Water	392x163	30/60	Cooling
	Global performance of a prototype brazed plate heat exchanger in a large Reynolds number range	R. Bogaert and A. Bölcs	Mineral Oil	236x113	22º	Cooling
	Recent Research And Developments In Plate Heat-Exchangers	Thonon B, Vidil R, Marvillet C	Review and conclusions about previous investigations for single phase, evaporation and condensation			
	Assessment of boiling and condensation heat transfer correlations in the modelling of plate heat exchangers	J.R. García-Cascales, F. Vera-García, J.M. Corberán-Salvador and J. Gonzálvez-Maciá	R22 and R-290	Study of heat transfer in PHEs, comparing different correlations for single and two phase flow, for the evaluation of heat transfer coefficients. Behaviour of a model for the characterization of refrigeration equipment.		Evaporation and condensation
Two phase flow	HFC-410A vaporisation inside a commercial brazed plate heat exchanger	Giovanni A. Longo and Andrea Gasparella	HFC-410°	278x72	65	Vaporization
	Refrigerant R134a vaporisation heat transfer and pressure drop inside a small brazed plate heat exchanger	G.A. Longo and A. Gasparella	R-134	278x72	65º	Vaporization

Two phase flow	Dimensional analysis for the heat transfer characteristics in the corrugated channels of plate heat exchangers	J.H. Lin, C.Y. Huang and C.C. Su	Dimensional analysis for the heat transfer characteristics in the corrugated channels of plate heat exchangers			
	Dimensional analysis on the evaporation and condensation of refrigerant R-134a in minichannel plate heat exchangers	Amir Jokar, Mohammad H. Hosni and Steven J. Eckels	Glicol-water mixtures and R-134a	311x112	60º with 34, 40 and 54 plates	Evaporation and condensation
	Experimental heat transfer coefficients during refrigerant vaporisation and condensation inside herringbone-type plate heat exchangers with enhanced surfaces	G. A. Longo, A. Gasparella and R. Sartori	R22	290x75	65º	Evaporation and pressure drop
	Experimental investigations of heat transfer and pressure drop during the condensation process within plate heat exchangers of the herringbone-type	Reinhard Würfel and Nikolai Ostrowski	Water and n-heptane	560x188	A:30-30, B1:30-60, B2:60-30, C: 60-60	Condensation
	Evaporation heat transfer and pressure drop of refrigerant R-410a in a plate heat exchanger	Hsieh YY, Lin TF	R410-Water	500x120	60º	Evaporation
	Experiments on the characteristics of evaporation of R410A in brazed plate heat exchangers with different geometric configurations	Dong-Hyouck Han, Kyu-Jung Lee and Yoon-Ho Kim	R22 Y R410A and Water	522x115	45, 55 y 70º	Evaporation and pressure drop
	Condensation heat transfer and pressure drop of refrigerant R-134a in a plate heat exchanger	Yi-Yie Yan, Hsiang-Chao Lio and Tsing-Fa Lin	R134a – Water	500x120	60º	Condensation
	Subcooled flow boiling heat transfer of R-134a and the associated bubble characteristics in a vertical plate heat exchanger	Y. Y. Hsieh, L. J. Chiang and T. F. Lin	R134a – Water	500x120	60º	Heating (Evaporation)
	Saturated flow boiling heat transfer and pressure drop of refrigerant R-410A in a vertical plate heat exchanger	Y. Y. Hsieh and T. F. Lin	R410 – Water	500x120	60º	Boiling
	Evaporation heat transfer and pressure drop of refrigerant R-134a in a plate heat exchanger	Yan YY, Lin TF	R134a – Water	500x120	60º	Evaporation

Table 1. Summary of works carried out for the estimation of heat transfer coefficients and pressure drop in Plate Heat Exchangers

Title	Author	Working Fluids	Heat Transfer Area (mm)	Chevron angle (From vertical)	Process studied
Effect of geometry and flow conditions on particulate fouling in plate heat exchangers	Thonon B, Grandgeorge S, Jallut C	Small scale: TiO12 Full scale: CaCO3	Small scale: 140x396 Full scale: 160x435	30, 45 y 60º	Cooling
Particulate fouling of corrugated plate heat exchangers. Global kinetic and equilibrium studies	S. Grandgeorge, C. Jallut* and B. Thonon	Deionized Water - TiO2	396x133	30 y 60º	Cooling
Liquid-side fouling of heat exchangers. an integrated r & d approach for conventional and novel designs	A. J. Karabelas, S. G. Yiantsios, B. Thonon and J. M. Grillot	CaCO3	100x45	30 y 60º	Cooling
Experimental-study of particulate fouling in an industrial plate heat-exchanger	Bossan D, Grillot Jm, Thonon B, Grandgeorge S	Water with several types of particulates	505x220	26.5	Cooling

Table 2. Summary of works carried out for the study of fouling

Title	Author	Working Fluids	Heat Transfer Area (mm)	Chevron angle (From vertical)	Process studied
Characteristic of two phase flow in a channel formed by chevron type plates	Yoichi Shiomi, Shigeyasu Nakanishi, Takafumi Uehara	Two phase flow: water- air	435x162	A:30-30, B1:30-60, B2:60-30, C: 60-60	Single and two phase flow. Variation of volumetric flux of fluids
Air–water two-phase flow and heat transfer in a plate heat exchanger	P. Vlasogiannis, G. Karagiannis, P. Argyropoulos and V. Bontozoglou	Air - water	430x123	60º	Heating. Variation of volumetric flux of fluids

Table 3. Summary of works carried out for the determination of flow patterns

2.3. Conclusions

From the summary of the works referenced above, which covers topics of interest in this thesis, the following can be concluded:

Regarding absorption systems, the high necessity of new machine designs is noticeable as well as new absorber configurations and methods to analyze the performance of absorption chillers. In this way, the adiabatic absorption is being investigated as one method for improving absorption processes, so that absorption and heat rejection are separated and individually optimized. In this way smaller absorbers are envisaged. The advantages of adiabatic absorption over simultaneous absorption-heat rejection are expected to increase owing to the problems encountered on wetting of heat exchanger wall by the solution. Also, the film of solution over the heat exchanger wall tends to increase on thickness with highly viscous solutions, such as water-LiBr, what precludes fast saturation.

Bearing in mind these research labours, the development of the innovative components, in particular the absorber, is inescapable to improve the heat and mass transfer processes involved in the cycle functioning. The design and building of the experimental facilities evaluated in this work is in line with this, as well as the study of operational implications of those components within the cycle. On the other hand, the effort aimed to calculation methods to analyze the performance of an absorption cycle is remarkable. The work published by Hellmann et al. has been followed by other investigators in order to obtain simple equations to control the machine. The extension of this model to adiabatic absorption cycles is motivating.

Absorption is as a research area of concern in which both industry and scientific community are interested in further studies and results.

About the state of the art on plate heat exchangers, it seems clear that single phase flow has been studied extensively, which is not the case for two-phase flow. It is relevant the increasing interest and effort to study new refrigerants, flow patterns inside the plate heat exchanger and to obtain new correlations for both heat transfer and frictional pressure drop for both evaporation and generation processes, but also condensation and absorption processes, being the temperature glide caused by generation and absorption particular issues when using solutions. There is not agreement on the governing mechanism on the flow boiling heat transfer coefficient,

owing to its complex nature and a complexity in geometry. Regarding to boiling mixtures limited data have been reported and more limited for multicomponent mixtures. Plate type generators and absorbers (PHE) are new devices that deserve a better characterization, as they could improve bulk, weight and cost issues in absorption machines. The need for investigation in this last topic seems obvious.

Since advantages of compact plate heat exchangers coincide with the needs identified for absorption process, regarding to improvement of heat transfer process, it is necessary more knowledge about calculation methods on two phase process. This would be very useful for designers in order to incorporate plate heat exchangers in the absorption design.

Chapter 3

EXPERIMENTAL SET UP

Index

NOMENCLATURE

LiBr	lithium bromide
$\dot{m}$	mass flow rate [kg/h]
P	absolute pressure [mbar]
PHE	plate heat exchanger
T	temperature [ºC]
U	measuring uncertainty
x_j	measured variable

Subscripts

chw	chilled water
set	established value
r	recirculated

3.1. Introduction

In this Chapter the experimental facility is described in detail. The different flow loops that comprise it are explained in terms of operation and instrumentation used. Some specifications of the equipment are provided. A second configuration, in which various changes were made in two loops, is also described as well as the data acquisition system, the experimental procedure and the uncertainty analysis procedure. In the last section, another experimental facility is described, which is specific for adiabatic absorbers, where flat-fan sheets absorber configuration were previously tested.

Fig. 3.1 shows a diagram of the single effect absorption test rig. It consists of four loops: the hot loop, the solution loop, the cold loop and the chilled water loop. Main components include: two evaporators, absorber, generator, condenser, sub-cooler and solution heat exchanger. Last four components are plate heat exchangers while the evaporators are fin-coiled tubes and the absorber is an adiabatic chamber. A computerized data acquisition system is used to register the measured data.

Aqueous LiBr solution inside the absorption chamber flows into two separated streams: strong solution (solution poor in water or concentrated solution) coming from the generator, and recirculated solution. The strong solution is separated from water vapor, which goes to the condenser, and directed to the absorber. Recirculated solution is extracted from the bottom of the absorption chamber and pumped to the sub-cooler, where most of the absorption heat is rejected and then the sub-cooled solution is returned to the absorber. Two fancoils receive the external fluid circulating through each evaporator. The objective of placing two evaporators is having a larger heat exchange area available and to guarantee the symmetry in the supply of vapor to the absorption vessel. Nevertheless, distribution problems in the refrigerant flow were detected; which is discussed in next sections.

In the following sections, each loop is described in detail.

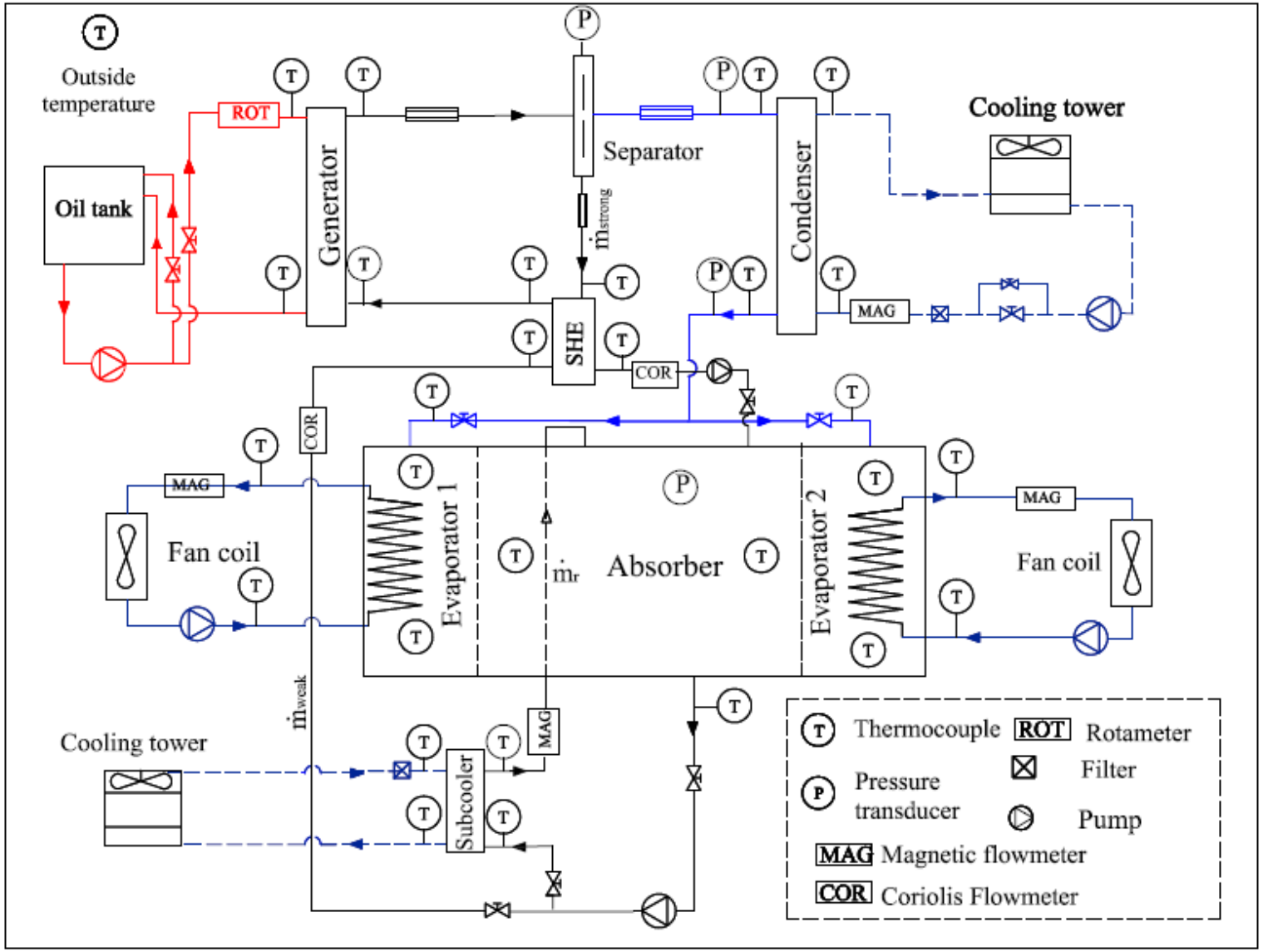

Fig. 3.1. Flow diagram of the test facility

3.2. Hot loop

Thermal oil is used as working fluid in this loop. This fluid is heated by electric resistances which give a maximum exchanged thermal power of 18 kW. The loop contains a pump that delivers the heated oil to the generator. To measure the oil flow rate, a rotameter is installed between the oil pump and the generator. Two valves are used to finely adjust the oil flow rate. Two type T thermocouples measure the oil temperature inside the inlet and outlet manifolds. The oil temperature is stabilized through an on – off control system, which uses a PT100 thermoresistance to measure the oil temperature inside the oil tank. With this control, the fluctuation of oil temperature is less than 6 ºC. Fig. 3.2. shows pictures of the components for this loop.

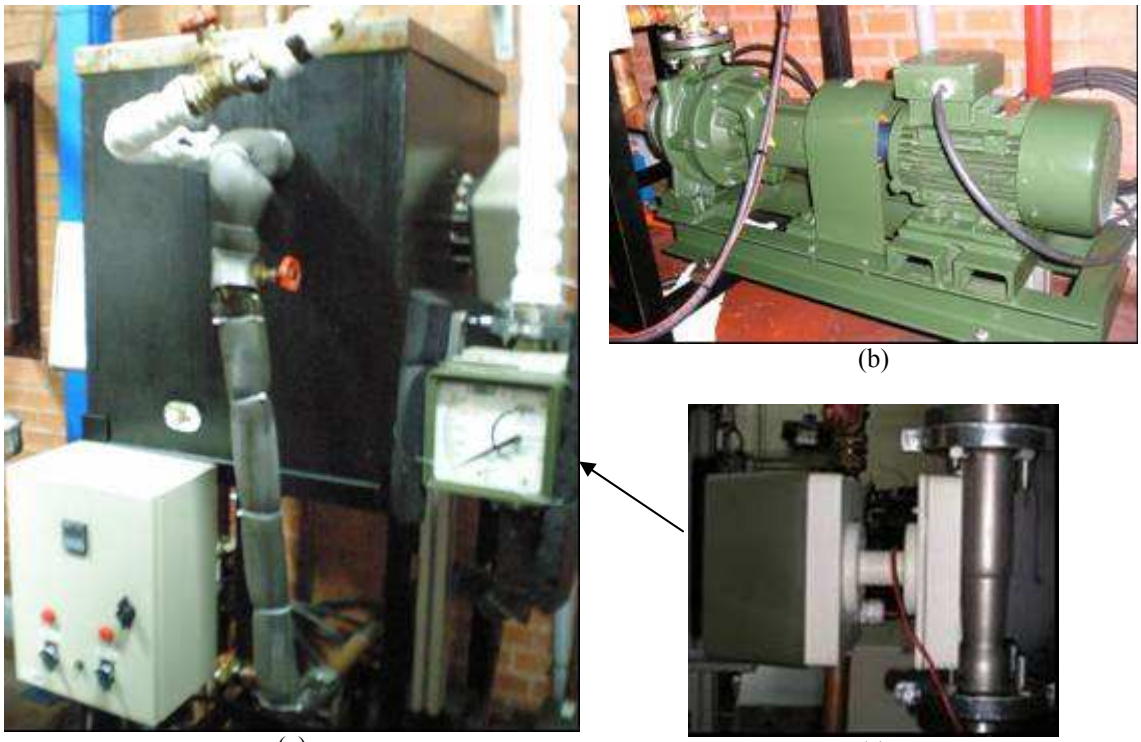

(a) (b) (c)

Fig. 3.2. (a) Oil tank and on-off control system. (b) Oil pump. (c) Rotameter flowmeter

3.3. Cooling water loop

The cooling loop uses a cooling tower to evacuate the condensation and absorption heats. The cooling water crosses in parallel configuration, both the condenser and subcooler for this purpose. This loop incorporates magnetic type flowmeters and valves to measure and adjust, respectively, the water flow rate. In the condenser, the cold water produces the phase change of the water steam coming from the separator. In the subcooler, the cooling water diminishes the temperature of the solution extracted from the absorber. Four thermocouples, positioned inside inlet and outlet manifolds of both the condenser and subcooler, measure the inlet and outlet temperature of the cold fluid. Two filters, installed at inlet of both PHEs, protect the loop against particles and dirt. Fig. 3.3 shows pictures of the components for this loop.

(a) (b)

Fig. 3.3: (a) Magnetic flowmeter. (b) condenser

3.4. Solution loop

The LiBr aqueous solution is the working fluid in this loop. The main components are: three PHEs (the generator, the solution heat exchanger and the subcooler), the separator and the absorber. The boiling solution flows through the generator from bottom to top. The separator divides the flow into water vapour and strong solution. The superheated steam goes to the condenser. Downstream, the subcooled water is delivered to the twin evaporators through a pressure-reducing pipe and it drips over the evaporators finned tubes, extracting heat from the water circulating inside them. This produces the useful cooling effect while the refrigerant evaporates. The fraction of water that is not evaporated mixes into the solution at the bottom of the vessel, being not recirculated to the evaporators.

The absorption process is carried out in the absorber, which consists of a vessel made out of stainless steel plates to ensure a steady behavior in the corrosive environment formed by the LiBr aqueous solution. It offers a wide optical access to the droplets or sheet formation zone by the use of 20 mm thick Pyrex® glass windows. At lateral, front and back sides there are round windows for visualization purposes, and at the top there is a complete rectangular area for the same purpose.

The strong solution coming from the separator is used to preheat the solution going to the generator (weak or diluted solution), due to its higher temperature, through the countercurrent solution heat exchanger. Then it goes to the absorption chamber and is dispersed as either falling drops or fan sheets, using an array of orifices or nozzles, depending on the absorber configuration (see Fig. 3.4). The drops or sheets absorb the water vapour which is generated in the two evaporators. At absorber exit, the weak solution mass flow rate is divided in two streams: the larger fraction (70% as mean value) is recirculated to the absorption vessel, passing through the subcooler. Both recirculated and strong solutions are mixed after the absorption process. The rest of the solution is delivered to the generator, closing the cycle. A volumetric pump is installed at absorber exit. It controls the flow rate of both weak solution streams through the change of the AC frequency. Two valves, installed after this solution pump, allow fine-adjustment of the flow rates. A secondary volumetric pump, installed in the weak solution circuit, allows the precise adjustment of flows rates, as in Water-LiBr machines there is a very low head available for effective flow control. To measure the flow rate,

the density and therefore the concentration of both the weak and strong solution, two Coriolis flowmeters are installed at inlet and outlet of the absorber respectively. The pressure inside the absorber is measured with an absolute pressure transducer (Fig. 3.5). A vacuum pump is used to extract non-condensable gases after opening the sealed enclosure and to reach a set pressure, activated only when the machine is not working.

Fig. 3.4. Array of orifices at the top of absorber for generating droplets, eyedroppers.

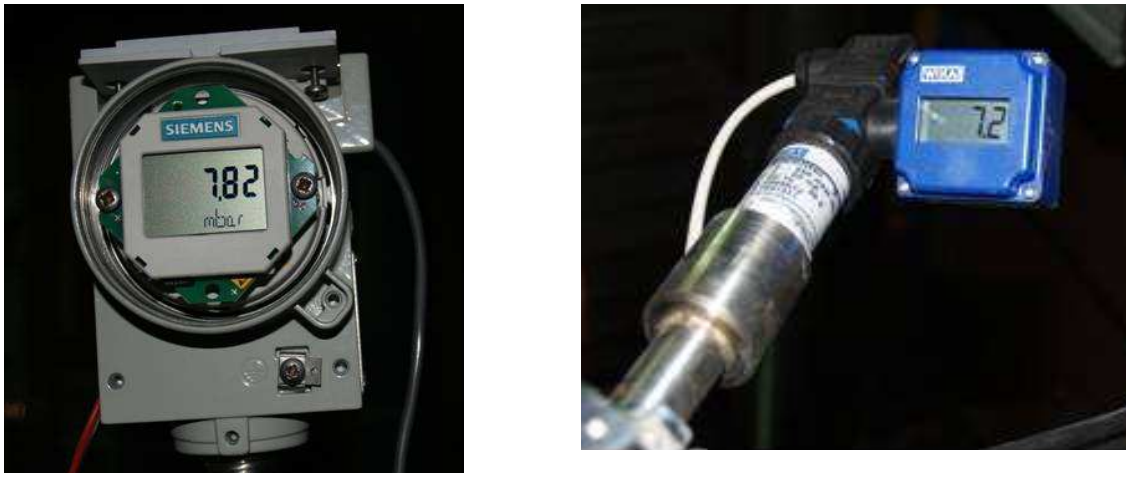

Fig. 3.5. Images of pressure sensors showing values of absorber pressure

There is a transparent pipe located at the generator exit (Fig.3.6) to allow observing the flow regime of the two phase flow. Another one, located at the condenser inlet, allows checking that the liquid is not entering into the condenser, thus checking the separator correct working.

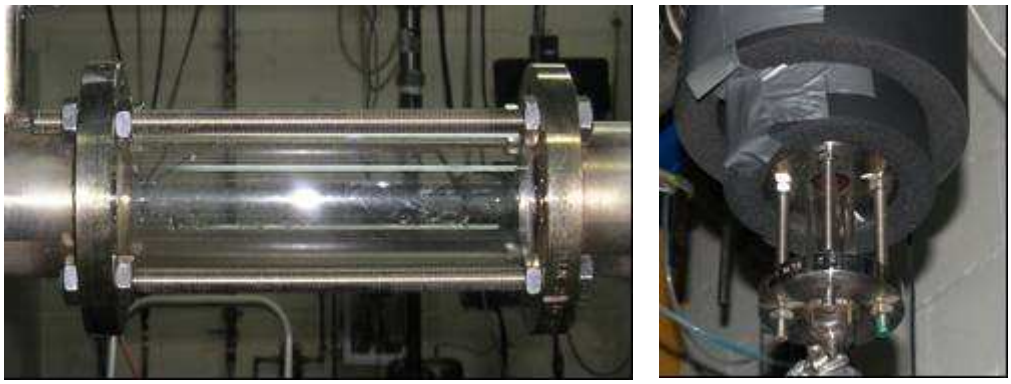

Fig. 3.6. Transparent pipes at generator exit (left) and separator outlet (right).

All PHEs in this loop (generator, condenser, solution heat exchanger and subcooler) incorporate type T thermocouples, which are located at inlet and outlet of the working fluid. A differential pressure sensor measures the pressure drop of the solution in the generator. There are also absolute pressure transducers positioned at inlet and outlet of the condenser. The PHEs have been manufactured by Alpha-Laval and are commercial size industrial heat exchangers.

Fig. 3.7 illustrates some components incorporated to this loop.

(a)

(b)

(c)

(d)

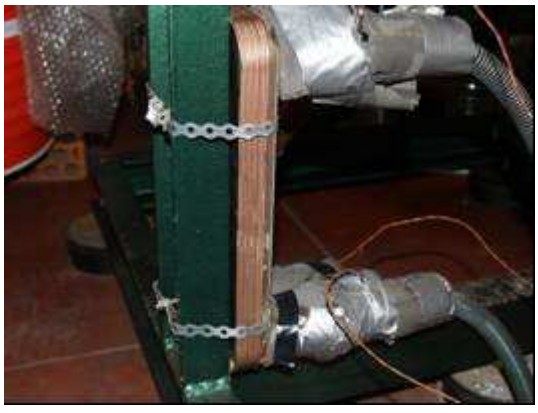

(e)

(f)

Fig. 3.7. (a) Generator (b) Separator (c) Diluted solution pump (d) Concentrated solution pump (e) Subcooler (f) Coriolis flow meter

3.5. Chilled water loops

External fluid, water in our case, circulating through each evaporator is sent to two fan-coils. Each loop contains a pump for recirculating the fluid, two temperature sensors, an expansion tank and a magnetic flowmeter to measure the flow rate (Fig. 3.8).

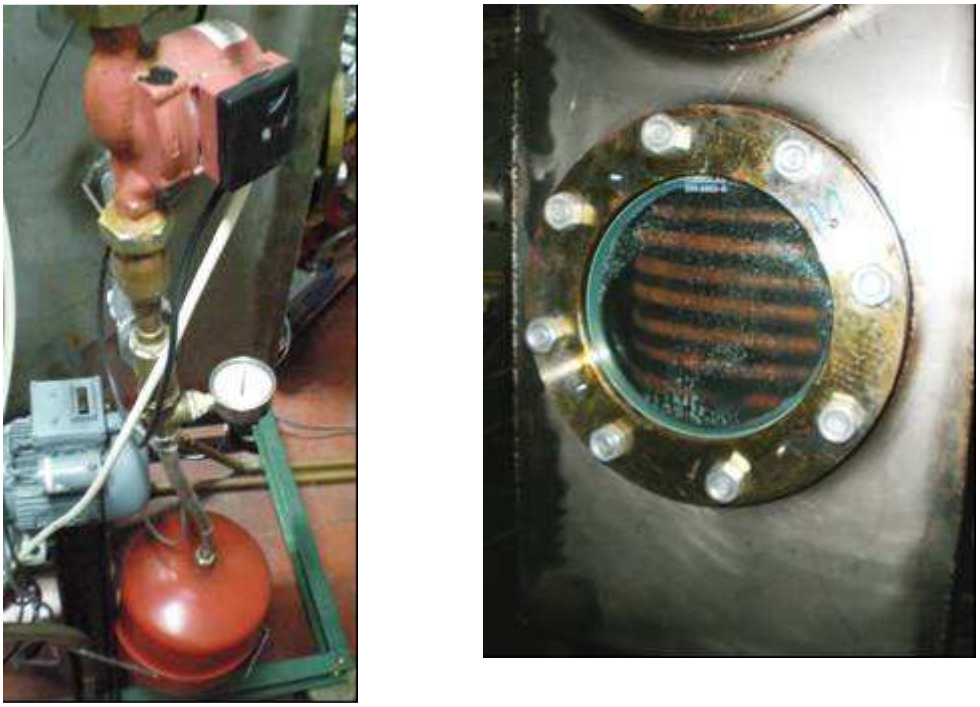

(a) (b)

Fig 3.8. (a) Pump and expansion tank (b) Evaporator observed through the lateral window

Fig. 3.9 gives an idea about the complete experimental test rig.

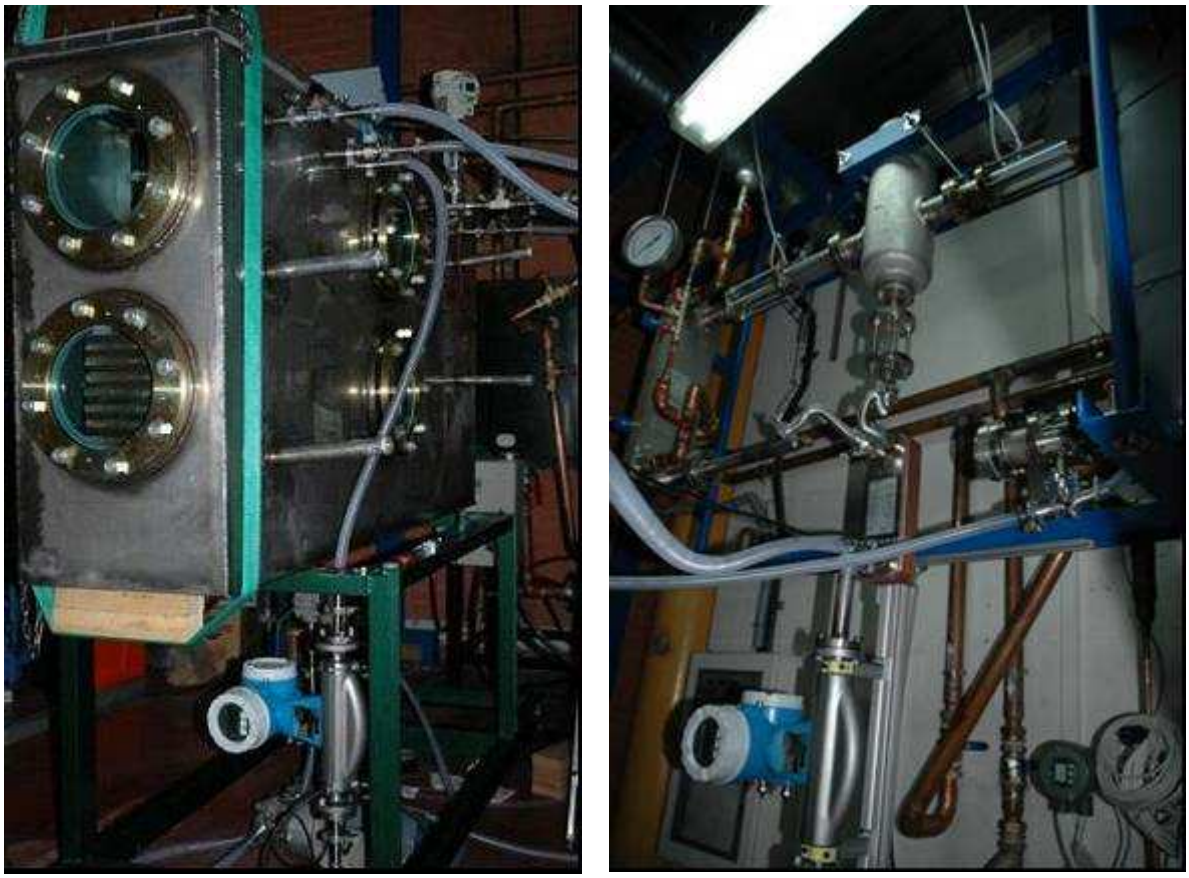

Fig. 3.9. Images of the absorption test rig.

3.6. Specifications of the components

Some specifications of the PHEs and pumps used in the experimental setup are listed below:

PLATE HEAT EXCHANGER	AlphaLaval Model	Number of plates	Height (mm)	Width (mm)	Heat transfer area per plate (m^2)
Generator	**CB76**	**10**	**617**	**192**	**0.095**
Condenser	**M6**	**30**	**920**	**320**	**0.13**
Subcooler	**CB26**	**10**	**310**	**111**	**0.025**
Solution heat exchanger	**CB26**	**20**	**310**	**111**	**0,025**

Table 3.1. Specification of Plate Heat Exchangers used in the experimental set up

Device	Manufacturer	Model	Working velocity (r.p.m)
Weak solution pump	**PulsaFeeder**	**GMC6-KCT-TLK-BT2**	**420 – 1210**
Strong solution pump	**PulsaFeeder**	**OMC1-KCE-KKJ**	**1420-1700**
Oil pump	**Saci**	**KDN 32 – 163 – 1 – 161**	**2900**

Table 3.2. Specification of pumps used in the experimental set up

3.7. *Second configuration*

The experimental facility has been changed to add a preheater and a generator, using the advantage of modular construction. The information of these new PHEs is shown in table 3.3. Another important change is that there is only one evaporator. A new set of experimental data was obtained from this new configuration. Fig. 3.10 and 3.11 show the diagram of the experimental setup and the added components, respectively, for this second configuration.

PHE	AlphaLaval Model	Number of plates	Height (mm)	Width (mm)	Heat transfer area per plate (m^2)
Generator	**CB14-30**	**30**	**207**	**77**	**0.12**
Preheater	**CB14-20**	**20**	**207**	**77**	**0.12**

Table 3.3. Specification of Plate Heat Exchangers used in a second configuration of the experimental set up

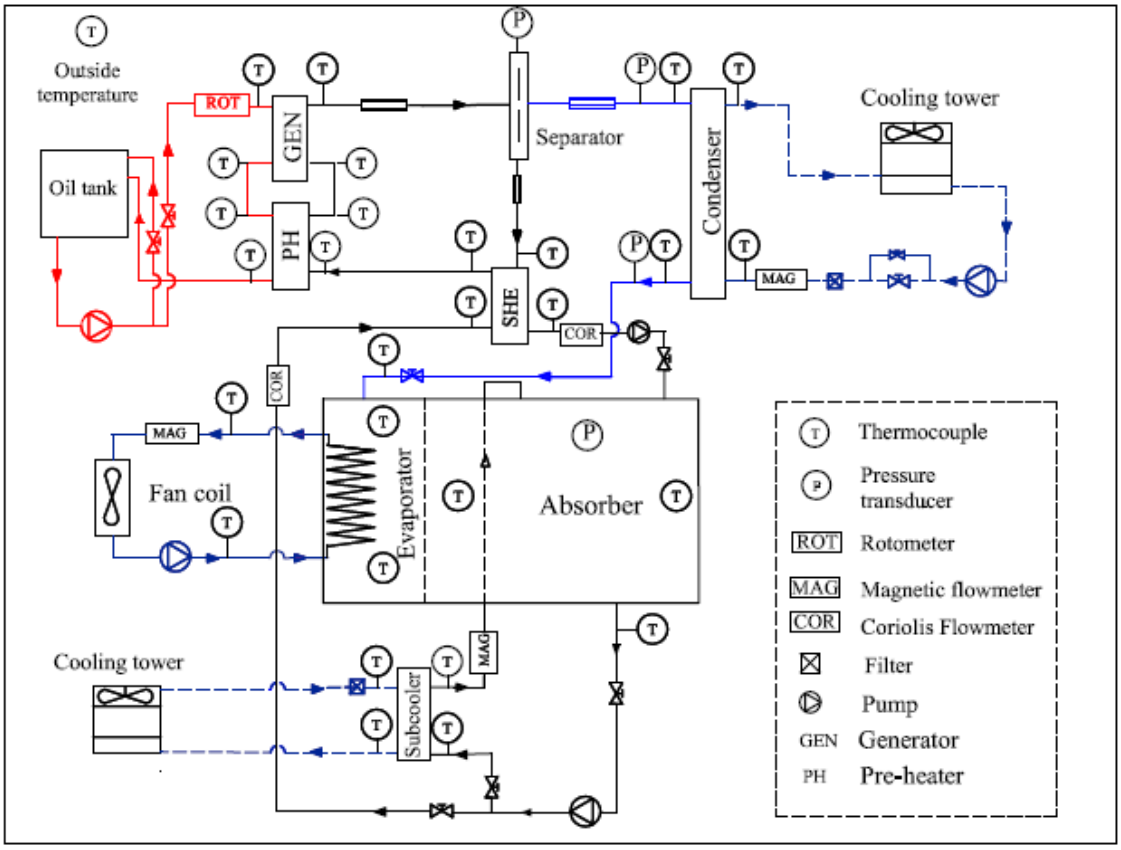

Fig. 3.10. Flow diagram of the test rig (2).

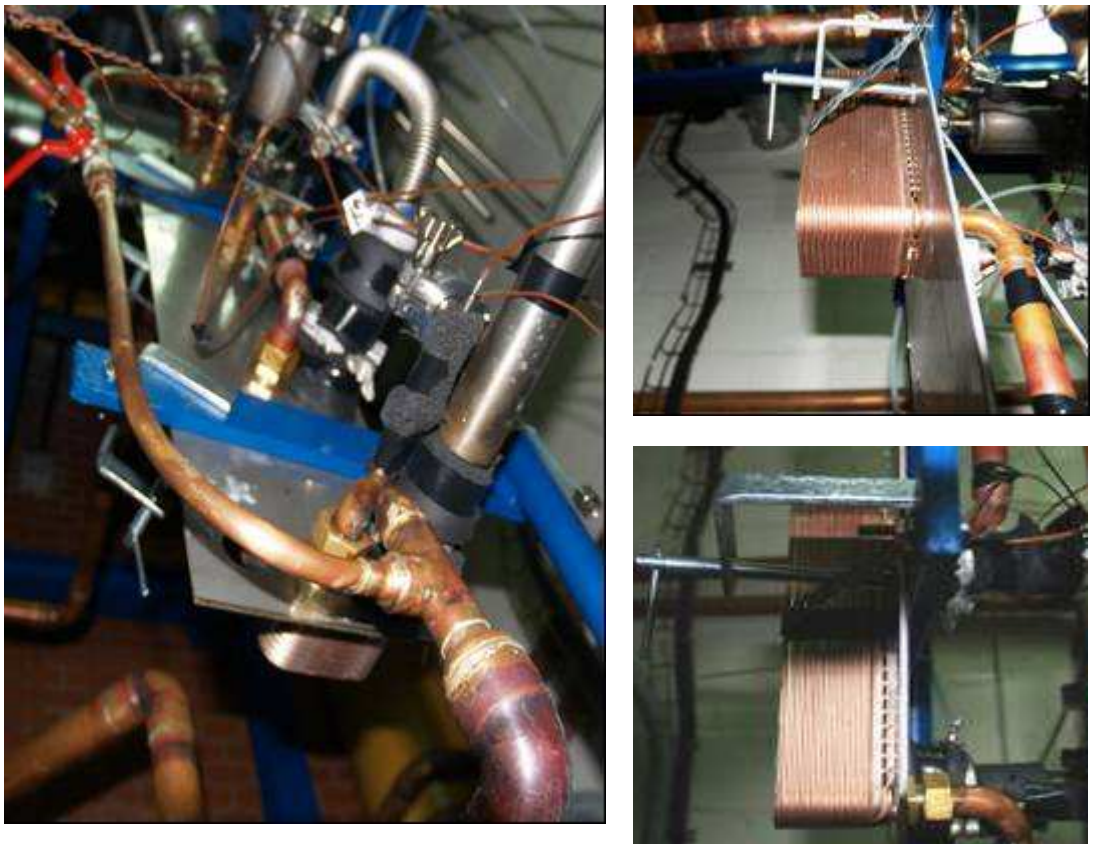

Fig. 3.11. System Generator - Preheater (left) and new PHEs: Generator (up) and Preheater (down)

The results of the experimental campaign carried out with this second configuration are under processing and are not presented in this thesis. However, this configuration is presented to demonstrate the feasibility of replacing system components easily and modularity of the machine.

3.8. Data acquisition

The data acquisition system is composed of two data-loggers, manufactured by Yokogawa, with 50 input ports available altogether, and a 24 V power supply. The oil flowmeter and the pressure transducers use the power supply to output an electric current of 4 to 20 mA. The input ports are read in intervals of 0,5 seconds by a computer program coded under National Instruments LabView® G environment (Fig. 3.12). Fig. 3.13 shows a picture of the data-loggers used.

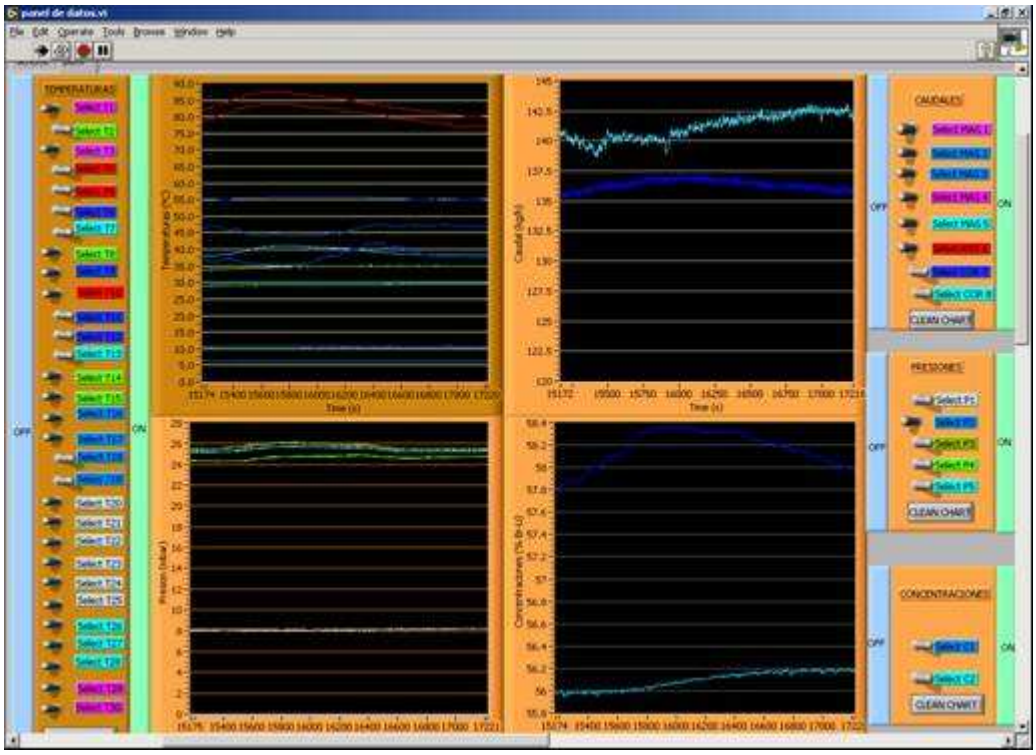

Fig. 3.12. Data panel of the data acquisition program

Fig. 3.13. Images of data-loggers

3.9. Experimental procedure

In each test the initial pressure inside the absorber-evaporators chamber is set to 7 mbar. A vacuum pump is activated to reach this pressure. There is an electro-valve that maintains this pressure value through an on-off control system. This system is activated only when the machine is not working.

The experimental procedure consists on periods of start-up, normal operation and shut down of the machine. Start-up begins with the thermal oil heating from ambient temperature to the temperature setpoint t_{set} while the oil is pumped to the generator. Solution pump is switched on and the weak solution flow rate $\dot{m}_{weak}$ to the generator is fixed at the desired value changing the frequency of the pump and adjusting the valves. The recirculated solution flow rate $\dot{m}_r$ varies according to the aperture of the valves and the driving frequency of the pump motor. Cooling tower flows are also switched on at this moment. The operating ranges of fixed and controlled parameters are given in Table 3.4.

Parameter	**Working Range**
Inlet oil temperature (***t_{set}***)	85 - 100 ºC
Weak solution mass flow rate ($\dot{m}_{weak}$)	170-360 kg/h
Recirculated solution mass flow rate ($\dot{m}_r$)	260-1050 kg/h
Oil mass flow rate	3800 kg/h
Cooling water mass flow rate (condenser)	1400 kg/h
Cooling water mass flow rate (sub cooler)	1600 kg/h
Chilled water mass flow rate (fancoils)	600 kg/h

Table 3.4. Operating ranges of fixed and controlled variables.

3.10. Data selection

The information obtained through the data acquisition system consists of time and the values of temperatures, mass flow rates, concentrations and pressures obtained in the experiments. With these data and using spreadsheet, plots corresponding to each variable are obtained in relation to time. These graphs yield the time interval where the conditions of stability are achieved.

After the oil temperature is stabilized at the desired value, which is then controlled by the on- off system, a critical variable to stabilize is the solution flow rate. The observation of its behavior determines the stability of the machine, as first estimate. The proper adjustment of solution flow, either by valves or the pump, is important to obtain the desired operating conditions. Fig. 3.14 indicates a time range where stability is achieved (where a time has passed to achieve equilibrium). In this figures some variables are plotted in order to show their evolution during a typical experiment. These variables are: inlet oil temperature, $T_{oil,i}$ (t_{set}) , outlet solution temperature at generator, $T_{G,o}$, outlet chilled water temperatures at evaporators 1 and 2, $T_{chw1,o}$ and $T_{chw2,o}$, mass flow rates and salt concentration of weak and strong solution $\dot{m}_{weak}$, $\dot{m}_{strong}$, X_{weak} and X_{strong}.

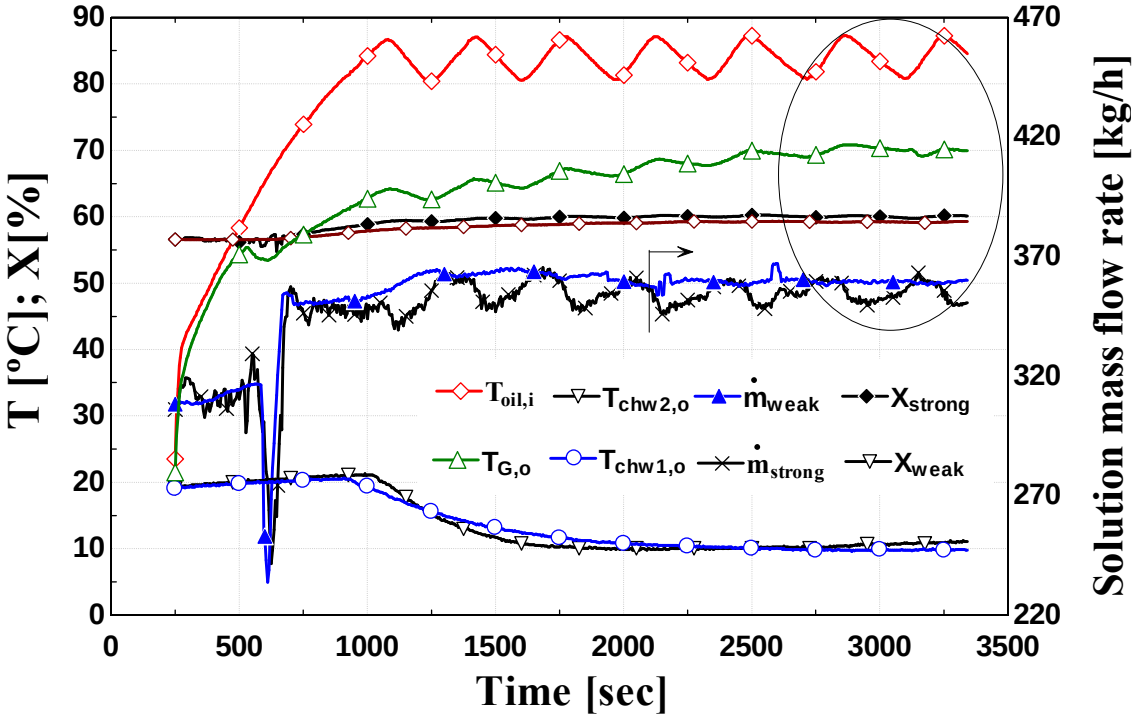

Fig. 3.14. Temperatures, concentration and flow rates vs. time during an experiment.

The stability of the working conditions is assured by selecting, from registered data, a period of time (20 min at least) in which temperatures, pressure and both $\dot{m}_{weak}$ and $\dot{m}_{strong}$ shows a constant behavior. This is identified by oscillations of oil temperature and high pressure with constant amplitude and a trend variation less than 0.3%, and 5% respectively.

With these ranges as a reference, the stability of the remaining variables is checked. An analysis of the oil temperature oscillation, i.e., a cycle in which this temperature fluctuates between a maximum and a minimum value (Fig. 3.15), yields the interval in which experiment data is averaged. Everything is done taking into account the stability of the other temperatures, which are generally fairly constant in time.

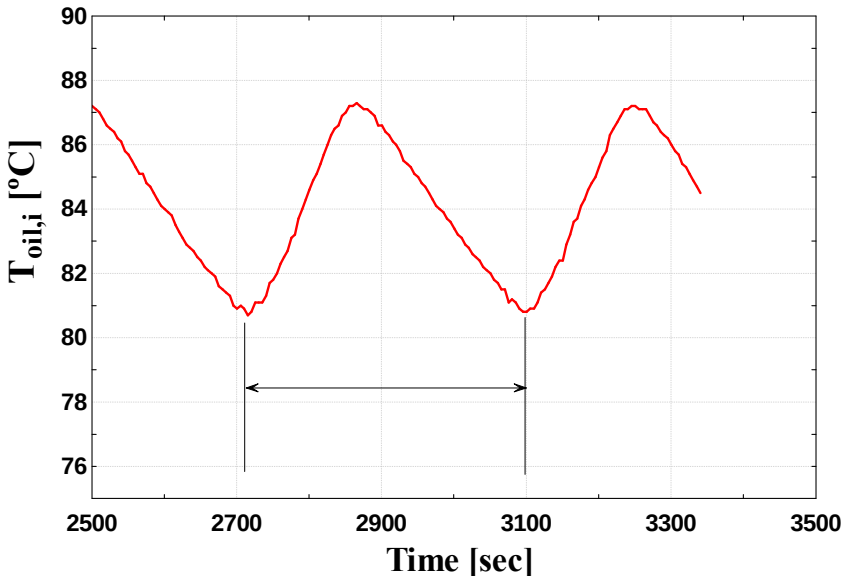

Fig. 3.15. Oil temperature at generator inlet vs. Time during an experiment.

After this procedure, the recorded data corresponding to all sensors connected to the data loggers are averaged.

3.11. Experimental uncertainty analysis

A calibration procedure was applied to all instruments described in Fig. 3.1. Using the calibration functions for every sensor, systematic errors were reduced as far as possible. The random uncertainty U for an experimental result R, which is function of n independent parameters $x_{i,}$ is estimated, according to a Gaussian statistics based algorithm, as:

$$U = \sqrt{\sum_{i=1}^{n}\left(\frac{\partial R}{\partial x_i}\cdot U_{x_i}\right)^2} \qquad ;\ R = f(x_1, x_2, \ldots x_n) \tag{3.1}$$

The uncertainty of instruments is given in Table 3.5. For the cases of thermocouples and pressures sensors, the uncertainty ranges given corresponds to minimum and maximum values for the whole set of calibrated instruments.

Appendix B describes the calibration process of sensors used in the experimental set-up and the resulting uncertainty of measured variables.

Instrument	**Quantity**	**Range**	**Uncertainty**
Thermocouple	30	5 - 110 ºC	±(0,2ºC - 0,6ºC)
Solution flow and density meter	2	150-400 kg/h	± 0,5%
Oil flowmeter	1	1000-3600 l/h	± 3,1%
Cooling water flowmeters	2	1200-1500 kg/h	± 1,1%
Recirculated solution flowmeters	1	200-1000 kg/h	± 1,3%
Fan coil flowmeters	2	400-600 kg/h	± 0,7%
Pressure sensors	4	7-130 mbar	±(1,8 - 3)%

Table 3.5. Sensors used in the experimental test rig.

3.12. Experimental set up specific for adiabatic absorbers

Experiments were conducted in a test chamber designed and built for the characterization of the distribution units of solution, before being tested in the complete adiabatic absorption cycle. The objective of these trials was to evaluate de absorption capability of one single fan sheet, before being incorporated to the complete absorption system, previously described.

The experimental set-up is shown in Fig. 3.16. The test section consists of a plenum chamber made out of stainless steel sheet to ensure an optimum behaviour in a corrosive environment with Water- LiBr solution. It also has a wide optical access to the fan sheet formation zone through windows of 20 mm Pirex in thickness, forming a triangular structure in the upper part.

The solution passes through several components in a closed loop. This loop is composed of the absorption chamber as test section, a variable-speed pump, a cold water tank and a Coriolis mass flow meter. The pump delivers the solution to the chamber. The mass flow rate is controlled by an AC motor through the change of the frequency. In order to cool down the solution that goes out from the chamber, it passes through flexible tubes to a tank of cold water. A Coriolis type meter measures simultaneously the mass flow, the density and the temperature of the solution. In addition, there are two valves in the loop at inlet and exit of the chamber to control filling and emptying operations. The absorption chamber is equipped with two absolute pressure transducer that measured the pressure upstream of the nozzle and inside the chamber. The solution temperature at chamber exit is measured by a T-type thermocouple. The fan sheet generated and the nozzle used in the experiments are shown in Fig. 3.17. The details of instrumentation used are given in Table 3.6.

In order to assure the steam supply to the chamber, a water tank heated with an electric heater is used. It has a valve to control the pressure inside the absorption chamber and a type T thermocouple to measure the temperature inside it.

A vacuum pump is used in order to obtain the vacuum pressure inside the chamber. It is equipped with a cold trap to separate the steam extracted from the enclosure. This trap is fed with cold water from a tank using a level pump to assure its operation.

Figs.3.18 and 3.19 show photographs of the experimental set up.

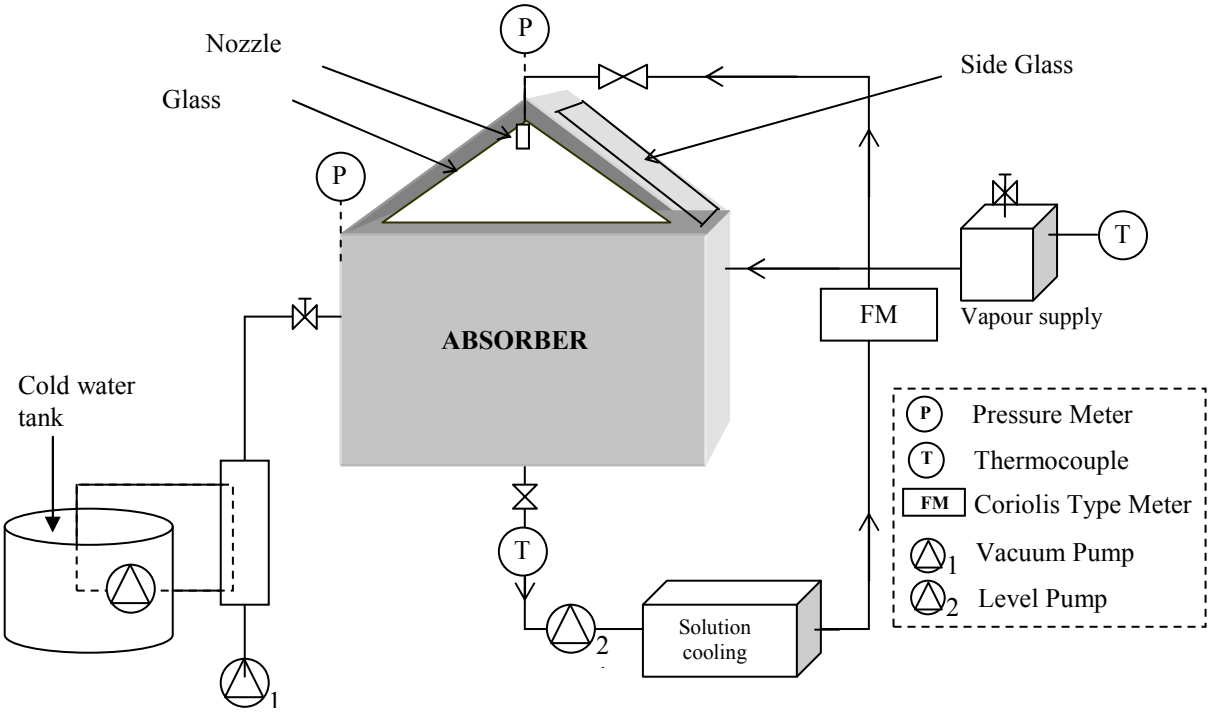

Fig. 3.16. Schematic view of the experimental set up specific for adiabatic absorbers

Instrument	**Type**	**Range**	**Accuracy**
Thermocouple.	T	20-40 ºC	± 0,1 ºC
Solution flow and density meter	Coriolis	(0.19<Q<600) Kg/h (0.3<ρ<5)Kg/l (-180<T<150)ºC	Mass Flow:+/- 0.1% VM Density: +/- 4 g/l Temperature: +/-1ºC
Pressure sensor	Absolute	8.3 – 250 mbar	0.5% (span offset)
Pressure sensor	Absolute	0-250 mbar	< 0.1% (span offset)

Table 3.6. Details of instrumentation used in the experimental set up specific for adiabatic absorbers

(a) (b)

Fig. 3.17. (a) Image of the nozzle used in the experiments. Source: www.spray.com.mx . (b) Front view of the fan sheet generated

Fig. 3.18. Schematic view of the experimental set up specific for adiabatic absorbers

Fig. 3.19. Lateral view of the experimental set up specific for adiabatic absorbers

Experimental procedure

In each test the pressure inside the chamber is maintained around 6 mbar. The vacuum pump is activated to obtain these pressure values. Then, the flow rate is selected by changing the frequency of the solution pump. Meanwhile, the pressure is maintained at the desired value. Next, the experimental data is taken every 30 seconds. The solution introduced to the chamber is weighed before starting each test. Once each experiment is finished, the diluted solution is weighed again. This is done to obtain the value of absorbed water, by subtraction. The solution concentration in the experiments ranges from 58 to 60%. When the solution reaches the minimum value, it is replaced with a concentrated solution with concentration of 60%.

The experiments are carried out for several flow rates, which range from 100 to 250 Kg/h of solution. The acquired data gave the values of density, pressure and temperature of solution for each flow rate tested.

The experiments aim to analyze the performances of the fan sheet in the absorption process by estimating the change of concentration of the solution with time. This will determine the refrigerant flow that a single fan sheet is capable of handling (absorption capacity).

In order to estimate the cooling capacity of the fan sheet the following procedure is used:

1. Concentration change in the solution:

$$X = \frac{m_{LiBr}}{m} = \frac{m_{LiBr}}{m_{LiBr} + m_{H_2O}} \tag{3.2}$$

$$\frac{dX}{dt} = -\frac{m_{LiBr} \cdot \frac{dm_{H_2O}}{dt}}{m^2} = -\frac{X}{m}\frac{dm_{H_2O}}{dt} \rightarrow \frac{dm_{H_2O}}{dt} = -\frac{m}{X}\frac{dX}{dt} \tag{3.3}$$

2. Defining the absorption capacity as the refrigerant flow that the sheet is able to absorb, the above parameter is:

$$\frac{dm_{H_2O}}{dt} = \dot{m}_{refrigerant} \tag{3.4}$$

3. The cooling capacity can be estimated as:

$$\dot{Q}_{fansheet} = \dot{m}_{refrigerant} \cdot h_{fg} \tag{3.5}$$

where h_{fg} is the phase change enthalpy of water at a given temperature.

The preliminary results obtained served to define the way forward in terms of experiments with this absorber configuration.

Values of cooling capacity obtained range from 0,05 and 5,3 kW.

Fig. 3.1 shows the concentration change of solution with time, for several experiments.

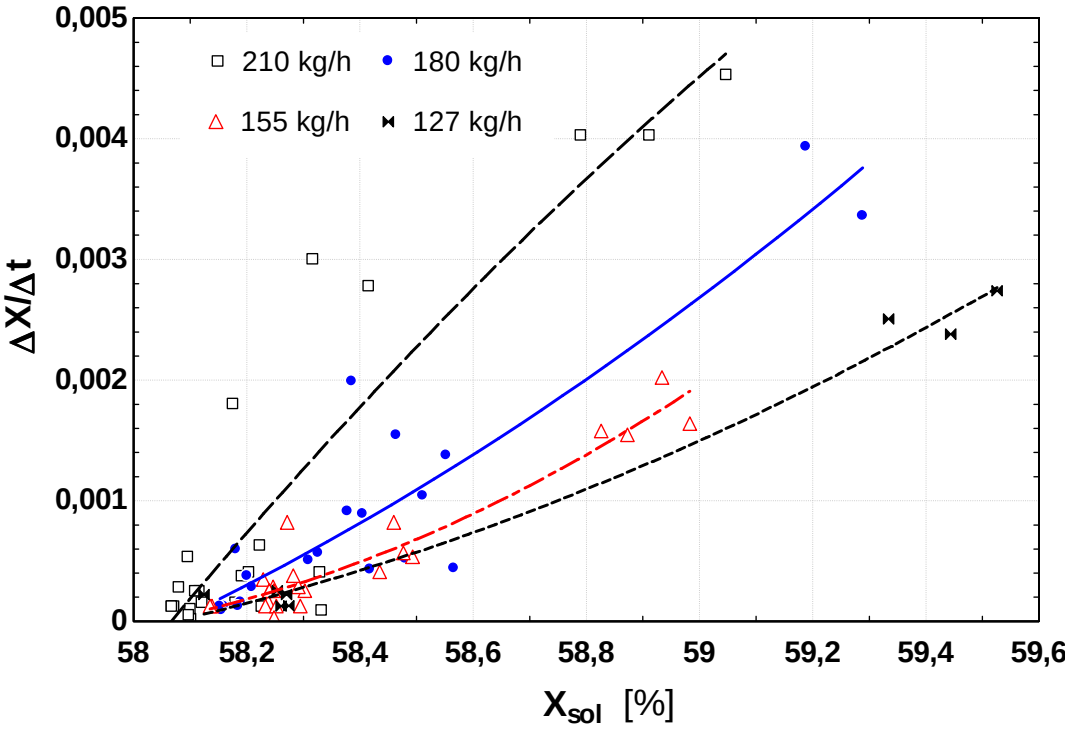

Fig. 3.20. Concentration change of solution vs. time for various flow rates.

Chapter 4

OVERALL TEST FACILITY PERFORMANCE

Index

NOMENCLATURE

COP	coefficient of performance
C	specific heat capacity ($kJkg^{-1}K^{-1}$)
D	Diameter (m)
f	friction factor
g	acceleration due to gravity
Gr	Grashof number
h	enthalpy ($kJkg^{-1}$)
L	Characteristic length
LiBr	lithium bromide
$\dot{m}$	mass flow rate (kgh^{-1})
Nu	Nusselt number
P	absolute pressure (mbar)
Pr	Prandtl number
PHE	plate heat exchanger
$\dot{q}$	thermal power per unit mass flow ($kJ\ kg^{-1}$)
$\dot{Q}$	thermal power (kW)
Ra	Rayleigh number
RR	recirculation ratio, $RR = \frac{\dot{m}_r}{\dot{m}_{weak}}$
SHE	solution heat exchanger
t	temperature, external (ºC)
T	temperature, internal (ºC)
T_∞	fluid temperature far from the surface of the object (ºC)
u	velocity (ms^{-1})
x	quality
X	concentration

Subscripts

A	absorber

C	condenser
ch	chilled
E	evaporator
f	friction
exp	experimental
G	generator
i	inlet
id	ideal
ins	insulation
l	liquid
m	material
o	outlet
r	recirculated
ref	refrigerant
set	established value
t	tube
v	vapour
V	at valve conditions
w	water

Greek letter:

α	Thermal diffusivity
β	Thermal expansion coefficient
ΔT_{lm}	Logarithmic mean temperature difference
η	efficiency
ρ	density
v	Kinematic viscosity

4.1. Introduction

In line with the general objective of this thesis, the experimental evaluation of the overall performance of the machine is presented in this chapter in terms of the cooling capacity and COP.

Once the overall performance of the machine is defined, it is necessary to carry out the particular detailed analysis of each component in order to explain their effects on the overall performance obtained. The analysis is focused firstly on the evaporators. Another important component to study is the solution heat exchanger, considering its efficiency and operation as an important effect to observe and concern. In addition, thermal losses calculations are included, which will be used for the analysis of results and a subsequent model is developed.

For all the evaluation parameters described next and for the thermo-physical and transport properties calculations, the software Engineering Equation Solver (EES) was used. Temperature, pressure, enthalpy and concentration of lithium bromide are based on correlations from the ASHRAE Handbook of Fundamentals (1989).

4.2. Preliminary experimental results

As it was stated in chapter 3, start-up of the machine begins with the thermal oil heating from ambient temperature up to the desired temperature t_{set}. After about 15 minutes vapour separation begins in the generator. Cold water production begins 10 minutes later. After shut down of the heating source the machine remains producing chilled water for about 45 min, while the solution is maintained circulating. Along this last period the pressure in the absorption chamber decreases.

The performance parameters corresponding to each operating conditions are obtained according the procedure explained on section 3.10.

From measured values of inlet and outlet water temperatures of both evaporators, cooling power is obtained from Eq. (4.1):

$$\dot{Q}_{E,\exp} = \dot{m}_{chw} \cdot C_w \cdot (t_{chw,i} - t_{chw,o}) \tag{4.1}$$

The heating power supplied to the generator was evaluated as:

$$\dot{Q}_{G,\exp} = \dot{m}_{oil} \cdot C_{oil} \cdot (t_{oil,i} - t_{oil,o}) \tag{4.2}$$

The experimental *COP* was calculated as the quotient of (4.1) and (4.2).

$$COP_{\exp} = \frac{\dot{Q}_{E,\exp}}{\dot{Q}_{G,\exp}} \tag{4.3}$$

Another parameter that is sometimes useful is the solution circulation ratio, named *f*, according to the definition given by Herold and Radermacher (1996).

$$f = \frac{\dot{m}_{weak}}{\dot{m}_{ref}} = \frac{X_{strong}}{X_{strong} - X_{weak}} \tag{4.4}$$

Figs. 4.1 to 4.4 show the behaviour of instantaneous parameters in a dynamic experiment carried out in the absorption test rig. Fig 4.1 illustrates the instantaneous cooling power and *COP*. In this experiment t_{set} was fixed at 90 ºC, the recirculation radio *RR* (the ratio of the solution mass flow rate recirculated to the absorber to solution mass flow rate sent to generator) was fixed at 1.7 and $\dot{m}_{weak}$ was varied from 170 up to 360 kg/h.

Fig. 4.2 shows the generation, condensation and evaporation temperatures for this experiment. As can be expected, the oscillating behaviour of the generation temperature, due to the on-off control, is followed by other parameters like *COP* (Fig. 4.1), the condensation pressure (Fig. 4.3) and the weak solution flow rate (Fig. 4.4). These oscillations are considered for the implementation in vehicles, which is proposed in the project CLIMABCAR. This is due to expected fluctuations in the temperature of generation, produced by changes in operating conditions of the engine, whose waste heat is used.

For all experiments $\dot{m}_{weak}$ was changed six times for each t_{set}. The steps in Fig. 4.4 represent these changes in $\dot{m}_{weak}$ and the corresponding $\dot{m}_r$.

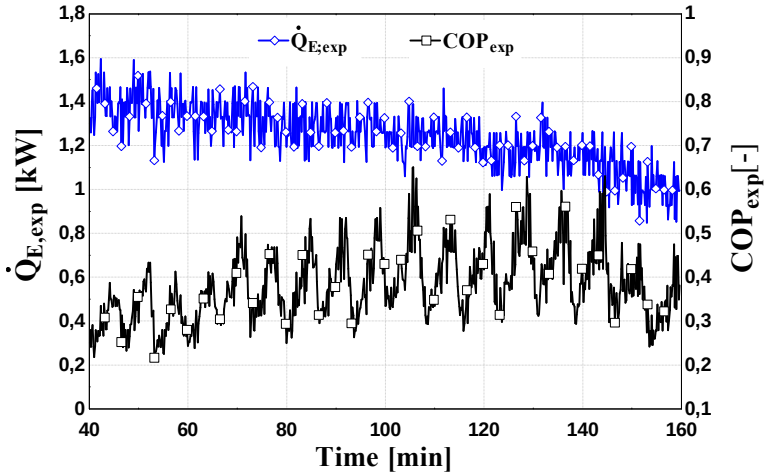

Fig. 4.1. Time evolution of cooling power and *COP* at t_{set} = 90 ºC, *RR* = 1.7, with variable $\dot{m}_{weak}$.

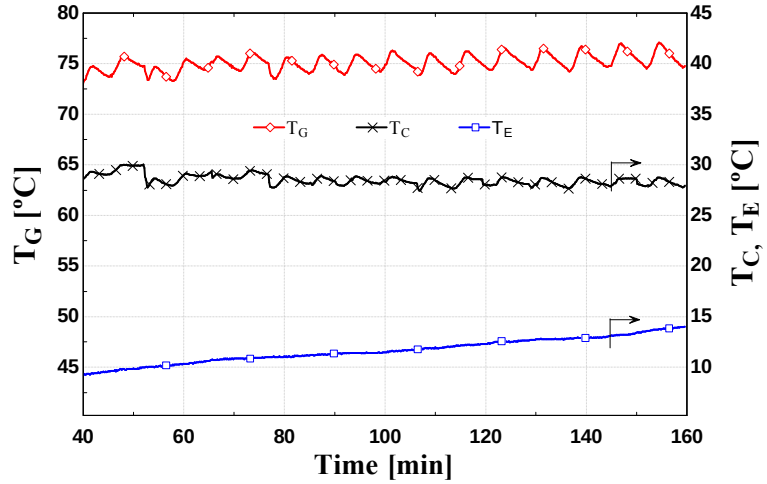

Fig. 4.2. Time evolution of generation temperatures (left scale). Condensation and evaporation temperatures (right scale).

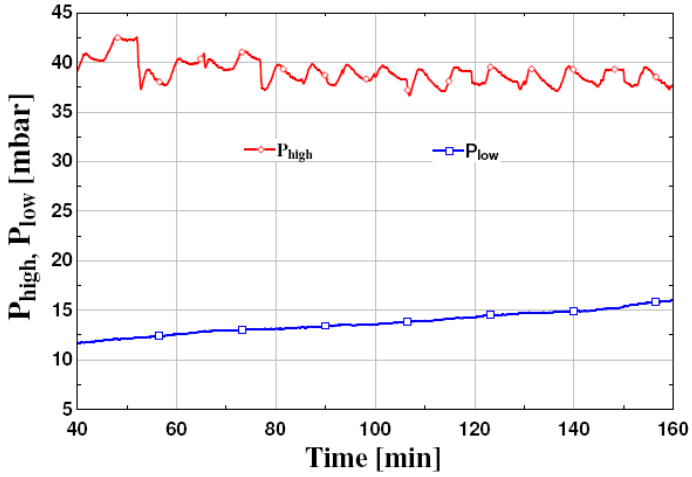

Fig. 4.3. Time evolution of condensation pressure (upper curve) and evaporation pressure (lower curve)

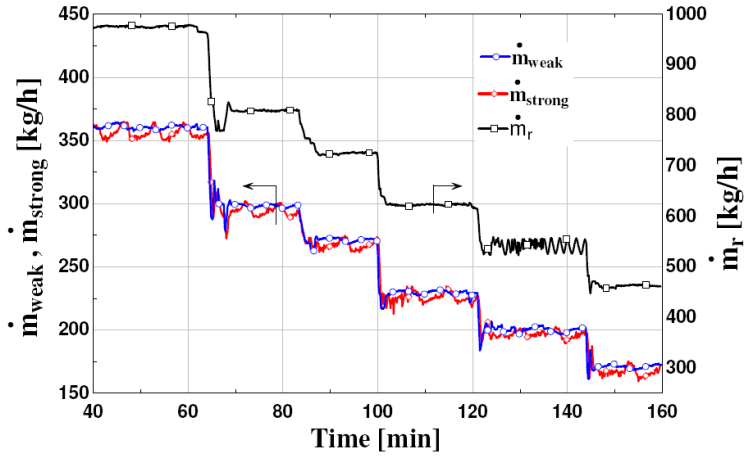

Fig. 4.4. Time evolution of weak and strong solution mass flow rates (left scale) and recirculated solution mass flow rate (right scale).

Fig. 4.5 shows that the concentration of weak solution also follows the oil temperature evolution, but out of phase. This is due to the heat capacity effects of the machine. Variations in the oil temperature allow observing the behaviour of this facility, when the operating parameters vary with time. The time difference between the maximum values of cooling capacity and the weak solution temperature at the generator exit, due to this heat capacity effects, was 1.83 minutes. This delay calculated from the thermal oil temperature entering to the generator was 2.13 minutes.

The difference between strong and weak solution concentration (Fig. 4.5) is higher for smaller values of $\dot{m}_{weak}$. For the complete experimental campaign, the minimum and maximum values of weak and strong solution concentration were 58% – 62% and 59% – 64%, respectively. From all experiments run it has been observed that when

$\dot{m}_{weak}$ is too low, and the oil temperature is too high, there is a risk of crystallization. Crystals are originated in the high pressure zone, passing to the low pressure zone.

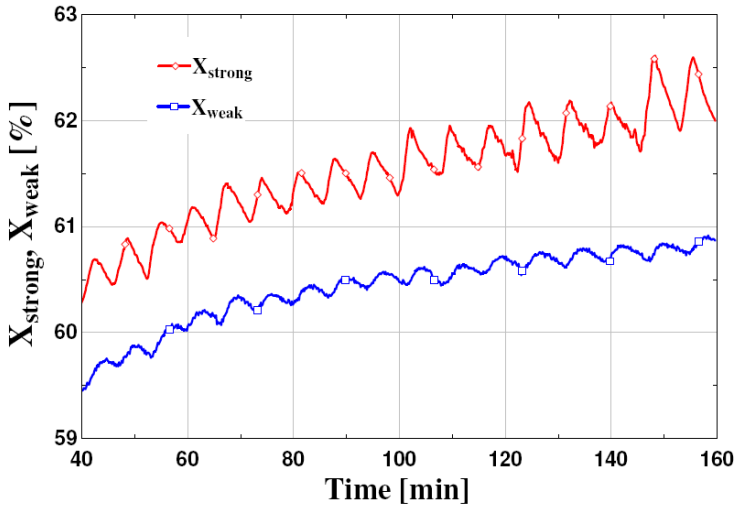

Fig. 4.5. Time evolution of strong and weak solution concentrations.

Fig. 4.6 represents solution cycle in a *P-T* plot for an evaporation temperature T_E= 13 ºC, condensation temperature T_C=29 ºC and absorption temperature T_A = 55 ºC, corresponding to minute 130 in Fig. 4.1-4.5. This diagram is extended for the adiabatic cycle, corresponding to this machine, in Chapter 5.

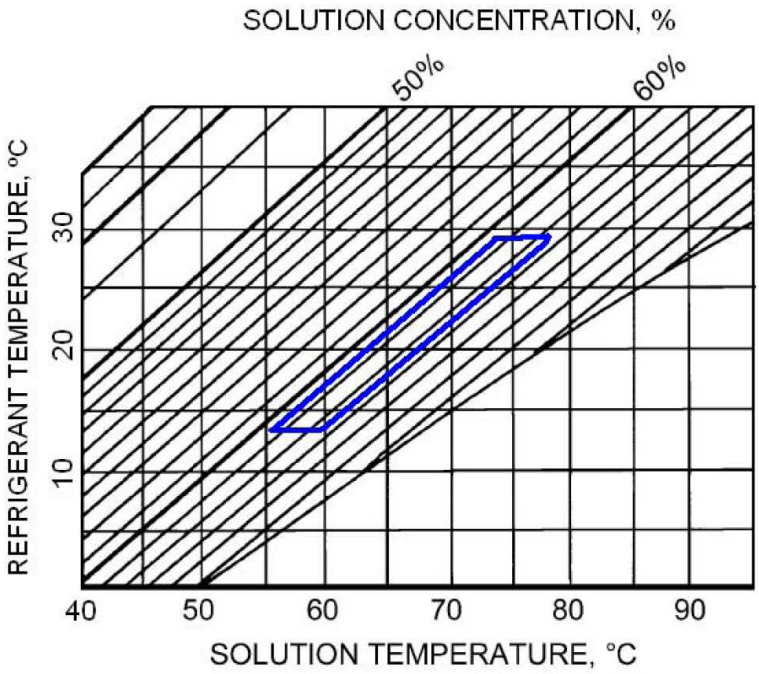

Fig. 4.6. Absorption cycle in a pressure – temperature plot.

The influence of the parameters which were varied in the experiments (t_{set} and $\dot{m}_{weak}$) on cooling power and *COP* was analyzed for 280 experimental points. Fig. 4.7 shows the different *COP* and $\dot{Q}_{E,\exp}$ obtained as a function of t_{set} for *RR* fixed at 1.9 and a $\dot{m}_{weak}$ fixed at 230 kg/h. There is a maximum value observed for a given t_{set} in both cases. This behaviour is similar for all values of $\dot{m}_{weak}$ proving that the variation of t_{set} always affects the *COP* and the cooling power. The existence of a maximum point, for the case of $\dot{Q}_{E,\exp}$, has a relation with the performance of the evaporators' couple in the machine. When t_{set} is higher, the quantity of vapour separated is higher (as shown on Fig. 4.8) and therefore there is more liquid water obtained in the condenser. It would be reasonable to expect an increase in $\dot{Q}_{E,\exp}$. But the performance of the evaporators makes them unable to evaporate all the condensed water. This will be discussed in detail in next section.

The decrease in cooling power, and the fact that at higher t_{set} the generation power is higher, jointly with an increase of the irreversibility in the machine, makes the *COP* to decrease. On the other hand, at lower values of t_{set} there is less vapour generated, producing a lower cooling capacity and therefore a lower *COP*. Maximum value of t_{set} observed was 90 ºC for $\dot{Q}_{E,\exp}$ and 85 ºC for *COP*.

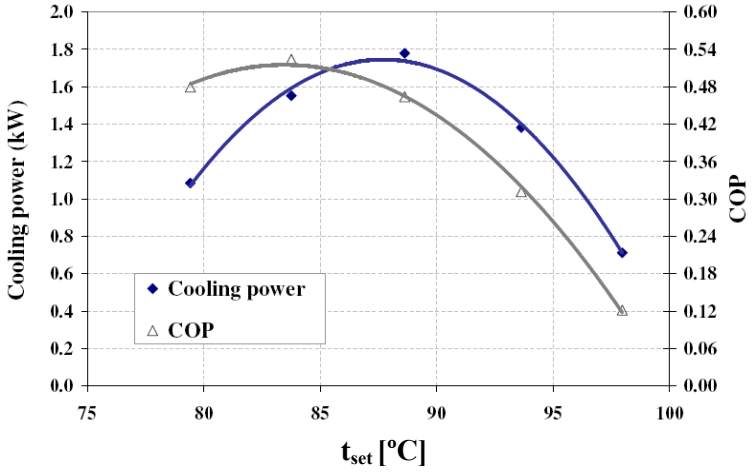

Fig. 4.7. Influence of hot fluid temperature on cooling power and *COP* at *RR* = 1.9 and $\dot{m}_{weak}$ = 230 kg/h.

Fig. 4.8 illustrates the solution circulation radio, calculated through Eq. (4.4). The influence of both controlled oil temperature and solution mass flow rate is clear. In general, f is inversely proportional to t_{set} and proportional to $\dot{m}_{weak}$.

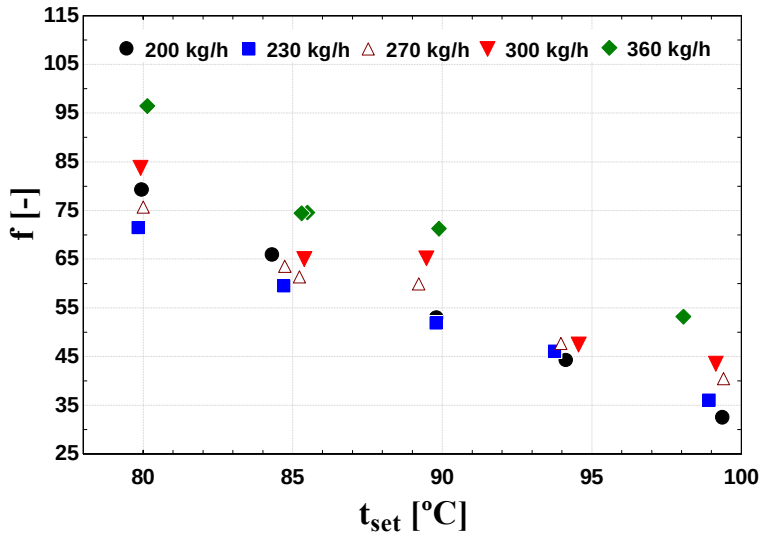

Fig. 4.8. Solution circulation ratio vs. t_{set} for different $\dot{m}_{weak}$

Fig. 4.9 shows the influence of $\dot{m}_{weak}$ on $\dot{Q}_{E,\exp}$ and *COP* at a fixed t_{set} (85 ºC) and *RR* fixed at 2.2. As $\dot{m}_{weak}$ increases the cooling power is higher. However the *COP* shows a maximum value at a given $\dot{m}_{weak}$. This optimal value of $\dot{m}_{weak}$ was in the range from 200 to 230 kg/h for t_{set} between 80 and 90 ºC. When t_{set} increases maximum values of $\dot{m}_{weak}$ decreases.

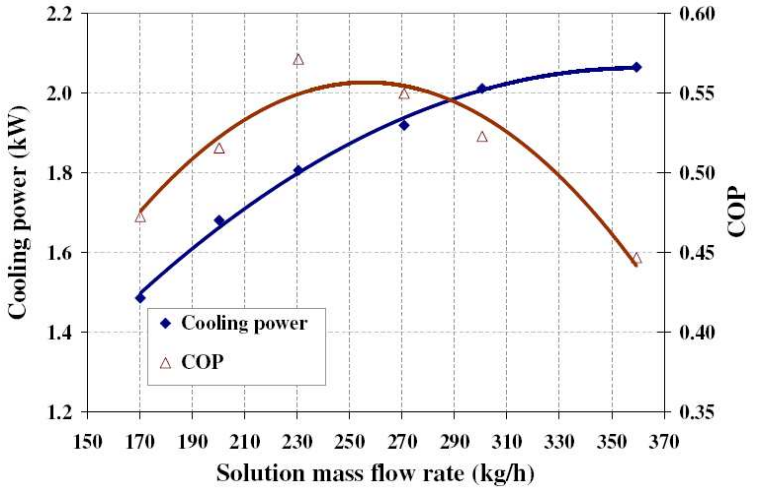

Fig. 4.9. Influence of solution flow rate trough the generator on cooling power at t_{set} = 85 ºC and *RR* = 2.2.

Results of this preliminary analysis show that:

- Due to the on-off control of the oil temperature, the small, but significant oscillating behaviour of this parameter is transmitted to condensation pressure, the concentration of the weak solution and *COP*. Special care had been taken with these oscillations, because in their peaks crystallization conditions could be reached in the strong solution.
- The time difference between the maximum values of cooling capacity and the thermal oil temperature entering the generator, due to heat capacity effects, was 2.13 minutes, for the operating conditions described above.
- The oil temperature at the inlet to generator t_{set} affects the cooling power and the instantaneous *COP*. There is a maximum value for t_{set} observed on both parameters. Maximum value of t_{set} observed was 90 ºC for $\dot{Q}_{E,\exp}$ and 85 ºC for *COP*. The source of this maximum point could be the limitation of evaporation rate due to a lack of performance of evaporators, producing the overflow of refrigerant. The decrease in $\dot{Q}_{E,\exp}$, and the fact that at higher t_{set} the generation power is larger and the irreversibilities in the machine are larger, makes the *COP* to decrease also. On the other hand, at lower values than optimum of t_{set} there is less vapour generated, producing a lower cooling capacity and therefore lower *COP*.
- As $\dot{m}_{weak}$ rises, the cooling power rises also. But the *COP* shows a decreasing tendency from a maximum value. This maximum value of $\dot{m}_{weak}$ was in the range from 200 to 230 kg/h for t_{set} between 80 and 90 ºC. When t_{set} increases optimal values of $\dot{m}_{weak}$ decreases.

This preliminary analysis gives an idea about the operational features of the machine, which yields the subsequent detailed analysis of components performance. This analysis is oriented to:

- Evaporators efficiency.
- Solution heat exchanger efficiency.
- Machine thermal losses.

In the following sections, the components performance is analyzed in detail in order to give the basis of the performance behaviour illustrated above.

4.3. Components performance and machine thermal losses

The drastic fall in the cooling capacity at high temperatures makes the present study to consider, first that all, the evaporators as the principal component to analyze, due to the obvious dependence of their performance and the cooling capacity obtained.

4.3.1. Evaporators

In the following, the evaporators' efficiency and refrigerant mass flow rate distribution to the evaporators will be estimated and discussed.

4.3.1.1. Evaporators efficiency

An energy balance in the evaporators allows the calculation of the maximum cooling capacity, as follows:

$$\dot{Q}_{E,ref} = \dot{m}_{ref} \cdot \left(h_{E,i} - h_{E,o} \right) \tag{4.5}$$

The inlet evaporator enthalpy $h_{E,i}$ was obtained from the enthalpy corresponding to the liquid water at condenser outlet (Eq. 4.6), assuming that isenthalpic processes take place in the expansion valve. The vapour enthalpy at the evaporator outlet $h_{E,o}$ was calculated considering that vapour is saturated (Eq. 4.7).

$$h_{iE,in} = f(T_{C,o}, P_{C,o}) \tag{4.6}$$

$$h_{E,o} = f(P_E, x = 1) \tag{4.7}$$

Eq. (4.5) gives the cooling capacity that would be obtained if the entire refrigerant were evaporated. In order to measure the quantity of evaporated refrigerant, and therefore the performance of evaporators, $\dot{Q}_{E,ref}$ is compared with the cooling capacity calculated through an energy balance on the external flow, see Eq. (4.1).

The fraction of refrigerant evaporated, named from now on efficiency of evaporators, is then obtained by dividing Eq. (4.5) and (4.1):

$$\eta_E = \frac{\dot{Q}_{E,\exp}}{\dot{Q}_{E,ref}} \tag{4.8}$$

The corresponding COP_{ref} is calculated using Eqs. (4.5) therefore allowing the comparison of maximum and experimental values:

$$COP_{ref} = \frac{\dot{Q}_{E,ref}}{\dot{Q}_{G,\exp}} \tag{4.9}$$

These parameters allow expressing the behaviour of the evaporators, because their variation with operating conditions of the machine is significant, as discussed below.

4.3.1.2. Refrigerant mass flow rate distribution

Estimation of the quantity of refrigerant going to each evaporator, $\dot{m}_1$ *and* $\dot{m}_2$, is important for the evaluation of their individual performance and its strong influence over the resulting global performance of the system.

Ideally, the refrigerant mass flow rate distribution is expected to be symmetrical. But in practice this is not the case, due to the different opening of expansion valves, or different length and height of both connecting pipes. Temperatures at the end of the process, after the expansion valves, will also be different as a consequence of the different pressure drop in each stream.

Fig. 4.10 represents the diagram of the refrigerant distribution system in the machine under study. The boundary of control volume goes from the condenser outlet to the inlet of evaporators. The expansion valves corresponding to each evaporator are represented as V_1 and V_2. The other valves (d_1 and d_2) represent the expansion process taking place inside the evaporators, in the orifices of distribution tubes. E_1 and E_2 represent the refrigerant conditions at the state of the evaporation process.

In the following, the analysis of the system is developed with the aim to determine the specific quantity of refrigerant going to each evaporator.

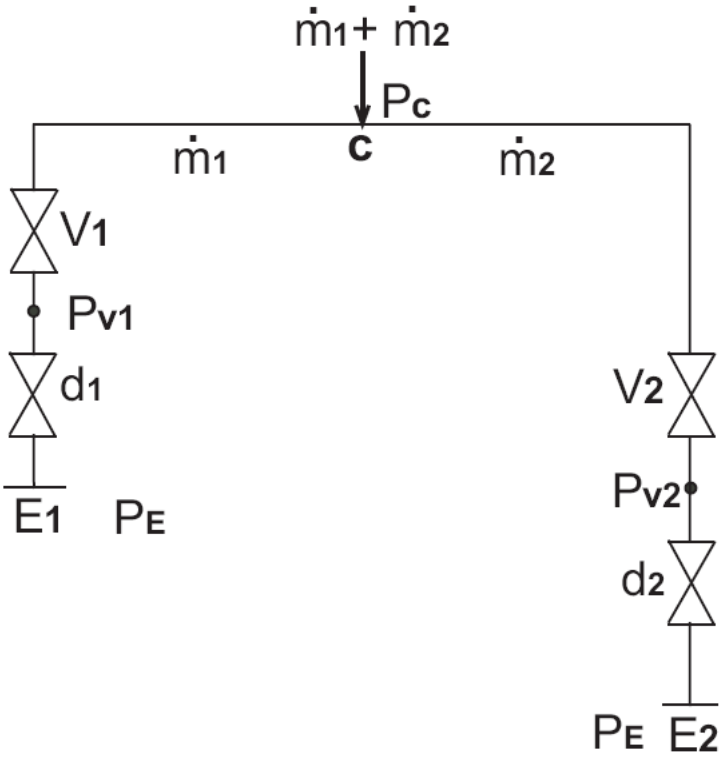

Fig. 4.10. Diagram of refrigerant mass flow rate distribution from condenser (c) to evaporators (E_1 and E_2).

High and low pressures, as well as temperatures after the expansion valves T_{V1} and T_{V2} are known from the experimental data. The following data are therefore known: P_C, P_{V1}, P_{V2}, P_E, h_C.

The unknown data is: $\dot{m}_1$, $\dot{m}_2$, ρ_{V1}, ρ_{V2}, ΔP_{fd1}, ΔP_{fd2}. The last two terms represent the pressure drop due to the expansion of refrigerant in the evaporators inlet (subscript d), corresponding to each valve. Fig 4.11 represents the Temperature-Entropy diagram of the process. This diagram aims to show the difference of output conditions (quality) of the refrigerant flow going to each evaporator. In most cases, the temperature of each flow is different, as seen in next section.

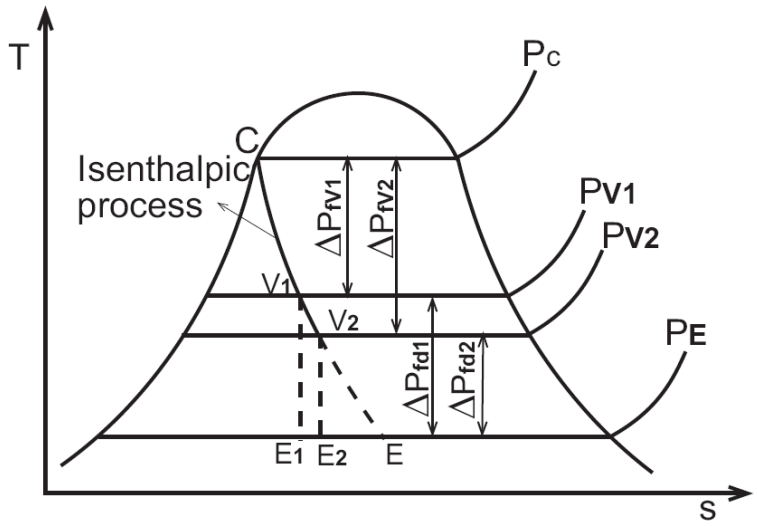

Fig. 4.11. Diagram Temperature – Entropy for the refrigerant distribution system

Knowing that $\Delta P_{fv} = K \cdot \frac{1}{2} \cdot \rho \cdot (v)^2 = K \cdot \frac{1}{2} \cdot \rho \cdot \left(\frac{\dot{m}}{\rho A_t} \right)^2$

We obtain: $\dot{m} = A_{efective} \cdot \sqrt{2 \cdot \rho \cdot \Delta P_{fv}}$ (4.10)

$$P_{V1} - P_E = \Delta P_{fd1} \tag{4.11}$$

$$P_{V2} - P_E = \Delta P_{fd2} \tag{4.12}$$

P_{V1} and P_{V2} are the saturation pressures corresponding to T_{V1} and T_{V2}, respectively. The two phase flow densities ρ_{V1} and ρ_{V2} can be estimated from h_C and T_{V1}, T_{V2}. From Eq. (4.10) and assuming that $A_{ed2}=A_{ed1}=A_{de}$.

$$\dot{m}_1 = A_{de} \cdot \sqrt{2 \cdot \rho_{V1} \cdot \Delta P_{fd1}} \tag{4.13}$$

$$\dot{m}_2 = A_{de} \cdot \sqrt{2 \cdot \rho_{V2} \cdot \Delta P_{fd2}} \tag{4.14}$$

Combining Eqs. (4.13) and (4.14):

$$\frac{\dot{m}_1}{\dot{m}_2} = \sqrt{\frac{\rho_{V1}}{\rho_{V2}} \cdot \frac{\Delta P_{fd1}}{\Delta P_{fd2}}} \tag{4.15}$$

$$\dot{m}_{ref} = \dot{m}_1 + \dot{m}_2 \tag{4.16}$$

Solving the equation system defined by Eqs. (4.11), (4.12), (4.15) and (4.16), the refrigerant mass flow rate distribution is estimated.

4.3.1.3. Results and discussion

Solution of the equation system previously explained allows the estimation of the quantity of refrigerant mass flow rate, $\dot{m}_{ref}$, received by each evaporator. Fig. 4.12 illustrates this distribution for the different experiments carried out. This figure is an illustrative example to have an idea about the distribution of the refrigerant and the corresponding inlet generator temperature (t_{Gi}= t_{set}) along the whole experimental campaign. In those experiments where the distribution is more equitable, the cooling power associated is higher. Besides, it has been detected that the distribution of $\dot{m}_{ref}$ ($\dot{m}_1$ and $\dot{m}_2$) is not symmetrical in some cases, and therefore one of the evaporators could be not operating. This situation also explains why $\dot{Q}_{E,\exp}$ slopes down when it is supposed to have an increasing tendency; i.e., when $t_{G,i}$ rises.

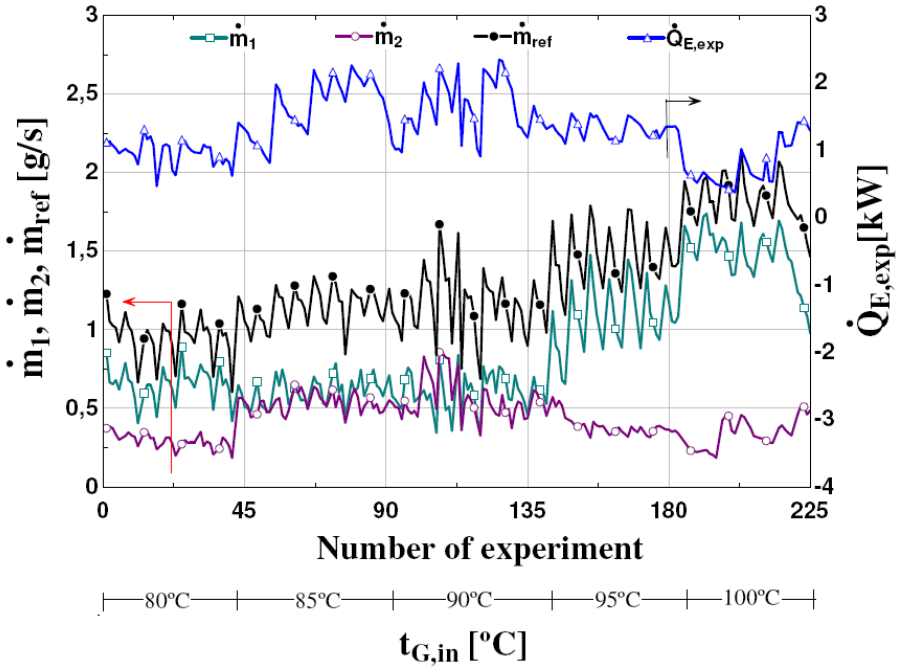

Fig. 4.12. Refrigerant distribution for different experiments.

Figs. 4.13 and 4.14 illustrate the quantity of refrigerant going to each evaporator vs. t_{Gi} and the total $\dot{Q}_{E,\exp}$ obtained, for several fixed values of solution mass flow rate $\dot{m}_{weak}$ and recirculation ratio *RR*.

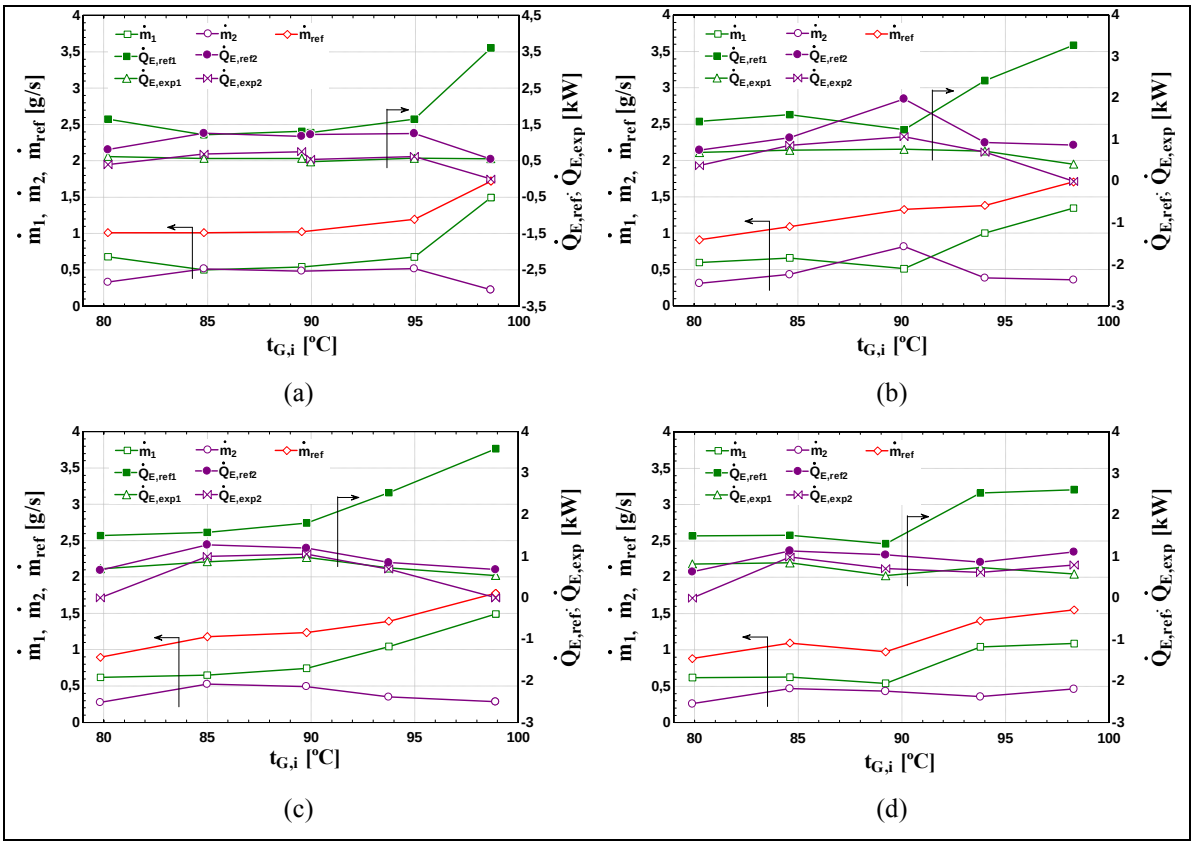

Fig. 4.13. Refrigerant distribution and corresponding experimental and maximum cooling capacity for each evaporator vs. t_{Gi}. $\dot{m}_{weak}$ =230 kg/h and RR=(a) 1,5;(b) 1,9; (c) 2.3 and (d) 2,7.

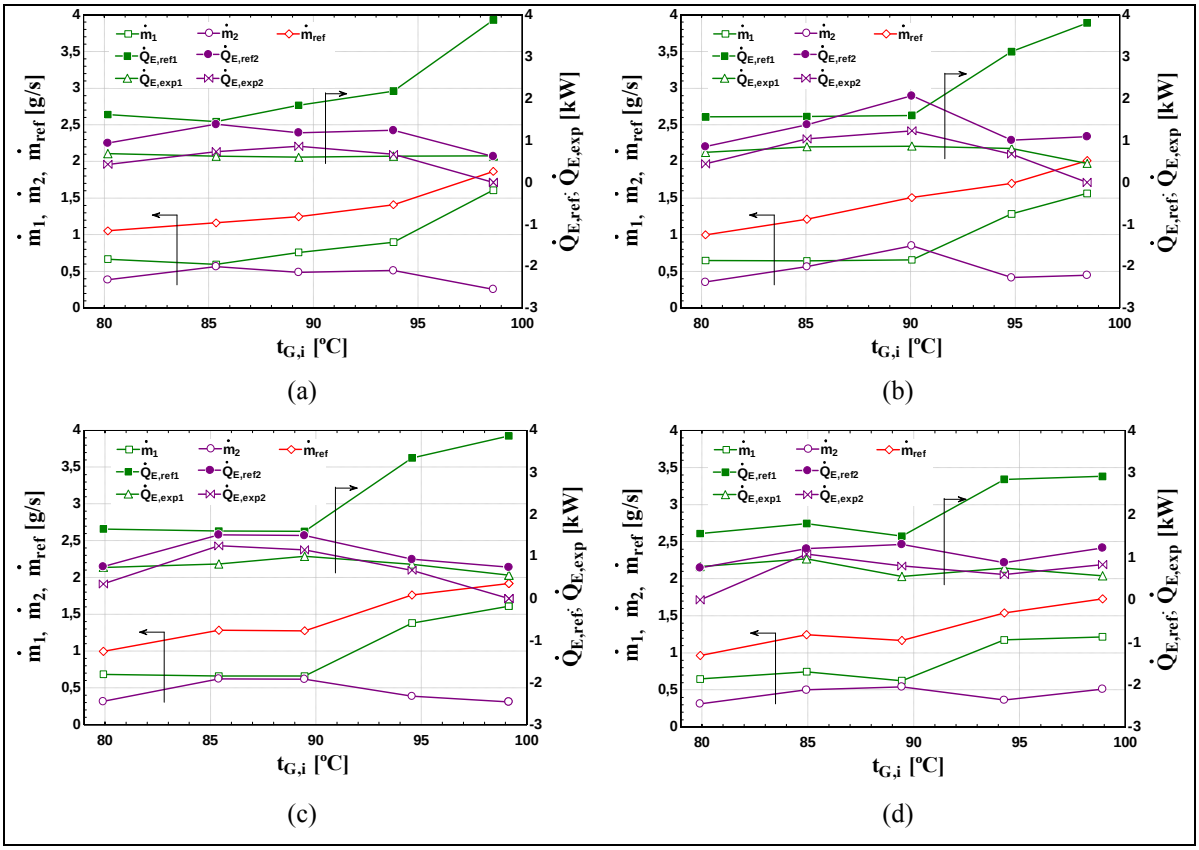

Fig. 4.14. Refrigerant distribution and corresponding experimental and expected cooling capacity for each evaporator vs. t_{Gi}. $\dot{m}_{weak}$ =300 kg/h and RR=(a) 1,5;(b) 1,9; (c) 2.3 and (d) 2,7.

Fig. 4.15 and 4.16 show the global performance parameters (evaporators efficiency η_E, cooling power and COP) obtained as a function of t_{Gi} for various *RR* and $\dot{m}_{weak}$. The cases plotted correspond to experimental data obtained for $\dot{m}_{weak}$ fixed to 230 kg/h and 300 kg/h. It can be noticed that, in general, $\dot{Q}_{ref}$ (expected cooling capacity) increases when t_{Gi} increases. This behaviour was found similar for all values of $\dot{m}_{weak}$.

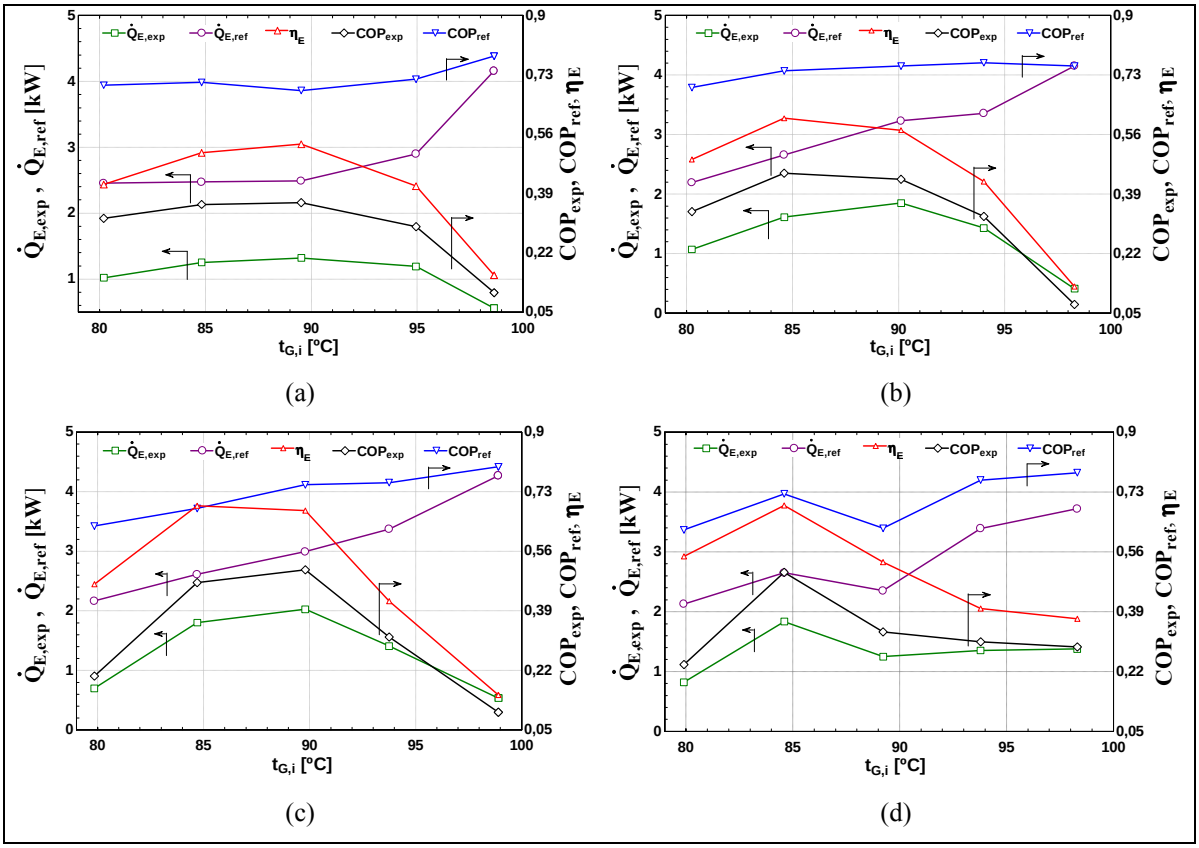

Fig. 4.15. Experimental and expected cooling capacity, evaporators' efficiency and COP vs. t_{Gi}. $\dot{m}_{weak}$ =230 kg/h and RR=(a) 1,5;(b) 1,9; (c) 2.3 and (d) 2,7.

The difference between this ideal value, $\dot{Q}_{E,ref}$, and the one obtained, $\dot{Q}_{E,\exp}$, is a clear evidence of the evaporators performance loss, which is also shown for each case plotted. The average loss in cooling capacity due to overflow obtained for the whole set of experimental points corresponds to 49 %. This low performance is a consequence of the current layout, where the excess of refrigerant is not recirculated to the evaporators and therefore it goes to the solution reservoir inside the absorber. This behaviour is similar to the one in the evaporator of some conventional absorption chillers such as Yazaki WFC-10 (Albers, 2005) under specific operation conditions.

Corresponding values of COP_{ref} and COP_{exp} show the same behaviour described for the cooling capacity. An appreciable difference is observed between expected and experimental values.

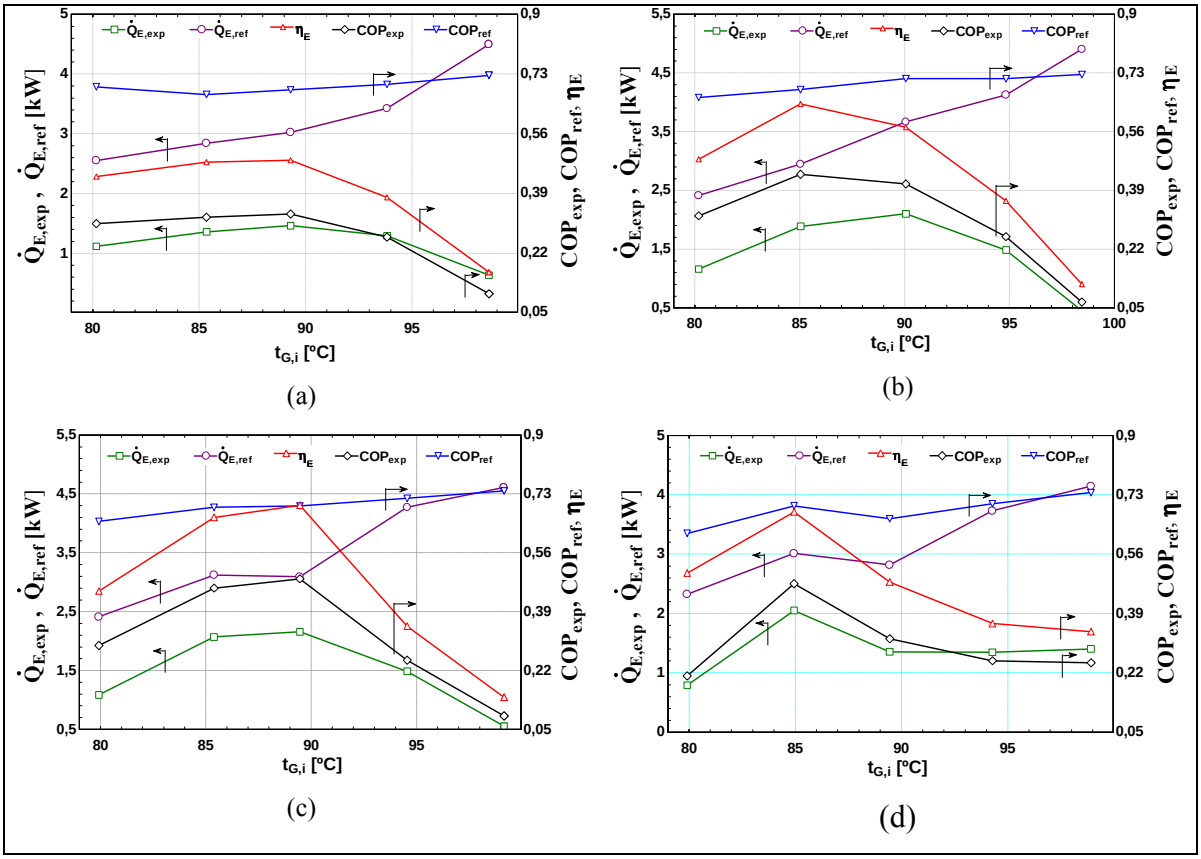

Fig. 4.16. Experimental and expected cooling capacity, evaporators' efficiency and COP vs. t_{Gi}. $\dot{m}_{weak}$ =300 kg/h and RR=(a) 1,5;(b) 1,9; (c) 2.3 and (d) 2,7.

In Fig. 4.17 it can be noticed that experimental cooling power is almost constant over the complete range of $\dot{Q}_{E,ref}$. In most cases, $\dot{Q}_{E,\exp}$ do not reach the expected or maximum value, $\dot{Q}_{E,ref}$.

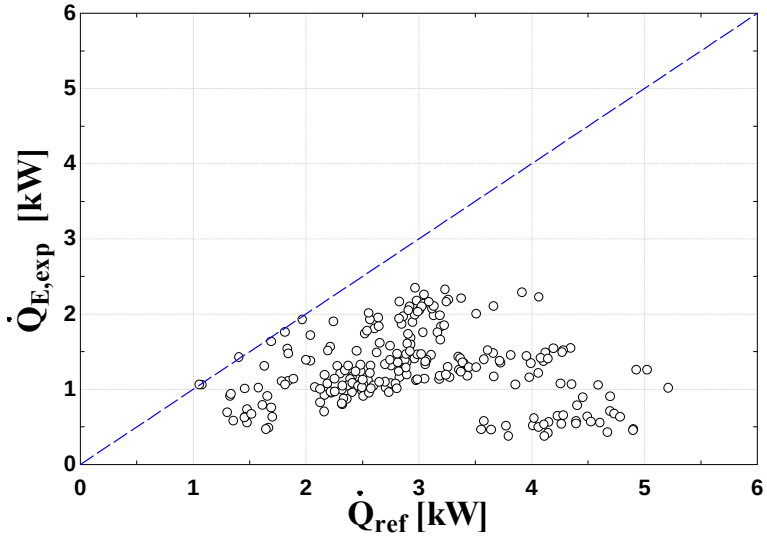

Fig. 4.17. Experimental vs. maximum cooling capacities.

This shows clearly that the drop system used for the spreading of the refrigerant on the fin tubes is not working as expected. Therefore, the spreading system must be improved in order to obtain a cooling capacity closer to the ideal one.

The above mentioned fact (that one of the evaporator runs dry) is noticeable when we observe that the individual cooling capacity, estimated through chilled water temperatures and mass flow rates, is close to cero.

In order to determine the cause for this inadequate operation, the information given by the outlet temperatures of the expansion valves, $T_{V1,o}$, $T_{V2,o}$ (temperature of refrigerant at evaporators inlet), is very useful. Fig. 4.18 illustrates these temperatures for the different experiments carried out. Figs. 4.19 represent the difference between these temperatures corresponding to each evaporator. This is also supported by the refrigerant mass flow rate $\dot{m}_{ref}$ distribution explained before, in which the value of temperatures T_{V1} and T_{V2} plays an important role in the estimation of properties and thermodynamic states, necessary to estimate such distribution. The proximity of T_{V1} and T_{V2} with the outlet condensed refrigerant temperature, $T_{c,o}$ also gives an idea of the path followed by the most quantity of refrigerant, in the case they are uneven. In those cases in which $t_{chw,i}$ and $t_{chw,o}$ are too close, the evaporator is not receiving refrigerant and therefore it is not producing any cooling effect. As example, see cases when $t_{G,i}$ =100ºC for the evaporator 2.

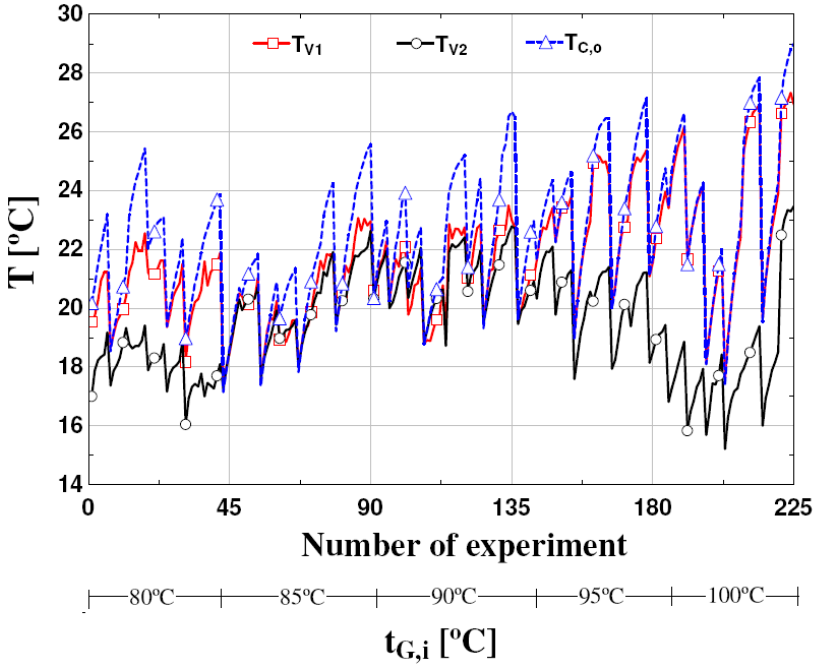

Fig. 4.18. Refrigerant temperatures after the expansion valves for different experiments.

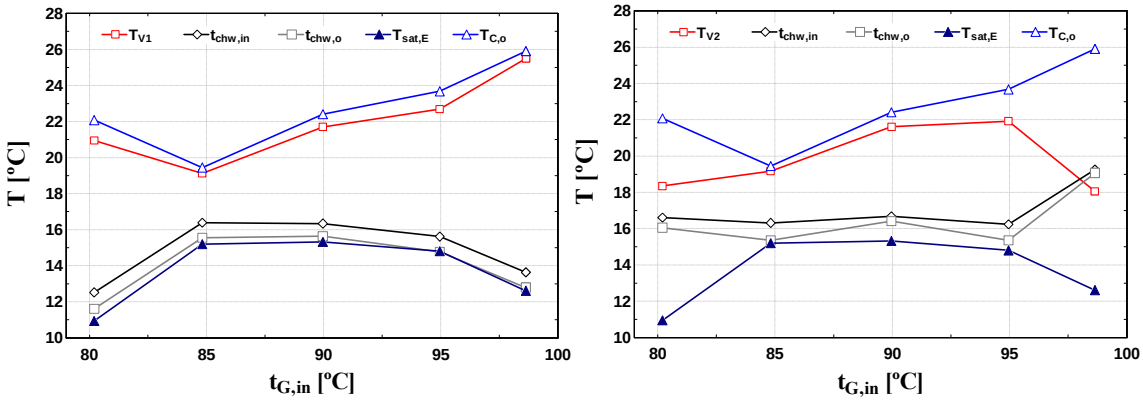

(a)

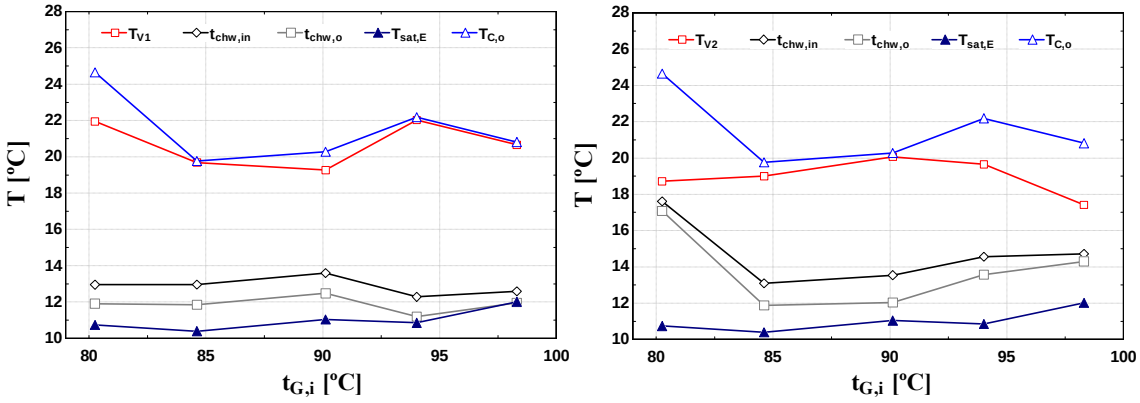

(b)

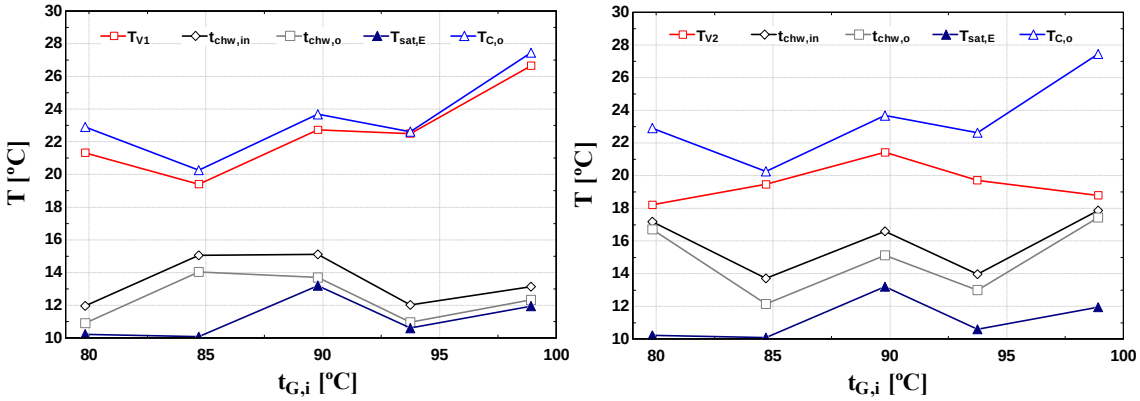

(c)

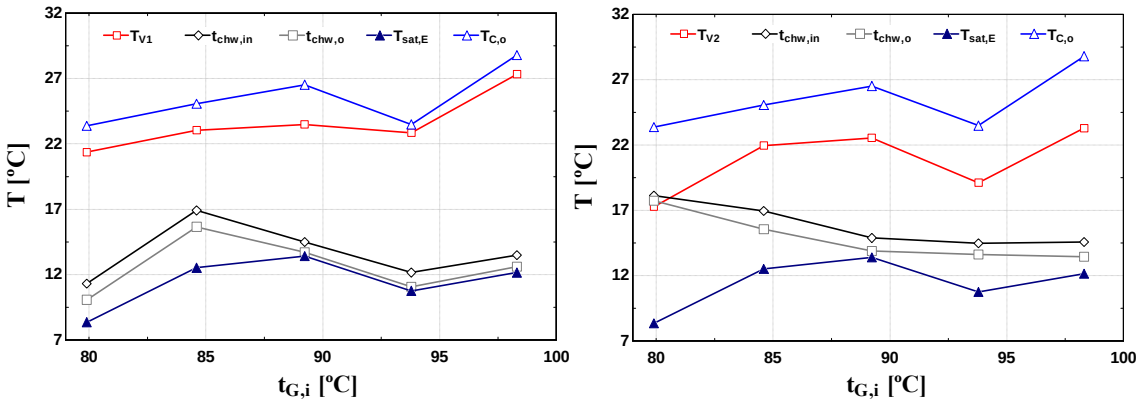

(d)

Fig. 4.19. Temperature of valve, chilled water, saturation and refrigerant at condenser outlet for evaporator 1 (left) and evaporator 2 (right) vs. t_{Gi}. $\dot{m}_{weak}$ =230 kg/h and RR=(a) 1,5;(b) 1,9; (c) 2.3 and (d) 2,7.

4.3.2. Solution heat exchanger

The solution heat exchanger efficiency, η_{she}, is one of the factors that affect greatly the resulting cooling power and COP of the facility. The η_{she} is defined as the ratio of the actual heat transfer to the maximum possible heat transfer for the given inlet conditions (Eq. 4.17).

$$\eta_{she} = \frac{\dot{Q}_{she}}{\dot{Q}_{\max}} \tag{4.17}$$

with

$$\dot{Q}_{she} = \left(\dot{m}c_p\right)_{cold}\left(T_{weak,o} - T_{weak,i}\right) = \left(\dot{m}c_p\right)_{hot}\left(T_{strong,i} - T_{strong,o}\right)$$

$$\dot{Q}_{\max} = \left(\dot{m}c_p\right)_{\min}\left(T_{strong,i} - T_{weak,in}\right) \tag{4.18}$$

Because of the design of the machine under study, the functioning of the strong solution circuit leads to take into account some particular operating conditions in the solution heat exchanger. The pressure drop in this circuit is higher than a conventional machine because of the existence of a Coriolis flow meter and the distribution system of the solution inside the absorber. The existence of a secondary volumetric pump installed in this circuit (see Fig. 3.1) avoids the fact that the strong solution overflows the separator and reaches the condenser. But in some cases, the strong solution side is not completely filled by the strong solution flow rate, as illustrated on Fig. 4.20.

As a consequence of this, the heat transfer process is obviously affected, reducing η_{she}. In order to illustrate this idea, the working temperatures and η_{she} in a sequence of an experiment is shown on Fig. 4.21. Oil temperature in the generator inlet, $t_{G,i}$, is set to 85ºC.

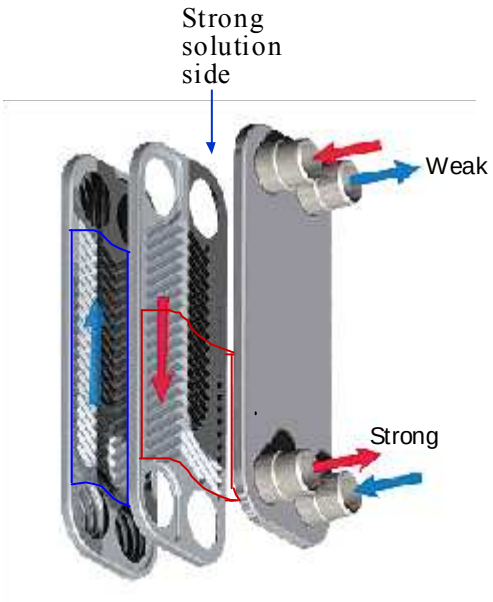

Fig.4.20. Illustration of the incomplete filling up of the strong solution side inside the solution heat exchanger. Source: **www.genemco.com/aloe/plate.html**

The η_{she} decreases abruptly while the outlet temperatures of both strong and weak solution change. In this period, the situation explained above occurred: the strong solution side is not completely filled. In the rest of the experiment, η_{she} keeps over 0.7, just as the working temperatures remain stable.

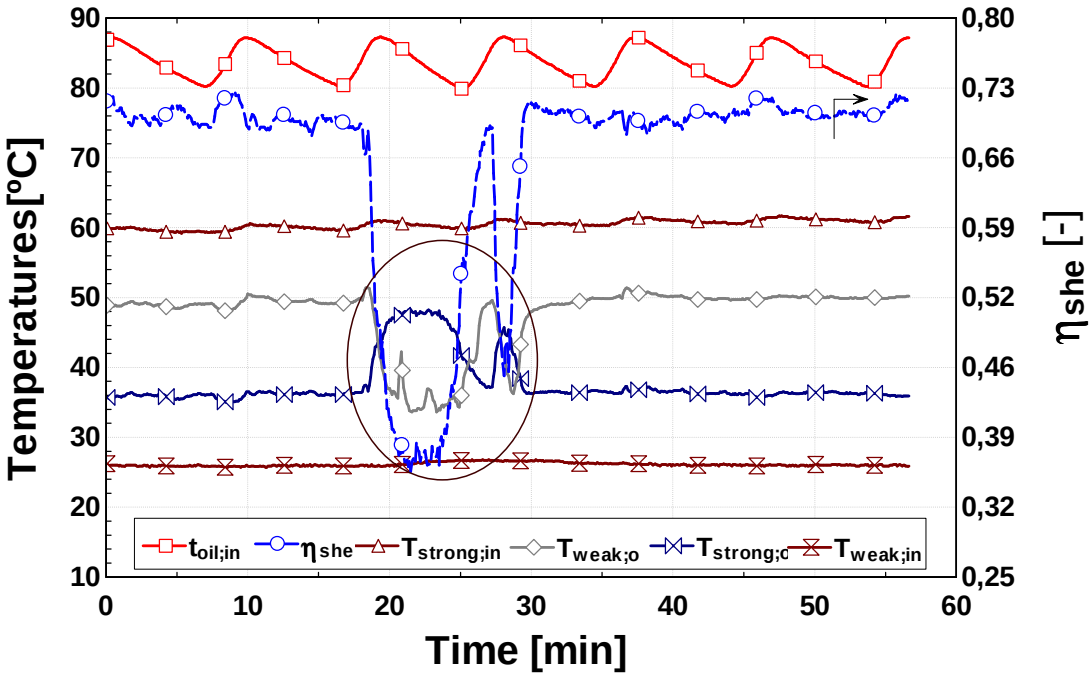

Fig. 4.21. Solution heat exchanger efficiency and working temperatures vs. time during an experimental run. $t_{G,i}$ = 85 ºC.

The effect of η_{she} variation over the corresponding generation power and COP in the same experiment is illustrated on Fig. 4.22. As the heat transfer process inside the PHE is affected, the weak solution temperature (going to the generator) is cooler, the generation heat is higher. Obviously the COP decreases. On the other hand, the strong solution temperature (going to the absorber) is higher, affecting also the absorber performance.

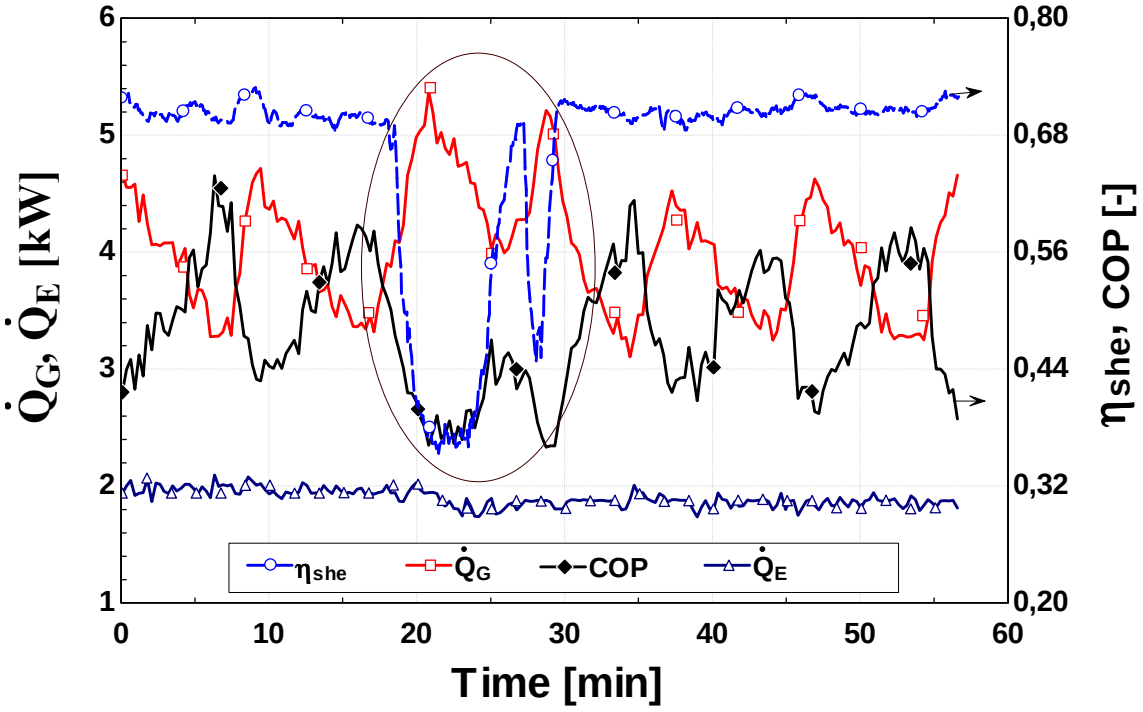

Fig. 4.22. Cooling and generation power (left scale), solution heat exchanger efficiency and COP (right scale) vs. time during an experimental run. $t_{G,i}$ =85 ºC.

Because of the lack of a control system to assure the filling up of the solution heat exchanger, the risk that this difficulty occurs increases when $\dot{m}_{weak}$ is reduced. The strong solution pump continues working at a frequency higher than the necessary to keep this heat exchanger completely filled in that side. This explains the sporadic drop of η_{she} during the test period, in which $\dot{m}_{weak}$ is varied in descending order. Fig. 4.23 shows such sporadic descent of η_{she} for a set of data selected according a common operating condition (RR=1,9).

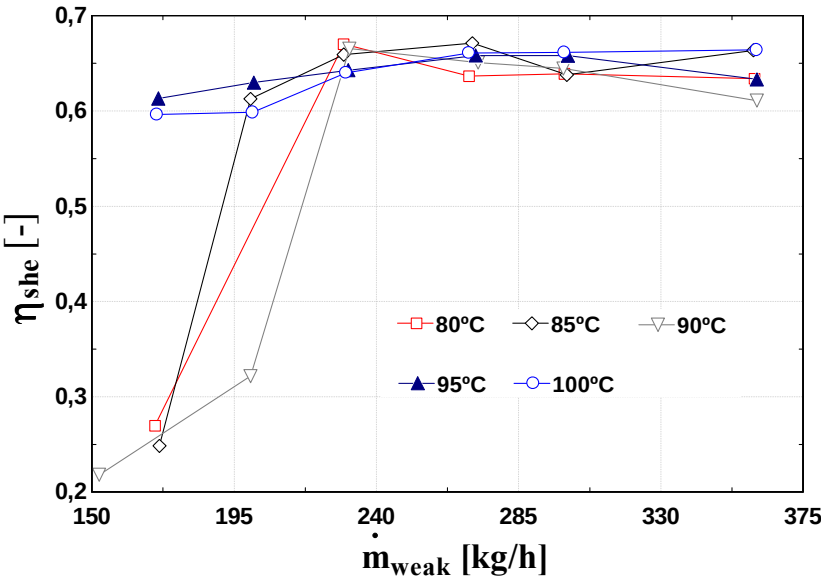

Fig. 4.23. Solution heat exchanger efficiency vs. solution mass flow rate for different external hot fluid temperature. RR is fixed at 1.9.

Each curve represent the η_{she} obtained for different values of $t_{G,i}$. As it is a situation resulting of a deficient filling up of the SHE, the η_{she} drop is not observed for all cases plotted. For example, this occurred when $t_{G,i}$ was 80, 85 and 90 ºC, but did not occur when $t_{G,i}$ was 95 and 100 ºC.

The situation described above must be identified and highlights the necessity of a control system in this kind of machines.

When $t_{G,i}$ is fixed at 95ºC, the resulting behaviour of η_{she} can be appreciated on Fig. 4.24a. Each curve represents different experiments for fixed values of RR, which ranges from 1.5 to 2.7. The change on *RR* does not seem to have a clear influence over η_{SHE}.

The effect of η_{she} over the *COP* is more notable, for a fixed $\dot{m}_{weak}$, considering its effect over the rise in $\dot{Q}_G$ and the corresponding drop of *COP* (Fig. 4.24b and 4.24c). Since the resulting *COP* depends on both cooling and generation powers, the rise in corresponding values of $\dot{Q}_G$ when η_{she} falls is obvious (see cases 1.5, 2.5 and 2.7) and it separates from the normal decreasing tendency with $\dot{m}_{weak}$ reduction.

The same variables are plotted for $t_{G,i}$=85ºC (Fig. 4.25).

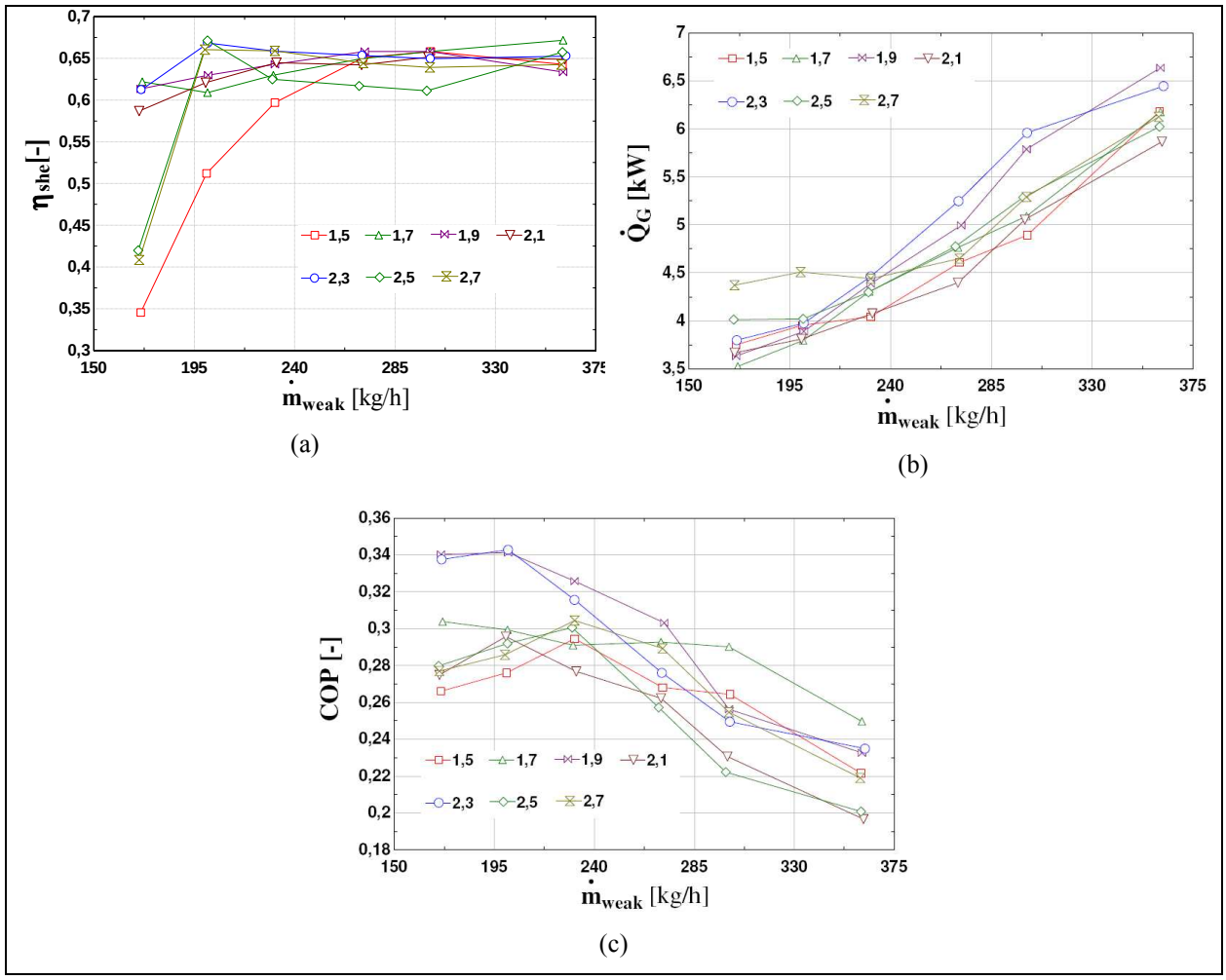

Fig. 4.24. Solution mass flow rate vs. the corresponding : (a) solution heat exchanger efficiency (b) generation power and (c) COP. $t_{G,i}$ is fixed to 95ºC and recirculation radio *RR* is variable.

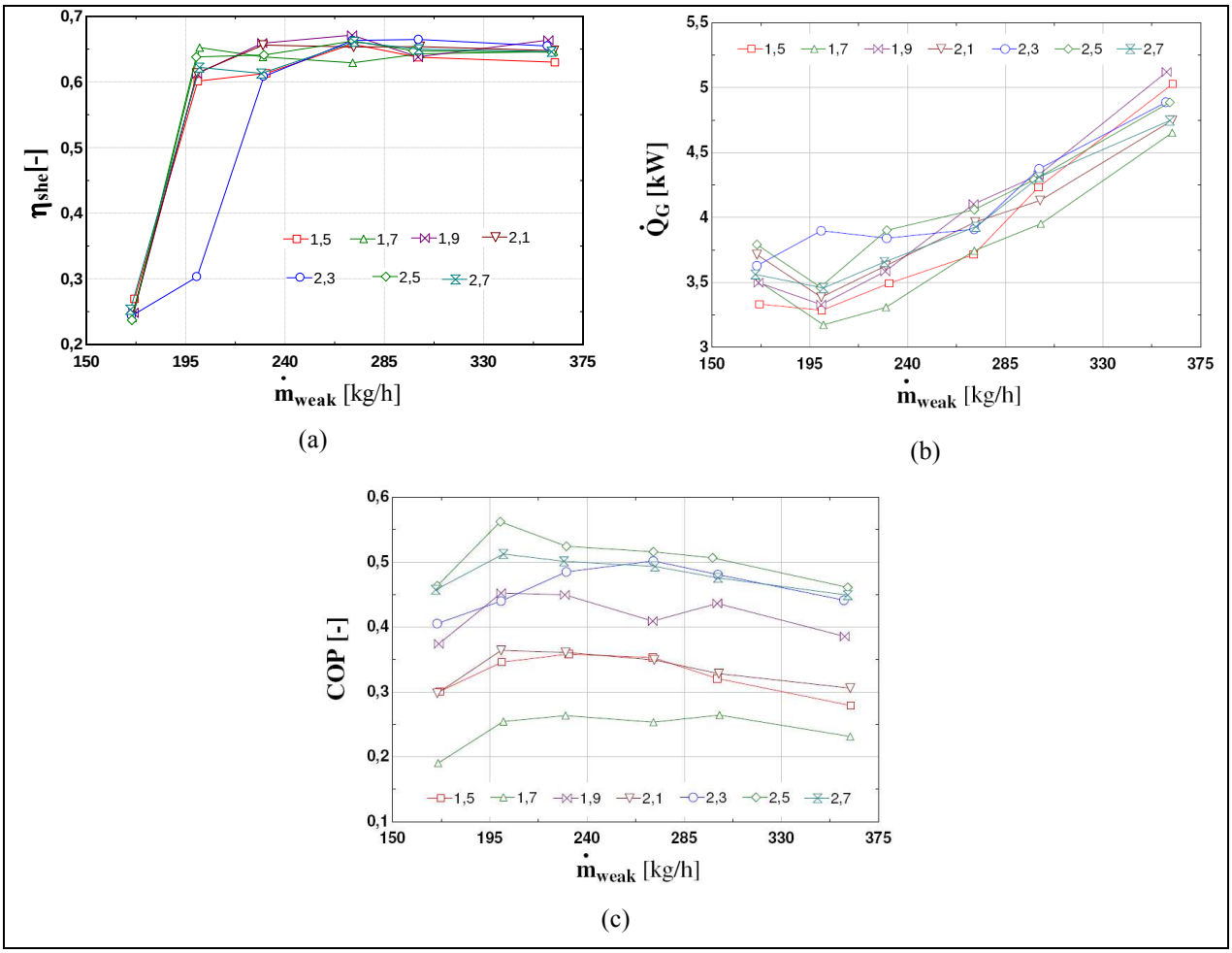

Fig. 4.25. Solution mass flow rate vs. the corresponding: (a) solution heat exchanger efficiency (b) generation power and (c) COP. $t_{G,i}$ is fixed to 85ºC and recirculation radio *RR* is variable.

4.3.3. Machine thermal losses

Convection heat transfer from equipments and pipes walls to the air are considered thermal losses which should be taken into account into the energy balances involved in the performance analysis. The estimation of these thermal losses occurring in the different loops of the experimental facility is presented next.

Thermal losses in pipes, transparent pipes, separator and PHE, forming part of a control volume around generator in the solution loop are grouped as

$$\dot{Q}_{lossG} = \dot{Q}_{loss,P} + \dot{Q}_{loss,TP} + \dot{Q}_{loss,S} + \dot{Q}_{loss,PHE} \tag{4.19}$$

With:

$\dot{Q}_{loss,P}$: Thermal losses in pipes

$\dot{Q}_{loss,TP}$: Thermal losses in transparent pipes

$\dot{Q}_{loss,S}$: Thermal losses in separator

$\dot{Q}_{loss,PHE}$: Thermal losses in plate heat exchanger

The corresponding thermal losses in the hot loop and absorber are called $\dot{Q}_{loss,oil}$ and $\dot{Q}_{lossA}$, respectively.

Evaporators are isolated from radiation heat through a double shell flat metallic plate. Due to the low density of vapour inside the chamber, convection effects were estimated as not significant.

With regard to the condenser, as it is isolated, the thermal losses to ambient are considered not significant as the cooling water and ambient temperature are very close. Besides, the outer surface average temperature will be higher than the cooling water temperature.

In order to estimate the thermal losses of the absorber, separator, pipes and heat exchangers, different correlations found in the literature (Incropera, 1999) for the Nusselt number (Stuart et al., 1975; Cebeci, 1974; Goldstein et al., 1973; Lloyd and Moran, 1974) have been used to evaluate the free convection of external surfaces according to the case, for similar geometries and operating conditions.

The correlations for natural convection outside of the machine walls are based on the Rayleigh number

$$Ra_L = Gr_L \cdot \mathrm{Pr} = \frac{g \cdot \beta \cdot (T_s - T_\infty) \cdot L^3}{\nu^2} \tag{4.20}$$

The empirical correlation that may be applied over the entire range of Ra_L (Incropera, 1999) is

$$\overline{Nu}_{L,D} = \left\{ A_1 + \frac{0.387 \cdot Ra_L^{1/6}}{\left[1 + (A_2 / \mathrm{Pr})^{9/16}\right]^{(8/27)}} \right\}^2 \tag{4.21}$$

With A_1 and A_2 according to Table 4.1. The properties of air, *Pr,* β and ν, are evaluated at a mean value between superficial and ambient temperature.

Geometry	**A_1**	**A_2**
Vertical plate	0,825	0,492
Horizontal long cylinder	0,6	0,559

Table 4.1. Constants values of Eq. (4.21)

Correlations used for vertical plate can also be used for vertical cylinders with height L if the thickness δ of boundary layer is less than the diameter D of the cylinder. This condition is satisfied when $\frac{D}{L} \geq \frac{35}{Gr_L^{1/4}}$ (Incropera, 1999).

For vertical cylinders that do not satisfy this condition, the following correction is used (Cebeci, 1974):

$$\xi = \frac{2\sqrt{2}}{Gr_L^{1/4}} \left(\frac{L}{r_o} \right) \tag{4.22}$$

The deviation of local Nusselt Number of Cylinder from that of a flat plate for various values of Pr is obtained from Fig. 4.26.

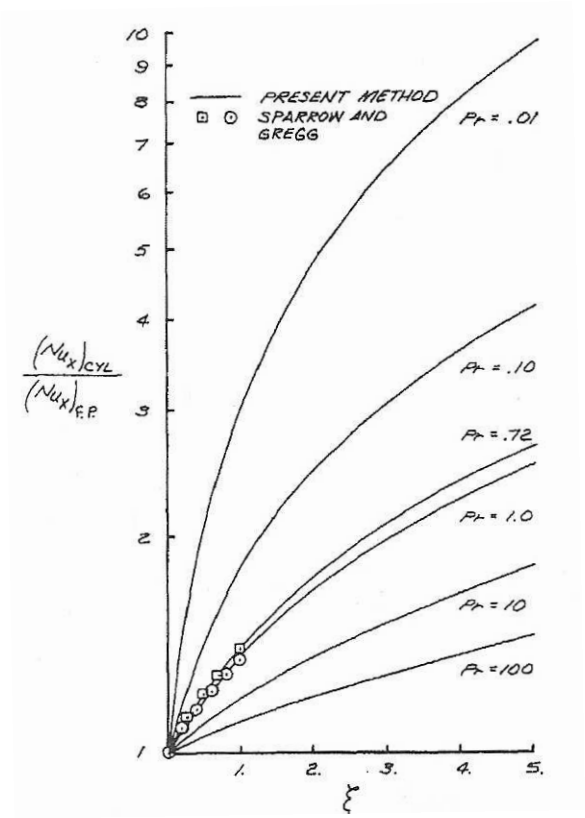

Fig. 4.26. Deviation of local Nusselt number of cylinder from that of a flat plate for various values of Pr. Source: (Cebeci, 1974).

For inclined plates the same Nusselt number correlations, as for vertical plate, can be used if g is replaced by $g \cdot \cos\theta$.

For horizontal plates, the following correlations were used for upper surface of heated plate or lower surface of cooled plate (Incropera, 1999).

$$\overline{Nu}_L = 0{,}54 \cdot Ra_L^{1/4} \qquad \left(10^4 \le Ra \le 10^7\right) \tag{4.23}$$

$$\overline{Nu}_L = 0{,}15 \cdot Ra_L^{1/3} \qquad \left(10^7 \le Ra \le 10^{11}\right) \tag{4.24}$$

and for lower surface of heated plate or upper surface of cooled plate

$$\overline{Nu}_L = 0{,}27 \cdot Ra_L^{1/4} \qquad \left(10^5 \le Ra \le 10^{10}\right) \tag{4.25}$$

The components isolated for the first experimental campaign were the generator, separator and condenser. An elastomeric foam (Fig. 4.27) with 30 mm thickness and k=0.038 W/mK, was used as thermal insulation material.

Fig. 4.27 Thermal isolation used: Elastomeric foam. Source: http://www.armacell.com

For those components isolated, thermal losses are estimated as follows:

$$\dot{Q}_{loss,i} = U_{loss,i} \cdot A_i \cdot \Delta T\,, \qquad \Delta T = T_{\sup} - T_{amb} \tag{4.26}$$

$$U_{loss,i} = \frac{1}{R_{cond} + R_{ins} + R_{conv}}; R_{cond} = \frac{e_m}{k_m}; R_{ins} = \frac{e_{ins}}{k_{ins}} \tag{4.27}$$

Where R_{cond} and R_{ins} are thermal resistances corresponding to conduction through wall and insulator material, respectively.

Results

Table 4.2 summarised the range of convective heat transfer of external surfaces analyzed.

Component	$\dot{Q}_{loss,i}$ **[W]**
Connexion tube SHE-Generator	4-17
Horizontal transparent pipes	9-14
Vertical transparent pipe	3-5
Oil pipes and tank	215-350
Absorber	70-245
Generator	11-18
Solution heat exchanger	2-8
Subcooler	1-4

Table 4.2. Thermal losses to environment from different components.

Thermal losses in the control volume of generator, $\dot{Q}_{lossG}$, represent as average value 8% of $\dot{Q}_G$. For the case of the absorber, $\dot{Q}_{lossA}$, is 5% of thermal power of subcooler. In the last case, that percentage represents a contribution to the operation of the subcooler, i.e., a spontaneous evacuation of heat that must be extracted from the solution in that component.

The relation between the controlled inlet oil temperature, t_{Gi}, and $\dot{Q}_{lossG}$ is illustrated in Fig. 4.28. In spite of the variation of other parameters ($\dot{m}_{weak}$ and RR) that causes the scattering of data, it is observed the obvious increasing tendency in both the external and internal circuits when t_{Gi} increases. Obviously, energy losses in hot external circuit, $\dot{Q}_{loss,oil}$, are higher than those in internal circuit due to the higher oil temperature and total area of the pipes exposed to ambient.

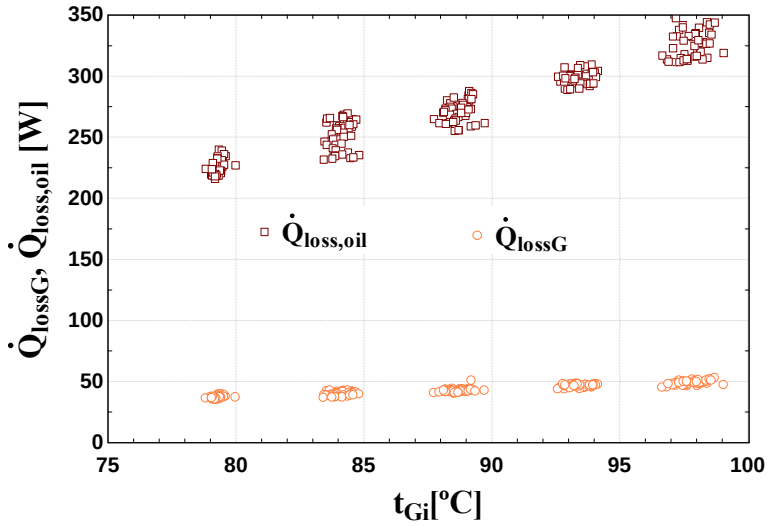

Fig. 4.28. Thermal losses of internal and external fluid in the generator

Thermal losses in the absorber, $\dot{Q}_{lossA}$, is a consequence of the wetting of the walls, where an absorption process takes place evacuating heat through the walls. According to this, as solution reservoir located at the end of absorber is heated from walls by radiation and conduction heat transfer, the absorber pressure also increases during the test process. $\dot{Q}_{lossA}$ is affected by both generation temperature and recirculated mass flow rate, $\dot{m}_r$.

Fig. 4.29 shows $\dot{Q}_{lossA}$ vs. $\dot{m}_r$ for different operating conditions (RR=1.5, 1.9, 2.1 and 2.5). In this case, the effect of $t_{G,i}$ over the thermal losses is not as obvious as the previous case, but in general, $\dot{Q}_{lossA}$ tends to increase when $t_{G,i}$ increases. The influence of $\dot{m}_r$ is clear in most cases: when $\dot{m}_r$ is increased, $\dot{Q}_{lossA}$ decreases as a results of the cooling effect of $\dot{m}_r$ inside the absorber.

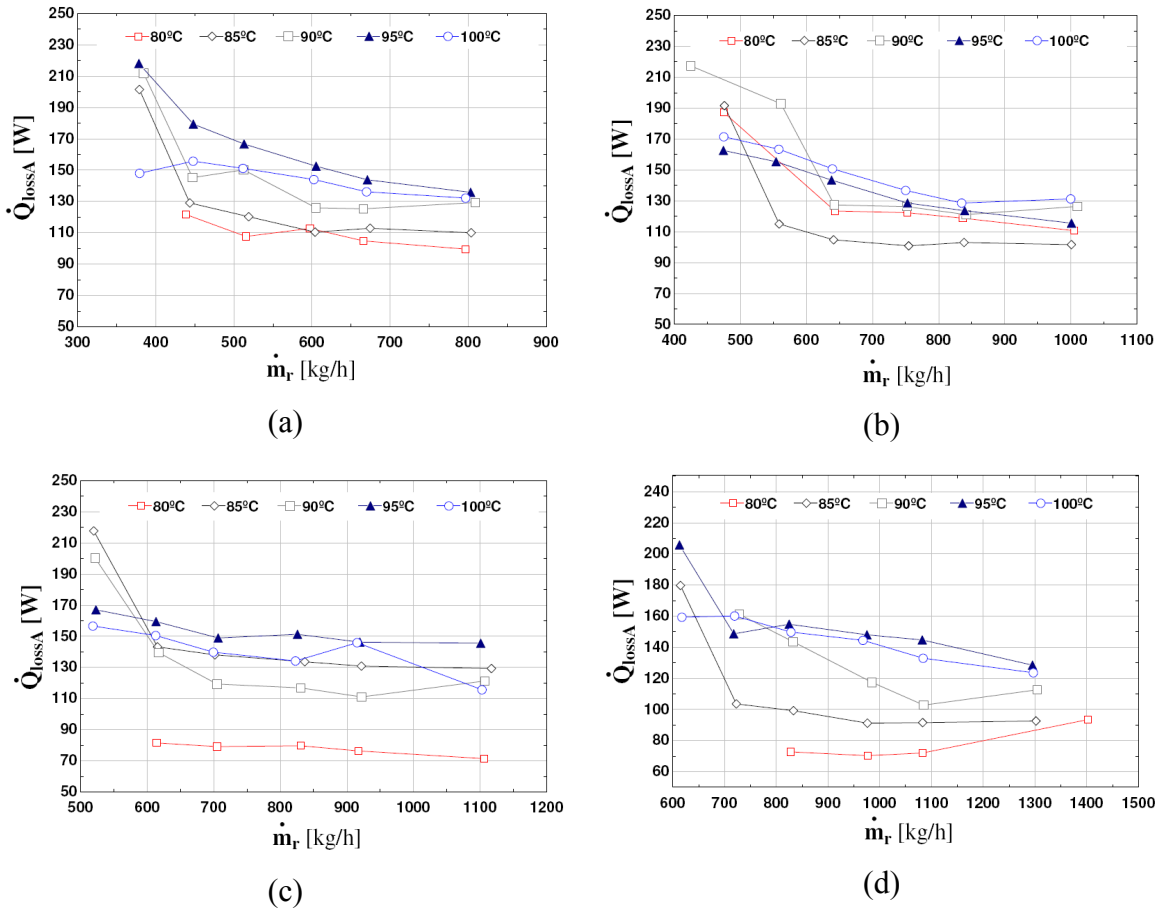

Fig. 4.29. Thermal losses of absorber vs. recirculated mass flow rate for different $t_{G,i}$. RR is fixed to (a) 1.5, (b) 1.9, (c) 2.1, (d) 2.5.

The results of the estimation of thermal losses will be used in subsequent calculation.

4.3.4. Temperature difference in the strong solution route

A noticeable difference was identified between solution temperature at generator outlet and separator outlet (points 1 and 3 in Fig. 4.30).

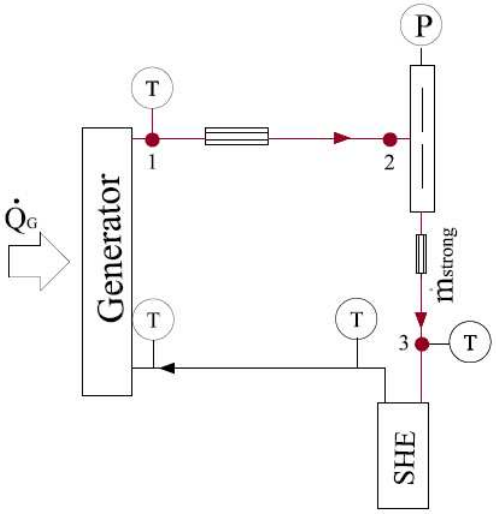

Fig. 4.30. Control volume on generator - separator in strong solution circuit

Fig 4.31 illustrates such difference in temperatures, for two different $t_{G,i}$ vs. solution mass flow rate, for a fixed RR. The temperature drop associated for all points tested, ranges from 4ºC to 10ºC, depending on controlled parameters.

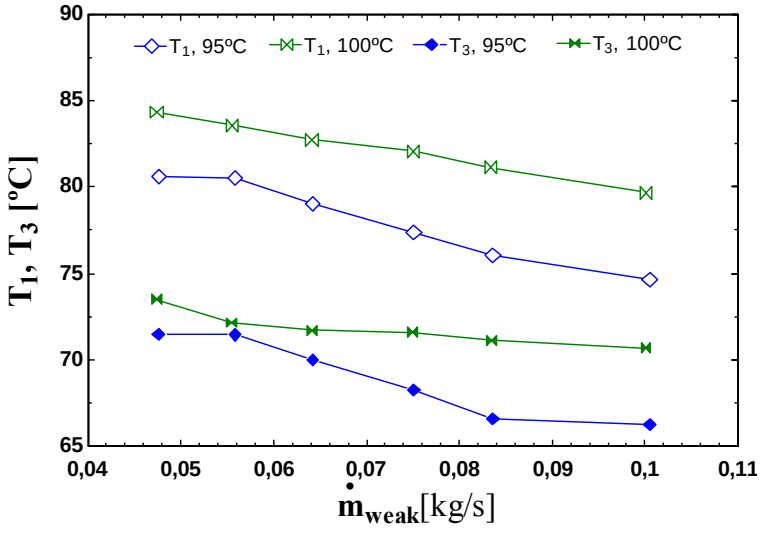

Fig. 4.31. Solution temperature at generator outlet and separator outlet vs. $\dot{m}_{weak}$ for two $t_{G,i}$ values and RR=2.3.

The thermal power associated to this difference is given by

$$\dot{Q}_{1-3} = \dot{m}_{strong} \cdot (h_1 - h_3) \tag{4.28}$$

Thermal losses calculation in pipes, transparent pipes and separator allowed checking that heat transfer thermal losses $\dot{Q}_{lossG}$ were not causing such difference. Fig. 4.32 allows observing that $\dot{Q}_{1-3} >> \dot{Q}_{lossG}$, compared to results showed on Fig. 4.28. The dependence with temperature is clear in both cases. The variation of solution mass flow rate affects proportionally to heat transfer losses, $\dot{Q}_{1-3}$. The great difference between $\dot{Q}_{1-3}$ and $\dot{Q}_{lossG}$ is at least one order of magnitude.

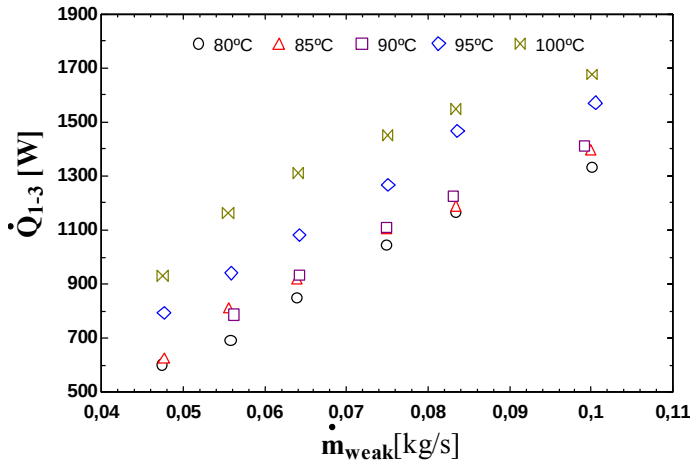

Fig. 4.32 . Thermal power associated to temperature difference between solution temperature at generator outlet and separator outlet against solution mass flow rate for different $t_{G,i}$. RR is fixed at 2.3.

Therefore, the cause of the difference in temperatures along the strong solution path can be explained because the solution was still boiling at the exit of generator. Consequently, the refrigerant separation kept on in the path followed by the solution, as shown schematically on Fig. 4.33 between points 1 and 2. This was observed during experiments through the transparent pipe, located at the exit of generator.

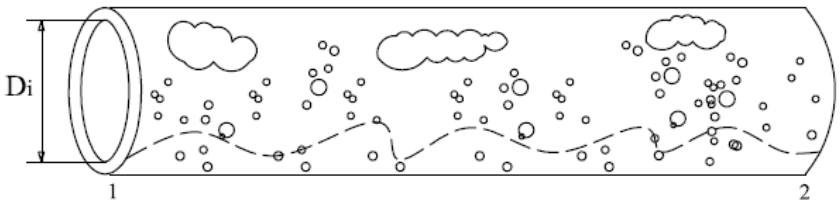

Fig. 4.33. Solution flow inside the connexion pipe from generator to separator

The above statement entails solving the following Eq. system in order to find the values of X_1, h_1, $\dot{m}_{strong,1}$, $\dot{m}_{ref,1}$ and $\dot{m}_{ref,1-3}$:

Considering the thermal losses, the energy balance in the generator yields

$$\dot{Q}_{G,\exp} = \dot{m}_{ref,1} \cdot h_{1,vapor} + h_1 \cdot \dot{m}_{strong,1} - \dot{m}_{weak} \cdot h_{weak,G} + \dot{Q}_{loss,G} \tag{4.29}$$

With $\dot{Q}_{G,\exp}$ from Eq. (4.2)

$$h_1 = h_{LiBr}(T_1, X_1) \tag{4.30}$$

The mass balance in the generator yields,

$$\dot{m}_{strong,1} = \dot{m}_{weak} - \dot{m}_{ref,1} \tag{4.31}$$

$$\dot{m}_{strong,1} \cdot X_1 = \dot{m}_{weak} \cdot X_{weak} \tag{4.32}$$

The enthalpy and concentration at the exit of generator can then be obtained.

Eq. (4.28) would be rewritten as:

$$\dot{Q}_{1-3} = \dot{m}_{strong,1} \cdot h_1 - \dot{m}_{strong} \cdot h_3 \tag{4.33}$$

And taking into account the vapour separation between points 1 and 3 (Fig. 4.30),

$$\dot{Q}_{1-3} = \dot{m}_{ref,1-3} \cdot h_{fg} \tag{4.34}$$

The total refrigerant mass flow rate produced will be

$$\dot{m}_{ref} = \dot{m}_{ref,1} + \dot{m}_{ref,1-3} \tag{4.35}$$

In order to verify the contribution of pressure drop to the temperature difference between 1 and 3:

$$P_1 = P_{LiBr}(T_1, X_1) \tag{4.36}$$

$$\Delta P_{1-2} = P_1 - P_{high} \tag{4.37}$$

As both P_{high} and inlet pressure to condenser, $P_{C,i}$, are measured experimentally, ΔP_{2-C} can be used as a reference value:

$$\Delta P_{2-C} = P_{high} - P_{C,i} \tag{4.38}$$

Results obtained from Eq. (4.37) for ΔP_{1-2} , illustrated in Fig. 4.34, are the same order of magnitude, although higher, as those obtained between P_{high} and $P_{C,i}$ (ΔP_{2-C}). The average value of ΔP_{1-2} is 6.3 mbar. Such value of pressure drop in the connexion tube is not enough to cause the temperature drops shown on Fig. 4.31. As the solution is still boiling while refrigerant is separated, the pressure drop along 1 and 3 ΔP_{1-3} is also calculated assuming saturated conditions.

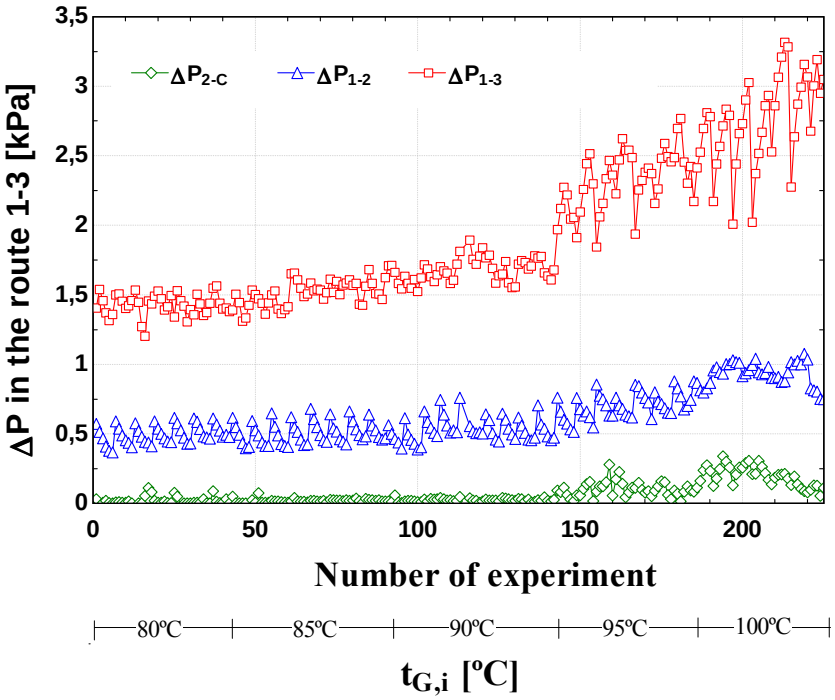

Fig.4.34. Pressure drop in connexion tube generator-separator for different experiments.

This pressure drop ranged from 15 to 33 mbar, according to variations in controlled oil temperature and $\dot{m}_{weak}$ as is illustrated on Fig. 4.35.

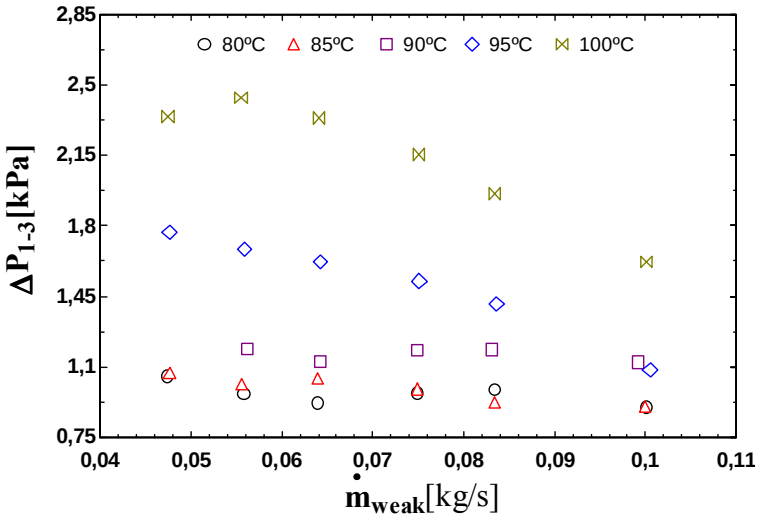

Fig. 4.35. Pressure drop between generator outlet and separator outlet vs. $\dot{m}_{weak}$ for various $t_{G,i}$ and RR=2,3.

The change in solution enthalpy between points 1 and 3 is not qualified as losses, because it generates an additional amount of steam. These results have been considered in the performance analysis.

4.4. The basic absorption model and comparison with experimental results

A basic thermodynamic model including the particular features in both design and operation of the facility analyzed is presented. Performance parameters, cooling capacity and *COP*, are expressed in terms of an ideal absorption model and compared with experimental results. The differences observed between ideal and experimental results help to validate the influence of components performances on the overall performance of the facility.

4.4.1. The basic absorption model

Fig. 4.36 represents the thermodynamic states of the ideal simple effect absorption cycle, assuming mechanical, thermal and chemical equilibrium and assuming mechanical degradation exclusively concentrated on expansion valves. Steady state mass and energy balance in components yield the following equations:

Evaporator:

$$\dot{Q}_{E,id} = \dot{m}_{ref,id} \cdot (h_2 - h_1); \quad h_1 = h_{10} \tag{4.39}$$

Considering $$\frac{\dot{m}_{ref,id}}{\dot{m}_{weak}} = \frac{X_{strong} - X_{weak}}{X_{strong}} \tag{4.40}$$

$$\dot{q}_{E,id} = \frac{\dot{Q}_{E,id}}{\dot{m}_{weak}} = \frac{X_{strong} - X_{weak}}{X_{strong}} \cdot (h_2 - h_1) \tag{4.41}$$

Generator:

Mass balance:

$$\dot{m}_{weak} = \dot{m}_{strong} + \dot{m}_{ref,id} \tag{4.42}$$

Energy balance:

$$\dot{Q}_{G,id} = \dot{m}_{strong} \cdot h_6 - \dot{m}_{weak} \cdot h_5 + \dot{m}_{ref,id} \cdot h_9; \; T_9 = T_6 \tag{4.43}$$

From (4.42): $$\frac{\dot{m}_{strong}}{\dot{m}_{weak}} = 1 - \frac{X_{strong} - X_{weak}}{X_{strong}} \tag{4.44}$$

$$\dot{q}_{G,id} = \frac{\dot{Q}_{Gi}}{\dot{m}_{weak}} = \left(1 - \frac{X_{strong} - X_{weak}}{X_{strong}}\right) \cdot h_6 - h_5 + \frac{X_{strong} - X_{weak}}{X_{strong}} \cdot h_9 \tag{4.45}$$

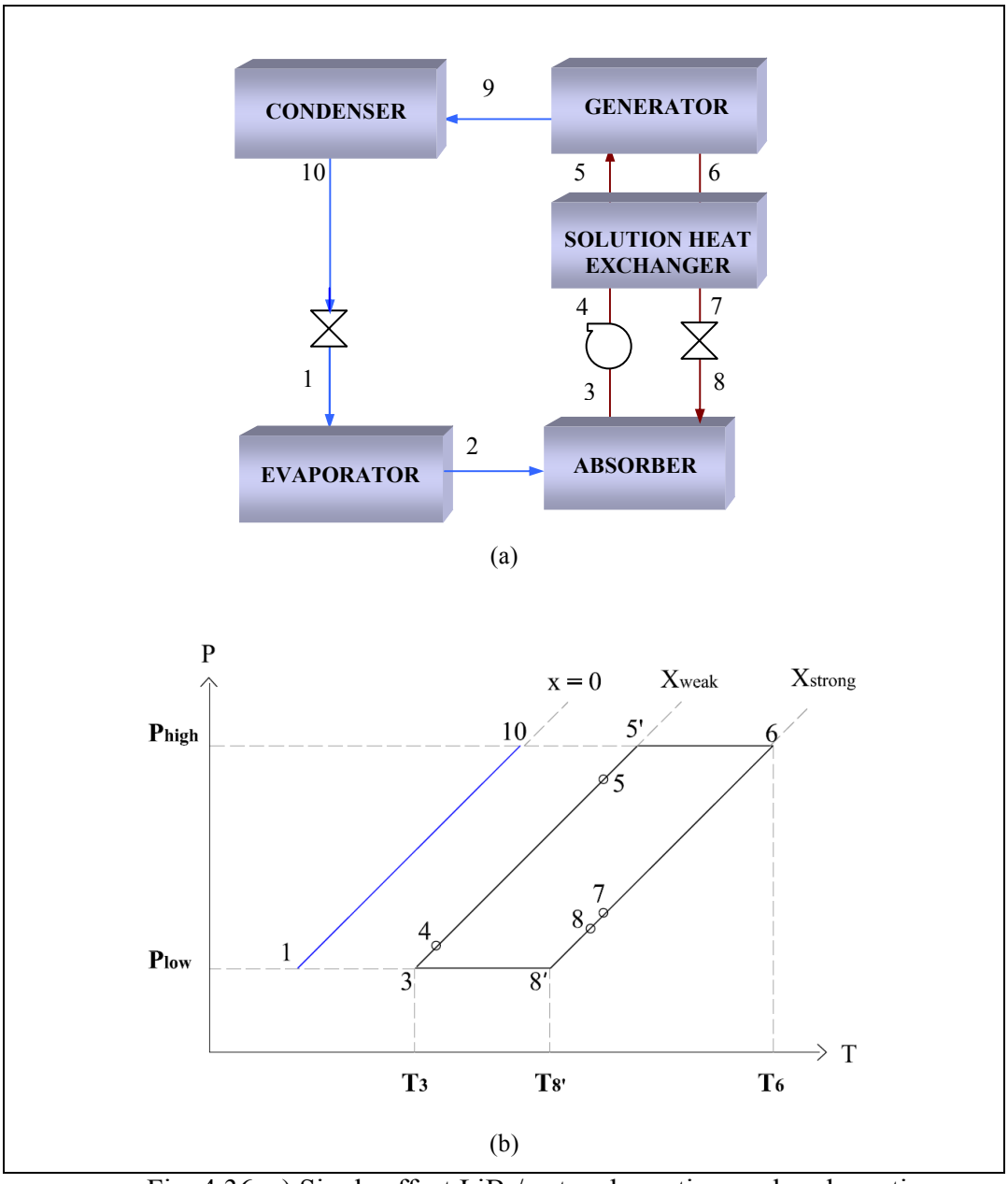

Fig. 4.36. a) Single effect LiBr/water absorption cycle schematic.
b) Diagram P(T)- T LiBr/water

Solution heat exchanger:

$$\eta_{she,id} = \frac{T_5 - T_3}{T_{5'} - T_3} = \frac{T_6 - T_8}{T_6 - T_{8'}} \tag{4.46}$$

$$\dot{Q}_{she,i} = \dot{m}_{weak} \cdot (h_5 - h_4) = \dot{m}_{strong} \cdot (h_6 - h_7) \tag{4.47}$$

$$h_4 - h_3 = w_{pi} \tag{4.48}$$

$$h_7 = h_8, \qquad h_5 - (h_3 + w_{pi}) = \left(1 - \frac{X_{strong} - X_{weak}}{X_{strong}}\right) \cdot (h_6 - h_8) \tag{4.49}$$

Assuming $\eta_{hex,i} = 1$, then $h_8 = h_{8'}$ (4.50)

$$\dot{q}_{she,id} = \left(1 - \frac{X_{strong} - X_{weak}}{X_{strong}}\right) \cdot (h_6 - h_8) \tag{4.51}$$

$$COP_{id} = \frac{\dot{Q}_{E,id}}{\dot{Q}_{G,id}} = \frac{\dot{q}_{E,id}}{\dot{q}_{G,id}} = \frac{\dfrac{X_{strong} - X_{weak}}{X_{strong}} \cdot (h_2 - h_1)}{\left(1 - \dfrac{X_{strong} - X_{weak}}{X_{strong}}\right) \cdot h_6 - h_5 + \dfrac{X_{strong} - X_{weak}}{X_{strong}} \cdot h_9} \tag{4.52}$$

The above expressions will be used next as a reference to evaluate the performance of the absorption facility.

4.4.2. Experimental performance parameters

Corresponding values per unit mass flow rate of experimental cooling capacity and *COP* are:

$$\dot{q}_{E,\exp} = \frac{\dot{Q}_{E,\exp}}{\dot{m}_{weak}} \tag{4.53}$$

$$\dot{q}_{G,\exp} = \frac{\dot{Q}_{G,\exp}}{\dot{m}_{weak}} \tag{4.54}$$

Then, the coefficient of performance is obtained:

$$COP_{\exp} = \frac{\dot{Q}_{E,\exp}}{\dot{Q}_{G,\exp}} = \frac{\dot{q}_{E,\exp}}{\dot{q}_{G,\exp}} \tag{4.55}$$

4.4.3. Results

4.4.3.1. Basic absorption model vs. Experimental results.

Fig. 4.37 and 4.38 illustrate the comparison of experimental performance parameters with those obtained through the basic model, Eqs. (4.41) and (4.52), for 280 test points. The dispersion observed in results corresponds both to the actual dispersion of $t_{G,i}$ and to the influence of other operating variables which vary according each test condition. The differences observed help identifying the influence of components performance, serving as a diagnosis. This influence is validated in the following section, according the analysis presented previously.

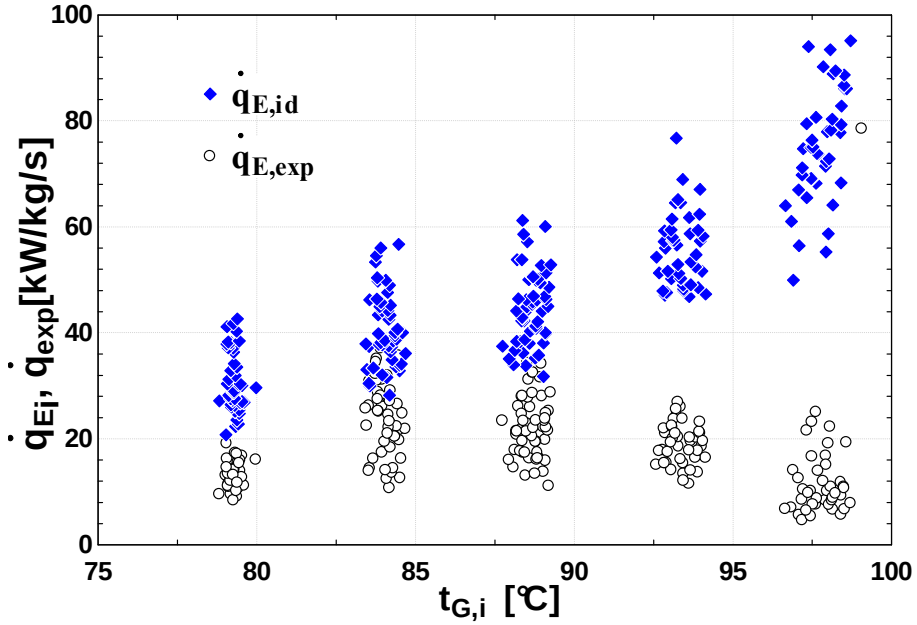

Fig. 4.37. Comparison of basic model and experimental results: Ideal and experimental cooling capacity vs. t_{Gi}

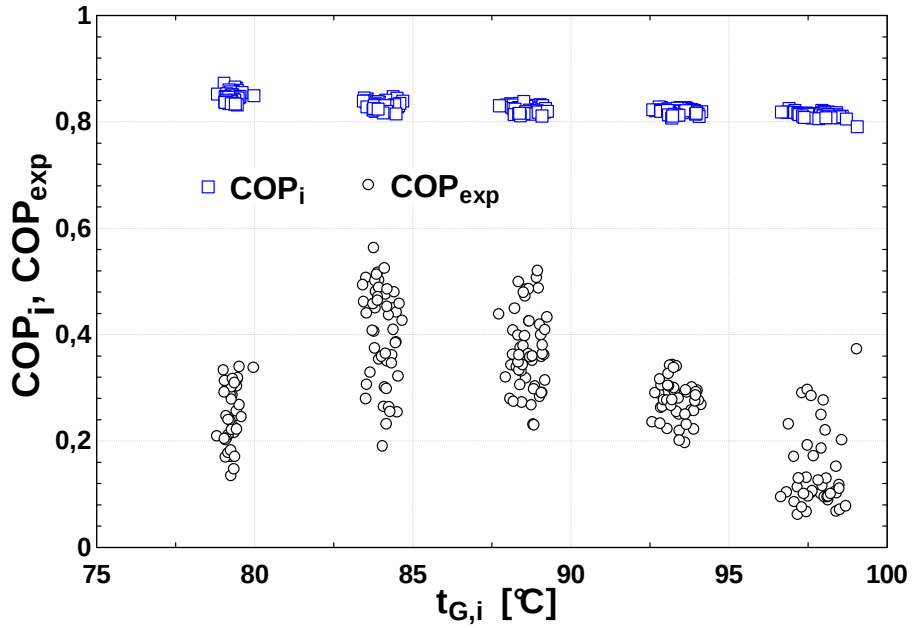

Fig. 4.38. Comparison of basic model and experimental results: Ideal and. experimental *COP* vs. t_{Gi}

4.4.3.2. Influence of components performance. Modified basic model.

The evaporators in this facility layout show low performance (see section 4.3.1). The obtained average η_E is 50%, which is considerably low. Taking into account the evaporators limitations explained above, the modified cooling capacity will be:

$$\dot{q}_{E,\mathrm{mod}} = \dot{q}_{Ei} \cdot \eta_E \tag{4.56}$$

The facility performance is also affected by the solution heat exchanger efficiency η_{she} and consequently it is considered in the analysis. Beside this, thermal losses and the thermal power associated to the temperature difference in the strong solution circuit $\dot{Q}_{1-3}$ (section 4.3.4) are also taken into account, named $\dot{q}_{G-sep}$.

Then, considering the real efficiency of the solution heat exchanger and the thermal power in the system generator-separator, the modified generation power will be:

$$\dot{q}_{G,\mathrm{mod}} = \dot{q}_{G,i} + \dot{q}_{she,i}\left(1-\eta_{she}\right) + \dot{q}_{G-sep} \tag{4.57}$$

As a result, the modified *COP* becomes:

$$COP_{\text{mod}} = \frac{\dot{q}_{E,\text{mod}}}{\dot{q}_{G,\text{mod}}} \tag{4.58}$$

Results obtained incorporating the specific behaviour of components to the basic model can be appreciated in Figs. 4.39 and 4.40. The predicted cooling capacity globally shows a good agreement with experimental results.

This indicates that the main causes of deviation have been included in the model, thus verifying the preliminary diagnosis.

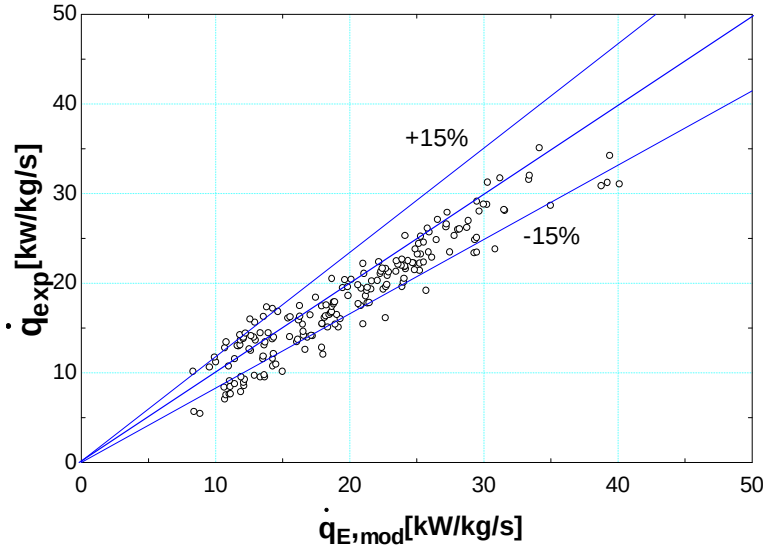

Fig. 4.39. Comparison of modified basic model and experimental results for cooling capacity per unit mass flow

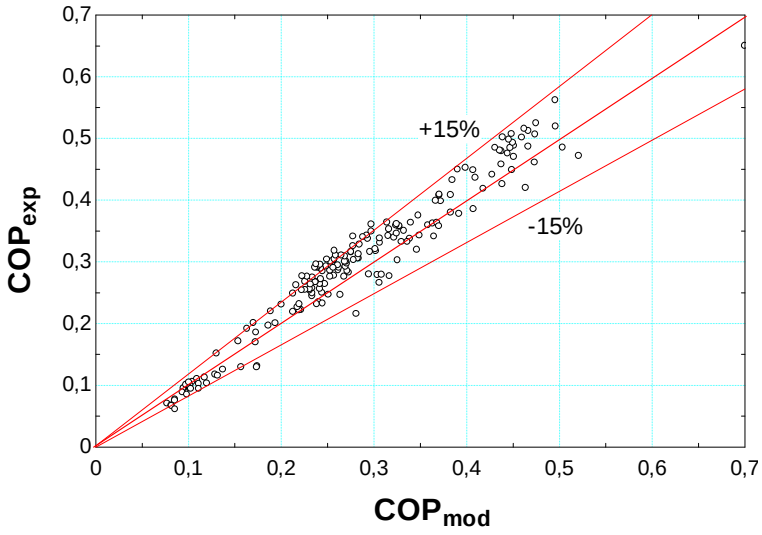

Fig. 4.40. Comparison of modified basic model and experimental results for COP

The differences observed between ideal and experimental results helped to identify the influence of components performances on the overall performance of the facility. The evaluation of the ideal and real cooling powers allowed validating a low performance of evaporators caused by both dry operation and overflow. Another influence factors which causes the deviation from ideal behaviour are the solution heat exchanger efficiency and the thermal power associated in the system generator-separator.

Taking into account the particular layout and operation features tested, a good agreement with experimental performance parameters and those obtained through a modified basic absorption model has been achieved. This model incorporates a quantified loss and/or efficiency separating from ideal and has been fitted to experimental data. However, there are systematic differences between the modified basic model and the experimental results (especially results for COP) that are attributable to the limited capacity of the simple model to describe an adiabatic absorption machine. In addition, for machines design and control purposes, a model that depends on few parameters is necessary.

Experimental results demonstrate the operational possibilities and flexibility of the design, showing a great potential in preliminary dimensioning calculations.

4.5. Conclusions

- Results of the preliminary analysis show the effect of controlled oil temperature at the inlet to generator, t_{set}, and solution mass flow rate $\dot{m}_{weak}$ on the cooling power and the instantaneous *COP*. A maximum value of both parameters was observed for a given t_{set} and $\dot{m}_{weak}$. The source of this maximum point is initially identified as the lack of performance of evaporators, and the effects of irreversibilities when increasing t_{set} on the *COP*. A detailed components performance analysis was conducted later in order to explain their effects on the overall performance obtained.

- An analysis of the evaporators system was developed with the aim to estimate their efficiency η_E and the quantity of refrigerant mass flow rate received by each evaporator. It has been detected that the distribution of $\dot{m}_{ref}$ is not symmetrical in some cases, leading to a partial or defective functioning of one evaporator. This explains why the cooling capacity slopes down when it is supposed to have an increasing tendency. The average η_E obtained for the totality of experimental points was 50%. This low performance is a consequence of being unable to evaporate all the condensed water. Liquid accumulation leads to overflow of refrigerant out of the evaporators. This shows clearly that the drop system used for the spreading of the refrigerant on the fin tubes is not working as expected and it must be improved in order to obtain a cooling capacity closer to the ideal one.

- The poor filling of the plate heat exchanger makes the η_{she} to decrease abruptly while the outlet temperatures of both strong and weak solution change because of this situation. The heat transfer process is obviously affected, reducing η_{she} and therefore reducing the *COP* of the machine. The situation described above must be identified and highlights the necessity of a control system in this kind of machines.

- Convection heat transfer from equipments and pipes walls to the air, were estimated. Thermal losses in the control volume of generator, $\dot{Q}_{lossG}$, represent as average value 8% of $\dot{Q}_G$. For the case of the absorber, $\dot{Q}_{lossA}$, is 5% of thermal power of subcooler,

being this case favourable for the operation of the subcooler. A general increasing tendency of thermal losses in the hot and solution loops was observed when inlet oil temperature increases. The increase in recirculated solution mass flow rate contributes to decrease $\dot{Q}_{lossA}$.

- It was verified that the energy associated to the difference between solution temperature at generator outlet and separator outlet was not caused by thermal losses to the environment nor pressure drop in the connection tube. Therefore, the cause of the difference in temperatures along the strong solution path can be explained because the solution was still boiling at the exit of generator. Consequently, the refrigerant separation kept on in the path followed by the solution.

- A basic thermodynamic model including the particular features in both design and operation of the facility analyzed was presented. Performance parameters are expressed in terms of an ideal absorption model and compared with experimental results. The differences observed between ideal and experimental results help to validate the influence of components performances on the overall performance of the facility. A good agreement with experimental performance parameters and those obtained through a modified basic absorption model has been achieved. However, there are systematic differences between such modified basic model and the experimental results, which are attributable to the limited capacity of this simple model to describe an adiabatic absorption machine. Therefore, for machines design and control purposes, a model that depends on few parameters is necessary. Next chapter deal with this point, where models that take into account these peculiarities are proposed.

- Experimental results demonstrate the operational possibilities and flexibility of the design, showing a great potential in preliminary dimensioning calculations.

Chapter 5

EXTENSION OF CHARACTERISTIC EQUATION TO ABSORPTION CHILLERS WITH ADIABATIC ABSORBERS

Index

NOMENCLATURE

Variables

COP coefficient of performance

C specific heat capacity of a liquid (kJ kg^{-1} K^{-1})

F correction factor for plate heat exchangers

h enthalpy (kJ kg^{-1})

LiBr lithium bromide

$\dot{m}$ mass flow rate (kg h^{-1})

Np Number of plates

NTU number of transfer units

P pressure

$\dot{Q}$ thermal power (kW)

RR recirculation ratio, $RR = \frac{\dot{m}_r}{\dot{m}_{weak}}$

t temperature, external (ºC)

T temperature, internal (ºC)

UA overall heat transfer coefficient (kW K^{-1})

X concentration, mass/solution mass

z logarithmic mean temperature difference divided by arithmetic mean temperature difference

Subscripts

A absorber, absorption

C condenser, condensation

ch chilled

cw cooling water

E evaporator, evaporation

eq equilibrium

G generator, generation

i inlet

I ideal

l liquid

lm logarithmic mean

o	outlet
of	overflow
r	recirculation
S	subcooler
she	solution heat exchanger efficiency
ref	refrigerant
v	vapour
w	water

Greek letter:

$\alpha, \beta, \lambda, \gamma$	characteristic equation parameters
ε_{SHE}	solution heat exchanger efficiency
η	efficiency
ΔT_{lm}	Logarithmic mean temperature difference

5.1. Introduction

Various researchers have developed models of conventional LiBr- H_2O absorption machines with the aim of predicting their performance. The effect of several operating variables or conditions on the functioning of the absorption refrigeration system is a common objective in the papers by Hellmann et al. (1998), Joudi and Lafta (2001), Florides et al. (2003), among others. The purpose of this section is to use the model developed by Hellmann et al. (1998), which is able to represent both the capacity and the *COP* of single effect absorption chillers and heat pumps by means of simple algebraic equations. These equations are expressed as a function of the so called characteristic temperature difference, which depends on the average temperature of the external heat carrier fluids, and a parameter representing the slope of an average solution isostere in the Dühring chart, *B*:

$$\dot{Q}_E = s \cdot \Delta\Delta t - \alpha \cdot \dot{Q}_{loss} \tag{5.1}$$

With

$$\Delta\Delta t =: t_G - t_A - B \cdot (t_C - t_E) \tag{5.2}$$

Based on the aforementioned work (Hellmann et al, 1998), cooling capacity is analyzed in terms of the characteristic temperature difference $\Delta\Delta t$. Previous works (Albers and Ziegler, 2005 and Kühn and Ziegler, 2005) illustrate the use of $\Delta\Delta t$ to analyze and predict the off-design performance of chillers with a diabatic absorber, meaning this simultaneous absorption and cooling. An extended version of the characteristic equation model has been developed and adapted to the facility features. The adjustment of both the original and extended model to the data is presented for a particular configuration that highlights the extended part.

5.2. Description of heat and mass transfer processes in components

The main aspects of heat and mass transfer processes in each component are described next. Each aspect mentioned is relevant to adapt the characteristic equations to this kind of machines.

Fig. 5.1 shows the solution cycle layout of refrigerant dew point against boiling point (Dühring diagram) diagram, in a schematic way. The subscript "I" corresponds to ideal conditions, given by the average temperature of an ideal diabatic absorption process in equilibrium at the corresponding pressure. In this way, T_{AI} and T_{GI} represent the average value of inlet and outlet temperatures of absorber and generator, respectively, at the corresponding pressures. This scheme is used in the following sections in order to explain important ideas about heat and mass transfer process in components.

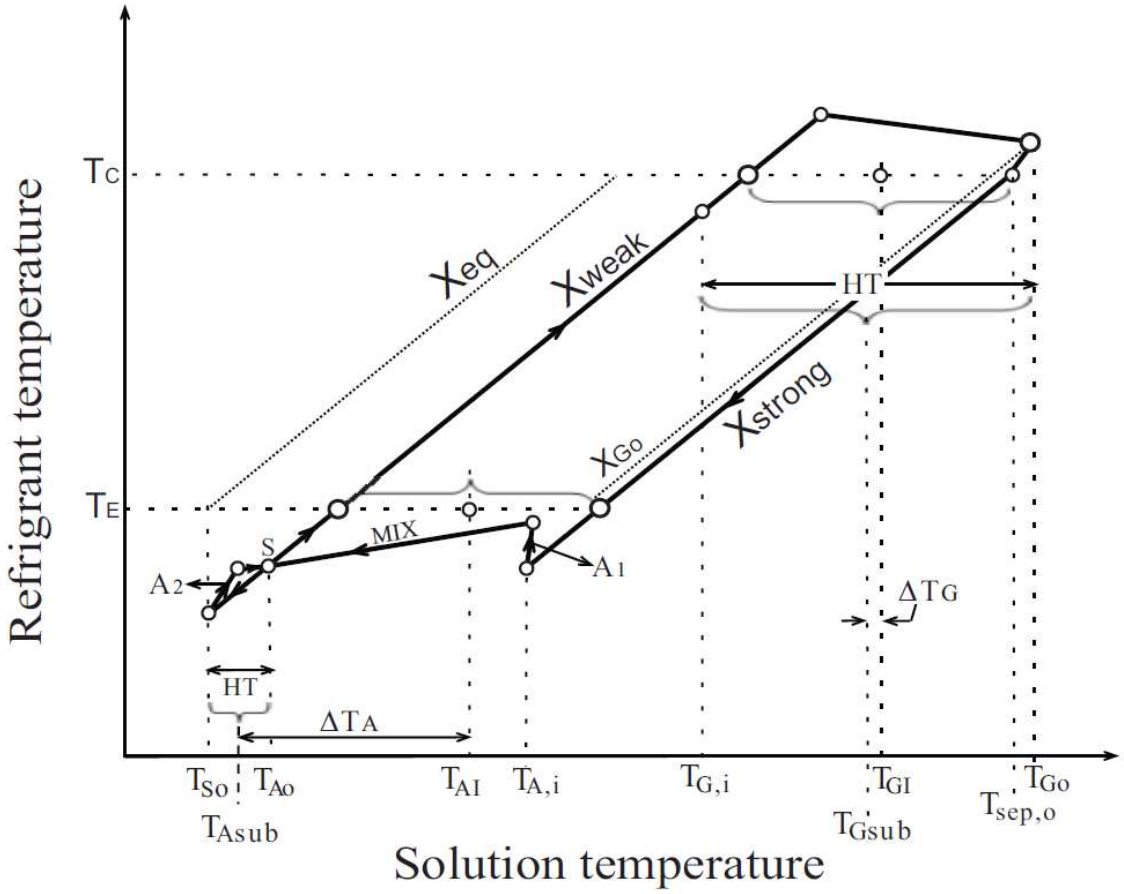

Fig. 5.1. Schematic diagram of solution cycle with adiabatic absorber on the Dühring diagram.

For the later description of heat and mass transfer processes in components, it is important to take into account that the use of a plate heat exchanger leads to apply a correction factor, F, if the number of plates is less than 50. F is a function of NTU and number of plates (Fig. 5.2). It is considered in order to take into account that the two external plates of the heat exchanger, transfer heat only by one of its sides (Hewitt, 1998).

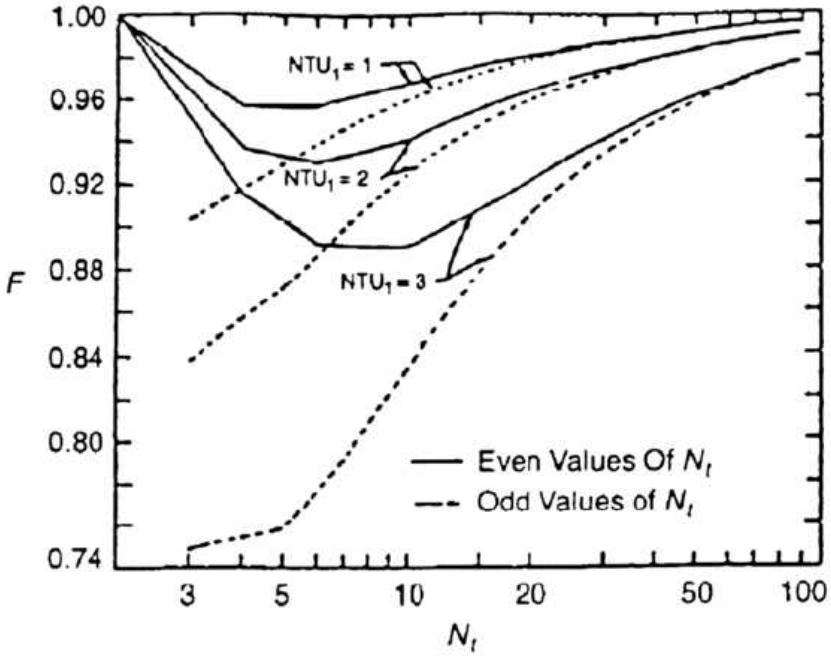

Fig. 5.2. The influence of odd and even number of thermal plates for 1 pass-1 pass counterflow exchanger performance. Source: Shah (1986)

5.2.1. Absorber

The control volume corresponding to absorber is shown on Fig. 5.3.

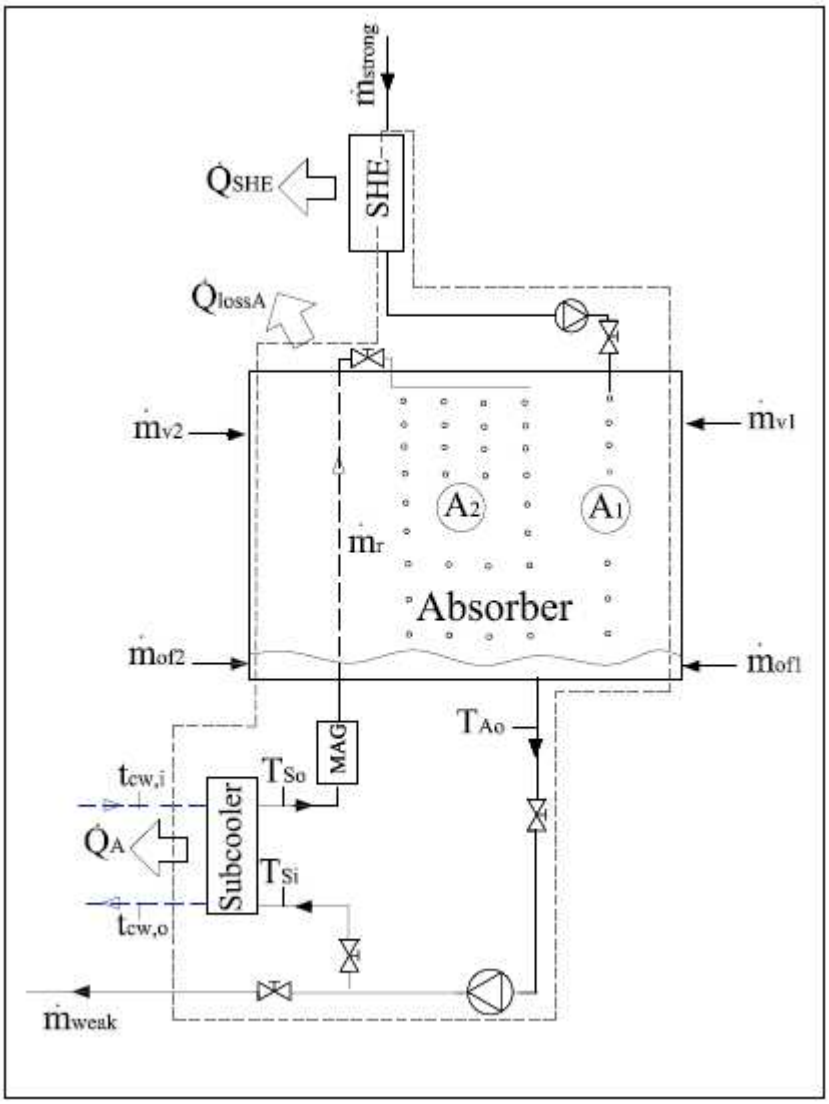

Fig. 5.3.Control volume of absorber

Main aspects:

- The subcooler has been included inside the control volume since both heat and mass transfer processes are included in diabatic absorbers. Thus, interactions of the whole with the outside are similar to those existing in a diabatic absorber: heat (both from the subcooler $\dot{Q}_A$ and losses to the environment $\dot{Q}_{lossA}$), input and output enthalpy flows corresponding to strong solution, refrigerant and weak solution. For machines equipped with circulation pump solution, the work done by them on the solution is included.
- Part of solution heat exchanger corresponding to the strong solution has been included in the control volume of absorber for compatibility with the methodology presented by Hellmann et al. (1998).

- Two adiabatic absorption processes, corresponding to strong and recirculated solution streams, are noted in Fig. 5.1 as A_1 and A_2 respectively. The solution temperature corresponding to strong and recirculated streams increases slightly while their concentration decreases during the absorption processes A_1 and A_2. Finally, the solution from both A_1 and A_2 falls into the pool, where it mixes up to the conditions of temperature and concentration of point S, to be pumped to the subcooler and the generator in parallel.
- The value of solution temperature at absorber outlet, T_{Ao}, is the same as that at subcooler entry, T_{Si} (point S in Fig. 5.1). This has been experimentally verified in our case.
- The mean value of inlet and outlet weak solution temperature in the subcooler is named T_{Asub}.
- Internal fluid temperature T_A: The heat transfer process takes place only in the subcooler. Then, temperatures of points T_{Ao} and T_{So} must be used to characterize this process, giving T_{Asub} (Fig. 5.1).

$$T_A = \frac{T_{Ao} + T_{so}}{2} = T_{Asub} \tag{5.3}$$

- The difference between T_{Asub} and T_{AI} is named as "absorber sub cooling" (ΔT_A). It indicates the difference in mean solution temperature between the heat transfer process which takes place in a diabatic absorber (supposed to work under saturated conditions) and the one that occurs in an adiabatic absorber (where the heat transfer take place far from saturated conditions).
- X_{weak} corresponds to the concentration measured at absorber outlet. X_{eq} corresponds to ultimate equilibrium concentration of the solution if the solution is brought to equilibrium adiabatically. The estimation of X_{eq} is explained in Chapter 6.
- UA_A is obtained from the energy balance in the subcooler: $\dot{Q}_A = UA_A \cdot \Delta T_{lmA} \cdot F_A$.
- External fluid temperature t_A is defined as:

$$t_A = \frac{t_{cw,o} + t_{cw,i}}{2} \tag{5.4}$$

Mass Balance:

$$\dot{m}_{weak} - \dot{m}_{strong} = \dot{m}_{v1} + \dot{m}_{v2} + \dot{m}_{of1} + \dot{m}_{of2} \tag{5.5}$$

Energy Balance:

$$\dot{Q}_A = (\dot{m}_{v1} + \dot{m}_{v2}) \cdot h_{vE} + (\dot{m}_{of1} + \dot{m}_{of2}) \cdot h_{lE} + \dot{m}_{strong} \cdot h_{strong} - \dot{m}_{weak} \cdot h_{weak} - \dot{Q}_{she} - \dot{Q}_{lossA} \quad (5.6)$$

$\dot{Q}_{lossA}$ is evaluated by using a model of heat transfer losses to ambient (see chapter 4).

5.2.2. Generator

Control volume corresponding to generator is shown on Fig. 5.4.

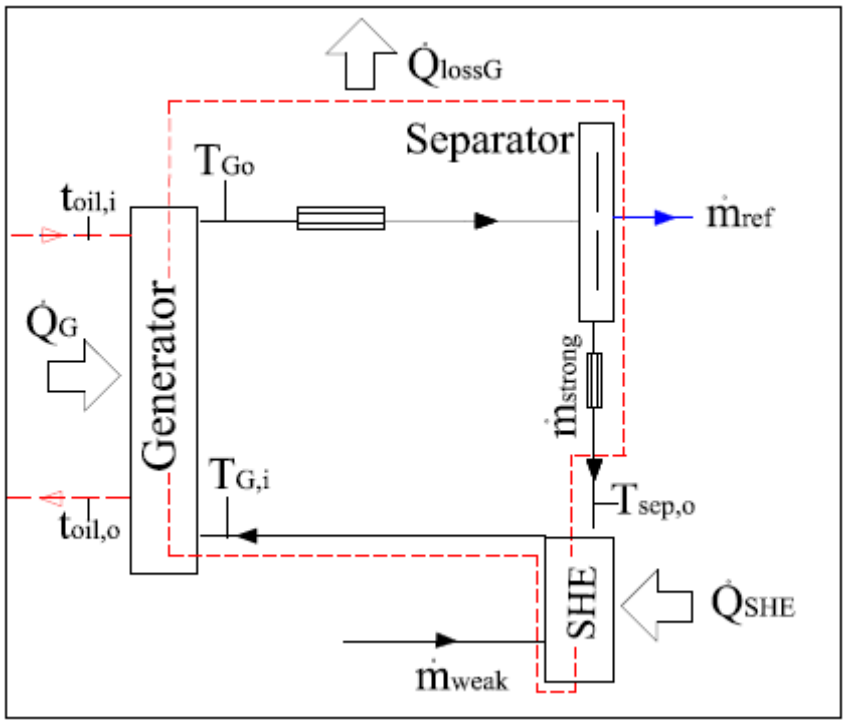

Fig. 5.4.Control volume of generator

Main aspects:

- The separator has been included inside the control volume since refrigerant separation is produced in the route from generator outlet to separator outlet, as explained in section 4.3.4. Interactions of the whole with the outside are similar to those existing in a diabatic absorber: heat (both from the generator $\dot{Q}_G$ and

losses to the environment $\dot{Q}_{lossG}$), input and output enthalpy flows corresponding to strong solution, refrigerant and weak solution.

- Part of the solution heat exchanger corresponding to the weak solution has been included in the control volume of absorber for compatibility with the methodology presented by Hellmann et al. (1998).
- The weak solution enters at generator into a sub cooled condition, $T_{G,i}$ depending on solution heat exchanger efficiency.
- Due to the pressure drop produced in the heat exchanger channels by density changes, an overheated condition of vapour is present in part of the PHE generator.
- The mean value of inlet and outlet solution temperature in the generator ($T_{G,i}$ and $T_{G,o}$) is named T_{Gsub}.
- The difference between T_{Gsub} and T_{GI} is named "generator subcooling" (ΔT_G). This quantity is smaller when the solution heat exchanger efficiency is higher.
- UA_G is obtained from the energy balance: $\dot{Q}_G = UA_G \cdot \Delta T_{lmG} \cdot F_G$.
- Finally, after the exit of heat exchanger, an adiabatic vapour separation is produced in a saturated condition, until condenser pressure is attained in the droplets separator vessel.
- Internal fluid temperature T_G (T_{Gsub} in Fig. 5.1):

$$T_G = \frac{T_{Gi} + T_{Go}}{2} = T_{Gsub} \tag{5.7}$$

- External fluid temperature t_G is defined as:

$$t_G = \frac{t_{oil,i} + t_{oil,o}}{2} \tag{5.8}$$

Mass Balance:

$$\dot{m}_{weak} - \dot{m}_{strong} = \dot{m}_{ref} \tag{5.9}$$

Energy Balance:

$$\dot{Q}_G = \dot{m}_{ref} \cdot h_{vG} + \dot{m}_{strong} \cdot h_{strong} - \dot{m}_{weak} \cdot h_{weak} - \dot{Q}_{she} + \dot{Q}_{lossG} \tag{5.10}$$

$\dot{Q}_{lossG}$ is evaluated by using a model of heat transfer losses to ambient (see chapter 4).

5.2.3. Evaporator

Control volume corresponding to evaporator is shown on Fig. 5.5. As can be seen, refrigerant distributor takes part of it.

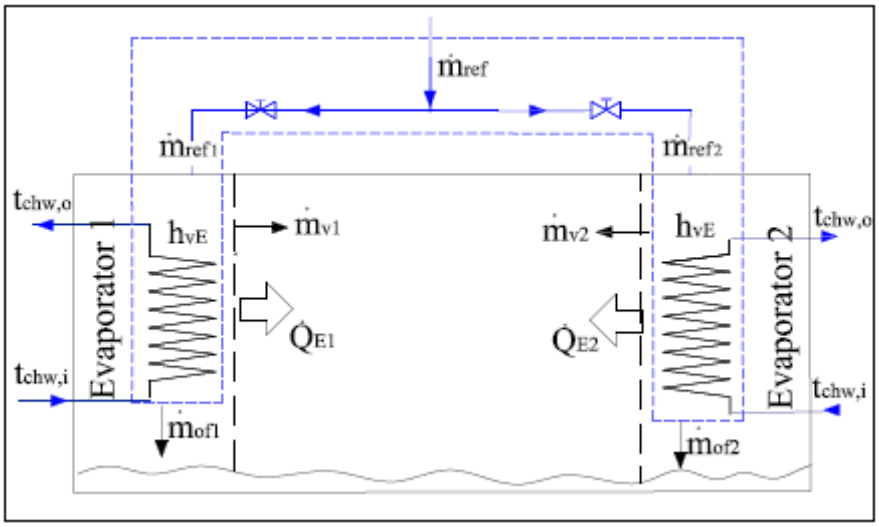

Fig. 5.5.Control volume of evaporator

Main aspects:

- A relevant aspect is that a non evaporated flow of refrigerant named “overflow”, represented as $\dot{m}_{of}$, is considered in this evaporator scheme, as a flow rate to absorber.
- Internal fluid temperature T_E: As both evaporators and absorber are located in the same vessel, the refrigerant saturation temperature corresponds to absorber pressure P_A. T_E is used to characterize thermally this component.
- External fluid temperature t_E is defined for each evaporator as:

$$t_{Ei} = \frac{t_{chwi} + t_{chwo}}{2} \tag{5.11}$$

In order to calculate t_E is necessary to weight the mean value of t_{E1} and t_{E2} with the corresponding chilled water mass flow rates, assuming that both streams mix to produce a single flow at t_E (Fig. 5.6).

The mass and energy balances would be:

$$\dot{m}_{chw_E} = \dot{m}_{chw_{E1}} + \dot{m}_{chw_{E2}} \tag{5.12}$$

$$\dot{m}_{chw_{E1}} \cdot Cp_w \cdot \left(t_E - t_{E1}\right) + \dot{m}_{chw_{E2}} \cdot Cp_w \cdot \left(t_E - t_{E2}\right) = 0 \tag{5.13}$$

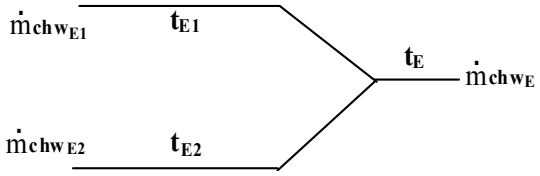

Fig. 5.6. Calculation scheme of external fluid temperature in the evaporator

t_E is obtained from (5.12) and (5.13):

$$t_{Ei} = t_{E1} \cdot \frac{\dot{m}_{chw_{E1}}}{\dot{m}_{chw_{E1}} + \dot{m}_{chw_{E2}}} + t_{E2} \cdot \frac{\dot{m}_{chw_{E2}}}{\dot{m}_{chw_{E1}} + \dot{m}_{chw_{E2}}} \tag{5.14}$$

Mass balance:

$$\dot{m}_{ref} = \dot{m}_{ref_1} + \dot{m}_{ref_2} \tag{5.15}$$

The terms on the right side of Eq. (5.15) corresponds to the distribution of refrigerant on both evaporators (see chapter 4).

And for the corresponding evaporator there will be an evaporated (used) and not evaporated (overflow) part of refrigerant:

$$\dot{m}_{ref_1} = \dot{m}_{v_1} + \dot{m}_{of_1} \tag{5.16}$$

$$\dot{m}_{ref_2} = m_{v_2} + \dot{m}_{of_2} \tag{5.17}$$

$\dot{m}_{v_1}$ designates the evaporated refrigerant.

Regarding the refrigerant mass flow rate that is not evaporated and the already defined evaporators efficiency η_E in Chapter 4, η_E can also be expressed as:

$$\eta_E = \frac{\dot{m}_v}{\dot{m}_{ref}} = \frac{\dot{m}_{ref} - \dot{m}_{of}}{\dot{m}_{ref}} = 1 - \frac{\dot{m}_{of}}{\dot{m}_{ref}} \tag{5.18}$$

Energy Balance:

$$\dot{Q}_E = \dot{Q}_{E1} + \dot{Q}_{E2} \tag{5.19}$$

$$\dot{Q}_{E1} + \dot{Q}_{E2} = \left(\dot{m}_{v_1} + \dot{m}_{v_2}\right) \cdot h_{vE} + \left(\dot{m}_{of_1} + \dot{m}_{of_2}\right) \cdot h_{lE} - \dot{m}_{ref_{oC}} \cdot h_{lC} \tag{5.20}$$

With

$$\dot{Q}_{E\,i} = \dot{m}_{vi} \cdot h_{vE} + \dot{m}_{ofi} \cdot h_{lE} - \dot{m}_{ref_i} \cdot h_{lC} \tag{5.21}$$

where the thermal losses in the refrigerant distributor have been neglected.

- Values of UA_E and ΔT_{lmE} used for later calculations are estimated by using the following equation system:

$$\dot{Q}_E = \dot{Q}_{E1} + \dot{Q}_{E2} = UA_{E1} \cdot \Delta T_{lm1} + UA_{E2} \cdot \Delta T_{lm2} \tag{5.22}$$

$$\dot{Q}_E = UA_E \cdot \Delta T_{lmE} \tag{5.23}$$

$$UA_E = UA_{E1} \cdot \frac{\Delta T_{lm1}}{\Delta T_{lmE}} + UA_{E2} \cdot \frac{\Delta T_{lm2}}{\Delta T_{lmE}} \tag{5.24}$$

If one of the evaporators does not receive any refrigerant, there is no heat exchange wet area (A_{Ei}=0), and the temperature difference ΔT_{lmE} is not defined. In those cases, UA_E and ΔT_{lmE} would be corresponding to the one evaporator that receives the refrigerant.

From Eq. (5.24):

$$\Delta T_{lmE} = \Delta T_{lm1} \frac{UA_{E1}}{UA_E} + \Delta T_{lm2} \frac{UA_{E2}}{UA_E} \tag{5.25}$$

Assuming that the overall heat transfer coefficients U do not change when the refrigerant mass flow rate is varied and the effective area of each evaporator is the wet area; then, it depends on the received refrigerant mass flow rate. Therefore, ΔT_{lmE} could be estimated as:

$$\Delta T_{lmE} = \Delta T_{lm1} \frac{m_{ref1_{used}}}{m_{ref}} + \Delta T_{lm2} \frac{m_{ref2_{used}}}{m_{ref}} \tag{5.26}$$

with

$$m_{ref1_{used}} = \frac{\left(\dot{m} \cdot c_p \cdot \Delta T\right)_{chw,E1}}{\left(h_{vE} - h_{lC}\right)} \text{ and } m_{ref2_{used}} = \frac{\left(\dot{m} \cdot c_p \cdot \Delta T\right)_{chw,E2}}{\left(h_{vE} - h_{lC}\right)} \tag{5.27}$$

5.2.4. Condenser

Control volume corresponding to condenser is shown on Fig. 5.7.

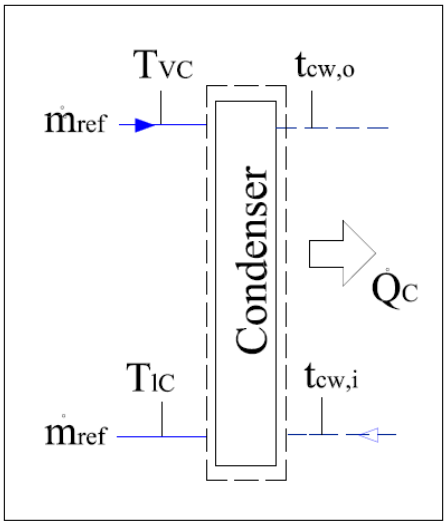

Fig. 5.7.Control volume of condenser

Energy balance:

$$Q_C = \dot{m}_{ref} \cdot (h_{vC} - h_{lC}) \tag{5.28}$$

- Vapour is entering at superheated condition.
- Internal fluid temperature T_C: The refrigerant saturation temperature T_C corresponding to condenser pressure P_C, is used to thermally characterize this component.
- External fluid temperature t_C:

$$t_C = \frac{t_{cwi} + t_{cwo}}{2} \tag{5.29}$$

- UA_C is estimated from the energy balance: $\dot{Q}_C = UA_C \cdot \Delta T_{lmC} \cdot F_C$

5.3. *Extension of the characteristic equation*

With the aim of implementing a model which is able to predict the cooling capacity and *COP* obtained for a wide range of operating conditions, applications of the characteristic equation model for an adiabatic absorption system has been explored. It will include the specific features involved in both the design and the operation (absorber subcooling, plate heat exchangers, two evaporators, off design flow rates, evaporator overflow). In the following, the procedure to adapt this model to such features is presented.

Regarding the heat transfer equations in the four major components, previous considerations made for each control volume were taken into account.

Then, following the analysis developed by Hellmann et al. (1998):

- The energy fluxes corresponding to each component are expressed as a function of $|t_i - T_i|$ $; i = E, C, A, G$.

$$\begin{aligned} \dot{Q}_C &= UA_C \cdot z_C \cdot (T_C - t_C) \cdot F_C \\ \dot{Q}_A &= UA_A \cdot z_A \cdot (T_A - t_A) \cdot F_A \\ \dot{Q}_G &= UA_G \cdot z_G \cdot (t_G - T_G) \cdot F_G \\ \dot{Q}_E &= UA_E \cdot z_E \cdot (T_E - t_E) \cdot F_E \end{aligned} \tag{5.30}$$

With

$$z_i = \frac{\Delta T_{lm,i}}{|t_i - T_i|} \tag{5.31}$$

The internal fluid temperatures are eliminated from Eq. (5.30), observing that the slope of concentration lines, in a Dühring diagram, is almost constant and for this, its value depends only on the solution concentration.

$$T_G - T_A - B \cdot (T_C - T_E) = 0 \tag{5.32}$$

B in Eq. (5.32) is the isostere line of Dühring diagram slope for an average solution concentration. T_G and T_A are generally considered as T_{GI} and T_{AI} (Fig. 5.1) respectively: But as previously explained, those are not the characteristics temperatures

for the real heat transfer processes due to subcooling; which are T_{Gsub} and T_{Asub}. Then, a definition of an apparent value of B, named B_{sub} is necessary to satisfy Eq. (5.32) in an adiabatic absorption behaviour:

$$B_{sub} = \frac{T_{Gsub} - T_{Asub}}{T_C - T_E} \tag{5.33}$$

This parameter can be related with B:

$$B_{sub} = B + \frac{\Delta T_A - \Delta T_G}{T_C - T_E} \tag{5.34}$$

Where, due to the subcooling process characteristic of the adiabatic absorbers, ΔT_A is the most relevant contribution, having an average value of 20ºK in the operating conditions tested. The average value for ΔT_G is 3ºK, for $\eta_{she} = 0{,}65$.

For a diabatic absorber, the four temperatures T_G, T_A, T_C and T_E must be specified when applying the characteristic equation. In adiabatic absorbers, at least ΔT_A must also be specified. Additionally, no matter of what type of absorber is, η_{she} should be specified to calculate ΔT_G.

Combining Eq. (5.30) and (5.32):

$$\frac{\dot{Q}_G}{UA_G \cdot z_G \cdot F_G} + \frac{\dot{Q}_A}{UA_A \cdot z_A \cdot F_A} + B_{sub} \cdot \left(\frac{\dot{Q}_C}{UA_C \cdot z_C \cdot F_C} + \frac{\dot{Q}_E}{UA_E \cdot z_E} \right) = t_G - t_A - B_{sub} \cdot (t_C - t_E) =: \Delta\Delta t \tag{5.35}$$

- For obtaining an equation for $\dot{Q}_E$ from Eq. (5.35) it is necessary to eliminate $\dot{Q}_G$, $\dot{Q}_A$ and $\dot{Q}_C$ through the energy balance on each component.

Energy balances are already specified on equations (5.6), (5.10), (5.20) and (5.28). Using another way to express those Equations, we have:

$$\dot{Q}_E = \dot{m}_{ref} \cdot (h_{vE} - h_{lc}) - \dot{m}_{of} \cdot (h_{vE} - h_{lE}) \cdot \tag{5.36}$$

The second term of Eq. (5.36) corresponds to the overflow of refrigerant:

$$\dot{Q}_{of} = \dot{m}_{of} \cdot (h_{vE} - h_{lE}) \tag{5.37}$$

$$\begin{aligned} \dot{Q}_C &= \dot{m}_{ref} \cdot (h_{vG} - h_{lC}) \\ \dot{Q}_A &= (\dot{m}_{ref} - \dot{m}_{of}) \cdot h_{vE} + \dot{m}_{strong} \cdot h_{trongsG} - \dot{m}_{weak} \cdot h_{weakA} - \dot{Q}_{she} + \dot{m}_{of} \cdot h_{lE} - \dot{Q}_{lossA} \\ \dot{Q}_G &= \dot{m}_{ref} \cdot h_{vC} + \dot{m}_{strong} \cdot h_{strongG} - \dot{m}_{weak} \cdot h_{weakA} - \dot{Q}_{she} + \dot{Q}_{lossG} \end{aligned} \tag{5.38}$$

As already explained in Chapter 4, thermal input from the ambient to the evaporators can be considered negligible because of its location within the low pressure shell next to the absorber. Additionally, the evaporators are insulated from absorber radiation heat through a double metallic flat plate (radiation shield). Heat loss of the condenser can be neglected because of its temperature, being near to the ambient.

Heat loss of the condenser can also be neglected because it is isolated and its operating temperature is near to the ambient.

Using equations (5.35)-(5.38), we express $\dot{Q}_C$, $\dot{Q}_A$ and $\dot{Q}_G$ as a function of $\dot{Q}_E$, knowing that:

$$\dot{m}_{ref} = \frac{\dot{Q}_E + \dot{Q}_{of}}{h_{vE} - h_{lC}} \tag{5.39}$$

As a result:

$$\begin{aligned}
\dot{Q}_C &= \frac{(h_{vC} - h_{lC})}{(h_{vE} - h_{lC})} \cdot (\dot{Q}_E + \dot{Q}_{of}) = C \cdot (\dot{Q}_E + \dot{Q}_{of}) \\
\dot{Q}_A &= \frac{(h_{vE} - h_{strongG})}{(h_{vE} - h_{lC})} \cdot (\dot{Q}_E + \dot{Q}_{of}) + \dot{m}_{weak} \cdot (h_{strongG} - h_{weakA}) - \dot{Q}_{hex} - \dot{Q}_{of} - \dot{Q}_{lossA} \\
&= A \cdot \dot{Q}_E + \dot{Q}_{of} \cdot (A-1) + \dot{Q}_{loss} - \dot{Q}_{lossA} \\
\dot{Q}_G &= \frac{(h_{vC} - h_{strongG})}{(h_{vE} - h_{lC})} \cdot (\dot{Q}_E + \dot{Q}_{of}) + \dot{m}_{weak} \cdot (h_{strongG} - h_{weakA}) - \dot{Q}_{hex} + \dot{Q}_{lossG} \\
&= G \cdot (\dot{Q}_E + \dot{Q}_{of}) + \dot{Q}_{loss} + \dot{Q}_{lossG}
\end{aligned} \tag{5.40}$$

With C, A and G assumed to be constants:

$$\begin{aligned}
C &= \frac{(h_{vC} - h_{lC})}{(h_{vE} - h_{lC})} \\
A &= \frac{(h_{vE} - h_{strongG})}{(h_{vE} - h_{lC})} \\
G &= \frac{(h_{vC} - h_{strongG})}{(h_{vE} - h_{lC})}
\end{aligned} \tag{5.41}$$

And defining $\dot{Q}_{loss}$ as:

$$\dot{Q}_{loss} = \dot{m}_{weak} \cdot (h_{strongG} - h_{weakA}) - \dot{Q}_{she} \tag{5.42}$$

According to Hellmann et al. (1998), "$\dot{Q}_{loss}$ is an equivalent for the solution heat exchanger loss, i.e. the heat required in the generator for heating and rejected in the

absorber for cooling the solution streams to the appropriate internal equilibrium temperature".

Combining Eqs. (5.35) and (5.40) results:

$$\dot{Q}_E = s \cdot \Delta\Delta t - \alpha \cdot \dot{Q}_{loss} - \beta \cdot \dot{Q}_{of} + \delta - \lambda \tag{5.43}$$

The characteristic parameters ($s, \alpha, \beta, \delta, \lambda$) are defined as:

$$s = \frac{1}{\frac{G}{UA_G \cdot z_G \cdot F_G} + \frac{A}{UA_A \cdot z_A \cdot F_A} + B \cdot \left(\frac{C}{UA_C \cdot z_C \cdot F_C} + \frac{1}{UA_E \cdot z_E} \right)}$$

$$\alpha = s \cdot \left(\frac{1}{UA_G \cdot z_G \cdot F_G} + \frac{1}{UA_A \cdot z_A \cdot F_A} \right)$$

$$\beta = s \cdot \left(\frac{G}{UA_G \cdot z_G \cdot F_G} + \frac{A-1}{UA_A \cdot z_A \cdot F_A} + \frac{B \cdot C}{UA_C \cdot z_C \cdot F_C} \right) \tag{5.44}$$

$$\delta = s \cdot \left(\frac{Q_{lossA}}{UA_A \cdot z_A \cdot F_A} \right)$$

$$\lambda = s \cdot \left(\frac{Q_{lossG}}{UA_G \cdot z_G \cdot F_G} \right)$$

Parameters β, δ, λ are new terms which are additional to the original characteristic equation parameters. Such parameters appear because of the effects on the performance of overflow and thermal losses in the absorber and generator, respectively.

5.4. *Results and discussion*

This section shows results of the extension of the characteristic equation model for all the experimental points obtained.

Fig. 5.8 illustrates the comparison of the experimental and predicted cooling capacity $\dot{Q}_E$, obtained by applying the characteristic equation model using "*B*" instead of "B_{sub}". The need of including the subcooling effects on B is revealed by the comparison with Fig. 5.9. In this case $\dot{Q}_E$ was obtained through the extended characteristic equation. The agreement observed is good and deviations are in the range of the overall uncertainty in the measured parameters.

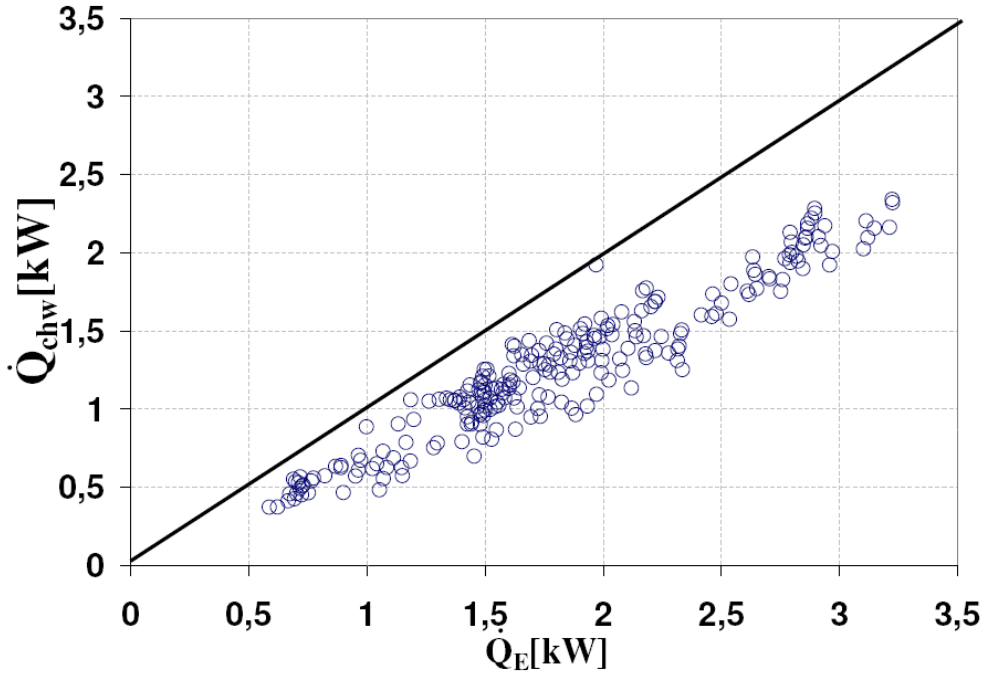

Fig. 5.8. Comparison of cooling capacity obtained trough extended characteristic equation, $\dot{Q}_E$, with experimental data $\dot{Q}_{chw}$. Results using *B*.

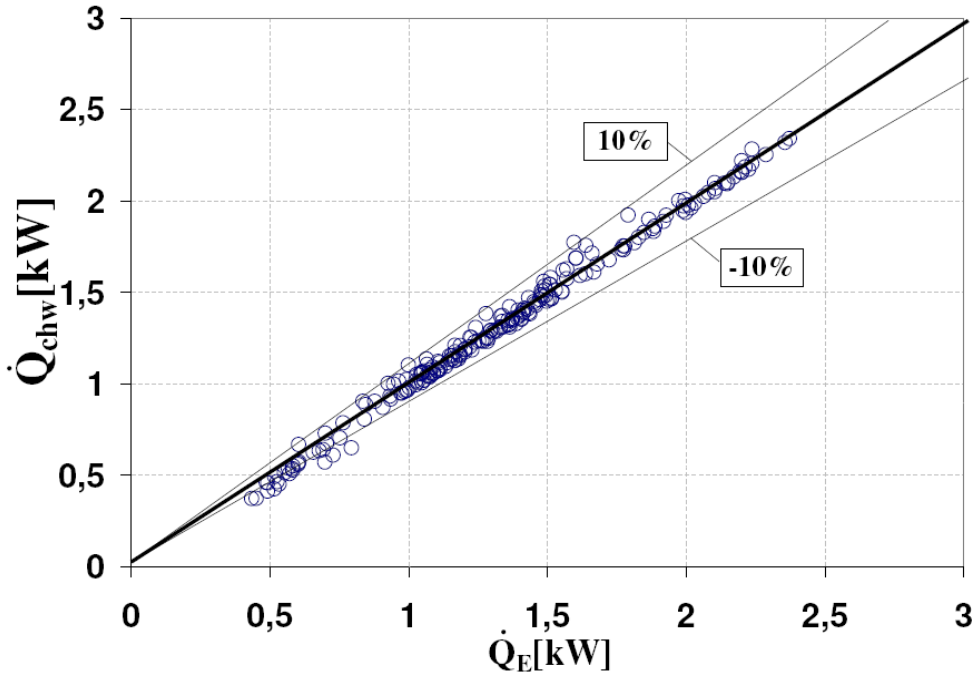

Fig. 5.9. Comparison of cooling capacity obtained trough extended characteristic equation, $\dot{Q}_E$, with experimental data $\dot{Q}_{chw}$. Results using B_{sub}.

The effect of overflow on $\dot{Q}_E$ is presented in Fig. 5.10. Obviously, as the fraction of non-evaporated refrigerant $\dot{m}_{of}$ increases, $\dot{Q}_E$ decreases.

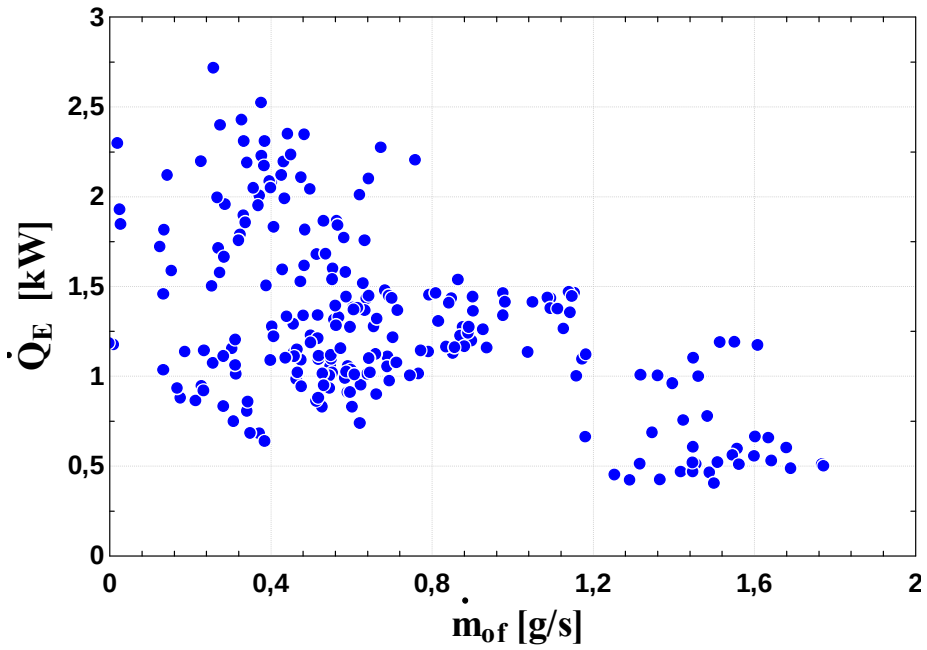

Fig. 5.10. Cooling capacity vs. overflow mass flow rate.

Thermal losses in pipes, plate heat exchangers, separator ($\dot{Q}_{lossG}$), represent an average value 8% of $\dot{Q}_G$. For the case of the absorber, $\dot{Q}_{lossA}$, is 5% of thermal power of subcooler (chapter 4). A noticeable difference was encountered between solution temperature at generator outlet and separator outlet. The associated temperature drop associated ranges from 4K to 10K (see difference between T_{Go} and $T_{sep,o}$ in Fig. 5.1). The estimation of the thermal losses allowed to state that these were not causing such a difference. However, it was observed that refrigerant production continued at the exit of the generator. This effect is enhanced by the additional pressure drop in the flow through the separator.

5.4. Conclusions

A characteristic equation has been adapted to a specially designed single effect LiBr absorption chiller and has been applied for experimental evaluation of system components and the whole chiller.

- An extension of the characteristic equation method to adiabatic absorption has been developed. For this kind of absorbers, a subcooling temperature must be specified.
- The effect of evaporator overflow has been characterized. Its influence on $\dot{Q}_E$ has been included in the extended characteristic equation.
- Taking into account the particular design and operation features, a good agreement between experimental performance parameters and those obtained through the extended characteristic equation has been achieved, even at off-design operation. This allows its use for simulation and control purposes.

Chapter 6

COMPARISON OF ABSORBER CONFIGURATIONS

Index

NOMENCLATURE

Variables

F_x	equilibrium factor in terms of concentration
$\dot{m}$	mass flow rate (kg h^{-1})
$\dot{Q}$	thermal power (kW)
$\dot{q}$	thermal power per unit mass flow (kJ kg^{-1})
RR	recirculation ratio
UA	overall heat transfer coefficient (kW K^{-1})
V	Volume
X	concentration, mass/solution mass

Subscripts

cw	cooling water
G	generation
i	inlet
eq	equilibrium
of	overflow
r	recirculated
ref	refrigerant

6.1. Introduction

The adiabatic absorber is configured in such a way that free-falling drops, sprays, liquid sheets in the form of a fan and inverse liquid jets (fountain alike) can be experimentally tested and compared. Two adiabatic absorber configurations, droplets and liquid sheets, were tested and evaluation parameters were experimentally estimated. Figures 6.1 and 6.2 illustrate the falling drops and fan sheet flow, respectively, in the absorbing vessel. The corresponding distribution systems are also illustrated. Both diameter of drops and intact length of a fan sheets depend on solution injection velocity. Typically, they are about 4 mm and 8 cm, respectively. In the case of fan sheet, the drops generated after the sheet break up are about 1 mm diameter. A comparison in terms of performance and absorption efficiency is presented for free falling drops and fan sheets adiabatic absorber configurations.

6.2. *Specific cooling capacity*

A single fan sheet is able to manage a flow rate equivalent to the flow rate managed by about 12 eyedroppers. The reduction of required space is considerable, leading to a significant reduction in the size of the absorber with no loss of benefits as shown later. This reduction in space has allowed the placement of a large number of fan sheets that are used to increase the recirculation ratio.

On the other hand, the rest of the machine is unable to handle a higher solution flow like the one resulting from using two sheets for the concentrated solution flow. This is especially limited by the evaporators overflow.

A specific flow quantity $\dot{q}$ is necessary for comparing the performance of both absorber configurations on a common base, for the reason that the quantity $\dot{m}_{weak}$ tested for fan sheet is lower than that tested for drops.

$$\dot{q}_{ref} = \dot{Q}_{ref} / \dot{m}_{weak} \tag{6.1}$$

$$\dot{q}_{E,\exp} = \dot{Q}_{E,\exp} / \dot{m}_{weak} \tag{6.2}$$

Experimental and maximum cooling capacity, $\dot{Q}_{ref}$ and $\dot{Q}_{E,\exp}$, have already been defined in Chapter 4.

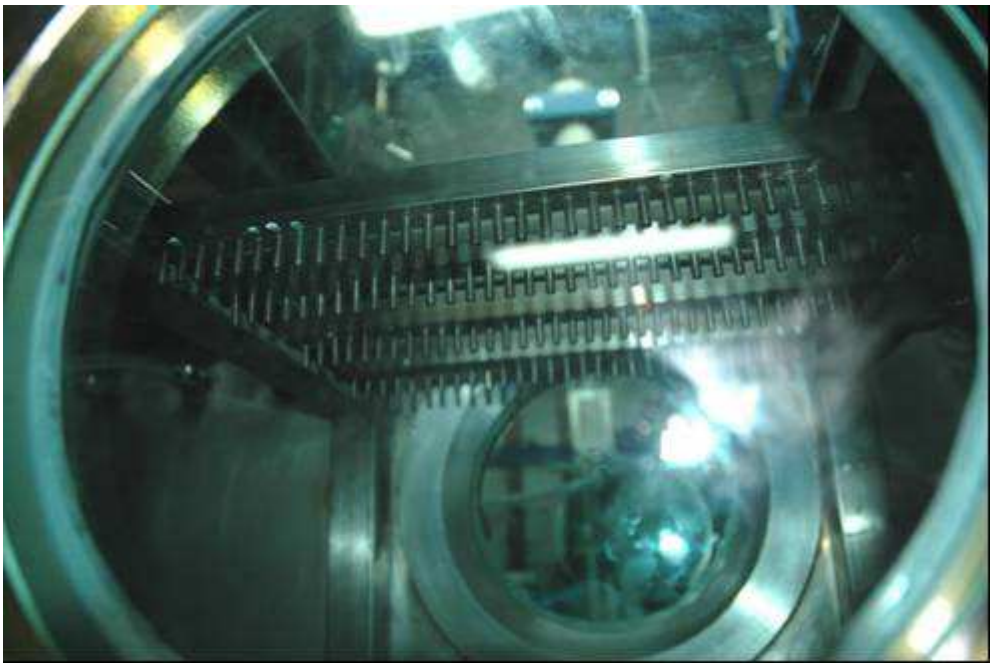

Fig. 6.1a. Distribution system of free falling drops

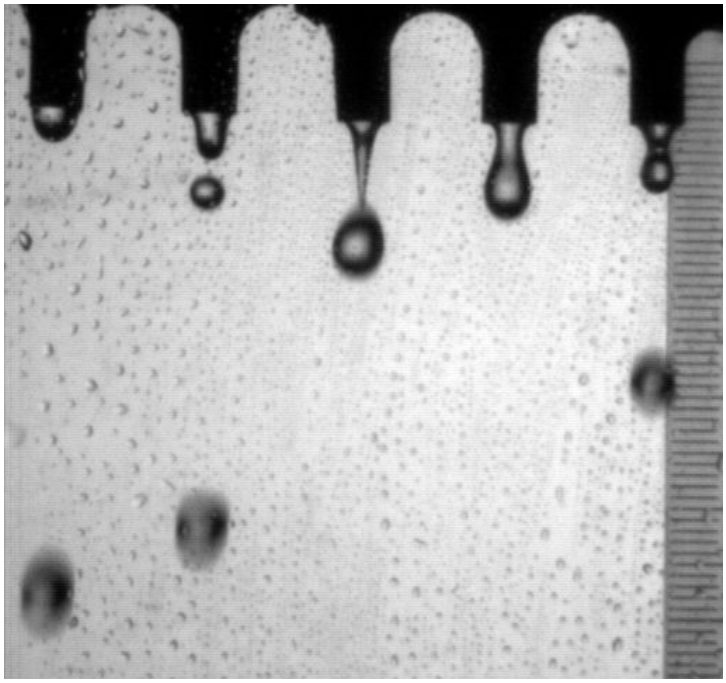

Fig. 6.1b. Falling drops (eyedroppers) flow in the absorption process. Divisions in the rulers on the right are in mm.

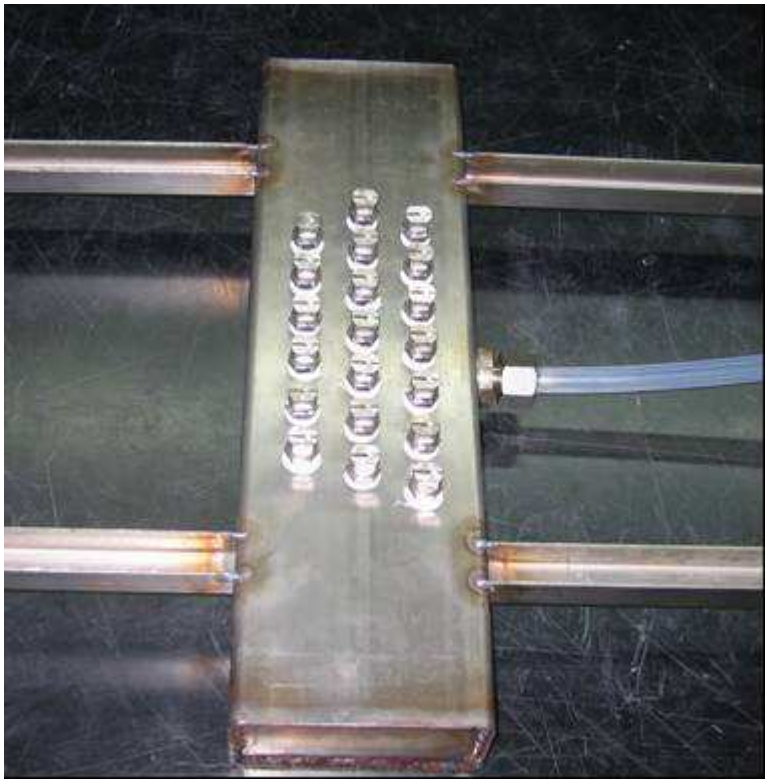

Fig. 6.2a. Distribution system of fan sheets, inverted position

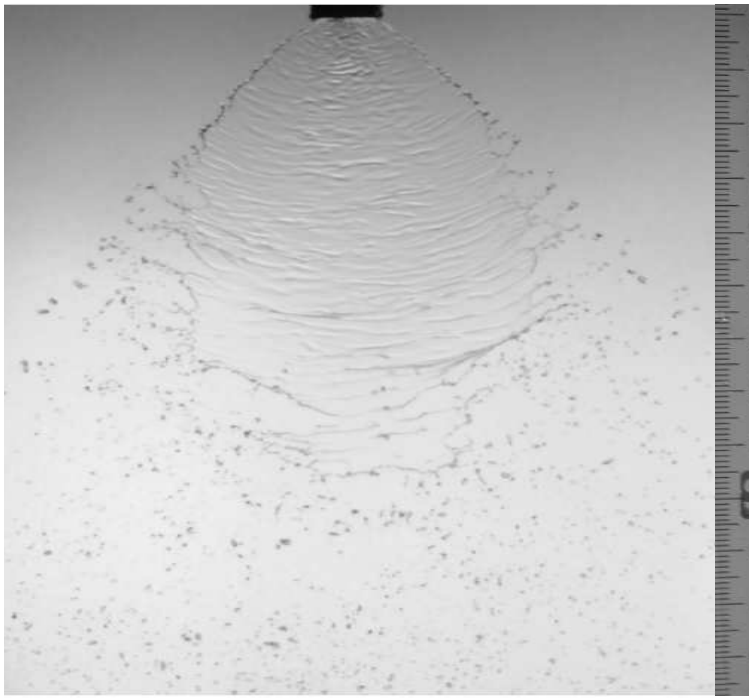

Fig. 6.2b. Front view of a single plane fan sheet in the absorption process.
Divisions in the rulers on the right are in mm.

6.3. *Approach to equilibrium factor*

The approach to equilibrium factor in the absorber F_x, also called absorber efficiency in older literature, is defined in Eq. (6.3). The absorption process can be characterized by using the measured values of the LiBr concentration at absorber inlet and outlet:

$$F_x = \frac{X_{weak,A} - X_{strong}}{X_{eq} - X_{strong}} \tag{6.3}$$

$X_{weak,A}$ is the actual concentration reached by the solution before mixing with the solution pool. Taking into account the contribution of the overflow mass flow rate $\dot{m}_{of}$ to the outlet concentration in the absorber:

$$X_{weak,A} = X_{weak} + \dot{m}_{of} \left/ \dot{m}_{weak} \right. \tag{6.4}$$

X_{eq} is the ultimate equilibrium concentration, which is calculated based on thermodynamic analysis: energy balances and known LiBr properties (Ryan et. al, 1995; Warnakulasuriya and Worek, 2006). Equilibrium state in the absorber is estimated by solving Eqs. (6.5) - (6.11), based on a control volume of absorber, reaching the equilibrium concentration at the absorber pressure (Fig. 6.3).
The overall mass balance yields:

$$\dot{m}_{strong} + \dot{m}_{ref} = \dot{m}_{eq} \rightarrow \frac{\dot{m}_{strong}}{\dot{m}_{eq}} + \frac{\dot{m}_{ref}}{\dot{m}_{eq}} = 1 \tag{6.5}$$

being $\dot{m}_{eq}$ the value of $\dot{m}_{weak}$ corresponding to the equilibrium condition.

The refrigerant mass balance yields:

$$\dot{m}_{strong} \cdot \left(1 - X_{strong}\right) + \dot{m}_{ref} = \dot{m}_{eq} \cdot \left(1 - X_{eq}\right) \tag{6.6}$$

Combining (6.5) and (6.6):

$$\frac{\dot{m}_{strong}}{\dot{m}_{eq}} = \frac{X_{eq}}{X_{strong}} \tag{6.7}$$

The energy balance in the absorber yields:

$$\dot{m}_{strong} \cdot h_{strong} + \dot{m}_{ref} h_{ref} = \dot{m}_{eq} h_{eq} + \dot{Q}_A \tag{6.8}$$

$$h_{eq} = f(T_{eq}, X_{eq}) \tag{6.9}$$

$$X_{eq} = f(P_{abs}, T_{eq}) \tag{6.10}$$

with

$$\dot{Q}_A = \dot{m}_r (h_{eq} - h_r), \quad h_r = h(T_{cw,i}, X_{eq}) \tag{6.11}$$

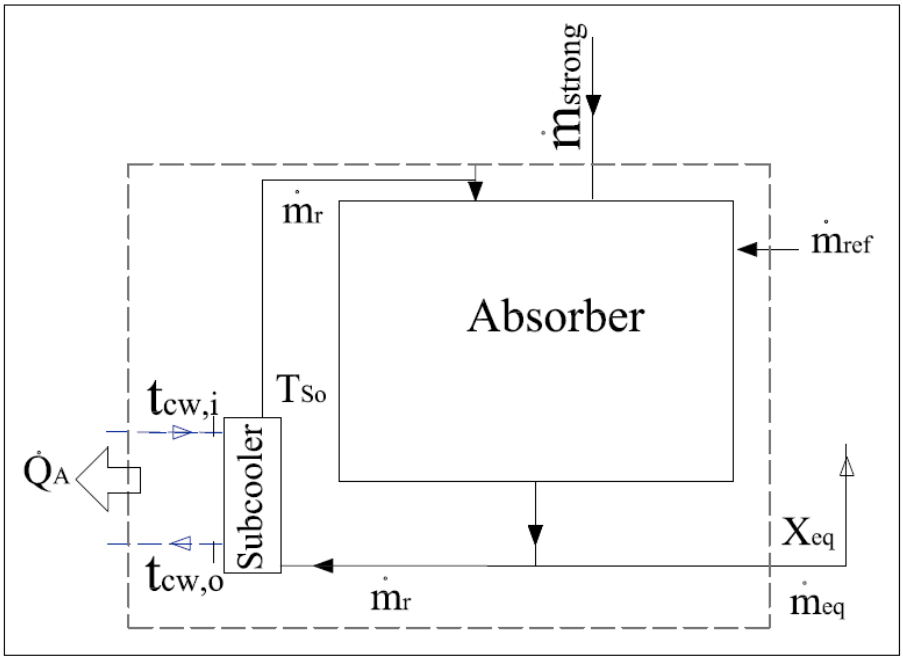

Fig. 6.3. Control volume of absorber in equilibrium.

F_x is used to evaluate the mass transfer process, instead of the coefficient of mass transfer, because of the uncertainty of the contact area for both configurations, which makes it difficult to express it in a quantitative way. F_x can also be expressed as a function of the temperatures when the measurement of solution concentration is complex at the inlet and outlet of absorber (Arzoz et al, 2005), which is not the case in this work.

All data were grouped according to the recirculation ratio *RR*,

$$RR = \frac{\dot{m}_r}{\dot{m}_{weak}} \tag{6.12}$$

Therefore, the dependence of F_x and UA_A with RR will be shown next.

6.4. Results and discussion

6.4.1. Heat and mass transfer in the absorber

The influence of the controlled recirculation ratio over the heat transmission UA_A is shown in Fig. 6.4, obtained with both absorber configurations under study. The parameter UA_A increases when *RR* increases for both cases. As mentioned on section 6.2, the space reduction achieved when using fan sheets allowed obtaining higher *RR*, which results in higher UA_A. The variation of $\dot{m}_{weak}$ affects clearly the heat transfer coefficient.

The approach to equilibrium factor F_x is much affected by $\dot{m}_{of}$ coming from the evaporators, which is manifested in Fig. 6.5. The results for an approach to equilibrium factor obtained if $\dot{m}_{of}$ is not considered, called $F_{x,i}$, are also shown for comparison purpose. $F_{x,i}$ is obtained for $X_{weak,A} = X_{weak}$ in Eq. (6.3), i.e., if all the refrigerant were evaporated and incorporated to the strong solution inside the absorber.

Because of the effect of $\dot{m}_{of}$ in the absorber performance, it is difficult to observe the influence of *RR* on F_x. In spite of this, when *RR* is increased F_x seems to increase for both fan sheets and free falling droplets configurations (Fig. 6.6).

6.4.2. Specific cooling capacity

Fig. 6.7 shows the results in terms of $\dot{q}_{ref}$ and $\Delta\Delta t$ for both fan sheets and droplets, for the same *RR*. Two sets of experiments with different solution mass flow rates $\dot{m}_{weak}$ are plotted for droplets in order to compare the common trends of experimental data with those obtained using fan sheets. Trend lines are drawn as dashed lines. In spite of the different range of $\Delta\Delta t$, the trend shows a higher $\dot{q}$ for the case of fan sheets compared with droplets. As a consequence, a significant reduction in the absorber size could be achieved. The ratio $V_A / \dot{Q}_E$ could be reduced from 450 l/kW, needed for falling drops, to 245 l/kW for fan sheets. If the size of each arrangement inside the absorber is considered (Fig. 6.1a and 6.2a), the space reduction achieved could be up to 50%.

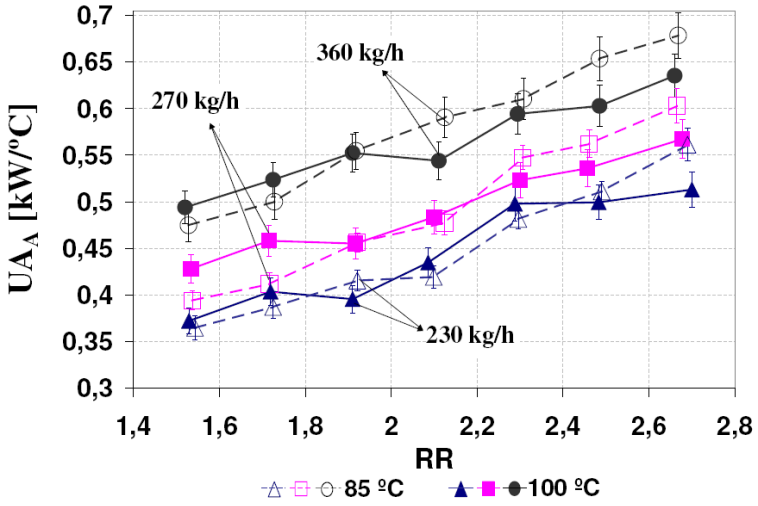

(a)

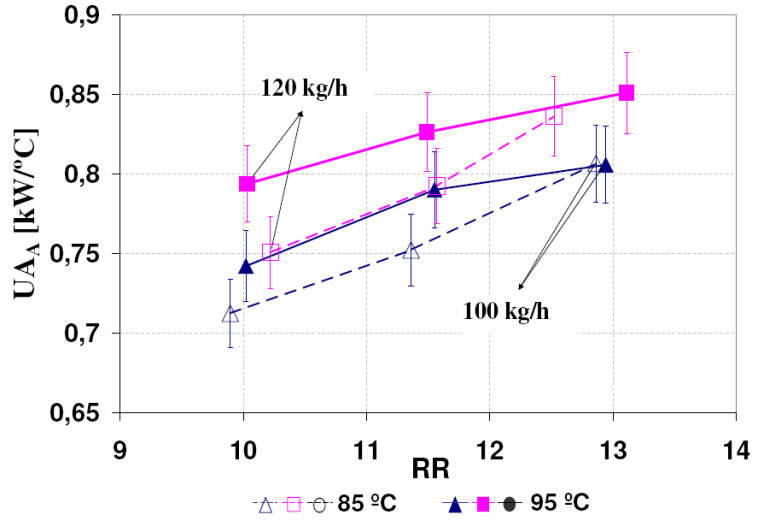

(b)

Fig. 6.4. Overall heat transfer coefficient UA_A vs. RR for different $\dot{m}_{weak}$ and $t_{G,i}$. a) Falling drop method. b) Fan sheets method

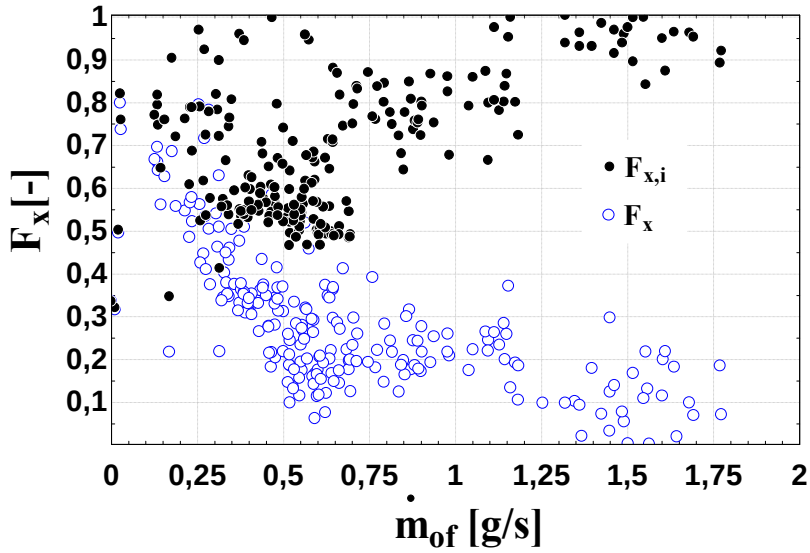

Fig. 6.5. Approach to equilibrium factor F_x vs. overflow mass flow rate.

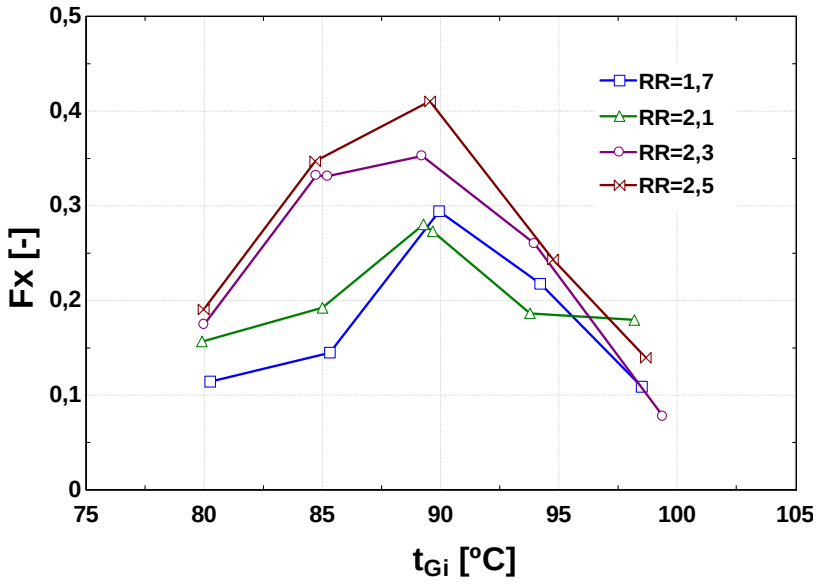

(a)

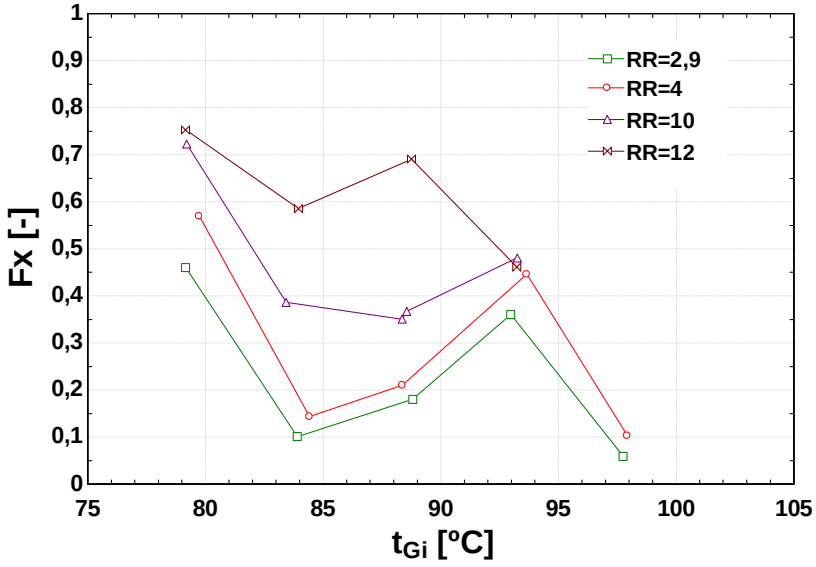

(b)

Fig. 6.6. (a) Approach to equilibrium factor vs. t_{Gi} for falling drop method. $\dot{m}_{weak}$ is fixed at 270 kg/h. (b) Approach to equilibrium factor vs t_{Gi} for fan sheets method. $\dot{m}_{weak}$ is fixed at 120 kg/h.

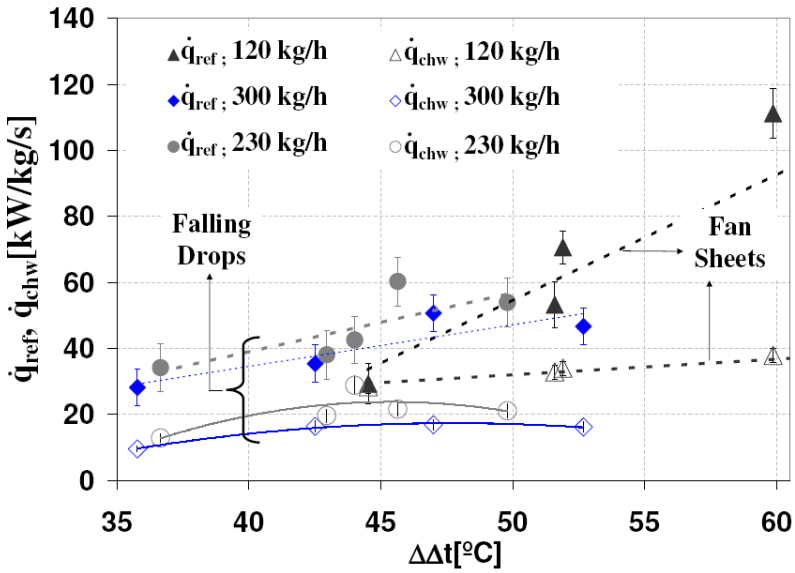

Fig. 6.7. Specific cooling capacity vs. $\Delta\Delta t$ for free falling drops and fan liquid sheets method for the same *RR*

6.5. Conclusions

- Two adiabatic absorber configurations, namely droplets and fan sheet, were tested and operational parameters have been experimentally determined.
- The absorber configuration based on fan sheets showed better performance parameters than the droplets configuration. A significant reduction in the absorber size (up to 50%) is possible.
- The absorber performance has been characterized trough two parameters: the thermal transmission conductance UA_A and the approach to equilibrium factor F_x. The influence of the controlled parameters on absorber performances has been shown.
- The UA_A has shown to be strongly dependent of recirculated mass flow rate. This way, the subcooling capacity of the absorber can be increased. As an increment in subcooling capacity help to the absorption process, an increment in RR could affect positively to the approach to equilibrium factor F_x.

Chapter 7

SINGLE AND TWO-PHASE HEAT TRANSFER AND PRESSURE DROP IN COMPACT PLATE HEAT EXCHANGERS

Index

NOMENCLATURE

Variables

A	heat transfer area (m^2)
b	corrugation depth (m)
C	specific heat capacity of a liquid (kJ kg^{-1} K^{-1})
D_h	hydraulic diameter (m)
e	plate thickness
f	friction factor
F	correction factor for plate heat exchangers
G	mass flux (kg m^{-2} s^{-1})
h	film heat transfer coefficient (W·m^{-2} C^{-1})
k	conductivity (W·m^{-1} C^{-1})
L	plate length (m)
LiBr	lithium bromide
$\dot{m}$	mass flow rate (kg s^{-1})
Np	Number of plates
Nu	Nusselt number
P	pressure (mbar)
PHE	Plate heat exchanger
Pr	Prandtl number $= \mu_f \cdot C_p / k_f$
$\dot{Q}$	thermal power (kW)
$\dot{q}$	heat flux (kW m^{-2})
Re	Reynolds number $= \rho \cdot u \cdot D_h / \mu_f$
T	temperature (ºC)
u	velocity (m s^{-1})
U	overall heat transfer coefficient (kW K^{-1})
W	plate width (m)
x_v	vapour quality
X	concentration, mass/solution mass

Subscripts

a	acceleration

c	cold, column
cw	cooling water
eq	equivalent
G	generator, generation
f	fluid, friction
foul	fouling
h	hot
i	inlet
o	outlet, outer
l	liquid
p	plate
sol	solution
t	total, tube
v	vapour
w	wall
1ph	single phase
2ph	two-phase

Superscripts

m	exponent of Reynolds number
n	exponent of Prandtl number

Greek letter:

β	Chevron angle, (º)
μ	viscosity ($kg \cdot m^{-1} \cdot s^{-1}$)
Λ	corrugation pitch (m)
ϕ	surface enlargement factor
ρ	density ($kg.m^{-3}$)
ΔT_{lm}	Logarithmic mean temperature difference.
ΔP	Pressure drop (mbar)

7.1. Introduction

The selection of compact plate heat exchangers to carry out heat transfer processes in the experimental absorption test rig is justified by the various benefits they offer, often highlighted in the open literature: higher heat transfer coefficients, less weight, size and cost than the conventional heat exchangers. Other significant advantage is the ability to stand extreme conditions and that even with highly viscous and low flow rates, turbulent or at least swirl flow can be obtained and the fouling rate is reduced (Cooper, 1983; Warnakulasuriya, 2008).

The brazed plate heat exchanger (BPHE) is the type installed in the test rig. In refrigeration applications BPHE are used instead of gasketed, mainly because they can withstand high operating pressure (Claesson, 2005) and also they offer higher reliability against leaks, besides being more compact.

As has been explained throughout the Thesis, three BPHE have been used in the experimental facility. The experimental characterization of commercially available PHEs working as a generator, subcooler and solution heat exchanger is described. For the case of generator, single and two-phase experimental data were obtained. For the cases of subcooler and solution heat exchanger, single phase heat transfer data have been obtained.

This chapter describes the heat transfer and pressure drop in the plate heat exchangers working in the absorption facility and studies their application for two-phase processes.

7.2. Plate geometry

The geometrical parameters that characterize a typical chevron corrugated plate (Fig. 7.1) are the chevron (β) angle the corrugation depth or amplitude (b), the corrugation pitch (Λ) and the "surface enlargement factor" (ϕ), defined as the ratio between the actual area and the projected area of the plates.

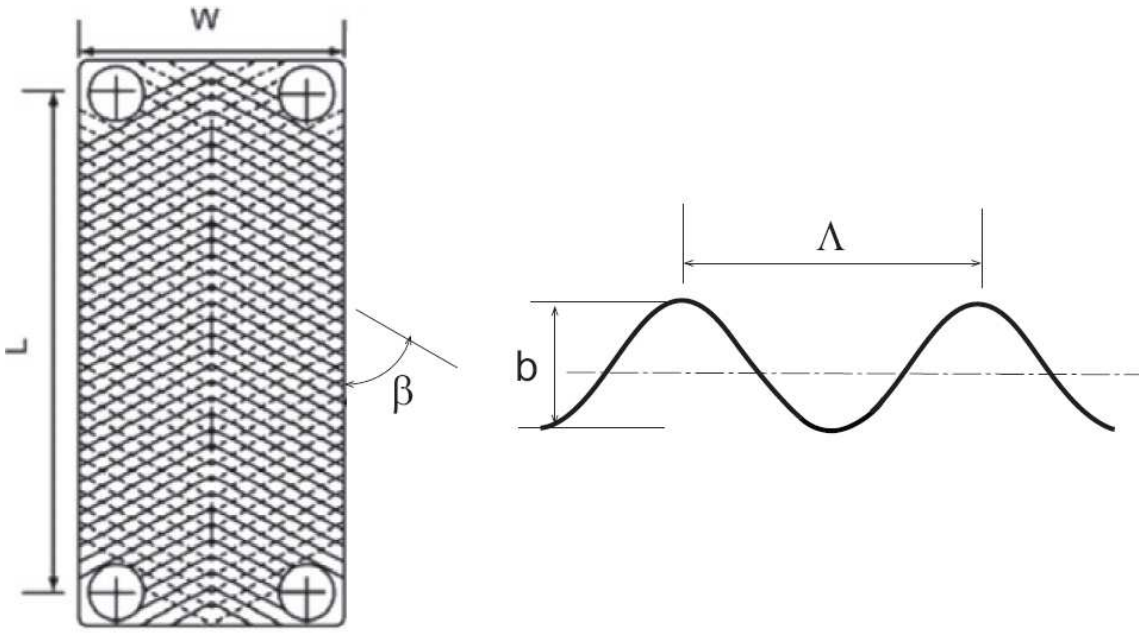

Fig. 7.1. Plate heat exchanger geometry. Source: Claesson, 2005.

It is not the purpose of this work to describe extensively the theory involved on PHEs. A more detailed general theory about PHEs, can be found in Cooper (1983), (Hewitt, 1998) and (Claesson, 2005), among others.

7.3. Correlations for single phase heat transfer and pressure drop

The literature review (chapter 2) demonstrates the large number of works published on heat transfer and pressure drop for single phase flow in plate heat exchangers. As the combinations of geometric parameters lead to a large number of cases, there is not any general theory or correlation that covers all of them.

Published results of other researchers on friction factor and Nusselt number are compared with the one obtained in this work. Some correlations depend on the chevron angle and they represent an intention to generalize some effects of the plate geometry. Several well known correlations available in the literature were selected taking into account a common chevron angle, β, and Reynolds number ranges for which the correlation is valid.

In the comparison it is included with particular interest the Bogaert and Bölcs correlations, because the exponent of the *Pr* number is not constant. Besides this, it is used by major Swedish manufacturer (Claesson, 2005). Eqs. from (7.1) to (7.14) have been extracted from both the original source (Bogaert and Bölcs, 1995; Muley and Manglik, 1997 and 1999, Yan and Lin, 1999; Warnakulasuriya et al, 2008) and works in which original correlations are explicitly given (García-Casales, 2007; Manglik, 1996).

The correlations used for comparison purposes, named by author, are listed bellow:

Nusselt number correlations:

- Wanniarachchi[+] et al.

$$Nu = j_{Nu} Pr^{1/3} \left(\eta / \eta_w \right)^{0.17} \tag{7.1}$$

where j_{Nu} is:

$$j_{Nu} = \sqrt[3]{j_{Nu,1}^3 + j_{Nu,t}^3}$$

with

[+] Valid for laminar, transition and turbulent flow regime (Muley and Manglik, 1996; García Casales, 2007)

$$j_{Nu,1} = \frac{3.65}{\left(90 - \frac{180\beta}{\pi}\right)^{0.445}} Re^{0.339}$$

$$j_{Nu,t} = \frac{12.6}{\left(90 - \frac{180\beta}{\pi}\right)^{1.142}} Re^{\left[0.646+0.00111\left(90-{}^{180\beta}/_{\pi}\right)\right]}$$

- Muley and Manglik

$$Nu = 0.44\left(\frac{6\beta}{\pi}\right)^{0.38} Re^{0.5} Pr^{\frac{1}{3}}\left(\frac{\eta}{\eta_w}\right)^{0.14} \qquad \text{for} \quad \begin{bmatrix} {}^{\pi}/_{6} \le \beta \le {}^{\pi}/_{3} \\ 30 \le Re \le 400 \end{bmatrix}$$

$$Nu = A(\beta)B(\phi)Re^{c(\beta)} Pr^{\frac{1}{3}}\left(\frac{\eta}{\eta_w}\right)^{0.14} \qquad \text{for} \quad \begin{bmatrix} {}^{\pi}/_{6} \le \beta \le {}^{\pi}/_{3} \\ 30 \le Re \le 400 \end{bmatrix} \qquad (7.2)$$

$$A(\beta) = 0.2668 - 0.006967 \cdot \beta + 7.244 \cdot 10^{-5} \cdot \beta^2$$
$$B(\phi) = 20.7803 - 50.9372 \cdot \phi + 41.1585 \cdot \phi^2 - 10.1507 \cdot \phi^2$$
$$C(\beta) = 0.728 + 0.0543 \cdot \sin(2\pi\beta/90 + 3.7)$$

- Yan and Lin .

$$Nu = 0.2121 Re^{0.78} Pr^{{}^{1}/_{3}} \qquad [200 \le Nu \le 2500] \qquad (7.3)$$

- Warnakulasuriya et al.

$$Nu = 0.292 Re^{0.705} Pr^{0.35} \qquad [250 \le Re \le 1100] \qquad (7.4)$$

- Bogaert and Bölcs

$$Nu = \begin{cases} 0.4621 Re^{0.4370} Pr^{\frac{1}{3}e^{\left(\frac{6.4}{\mathrm{Pr}+30}\right)}} \left(\frac{\mu}{\mu_w}\right)^{\frac{0.3}{(\mathrm{Re}+30)^{0.125}}} & [0 < Re < 20] \\ 1.73 Pr^{\frac{1}{3}e^{\left(\frac{6.4}{\mathrm{Pr}+30}\right)}} \left(\frac{\mu}{\mu_w}\right)^{\frac{0.3}{(\mathrm{Re}+30)^{0.125}}} & Re = 20 \\ 0.0875 RePr^{\frac{1}{3}e^{\left(\frac{6.4}{\mathrm{Pr}+30}\right)}} \left(\frac{\mu}{\mu_w}\right)^{\frac{0.3}{(\mathrm{Re}+30)^{0.125}}} & [20 < Re < 50] \\ 4.4 Pr^{\frac{1}{3}e^{\left(\frac{6.4}{\mathrm{Pr}+30}\right)}} \left(\frac{\mu}{\mu_w}\right)^{\frac{0.3}{(\mathrm{Re}+30)^{0.125}}} & Re = 20 \\ 0.4223 Re^{0.6012} Pr^{\frac{1}{3}e^{\left(\frac{6.4}{\mathrm{Pr}+30}\right)}} \left(\frac{\mu}{\mu_w}\right)^{\frac{0.3}{(\mathrm{Re}+30)^{0.125}}} & [50 < Re < 80] \\ 5.95 Pr^{\frac{1}{3}e^{\left(\frac{6.4}{\mathrm{Pr}+30}\right)}} \left(\frac{\mu}{\mu_w}\right)^{\frac{0.3}{(\mathrm{Re}+30)^{0.125}}} & Re = 80 \\ 0.26347 Re^{0.7152} Pr^{\frac{1}{3}e^{\left(\frac{6.4}{\mathrm{Pr}+30}\right)}} \left(\frac{\mu}{\mu_w}\right)^{\frac{0.3}{(\mathrm{Re}+30)^{0.125}}} & Re > 80 \end{cases} \tag{7.5}$$

- Martin*

$$Nu = 0.122 Pr^{1/3} \left(\frac{\mu}{\mu_w}\right)^{1/6} f \,\mathrm{Re}^2 \sin(2\beta)^{0.374} \tag{7.6}$$

Friction factor correlations:

- Wanniarachchi et al.

$$\varphi = 90 - \beta$$

$$f = \sqrt[3]{f_1^3 + f_t^3}$$

$$f_l = \frac{1774\phi^2}{\varphi^{1.026} Re} \tag{7.7}$$

$$f_t = \frac{46.6\phi^{(1+0.00423\varphi - 0.0000223\varphi^2)}}{\varphi^{1.08} Re^{1+0.00423\varphi - 0.0000223\varphi^2}}$$

* No Re given, but proved for 400<Re<10000 (García C. et al, 2007)

- Muley and Manglik

$$f = \begin{cases} \left[\left(\dfrac{40.32}{Re}\right)^5 + (8.12Re^{-0.5})^5\right]^{0.2} & [2 \le Re \le 200] \\ 1.274Re^{-0.15} & [Re \ge 1000] \end{cases} \quad (7.8)$$

- Warnakulasuriya et al.

$$f = 23.1Re^{-0.205} \quad [250 \le Re \le 1100] \quad (7.9)$$

- Bogaert and Bölcs

$$f = \begin{cases} 58.5Re^{-0.757} & [0 < Re < 20] \\ 5 & \mathrm{Re} = 30 \\ 2.6 + 120.797 / Re^{1.051} & [30 < Re < 200] \end{cases} \quad (7.10)$$

- Martin

$$\frac{1}{\sqrt{f}} = \left\{ \frac{\cos(\beta)}{\left[0.18\tan(\beta) + 0.36\sin(\beta) + \dfrac{\xi_0}{\cos(\beta)}\right]^{1/2}} + \frac{1-\cos(\beta)}{\left[3.8(\xi_{1,0})\right]^{1/2}} \right.$$

$$\mathrm{Re} < 2000 \begin{cases} \xi_0 = 64 / Re \\ \xi_{1,0} = \dfrac{597}{Re} + 3.85 \end{cases} \quad (7.11)$$

$$\mathrm{Re} < 2000 \begin{cases} \xi_0 = (1.8\log_{10}\mathrm{Re} - 1.5)^{-2} \\ \xi_{1,0} = \dfrac{39}{Re^{0.289}} \end{cases}$$

- Kovalenko and Maslov

$$f = \begin{cases} 17500Re^{-1}(2\Lambda / L) & [0 < Re < 15] \\ 915Re^{-0.25}(2\Lambda / L) & [50 < Re < 20000] \end{cases} \quad (7.12)$$

- Focke

$$f = \begin{cases} 1.2575 + 188.75Re^{-1} & [90 < Re < 400] \\ 6.7Re^{-0.209} & [400 < Re < 16000] \end{cases} \quad (7.14)$$

7.4. System analysis

7.4.1. Single phase heat transfer

Estimation of overall heat transfer coefficient (Eq. 7.18) is based on the following assumptions:

- The plate heat exchanger operates in steady conditions.
- The overall heat transfer coefficient, U, is based on log-mean temperature difference, ΔT_{lm}, of the heat exchanger.
- The temperatures and velocities of the fluids are uniforms trough the cross section of the channel.
- Fouling effects are negligible.
- There is not heat conduction in the direction of the fluid.
- In all the analysis, the properties of working fluids are calculated for the mean temperature between inlet and outlet.

7.4.1.1. Overall heat transfer coefficient

The following equation was used to find the heat transfer from each side and hence the overall experimental heat transfer coefficient:

$$\dot{Q} = \dot{m} \cdot C_p \cdot \Delta T \tag{7.15}$$

where ΔT is the temperature difference between the flow inlet and outlet.

Overall heat transfer coefficient can be obtained based on the log mean temperature difference:

$$\dot{Q} = U \cdot A \cdot \Delta T_{lm} \cdot F \tag{7.16}$$

where A is the projected area multiplied by the number of plates, used here like the heat transfer area. F is the ΔT_{lm} correction factor. The logarithmic mean temperature difference is (Incropera, 1999):

$$\Delta T_{lm} = \frac{\Delta T_2 - \Delta T_1}{\ln\left(\Delta T_2 / \Delta T_1\right)} \tag{7.17}$$

For counterflow exchanger:

$$\Delta T_1 = T_{h,i} - T_{c,o}$$

$$\Delta T_2 = T_{h,o} - T_{h,i}$$

From Eqs. (7.15) and (7.16), experimental overall heat transfer coefficient is calculated as:

$$U = \frac{\dot{m} \cdot C_p \cdot \Delta T_{lm}}{A \cdot \Delta T_{lm} \cdot F} \tag{7.18}$$

Overall heat transfer coefficient also can be calculated from:

$$\frac{1}{U} = \frac{1}{h_h} + \frac{1}{h_c} + \frac{e}{k_p} \tag{7.19}$$

where h_h and h_c are obtained using

$$h = \frac{Nu \cdot k_p}{D_h} \tag{7.20}$$

The third term in Eq. (7.19) represents the conduction resistance corresponding to the unit of heat transfer area.

Empirical correlations using Eq. (7.21) are used to find the Nusselt number and therefore the film heat transfer coefficient:

$$Nu = C \cdot Re^m \cdot Pr^n \tag{7.21}$$

with

$$\mathrm{Re} = \frac{\rho_f \cdot u_f \cdot D_h}{\mu_f} \tag{7.22}$$

u_f is the mean velocity in the channel section:

$$u_f = \frac{\dot{m}_f}{\rho_f (Np/2)\Lambda w} \tag{7.23}$$

and

$$\mathrm{Pr} = \frac{\mu_f \cdot C_p}{k_f} \tag{7.24}$$

Depending on flow conditions (Re, Pr, μ/μ_w) and chevron angle, reported values (Manglik, 1996) of constants m and n of Eq. (7.21) have the following range: $0.05 < C < 1.12$; $0.33 < m < 0.85$ and $0.30 < n < 0.45$.

7.4.1.2. The Wilson plot method

As above mentioned, due to the large variety of existing plates and geometries in the market, there is not enough general information to predict the thermal behaviour of the fluid inside a plate heat exchanger. This makes unfeasible the use of a standard correlation for all plate heat exchangers. Therefore, it is necessary to experimentally characterize the heat exchangers used in our experiments.

The Wilson plot is a technique to estimate the film coefficients in several types of heat transfer processes and to obtain general heat transfer correlations from measured values. The difficulties related to analytical solution of convection problems and measurement of surface temperature for an imposed heat flow makes it a method of interest to calculate the convective heat transfer coefficient of heat exchangers.

In the following, the basis of Wilson plot method is given, based on the document published by Fernández-Seara et. al. (2005). The general premises are given for a shell and tube heat exchanger, in order to explain the method. Then, it will be applied to the case studied here, for PHEs.

This method, proposed to evaluate the film heat transfer coefficient in shell and tube condensers, is based on the separation of the overall thermal resistance into convective thermal resistance and the remaining thermal resistances involved in the global process. The basic principles of heat transfer show that the overall thermal resistance is the sum of the thermal resistances in series corresponding to each one of

the different heat transfer processes, as expressed in Eq. (7.19). Referring to outer surface in a shell and tube condenser (the original application):

$$\frac{1}{U_o \cdot A_o} = \frac{1}{h_o \cdot A_o} + \frac{1}{h_{foul,o} \cdot A_o} + \frac{\ln(d_o / d_i)}{2 \cdot \pi \cdot k_t \cdot L_t} + \frac{1}{h_{foul,i} \cdot A_i} + \frac{1}{h_i \cdot A_i} \tag{7.25}$$

Taking into account the specific conditions of the condensation process, the thermal resistances due to the outside tubes convection process, the outer and inner fouling films and the tube wall can be considered constant (Eq.7.26), where C_1 is the constant.

$$\frac{1}{h_o \cdot A_o} + \frac{1}{h_{f,o} \cdot A_o} + \frac{\ln(d_o / d_i)}{2 \cdot \pi \cdot k_k \cdot L_t} + \frac{1}{h_{f,i} \cdot A_i} = C_1 \tag{7.26}$$

The film heat transfer coefficient for a turbulent flow in circular tubes can be obtained from Eq. (7.27), with the exponent of the Prandtl number assumed known and equal to 0.4.

$$\frac{1}{h_i \cdot A_i} = \frac{1}{C \cdot \mathrm{Re}^m \cdot \mathrm{Pr}^{0.4} \left(\frac{k_l}{d_i} \right) \cdot A_i} = C_2 \cdot \frac{1}{\mathrm{Re}^m} \tag{7.27}$$

Then, the overall thermal resistance is obtained as a linear function of $1/\mathrm{Re}^m$, as shown in Eq. (7.28), which tell us C_1 is the intercept of the regression line and the overall thermal resistance axis and C_2 is the slope of the straight line (Fig. 7.2).

$$\frac{1}{U_o \cdot A_o} = C_1 + C_2 \cdot \frac{1}{\mathrm{Re}^m} \tag{7.28}$$

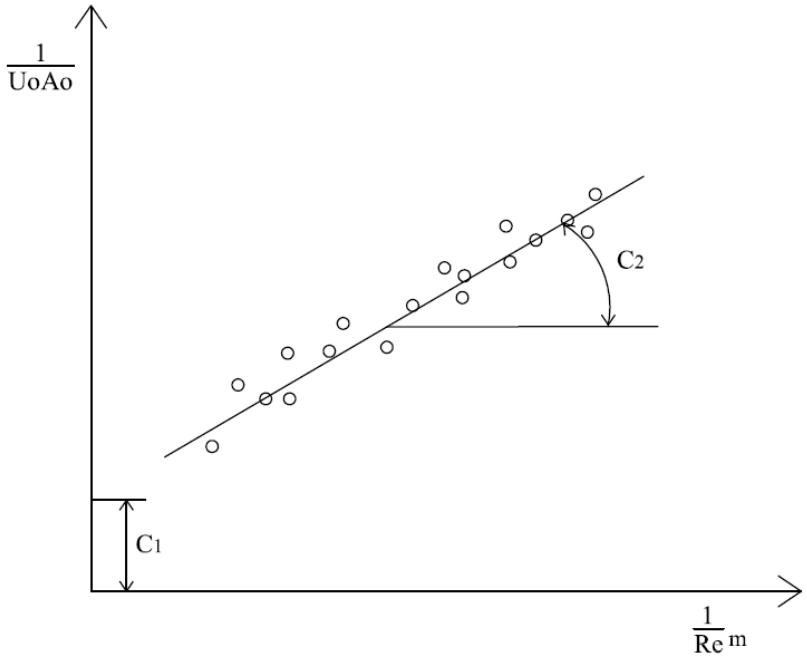

Fig. 7.2. Wilson plot of Eq.7.28

If the value of the exponent m is assumed, then the experimental values of the overall thermal resistance can be represented as a function of the experimental values of $1/Re^m$ and the equation of the straight line that fits the experimental data can be obtained by a simple linear regression. Once the constants C_1 and C_2 are determined, then the external and internal convection coefficients for a given flow rate and the unknown parameter C in equations (7.27) can be calculated.

7.4.1.3. The modified Wilson plot method

In the cases in which there is not a dominant resistance and one of the film coefficients is unknown, it is necessary to apply a calculation technique different from the Wilson plot method.

Moreover, the Wilson method requires the assumption of the exponents of the Reynolds and the Prandtl dimensionless numbers. Therefore, a modification of the method is commonly applied to overcome these limitations. This variation is known as the modified Wilson plot method.

The modified Wilson plot method is based on the described Wilson plot method but takes into account a second linear equation obtained by applying logarithms to both sides of Eq. (7.28) plus an iteration procedure.

After applying logarithms to both sides of equation (7.28) and rearranging it, Eq. (7.29) is obtained. It results in a linear equation of the term $\ln[1/((1/U_oA_o) - C_1)]$ as a function of ln(Re), with the term $\ln(1/C_2)$ being the intercept between the straight line and the vertical axis and the parameter m the slope of the straight line (Fig. 7.3).

$$\ln\left(\frac{1}{(1/U_o A_o)-C_1}\right)=\ln\left(\frac{1}{C_2}\right)+m\cdot\ln(\mathrm{Re}) \tag{7.29}$$

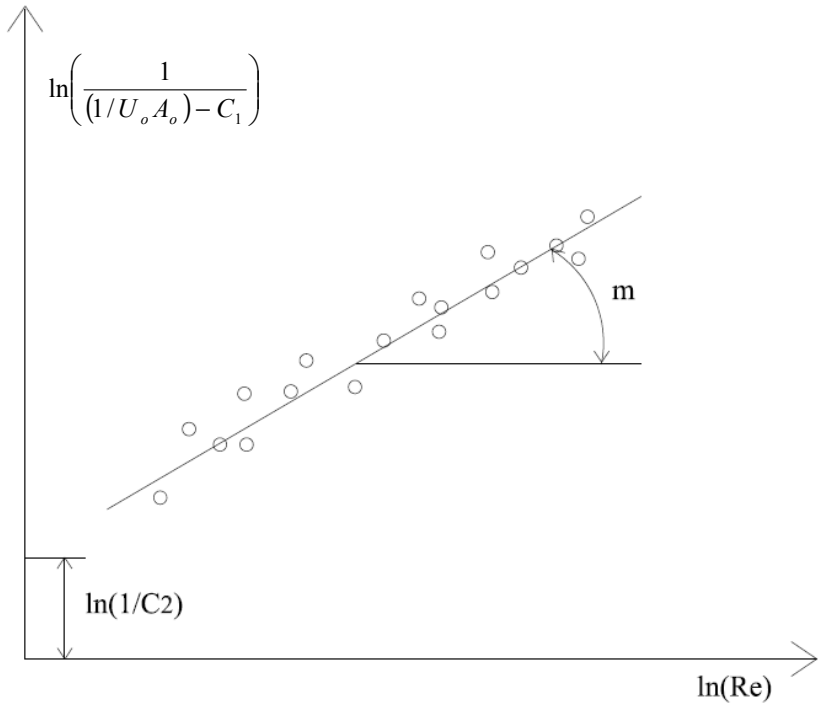

Fig. 7.3. Wilson plot of Eq.7.29

The iteration procedure for obtaining the value of the exponent m consists of:

1. The application of the Wilson plot method assuming the value of the exponent m. Then the values of C_1 and C_2 are obtained.
2. Taking into account the values of the overall thermal resistance and the Reynolds number obtained from the measured experimental data, the values of the term $\ln[1/((1/U_oA_o) - C_1)]$ are plotted as a function of ln(Re). Then, the equation of the straight line that fits the experimental data is obtained by a simple linear regression.
3. The value of the parameter m is obtained from the equation of the straight line since m is the slope of the line, according to Eq. (7.29).

4. If the value of m obtained is equal to the value initially assumed, then the process is finished and the value of the exponent m is determined. Otherwise, the iteration process is repeated from step 1 taking a new value of m.

Therefore, the general correlation is determined assuming only the value of the exponent of the Prandtl number, n.

7.4.1.4. Use of the modified Wilson plot method in PHEs

Although Wilson plot method was first used for shell and tube heat exchanger, it may be modified for vertical plates in PHEs/BPHEs, as presented next. Many works have reported the use of this technique for estimation of film heat transfer coefficients (Jokar et al., 2004; Longo et al., 2004; Hsieh and Lin, 2003 and 2002; Yan and Lin, 1999; Muley an Manglik, 1999 and 1996; among others).

Applying the ideas previously explained, for the case in which both sides are unknown and considering that both sides of the PHE have the same geometry, the procedure to use the modified Wilson plot technique is explained next.

The form of viscosity correction $(\mu/\mu_w)^{0.14}$ has been included in calculations, considering the effect of temperature on viscosity, being the Water-LiBr a viscous solution, as well as the thermal oil. The use of viscosity correction is used by many researchers, among them Muley and Manglik citing other reference (Sieder and tate, 1936).

with

$$h = C\,\mathrm{Re}^{m}\,\mathrm{Pr}^{n}\left(\frac{\mu}{\mu_w}\right)^{0,14}\left(\frac{k}{D_h}\right) \tag{7.30}$$

By substituting Eq. (7.30) in Eq. (7.19) and rearranging yields

$$\left(\frac{1}{U}-\frac{e}{k_p}\right)h'_h = \frac{1}{C_h}+\frac{1}{C_c}\frac{h'_h}{h'_c}; \qquad h = Ch'_h \tag{7.31}$$

Rewriting (7.31):

$$\left(\frac{1}{U}-\frac{e}{k_p}\right)\mathrm{Re}_h^m\,\mathrm{Pr}_h^n\left(\frac{\mu}{\mu_w}\right)_h^{0.14}\left(\frac{k_h}{D_h}\right)=\frac{1}{C_h}+\frac{1}{C_c}\frac{\mathrm{Re}_h^m\,\mathrm{Pr}_h^n\,k_h(\mu/\mu_w)_h^{0.14}}{\mathrm{Re}_c^m\,\mathrm{Pr}_c^n\,k_c(\mu/\mu_w)_c^{0,14}} \tag{7.32}$$

A first plot is obtained by using Eq. (7.32). Taking an initial value for m, values for C_h and C_c can be obtained as the intercept and the slope, respectively, by using the linear regression method.

After applying logarithms to both sides of equation (7.32) and rearranging again it results:

$$\ln\left(\left(\left(\frac{1}{U}-\frac{e}{k_p}-\frac{1}{C_c\,\mathrm{Re}_c^m\,\mathrm{Pr}_c^n(k_c/D_h)(\mu/\mu_w)_c^{0.14}}\right)\mathrm{Pr}_h^n(k_h/D_h)(\mu/\mu_w)_h^{0.14}\right)^{-1}\right) \tag{7.33}$$
$$=m\ln(\mathrm{Re}_h)+\ln(C_h)$$

A new value for m is obtained and iteration continues until convergence.

7.4.2. Single phase pressure drop

Pressure drop is one of the main parameters to be considered when designing and operating a PHE, because it is considered high in comparison with other kind of heat exchanger. In fact, this particularity will make the study of phase change process more complex (as the one that take place in the generator) using PHEs. According to Muley and Manglik (1999), while the chevron surface corrugations promote higher heat transfer coefficients, there is a higher pressure drop penalty. The friction factors could be 13 to 44 times higher compared with flat plate, increasing with β. In a plate heat exchanger, the pressure drop requirements can be closely met due to the flexibility involved in the choice of plates with respect to the size, configuration, number and the arrangement of flow passes (Warnakulasuriya, 1999).

The friction factor of the PHEs used in this work is defined based on the hydraulic diameter and the projected length between the inlet and outlet ports:

$$f = \frac{\Delta P_f}{2 \cdot \rho \cdot u_m^2 \cdot \left(\frac{L}{D_h} \right)} \tag{7.34}$$

From the measured overall pressure drop across the generator, the frictional pressure drop for single phase flow can be calculated as:

$$\Delta P_f = \Delta P_t - \Delta P_{port} - \Delta P_c \tag{7.35}$$

ΔP_t is the total pressure drop measured with the differential pressure transducer, ΔP_{port} is the pressure losses at outlet and inlet manifolds of the PHE and ΔP_c is the pressure of the fluid column inside the PHE. Regarding ΔP_{port}, a widely cited reference giving an empirically estimated correlation for this pressure drop, empirically estimated is Shah and Focke (1988):

$$\Delta P_{port} = 1{,}5 \cdot \left(\frac{G_{port}^2}{2 \cdot \rho} \right) \tag{7.36}$$

And ΔP_c can be evaluated as:

$$\Delta P_c = \rho \cdot g \cdot L \tag{7.37}$$

The general form of empirical correlation used to find the dependence of the experimental friction factor on the Reynolds number and flow conditions is:

$$f = \frac{C}{\mathrm{Re}^a} \tag{7.38}$$

where C and a are constants depending on Re and Pr numbers.

7.4.3. Two-phase Heat transfer

The procedure to quantify the flow boiling heat transfer coefficient of the solution flow from the measured data is explained in the following.

In the solution side, the boiling process does not necessarily take place from the entry, because the solution can enter in a subcooled state. If the solution heat exchanger

is efficient enough boiling can appear in it and thus, boiling occurs in the entire generator surface. If the solution enters in subcooled state, the heat transfer in the entrance occurs in single phase flow and then the boiling starts. Fig. 7.4 attempts to illustrate the process tanking place in the generator in order to explain the subsequent analysis. Observe that solution temperature distribution take into account the important effect of pressure drop in the PHE, which is included in the data analysis.

As illustrated in Fig. 7.4, there is a single phase heat transfer solution region (the entrance section) and a boiling region. The overall heat transfer coefficient, named from now on U_{2ph}, is calculated as:

$$U_{2ph} = \frac{\dot{Q}_{2ph}}{A_{2ph} \cdot \Delta T_{lm2ph}} \tag{7.39}$$

In order to estimate the area, A_{2ph}, the boiling heat transfer, $\dot{Q}_{2ph}$, and the logarithmic temperature difference ΔT_{lm2ph} corresponding to two-phase region it is necessary to consider the following equation system presented:

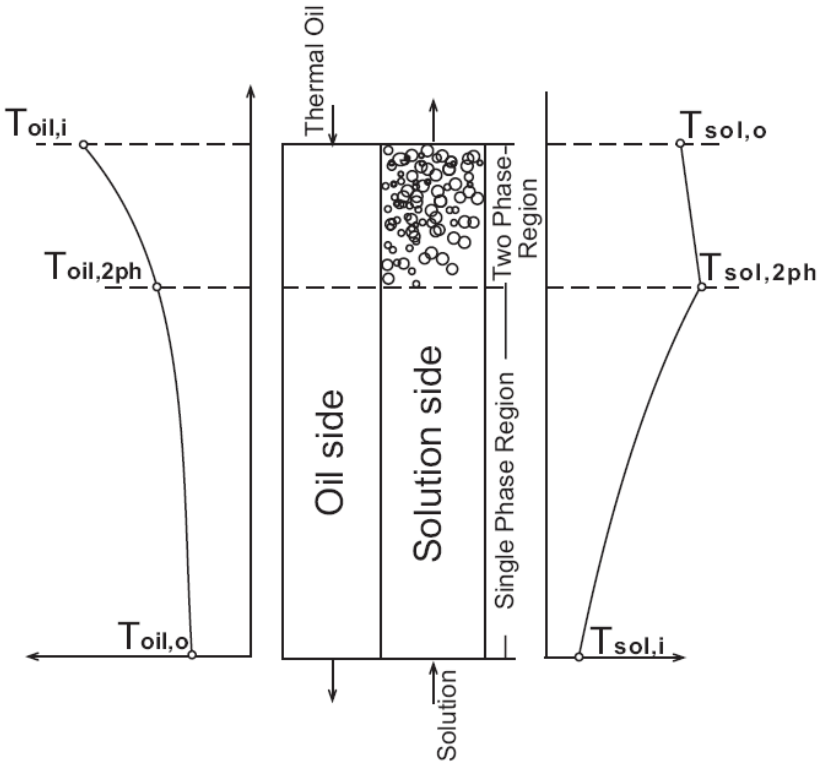

Fig. 7.4. Scheme of temperature distribution in the generator. Based on (Hsieh and Lin, 2002)

$$\dot{Q}_{2ph} = \dot{Q}_G - \dot{Q}_{1ph} \tag{7.40}$$

$$\Delta T_{lm\,2ph} = \frac{(T_{oil,i} - T_{sol,o}) - (T_{oil,2ph} - T_{sol,2ph})}{\ln\left[\frac{(T_{oil,i} - T_{sol,o})}{(T_{oil,2ph} - T_{sol,2ph})}\right]} \tag{7.41}$$

where $T_{oil,2ph}$ and $T_{sol,2ph}$ are respectively the temperatures of the oil and solution at the position in which solution starts to boil in the generator. They are deduced from:

$$\dot{Q}_G = \dot{m}_{oil} \cdot C_{p,oil} \cdot \left(T_{oil,i} - T_{oil,o}\right) \tag{7.42}$$

$$\dot{Q}_{oil,1ph} = \dot{m}_{oil} \cdot Cp_{oil} \cdot \left(T_{oil,2ph} - T_{oil,o}\right) = \dot{m}_{sol} \cdot Cp_{sol} \cdot \left(T_{sol,2ph} - T_{sol,in}\right) \tag{7.43}$$

And

$$\dot{Q}_{oil,1ph} = \dot{Q}_{sol,1ph} = U_{1ph} A_{1ph} \Delta T_{lm,1ph} \tag{7.44}$$

$$\Delta T_{lm,1ph} = \frac{(T_{oil,2ph} - T_{sol,2ph}) - (T_{oil,o} - T_{sol,in})}{\ln\left[\frac{(T_{oil,2ph} - T_{sol,2ph})}{(T_{oil,o} - T_{sol,in})}\right]} \tag{7.45}$$

$$\frac{1}{U_{1ph}} = \frac{1}{h_{sol,1ph}} + \frac{1}{h_{oil}} + R_{wall} \tag{7.46}$$

Previous single phase experiments allow quantifying $h_{sol,1ph}$ and h_{oil}. Then, Eq (7.43) and (7.44) can be solved by numerical iteration.

Introducing the single and two-phase pressure drop:

$$\Delta P_t = \Delta P_{1ph} + \Delta P_{2ph} \tag{7.47}$$

$$\Delta P_{1ph} = \Delta P_f + \Delta P_c + \Delta P_{port} = 2 f_{1ph} \rho u_m^2 L_{1ph} / D_h + \rho g L_{1ph} + 1{,}5 G_{port}^2 / 2\rho \tag{7.48}$$

f_{1ph} is known from previous obtained correlations (section 7.4.2) for solution side in the same plate heat exchanger.

$$L_{1ph} = A_{1ph} / P \tag{7.49}$$

$$P = A_t / L \tag{7.50}$$

where P is the perimeter

$$A_t = A_{1ph} + A_{2ph} \tag{7.51}$$

$$P_{G,i} = P_{G,o} + \Delta P_t \tag{7.52}$$

$$P_{i,2ph} = P_i - \Delta P_{1ph} \tag{7.53}$$

$$T_{sol,2ph} = f(X_{sol}, P_{i,2ph}) \tag{7.54}$$

The flow boiling heat transfer coefficient in the solution side is estimated from:

$$\frac{1}{h_{sol,2ph}} = \frac{1}{U_{2ph}} - \frac{1}{h_{oil}} - R_{wall} \tag{7.55}$$

The quality of vapour is:

$$x_v = \frac{\dot{m}_v}{\dot{m}_{weak}} \tag{7.56}$$

7.4.4. Two-phase pressure drop

Because of the flow acceleration when the liquid evaporates and the decrease in fluid density, the pressure drop associated to this ΔP_a must be taken into account. Therefore, in order to calculate the frictional component of the pressure drop in a two-phase flow, Eq. (7.57) is followed.

$$\Delta P_f = \Delta P_t - \Delta P_a - \Delta P_c - \Delta P_{port} \tag{7.57}$$

$$\Delta P_a = \left(\dot{m}_{eq}\right)^2 \cdot \left(\upsilon_v - \upsilon_l\right) \cdot \Delta x \tag{7.58}$$

where υ_v and υ_l are the specific volume of liquid and vapor phase, Δx is the vapour quality change between inlet and outlet (or the steam quality at manifold outlet, if the inlet flow is a single phase one).

$$\Delta P_c = g \cdot \rho_m \cdot L \tag{7.59}$$

$$\Delta P_{port} = \frac{1{,}5 \cdot \left(\dot{m}_{eq}\right)^2}{2 \cdot \rho_m} \tag{7.60}$$

with

$$\rho_m = \left[x_m / \rho_v + \left(1 - x_m\right) / \rho_L\right]^{-1} \tag{7.61}$$

ρ_m is the average two-phase density between inlet and outlet calculated at the average vapour quality x_m between the inlet and outlet.

$$\dot{m}_{eq} = \dot{m} \cdot \left[\left(1 - x_m\right) + x_m \cdot \left(\frac{\rho_l}{\rho_v}\right)^{1/2}\right] \tag{7.62}$$

Then, the equivalent Reynolds number will be:

$$\mathrm{Re}_{eq} = \frac{\dot{m}_{eq} \cdot D_h}{\mu_l} \tag{7.63}$$

The friction factor can be correlated as:

$$f_{2ph} = C' \mathrm{Re}_{eq}^m \tag{7.64}$$

7.5. Heat Transfer and Pressure Drop Analysis in Plate Heat Exchangers

The experimental results and correlations obtained for three plate heat exchangers, functioning as generator, subcooler and solution heat exchanger are shown and analyzed next. Single phase heat transfer analysis was carried out for all cases. Pressure drop measurements were collected for generator and a single and two-phase heat transfer and pressure drop analysis was carried out for this component. The case of condenser is not analyzed in this work. It is not a critical element in limiting the power of the machine under study. The subject of interest in this work is the analysis of BPHE working with water-LiBr solution.

7.5.1. Subcooler

The study and characterization of the subcooler is important to put into practice the concept of adiabatic absorption. The addition of this external heat exchanger is necessary in order to cool the solution.

The Wilson plot method and its modifications, applied in this section, allow the estimation of such heat transfer coefficient based on the experimental measurements and the subsequent construction of appropriated correlations, as above explained. The obtained results will be useful to predict the functioning of the PHE for research and simulation.

A photograph of Alfa Laval model **CB26** is shown on Fig. 7.5. It is a single pass brazed PHE, working in counter current flow configuration. It contains 10 corrugated plates with an effective heat transfer area per plate of 0,025 m^2. As explained on chapter 3, the cold fluid is water coming from the cooling tower and the hot fluid is the LiBr solution, shown schematically in Fig. 7.6.

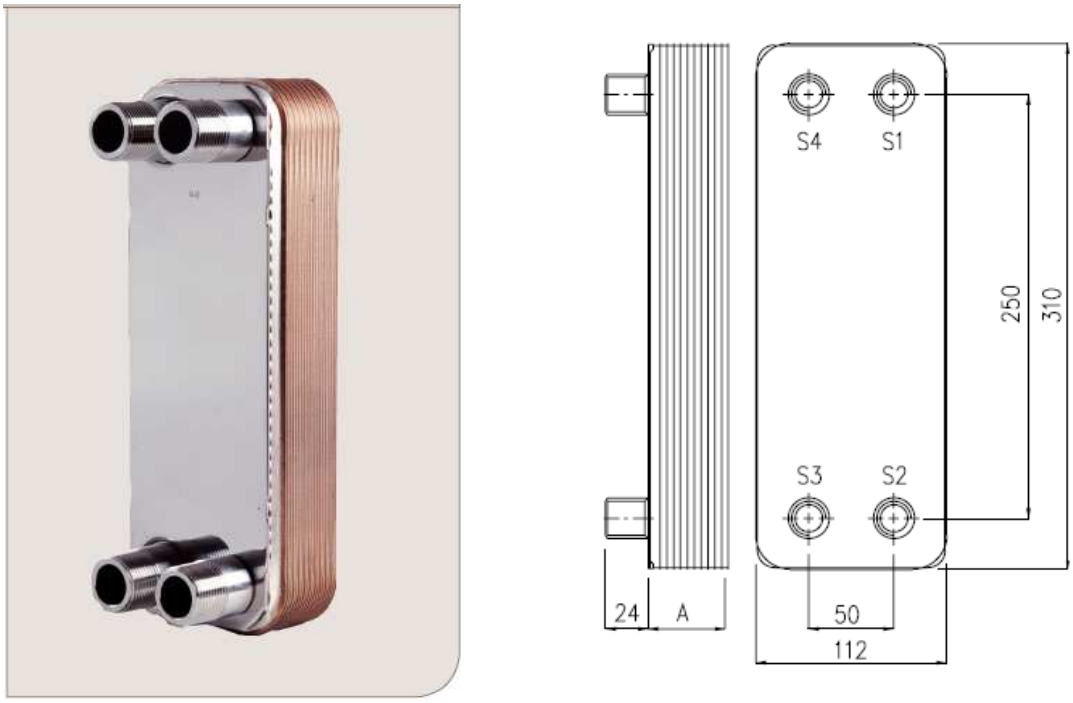

Fig. 7.5. Photography of the Brazed PHE operating as sub-cooler: Alfa Laval model CB26. Source: alfalaval.com

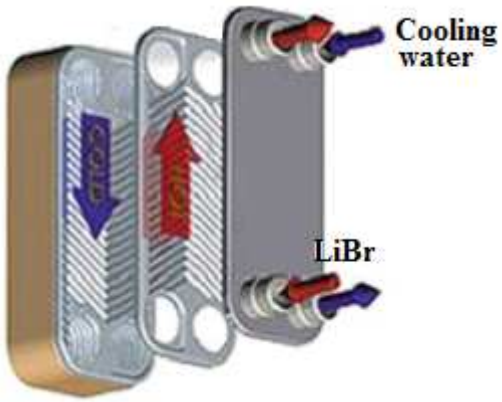

Fig. 7.6. Flow operation of cold and hot fluids in the subcoler. Based on: alfa-biz.com

7.5.1.1. Application of the Modified Wilson Plot Method

Ranges of solution mass flow rate and temperatures of the fluids for the experimental campaign are given in Table 7.1. The water mass flow rate was kept approximately constant at 420 g/s.

Variable	Water	Solution
Mass flow rate	403 - 430 g/s	70 - 270 g/s
Inlet temperature	17 – 30 ºC	30 – 43 ºC
Outlet temperature	19 – 31 ºC	22 – 32 ºC
Solution concentration		57 – 63 %

Table 7.1. Operating condition ranges of mass flow rates and temperatures of fluids during the experimental campaign for the subcooler.

Applying the procedure explained on section 7.4.1.4, a value for m is assumed. It is recommended that the influence of the Prandtl number on the Nusselt number to be characterised by an exponent of 1/3 following Garcia-Casales (2007). Also, according to Muley and Manglik (1997) this value is reasonable for moderate viscous flows.

From Eq. (7.15), the experimental value of the overall heat transfer coefficient U is obtained from external and internal flows. μ_w is calculated at wall condition assuming T_w as the average temperature between the water and solution mean temperature:

$$T_w = \frac{\left(T_{cw} + T_{sol}\right)}{2} \tag{7.63}$$

$$T_{mean} = \frac{\left(T_i + T_o\right)}{2} \tag{7.64}$$

The Wilson plot of Eq. (7.32) is illustrated in Fig. 7.7 for resulting m, with:

$$Y_1 = \left(\frac{1}{U} - \frac{e}{k_p}\right) \mathrm{Re}_{sol}^{m} \, \mathrm{Pr}_h^{1/3} \left(\frac{\mu}{\mu_w}\right)_h^{0.14} \left(\frac{k}{D_h}\right) \tag{7.65}$$

And

$$X_1 = \frac{\mathrm{Re}_{sol}^{m} \, \mathrm{Pr}_{sol}^{1/3} \, k_h \left(\mu/\mu_w\right)_{sol}^{0.14}}{\mathrm{Re}_{cw}^{m} \, \mathrm{Pr}_{cw}^{1/3} \, k_{cw} \left(\mu/\mu_w\right)_{cw}^{0.14}} \tag{7.66}$$

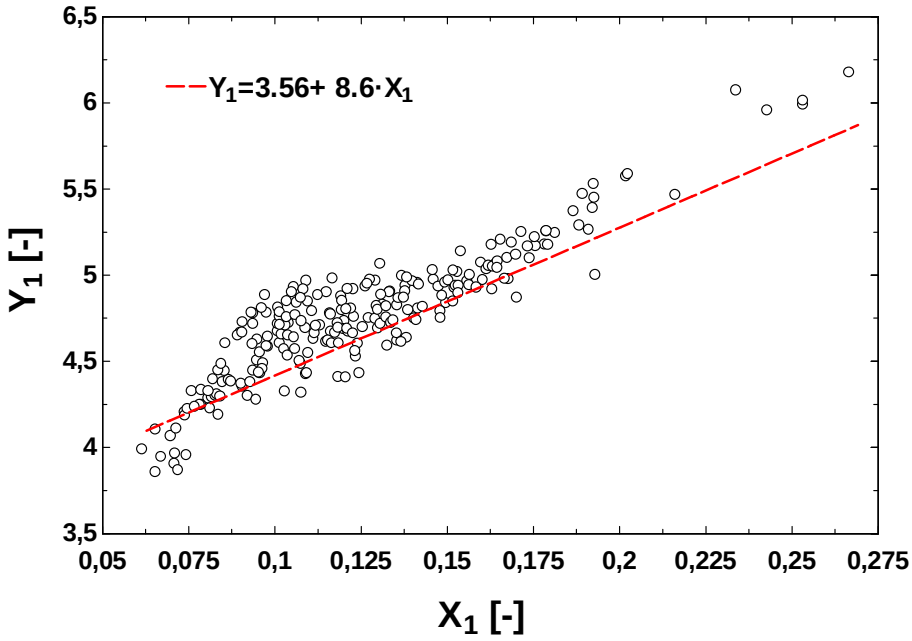

Fig. 7.7. Wilson plot of Eq. (7.32) for the subcooler

And from Eq. (7.33):

$$Y_2 = \ln\left(\left(\left(\frac{1}{U} - \frac{e}{k_p} - \frac{1}{C_{cw}\,\mathrm{Re}_{cw}^{m}\,\mathrm{Pr}_{cw}^{1/3}\left(k_{cw}/D_h\right)\left(\mu/\mu_w\right)_{cw}^{0.14}}\right)\mathrm{Pr}_{sol}^{1/3}\left(k_{sol}/D_h\right)\left(\mu/\mu_w\right)_{sol}^{0.14}\right)^{-1}\right) \tag{7.67}$$

And

$$X_2 = m\ln\left(\mathrm{Re}_{sol}\right) \tag{7.68}$$

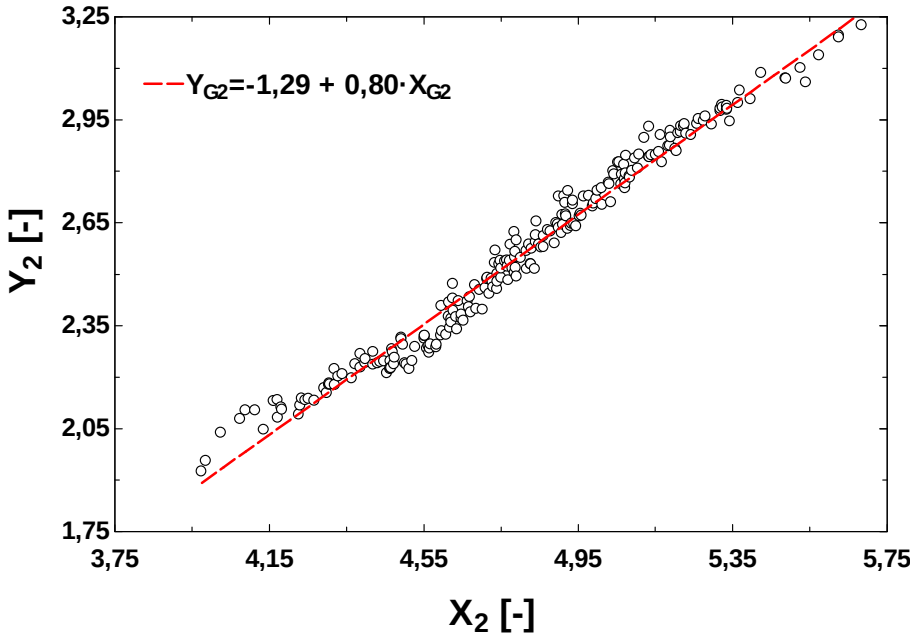

Fig. 7.8. Wilson Plot of Eq. (7.33) for the subcooler

The constant for the hot fluid C_{sol} is obtained as $C_{sol} = e^{Y(0,Y_2)}$.

7.5.1.2. Results and discussion

After this analysis, the Nusselt number calibration equations for both hot and cold side in the plate heat exchanger under study are found:

For hot (solution) side: $24 < Pr_{sol} < 34$

$$Nu = 0{,}274 \cdot \mathrm{Re}^{0.8} \cdot \mathrm{Pr}^{1/3} \left(\mu / \mu_w\right)_{sol}^{0.14} \qquad [50 < \mathrm{Re} < 300] \qquad (7.69)$$

For cold (water) side: $5{,}5 < \mathrm{Pr_c} < 7{,}5$

$$Nu = 0{,}11 \cdot \mathrm{Re}^{0.8} \cdot \mathrm{Pr}^{1/3} \cdot \left(\mu / \mu_w\right)_{c}^{0.14} \qquad [1.600 < \mathrm{Re} < 2.300] \qquad (7.70)$$

Experimental heat transfer coefficient is compared to calculated values, obtained through Eqs. (7.69) and (7.70). See results on Fig. 7.9. Most of the experimental points are in the zone of 5% of deviation.

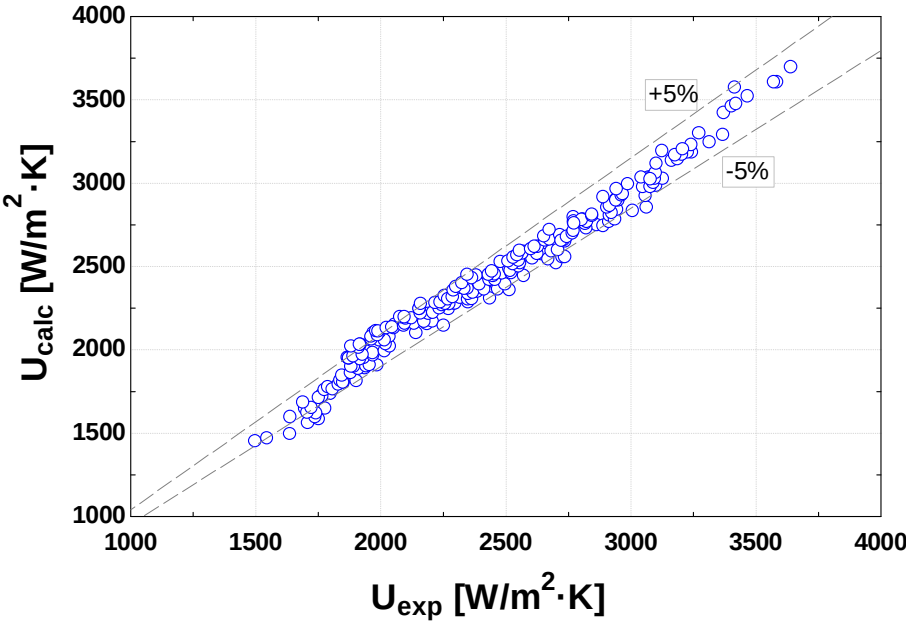

Fig. 7.9. Experimental vs. calculated heat transfer coefficient for the subcooler

The resulting range of U and Nu are:

$$1500 < U < 3650$$

$$20 < Nu < 80$$

Local velocities, which affect the heat transfer coefficient, are very dependent on the mass flow rate. This affirmation, illustrated in the work of Warnakulasuriya et al. (2008) was also found in this work. Fig. 7.10 manifest the variation of U_{exp} vs. the recirculated mass flow rate for all experimental points analyzed.

Here the expected influence of the recirculated mass flow rate $\dot{m}_r$ is clear. As $\dot{m}_r$ is higher and U increases, with more pronounced effect at lower $\dot{m}_r$.

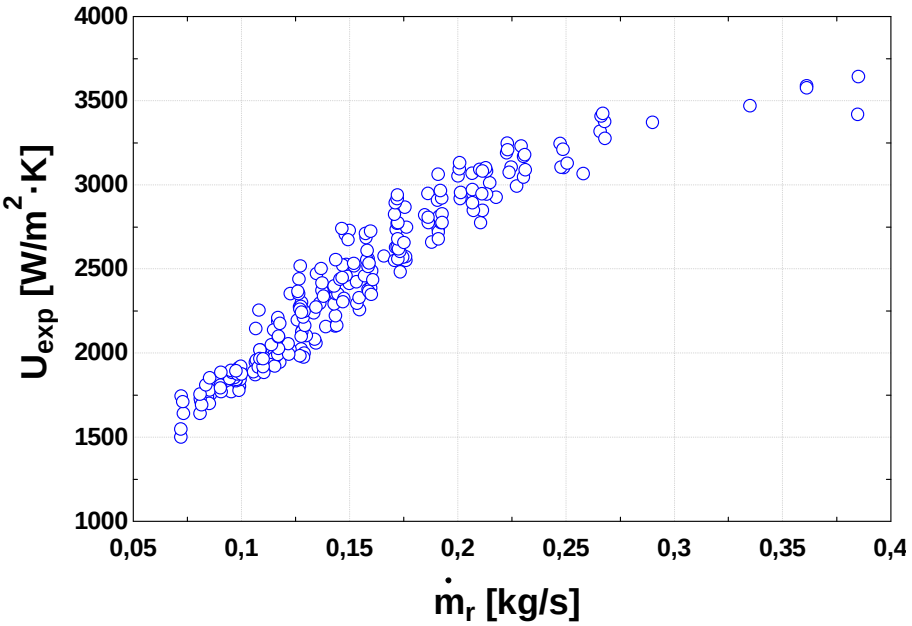

Fig. 7.10. Experimental overall heat transfer coefficient of LiBr vs. recirculated mass flow rate.

The calculated values, $U_{calc,}$ match the experimental results for all range of Reynolds number, which is enhanced by inclusion of viscosity correction in the correlations obtained (Fig. 7.11).

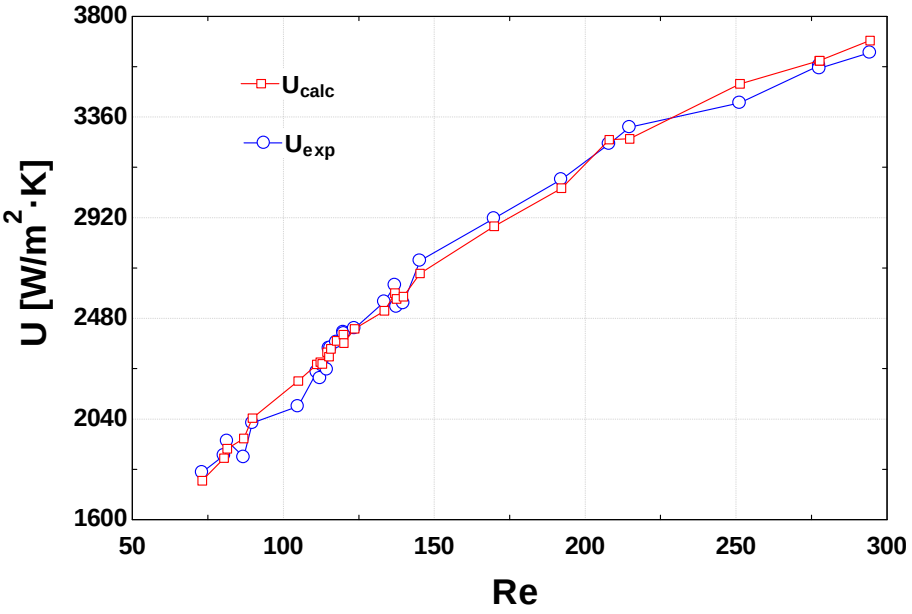

Fig. 7.11. Calculated and experimental values of overall heat transfer coefficient vs. Reynolds number. $T_{sol,in}$ = 36ºC.

As already explained in Chapter 2, devoted to state of the art, the heat transfer and pressure drop in plate heat exchangers are the scope of many investigations. In Fig.

7.12 the experimental data are compared with correlations reported in the open literature, given in section 7.3, according to the corresponding valid Re range reported.

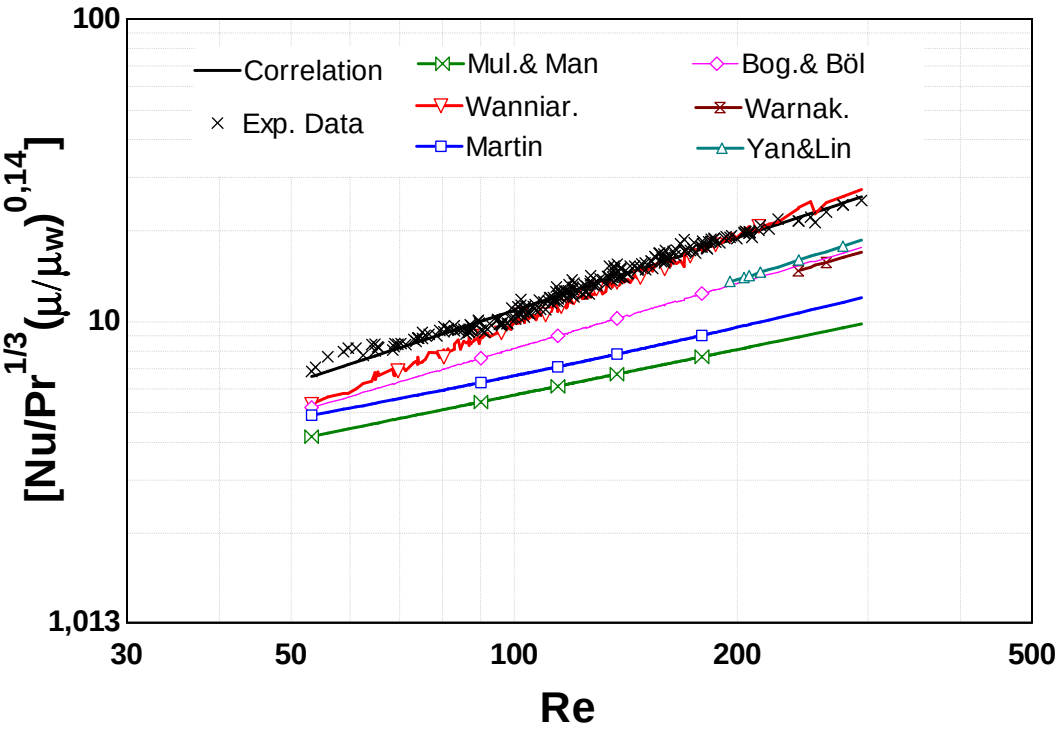

Fig. 7.12. Comparison of Nusselt number data with published correlations

There is a good agreement between the experimental values obtained in the present work and Wanniarachchi et al. prediction, although at low Reynolds number some deviation is observed. The rest of correlations under predict the data, being the Muley and Manglik, and Martin correlations those that deviate most with a distinct slope compared to the rest of correlations. Bogaert and Bölcs, Warnakulasuriya and Worek, and Yan and Lin correlations are closer.

7.5.2. Solution heat exchanger

The ranges of variables and non dimensional numbers corresponding to weak and strong solution are given in table 7.2.

Variable	Weak solution	Strong solution
Mass flow rate	11,5-100 g/s	11-99 g/s
Inlet temperature	29-42 ºC	61-80 ºC
Outlet temperature	39-65 ºC	40-66 ºC
Solution concentration	57,9-62,5	59-65 %

Table7.2. Operating condition ranges of mass flow rates and temperatures of fluids during the experimental campaign for the solution heat exchanger

The manufacturer's model of the solution heat exchanger installed is the same as the one used as a subcooler. The correlation obtained above can then be used to find the calculated overall heat transfer coefficient, U_{calc}. Fig. 7.13 shows the results obtained for U_{calc}, compared with the experimental results. The match is not as accurate as for the case of subcooler, but most of the points are in the zone of 10% deviation. The difference could be associated to the operational aspects discussed in section 4.3.2.

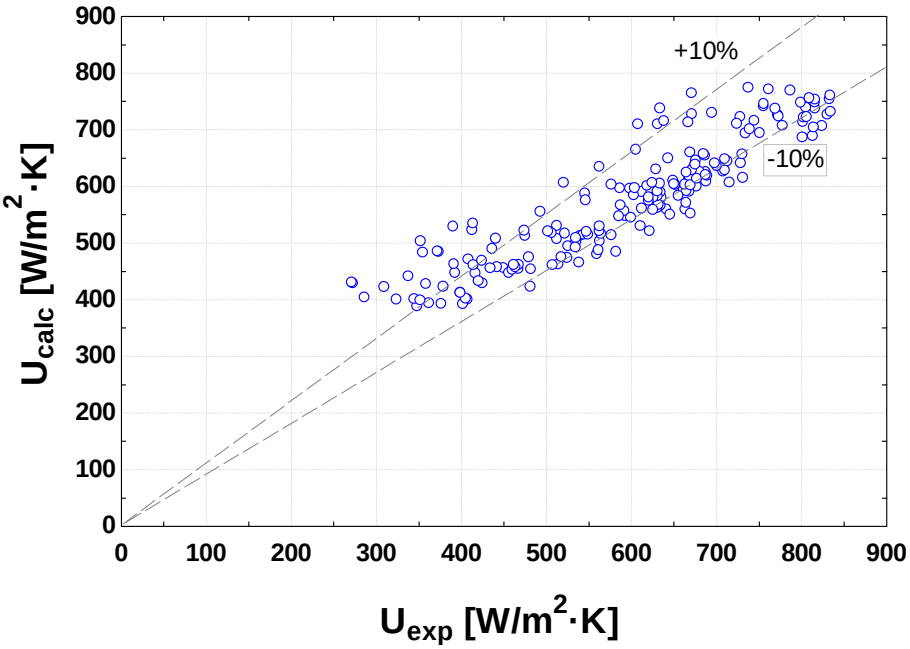

Fig. 7.13. Experimental vs. Calculated heat transfer coefficient in the Solution heat exchanger

7.5.3. Generator

In the following, the characterization of an upflow vertical plate heat exchanger acting as generator is described in terms of heat transfer and pressure drop. The analysis of flow boiling of a zeotropic binary mixture inside a vertical PHE, the application of the results to numerical simulation, and optimized design purposes enhance the interest and importance of this study.

Geometrical data

The photograph of Alfa Laval model **CB76** is shown on Fig. 7.14. It is a single pass brazed PHE, working in counter current flow configuration. As explained on Chapter 3, the hot fluid is thermal oil coming from the oil tank. In the cold side of the PHE, the water-LiBr solution is forced to flow with a solution pump.

(a) (b)

Fig. 7.14 (a) Photography of the Brazed PHE operating as generator: Alfa Laval model CB76. Source: alfalaval.com (b) Operation scheme of cold and hot fluids in the generator. Based on: www.bcb-plzen.eu

The detailed geometry data of the PHE is described on Fig. 7.15, which shows one of the 10 plates which make up the generator.

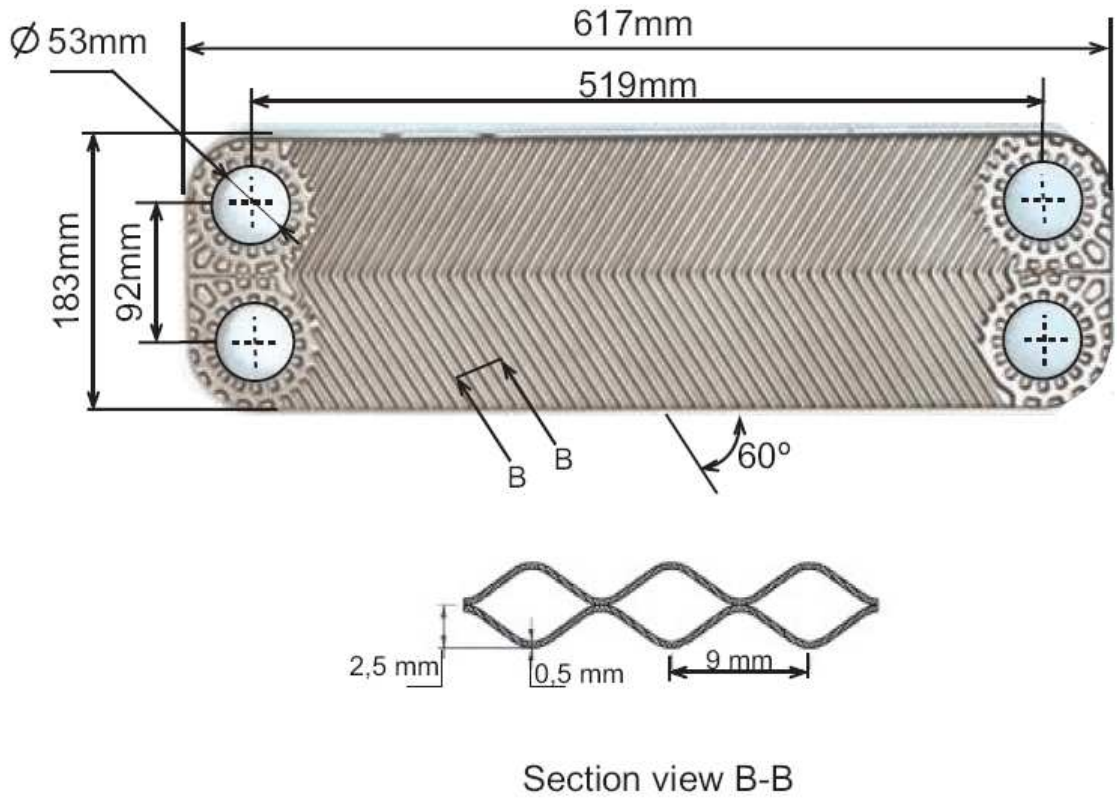

Fig. 7.15. Geometrical details of the plate heat exchanger (model Alfa Laval CB76)

For calculations purpose, the geometrical parameters used to correlate pressure drop and heat transfer are the hydraulic diameter, calculated as $D_h = 2 \cdot b / \phi$, and the length between ports centres as characteristic length.

The surface enlargement factor ϕ is calculated in the generator as (Martin, 1996):

$$\phi = \frac{1}{6}\left[1 + \sqrt{1 + x^2} + 4\sqrt{1 + \frac{x^2}{2}}\right]; \quad x = \frac{\pi b}{\Lambda} \tag{7.71}$$

Calculation basis

Referring important ideas highlighted in the literature, the study of two-phase flow is based on the following:

- The distinctive change in the slope of friction factor vs. Reynolds data, at a given Re number for single phase data suggests the onset and intensification of swirling flows (Muley and Manglik, 1997). This could indicate the beginning of a transition regime between laminar and turbulent flow in the PHE.

- An important source of uncertainty in the h_{2ph} calculation is the quantification of the h_{1ph}. Therefore, the low total uncertainty first requires a good fit of the h_{1ph} correlation (Corberán et al., 2002). Most of the works that deal with two-phase studies in PHEs determines first the single phase correlation for the specific PHE under study (Yan and Lin., 1999; Hsieh and Lin, 2001 and 2003; Han et al., 2003; Longo et al., 2006 and 2007 among others).
- The data reduction methodology can perfectly include the effect of pressure drop in the analysis with no important difficulties added, if experimental measurements are available (Corberán et al., 2002).

Taking into account the above mentioned ideas, single phase experiments were developed for heat transfer and pressure drop for both water and water-LiBr solution. Determination of Fanning friction factor allows identifying the change of flow regimes along the PHE under study and therefore the processing of the data for the subsequent determination of single phase heat transfer coefficients. The Wilson plot method, also applied for the case of subcooler, is applied in identical way for the generator to find h_{1ph}. Finally, the pressure drop is included as an important variable in the two-phase analysis.

7.5.3.1. Results and discussion

7.5.3.1.1. Single phase pressure drop

The total pressure drop obtained in the experimentation allows the determination of Fanning friction factor *f*. The experimental conditions correspond to Reynolds numbers range of $100 < Re < 700$, for experiments with water and $15 < Re < 40$ for experiments with water-LiBr solution. The contributions of gravitational, ports and frictional pressure drop were estimated by applying the data reduction explained on section 7.4.2. The gravitational pressure drop represents on average 85% of the total pressure drop for the case of experiments carried out with solution.

Results obtained for both water and solutions tests are presented on Figs. 7.16 and 7.17 respectively. For both cases, the power-law equation which describes the dependence of experimental f on Re is shown.

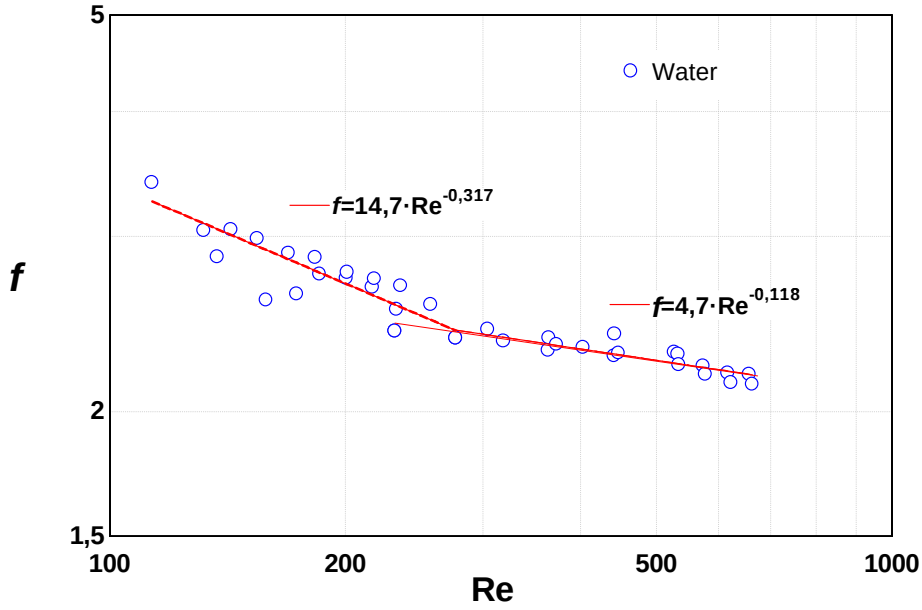

Fig. 7.16. Friction factor vs. Reynolds number. Results for experiments with water

Observing first the results for water, the degree of turbulence effect seems to increase for Re ≈ 250, which is indicated by a difference in slope of the *f-Re* data. This could be the beginning of turbulent regime.

For the case of water-LiBr, the mass flow rate range is restricted because of the experimental configuration, in order to avoid the solution to reach the condenser. Besides this, the high viscosity of the solution makes the corresponding Re to be low. In spite of the reduced Re range, some scatter of data is observed at $Re \approx 20$, showing an abrupt change at this value. Another change in the slope can be noticed at lower Re. Other investigations (Muley and Manglik, 1997; Bogaert and Bölcs, 1995) have also found this behaviour for high viscous fluids (low Re). They have suggested that for $Re > 20$ the onset and intensification of swirling flow occurs for their experiments. Therefore, the region $20 < Re < 300$ can be considered as indicative of transition regime.

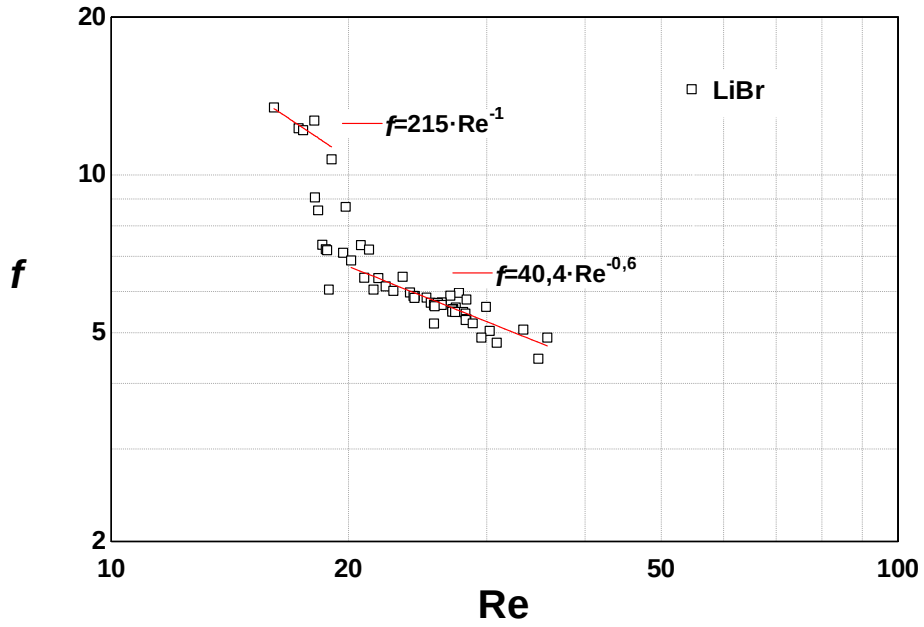

Fig. 7.17. Friction factor vs. Reynolds number. Results for water- LiBr solution

Correlation equations for single phase friction factor

The friction factor is fitted by empirical correlations of the type a/Re^b which allows the comparison with other researches.

As above mentioned, the analysis of separated data for both water and solution enables to distinguish changes in the flow regime of the data. Although the correlations obtained for each fluid are given individually on Figs. 7.16 and 7.17, a unique correlation is able to describe the data for the complete range of transition regime, $20 < Re < 300$, with an acceptable deviation. Fig. 7.18 shows the values of obtained correlations compared to experimental *f*.

$$f = \begin{cases} 215/\mathrm{Re} & 0 < \mathrm{Re} < 20 \\ 18{,}9 \cdot \mathrm{Re}^{-0{,}369} & 20 < \mathrm{Re} < 300 \\ 4{,}7 \cdot \mathrm{Re}^{-0{,}118} & 300 < \mathrm{Re} < 700 \end{cases} \tag{7.72}$$

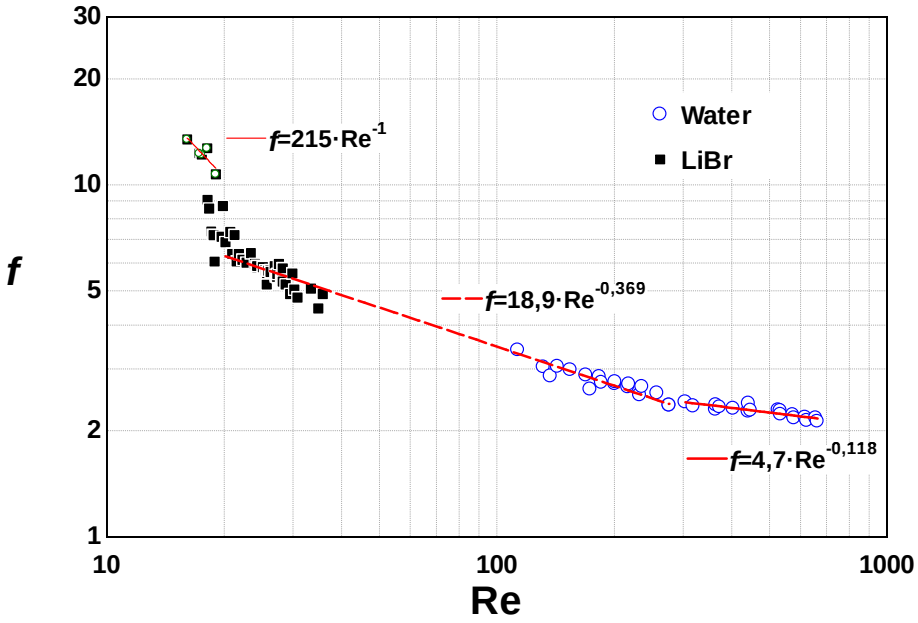

Fig. 7.18. Experimental and calculated friction factor vs. Reynolds number. Lines correspond to values calculated through correlations given on Eq. 7.72.

Fig. 7.19 presents the comparison of published correlations given in section 7.3, according to the corresponding valid Re range reported, with experimental *f*.

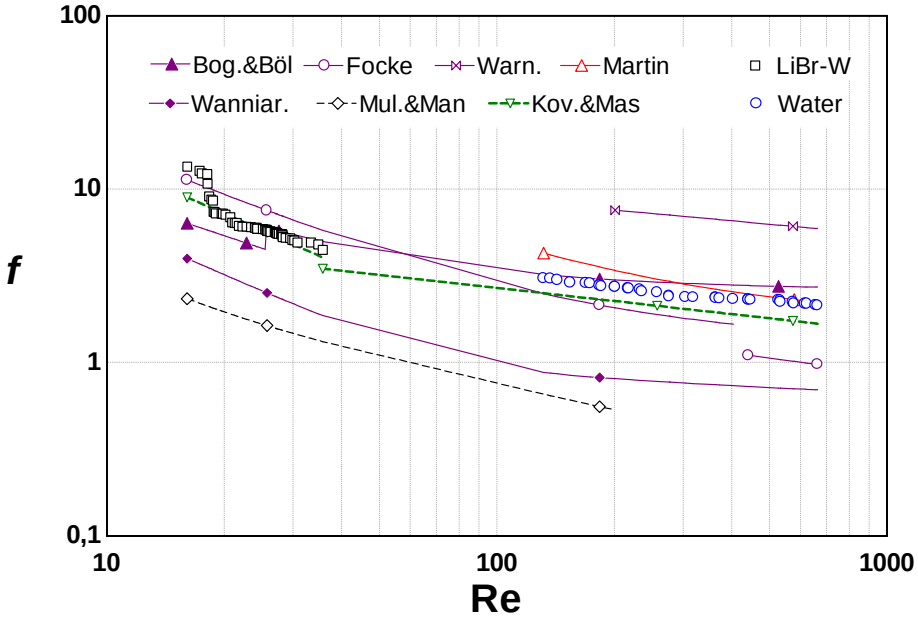

Fig. 7.19. Comparison of experimental *f* with results reported in literature.

The obtained correlations match well with Bogaert and Bölcs, Focke and Kovalenko and Masdov predictions, for the majority of points in the complete *Re* range tested. For *Re* > 300, obtained for water, the match is very good with Martin. Muley and

Manglik as well as Wanniarachchi correlations under predicts our own experimental results. Warnakasuriya correlation over predicts them. In spite that all correlations were selected according several common geometrical parameters and flow conditions, the different port orientation, flow distribution channels, plate width and length could be the reason for these differences (Muley an Manglik, 1996). Results given by Warnakasuriya are calculated by diving by 1/2 instead of 2 (Eq. 7.34), which could explain the higher values obtained.

7.5.3.1.2. Single phase heat transfer results

Considering the results obtained in the previous section, the heat transfer analysis was focussed on finding the appropriate correlation for the film heat transfer coefficients in the corresponding flow regime.

Both the original and the modified Wilson plot technique (Shah, 1990) were used to find the film heat transfer coefficients corresponding to each flow regime. The first case is applied when the other side is already known from previous estimation carried out on the same plate heat exchanger. Because of the existence of viscous process liquids, the term of viscosity $(\mu/\mu_w)^{0,14}$ is included, as done in section 7.5, for the subcooler. This term shows an average value of 0,993 and 1,004 for the oil and the water side, respectively. Reynolds and Prandtl numbers ranges for the considered flow regimes are given with the resulting correlations equations.

Results obtained from the application of Wilson plot technique for both water and Solution are plotted on Fig. 7.20. The Nusselt number calibration equations are also indicated. Fig. 7.21 shows the calculated overall heat transfer coefficient against the experimental values, corresponding to the cases presented previously on Fig. 7.20.

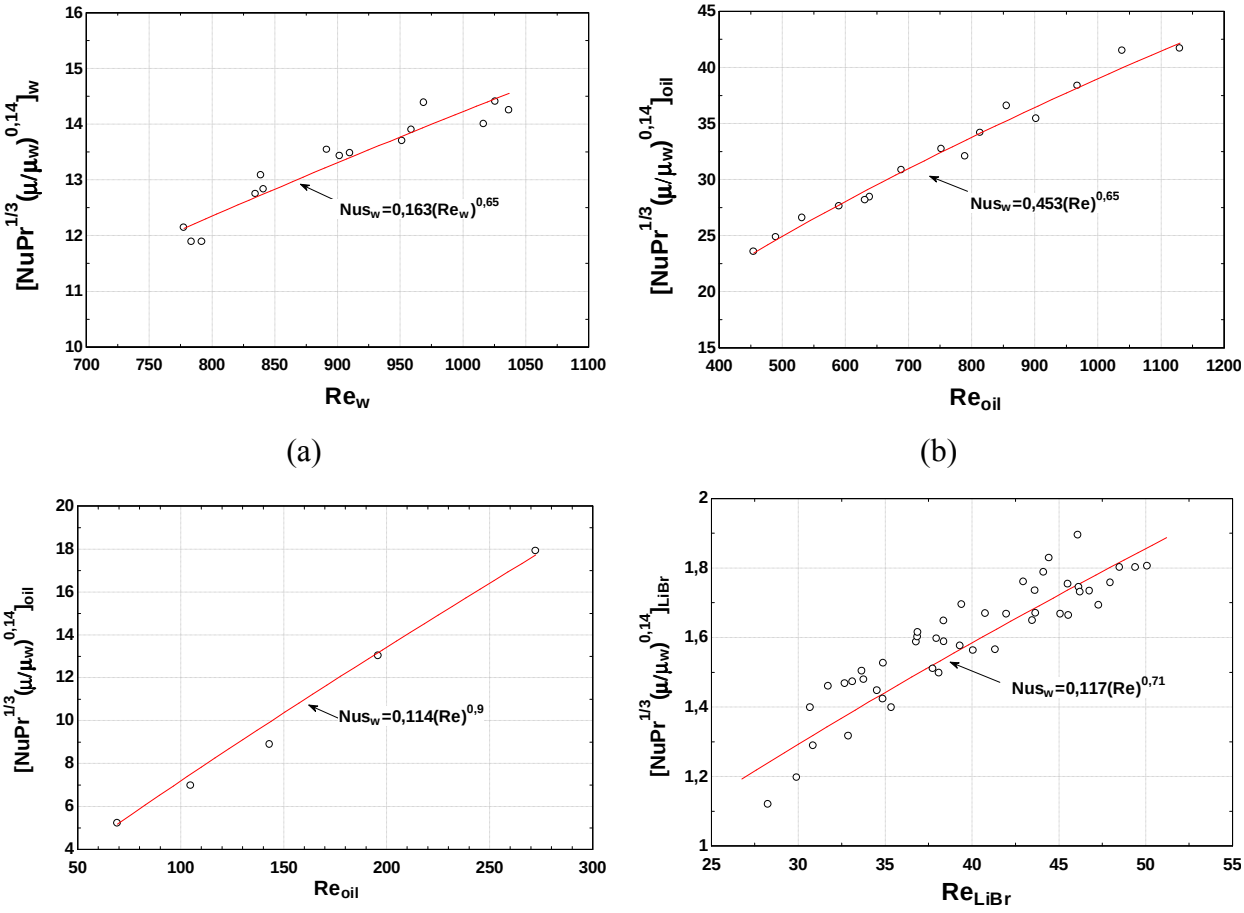

Figure 7.20. Nusselt number correlation: a) Water. Turbulent flow regime. b) Oil. Turbulent flow regime. c) Oil. Transition flow regime. d) Water-LiBr solution. Transition flow regime

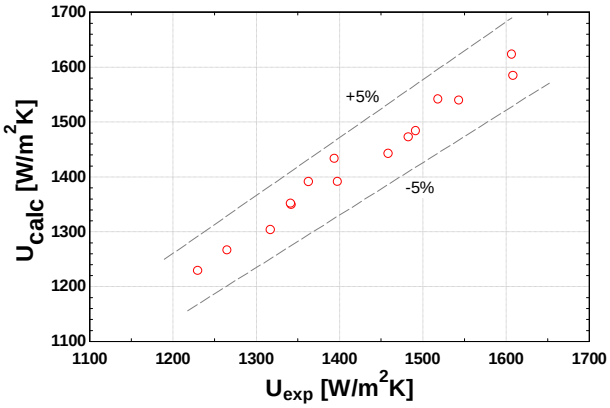

(a)

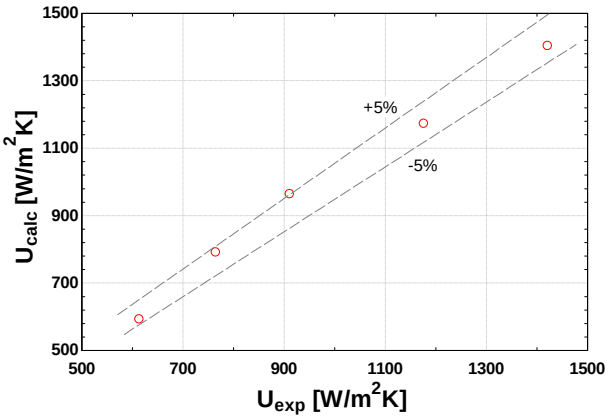

(b)

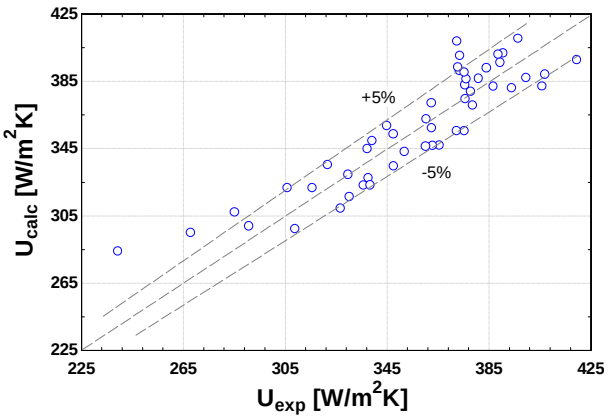

c)

Fig. 7.21. Single phase experimental vs. calculated heat transfer coefficient a) Water and Oil experiments in turbulent flow regime. b) Oil. Transition flow regime.c) Water-LiBr solution. Transition flow regime

Correlations equations for single phase heat transfer

Just like for the case of *f*, the correlations obtained for each fluid, with different Re and Pr, are given individually on Figs. 7.20. The Nusselt number calibration equations, corresponding to specific operating conditions for this case, are:

$$Nu = \begin{cases} 0{,}117 \cdot \mathrm{Re}^{0{,}71} \cdot \mathrm{Pr}^{1/3} \cdot \left(\dfrac{\mu}{\mu_w}\right)^{0{,}14} & 25 < \mathrm{Re} < 50; \quad 15 < \mathrm{Pr} < 25 \\ 0{,}114 \cdot \mathrm{Re}^{0{,}9} \cdot \mathrm{Pr}^{1/3} \cdot \left(\dfrac{\mu}{\mu_w}\right)^{0{,}14} & 50 < \mathrm{Re} < 300; \quad 140 < \mathrm{Pr} < 150 \\ 0{,}453 \cdot \mathrm{Re}^{0{,}65} \cdot \mathrm{Pr}^{1/3} \cdot \left(\dfrac{\mu}{\mu_w}\right)^{0{,}14} & 400 < \mathrm{Re} < 1.200; \quad 39 < \mathrm{Pr} < 53 \\ 0{,}163 \cdot \mathrm{Re}^{0{,}65} \cdot \mathrm{Pr}^{1/3} \cdot \left(\dfrac{\mu}{\mu_w}\right)^{0{,}14} & 700 < \mathrm{Re} < 1.100; \quad 1{,}6 < \mathrm{Pr} < 1{,}95 \end{cases} \tag{7.73}$$

In Fig. 7.22, the experimental data are compared with predictions for Nu from correlations found on the literature, listed on section 7.3.

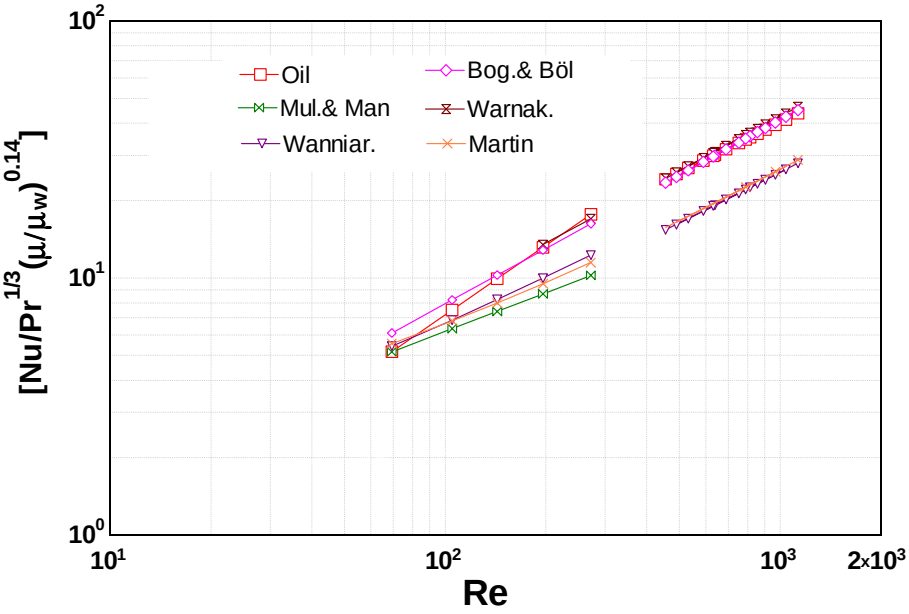

Fig. 7.22. Comparison of Nusselt number data with previous correlations

Some remarks can be raised from this comparison: The data for thermal oil agrees with Warnakulasuriya et al., which were obtained for highly viscous fluids with similar Pr. The agreement is also very good with Bogaert and Bölcs in the transition and turbulent zone. Wanniarachchi et al., Muley and Manglik, and Martin correlations under predicts the transition and turbulent region in most cases. In the low Re regions all correlations compared here, according to valid Re numbers, over predicts the experimental data obtained. The different properties of tested fluids in the low Re zone could explain the poor agreement in this zone. For the case of Bogaert and Bölcs experiments, the secondary fluid is water, not a viscous fluid like Water-LiBr solution. This is also the case for Muley and Manglik experiments.

Correlations obtained for *f* and Nu are an important piece of the two-phase heat transfer analysis, presented in the following.

7.5.3.1.3. Two-phase heat transfer and pressure drop

In the following, results obtained at two phase conditions for 257 experimental points are given in terms of single and two-phase parameters for the corresponding regions described in section 7.4.3: heat transfer coefficients, pressure drop, temperatures and areas distribution along the generator. Ranges of solution mass flux, temperatures

and pressure of the fluids for the complete experimental campaign are given in Table 7.3.

Variable	**Range**
Solution mass flux, G	5 - 45 kg/sm^2
Inlet oil temperature, $T_{oil,i}$	79 – 104 ºC
Outlet oil temperature, $T_{oil,o}$	77 – 102 ºC
Inlet solution temperature, $T_{sol,i}$	44 - 71 ºC
Outlet solution temperature, $T_{sol,o}$	67– 89 ºC
High pressure	30 – 60 mbar
Solution concentration, X	57 – 63 %

Table 7.3. Operating condition ranges of mass flux, temperatures and pressure during the experimental campaign for the generator.

The oil mass flux was kept constant at 460 kg/sm^2. Following the process explained in detail in section 7.4.3, some results of single and two-phase parameters for some cases is offered in Table 7.4. Figs 7.23 represent five selected cases for a fixed mass flux G. Temperatures distribution of oil and solution, concentration and pressures values are plotted as a function of generator flow path length.

Case	G [Kg/sm^2]	$T_{oil,in}$ [°C]	$T_{LiBr,in}$ [°C]	X_{in} [%]	Q_{1ph} [kW]	Q_{2ph} [kW]	ΔP_{1ph} [kPa]	ΔP_{2ph} [kPa]	$T_{LiBr,2ph}$ [°C]	$h_{LiBr,1ph}$ [W/m^2°C]	$h_{oil,1ph}$ [W/m^2°C]	U_{1ph} [W/m^2°C]	U_{2ph} [W/m^2°C]	h_{2ph} [W/m^2°C]	A_{1ph} [m^2]	A_{2ph} [m^2]	L_{1ph} [m]	L_{2ph} [m]
1	44	80	55	58	4,2	0,3	7,2	1,8	76,5	533,7	3639	458	222	239	0,89	0,22	0,42	0,1
2	37	80	56	59	3,4	0,4	7,0	1,9	77,1	468,3	3650	409	307	340	0,87	0,24	0,41	0,11
3	33	80	57	59	3,0	0,6	6,8	2,0	77,3	432,2	3657	381	386	438	0,86	0,26	0,4	0,12
4	28	80	56	59	2,7	0,7	6,7	2,0	77,2	381,7	3649	341	429	495	0,85	0,27	0,39	0,12
5	24	80	48	59	3,1	0,5	6,6	1,8	76,6	337,4	3624	305	307	339	0,83	0,28	0,39	0,13
6	21	80	47	59	2,7	0,6	6,4	1,7	76,8	300,1	3627	274	331	369	0,81	0,3	0,38	0,14
7	44	85	58	60	4,5	0,2	7,1	2,3	81,0	522,0	3777	451	117	121	0,87	0,24	0,4	0,11
8	37	85	59	60	3,5	0,5	6,8	2,3	81,3	453,4	3789	399	231	249	0,83	0,28	0,39	0,13
9	33	85	60	60	3,2	0,6	6,6	2,5	81,8	419,3	3807	372	280	305	0,81	0,3	0,38	0,14
10	28	85	60	61	2,6	0,7	6,3	2,4	81,7	369,9	3804	333	303	333	0,78	0,33	0,36	0,15
11	24	85	60	61	2,4	0,9	6,1	2,5	81,7	336,0	3803	305	340	378	0,75	0,36	0,35	0,17
12	21	85	49	61	2,9	0,7	6,2	2,1	80,7	287,8	3761	265	258	280	0,77	0,34	0,36	0,16
13	44	90	59	60	5,1	0,5	6,9	3,5	85,3	539,4	3910	466	218	233	0,84	0,27	0,39	0,13
14	37	89	61	60	3,9	0,7	6,5	3,4	85,2	470,1	3906	413	299	328	0,81	0,3	0,38	0,14
15	33	90	62	60	3,5	1,0	6,3	3,7	85,8	431,9	3929	384	339	376	0,78	0,33	0,36	0,16
16	28	90	60	60	3,2	1,0	6,2	3,6	86,0	379,1	3930	341	370	414	0,78	0,34	0,36	0,16
17	24	89	55	61	3,2	0,8	6,5	3,0	85,4	335,1	3896	305	322	356	0,8	0,31	0,37	0,14
18	44	94	61	60	5,4	0,9	6,5	4,4	88,9	539,7	4028	468	261	282	0,8	0,31	0,37	0,15
19	37	94	64	60	4,1	1,0	6,2	4,5	88,9	478,0	4031	421	334	369	0,77	0,34	0,36	0,16
20	33	94	66	60	3,5	1,3	6,0	4,6	89,8	446,2	4060	396	411	465	0,75	0,37	0,35	0,17
21	28	95	67	60	2,9	1,4	5,7	4,5	90,5	401,0	4084	360	466	536	0,72	0,4	0,33	0,18
22	24	94	68	60	2,4	1,4	5,5	4,1	90,6	363,3	4086	330	491	570	0,7	0,41	0,33	0,19
23	21	94	68	60	2,0	1,5	5,5	3,8	90,6	321,8	4057	295	528	621	0,69	0,42	0,32	0,2
24	44	98	61	59	6,1	1,1	6,7	4,9	92,1	557,2	4110	482	334	368	0,83	0,28	0,39	0,13
25	36	99	63	59	4,8	1,9	5,7	6,8	93,0	499,9	4167	439	421	476	0,72	0,39	0,34	0,18
26	33	99	65	59	4,2	1,9	5,6	6,4	92,9	467,6	4165	414	454	520	0,71	0,4	0,33	0,19
27	28	99	67	59	3,4	2,3	5,2	6,5	93,7	421,4	4193	378	512	596	0,66	0,45	0,31	0,21
28	24	99	68	59	2,8	2,4	4,9	6,4	93,9	381,0	4205	345	533	624	0,63	0,49	0,29	0,23
29	21	98	69	59	2,3	2,3	4,7	6,0	93,6	339,9	4160	311	536	630	0,61	0,5	0,28	0,23

Table 7.4. Operating conditions and resulting single and two-phase parameters for 28 cases among 237. Blue coloured cases correspond to those shown in Figure 7.23.

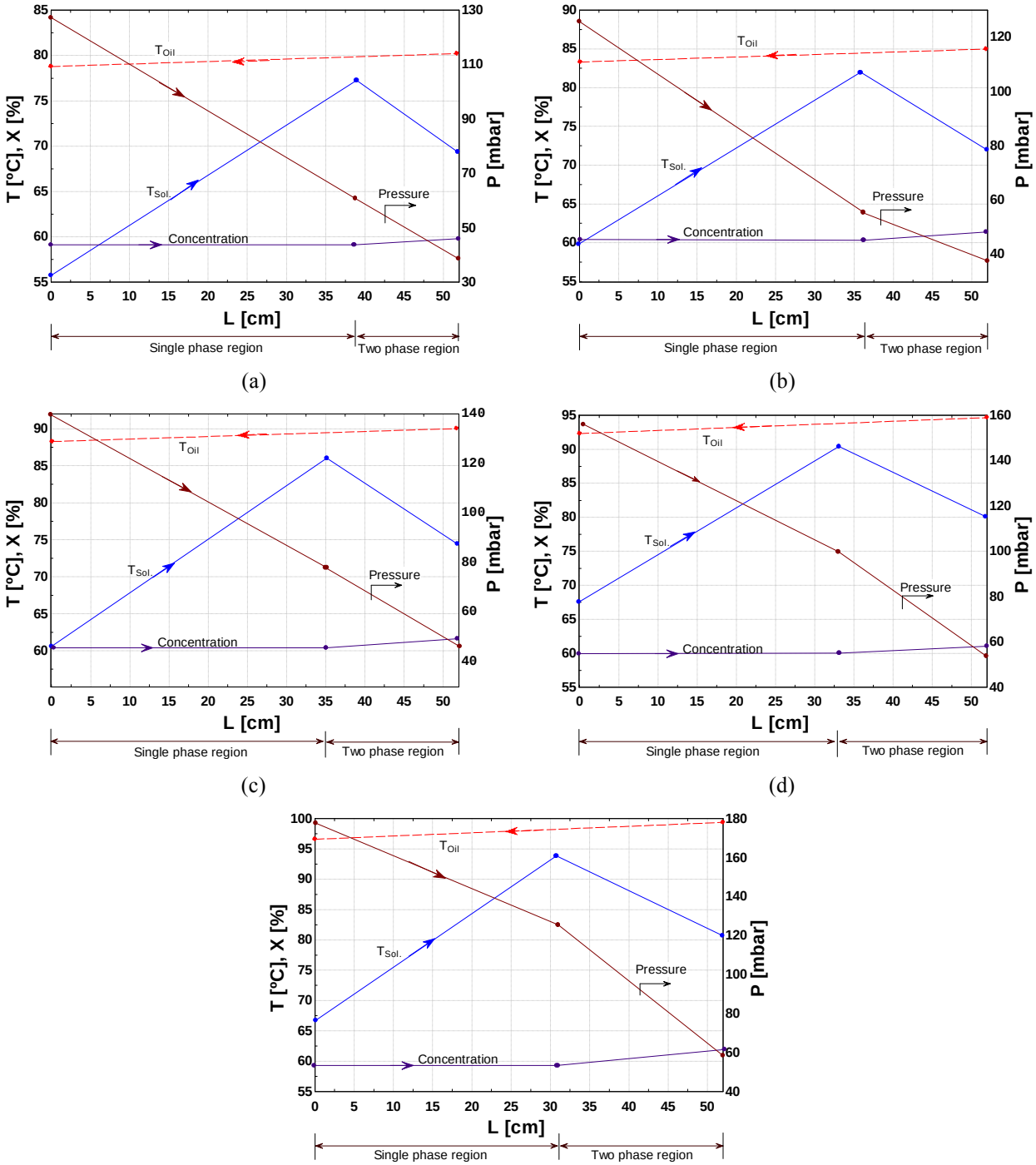

Fig. 7.23: a) Case 4. b) Case 10. c) Case 16. d) Case 21 e) Case 27

It is worth noting some aspects:

– For the cases showed, the single phase area A_{1ph} is larger than two phase area A_{2ph} except for higher hot fluid temperatures, $T_{oil,i}$. When $T_{oil,i}$ is increased the percentage of A_{2ph} also increases. In few cases, the percentage of A_{2ph} can reach up to 50% at low mass flux G. The ratio of areas is determined the degree of subcooling of the

weak solution. This in turn depends on the solution heat exchanger efficiency. As in this facility, such efficiency is low in certain cases (Chapter 4), there is a significant subcooling at the generator entry. This has motivated a new design for the generator system, which include a preheater. Fig. 7.24 manifests this situation, for G=21 kg/m^{2}s.

- Single phase pressure drop ΔP_{1ph} is significant and in some cases higher than two phase pressure drop ΔP_{2ph}. This leads to a significant change in conditions (temperature) which begins the process of steam separation. The principal weigh of ΔP_{1ph} corresponds to ΔP_c and not to frictional pressure drop.
- Regarding to solution temperatures distribution, it is noted that due to the pressure drop along the PHE, the solution temperature at the entry of two phase region $T_{sol,2ph}$ is higher than $T_{sol,o.}$ It is also interesting to note that the temperature profiles show a point of minimum temperature difference between the two flows.
- Another important aspect is that the single heat transfer coefficient h_{1ph} is some times higher than $h_{2ph.}$ As the proportion of separated vapour is small (the change of concentration solution is very small), high values of h_{2ph} are not expected. The cases in which h_{2ph} is higher than h_{1ph} are influenced by the mass flux G and $T_{oil,i}$. Fig. 7.25 illustrates several cases in which G is varied. The ratio $h_{1ph/}\, h_{2ph}$, shown on the right scale, diminishes when G is increased.

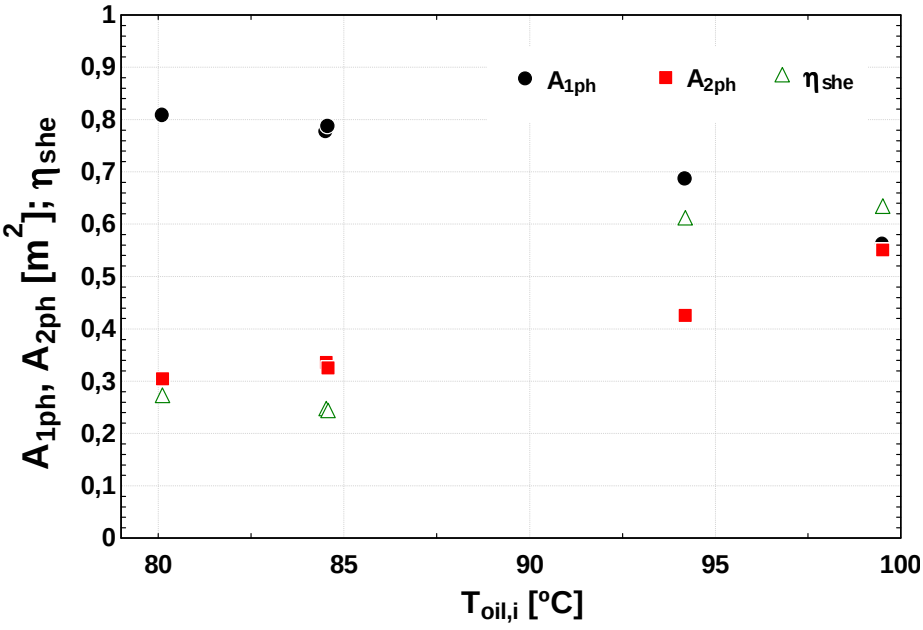

Fig. 7.24. Distribution of single and two phase area for a mass flux fixed at 21 kg/m^{2}s.

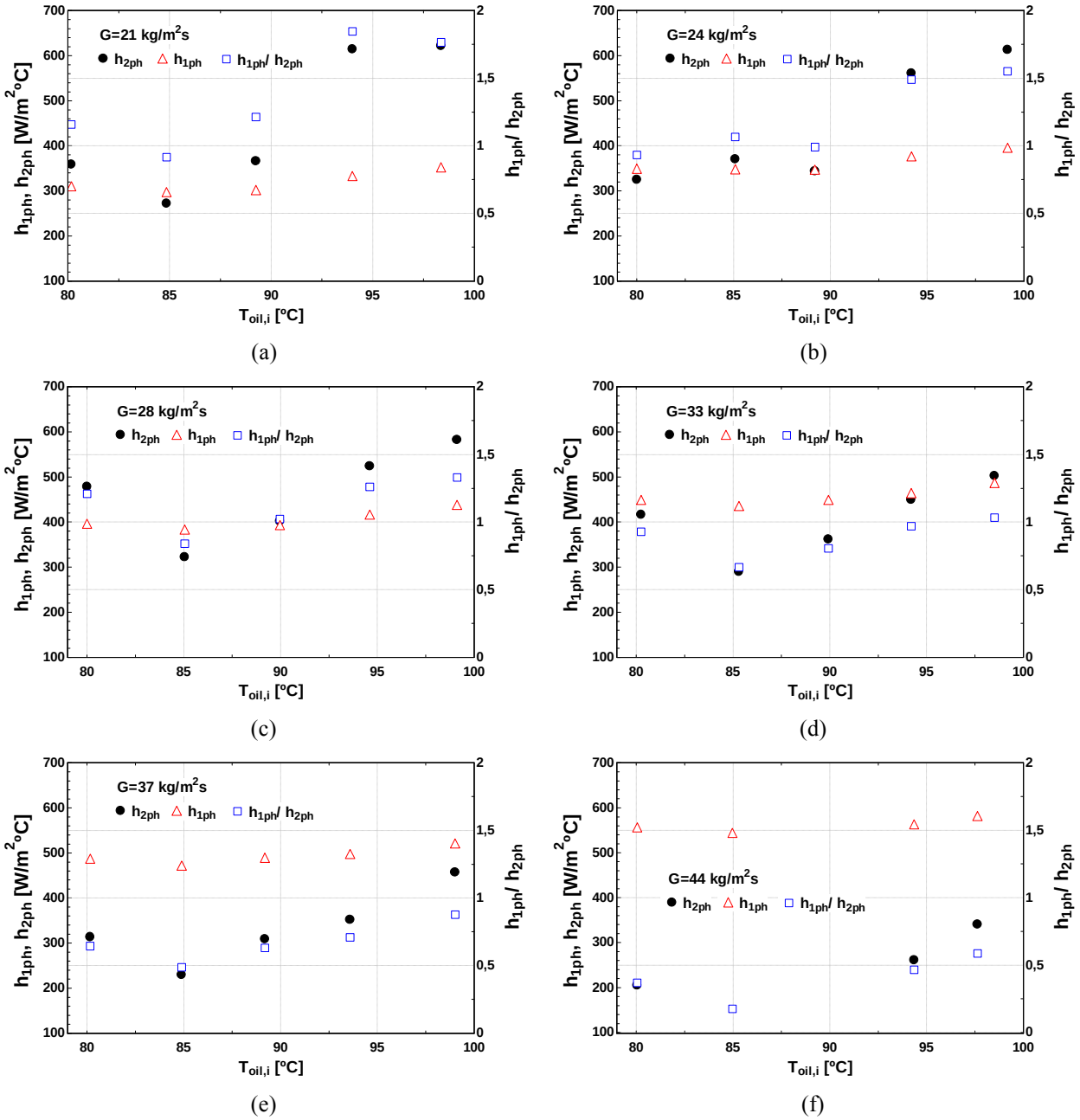

Fig. 7.25. Influence of mass flux and controlled inlet oil temperature on the single and two-phase heat transfer coefficients. a) G=21 kg/m^{2}s. b) G=24 kg/m^{2}s. 10. c) G=28 kg/m^{2}s. d) G=33 kg/m^{2}s e) G=37 kg/m^{2}s. f) G=43 kg/m^{2}s

7.6. Conclusions

- Experimental results for single phase heat transfer and pressure drop are obtained and compared to reported correlations in the literature. For the case of correlation equations of Nusselt number obtained for operating conditions in the subcooler, a good agreement is found between the experimental values and Wanniarachchi et al. prediction. Bogaert and Bölcs, Warnakulasuriya and Worek, and Yan and Lin correlations are nearer. For the case of calibration equations of Fanning friction in the generator, the match is close to Bogaert and Bölcs, Focke and Kovalenko and Masdov, for the majority of points in the complete Re range tested.
- For the case of two-phase calculations, the experimental heat transfer coefficients, pressure drop, areas and temperature distribution corresponding to each zone are obtained. It is verified that boiling heat transfer coefficients are in some cases higher than single heat transfer coefficients and that the single phase pressure drop ΔP_{1ph} is significant, in some cases higher than the two-phase pressure drop ΔP_{2ph}.

Chapter 8

CONCLUSIONS AND FUTURE WORK

8.1. Conclusions

The work carried out in this thesis has met the goals originally proposed, which focus on the experimental evaluation of the overall and components performance of an adiabatic absorption facility, development of thermodynamic models to represent such performance (including the specific features involved in both the design and the operation) and finally the study of heat transfer and pressure drop processes in plate heat exchangers working with water-LiBr solution.

A summary of the main conclusions of each part of this thesis is presented below.

- Regarding overall test facility performance:

– The effect of controlled oil temperature at the inlet to generator t_{Gi}, and of the solution mass flow rate $\dot{m}_{weak}$ on the experimental cooling capacity $\dot{Q}_{E,\exp}$ and the instantaneous *COP* has been described. A maximum point was noticed for $\dot{Q}_{E,\exp}$ and *COP* at given values of t_{Gi} and $\dot{m}_{weak}$. This was initially justified by the low performance of evaporators, and the effects of irreversibilities, leading to a reduction of the *COP* when increasing oil temperature.

– A performance analysis of the evaporators revealed that the distribution of refrigerant mass flow rate $\dot{m}_{ref}$ was not symmetrical in some cases, leading to a partial or defective functioning of one evaporator. This explains why the cooling capacity slopes down when it is expected to be increasing, i.e., when $t_{G,i}$ rises. The average evaporators' efficiency η_E obtained for the whole set of experimental points was 50%. Liquid accumulation leads to overflow of refrigerant out of the evaporators. Therefore, the distribution system used for the spreading of the refrigerant on the fin tubes was not working as expected and it must be improved in order to obtain a cooling capacity closer to the ideal one.

– The solution heat exchanger efficiency η_{SHE} and its influence over the overall system performance were analyzed. The poor filling of this plate heat exchanger makes η_{she} to decrease abruptly in that situation. The heat transfer process is affected, reducing η_{she} and therefore reducing the *COP* of the machine. The

situation described above highlights the necessity of a control system in this kind of facilities.

- Convection heat transfer from components and pipe walls to the air were calculated. Thermal losses in the control volume of generator, $\dot{Q}_{lossG}$, represent as average value 8% of $\dot{Q}_G$. For the case of the absorber, $\dot{Q}_{lossA}$, was 5% of thermal power of subcooler. When inlet oil temperature increases a general increasing tendency of thermal losses in the oil and solution loops was observed. The increase in recirculated solution mass flow rate $\dot{m}_r$ contributes to decrease $\dot{Q}_{lossA}$ as a result of the cooling effect of $\dot{m}_r$ inside the absorber.
- A noticeable difference in temperature was identified between solution at generator outlet and separator outlet. It was verified that the energy associated to this difference was not caused by thermal losses to the environment nor pressure drop in the connection tube. The cause of the difference in temperatures along the strong solution path can be explained as the solution was still boiling at the exit of the generator. Consequently, the refrigerant generation kept on in the path followed by the solution.
- A basic thermodynamic model including the particular features, in both design and operation, of the facility analyzed has been presented. Performance parameters were expressed in terms of an ideal absorption model and compared with experimental results. The differences observed between ideal and experimental results help to envisage the influence of components performances on the overall performance of the facility. A good agreement with experimental performance parameters and those obtained through a modified basic absorption model has been achieved.

- Regarding extended characteristic equation:

- An extension of the characteristic equation method to adiabatic absorption has been developed. The extension needs a subcooling temperature.
- The effect of evaporator overflow has been characterized. Its influence on the cooling capacity $\dot{Q}_E$ has been included in the extended characteristic equation. This is necessary to describe the operation of some commercial absorption chillers.
- Taking into account the particular design and operation features, a good agreement between experimental performance parameters and those obtained through the

extended characteristic equation has been achieved, even at off-design operation. This allows its use for predicting the performances and for planning control strategies.

- Regarding comparison of absorber configurations

Two adiabatic absorber configurations, namely droplets and fan sheet, were tested and operational parameters have been experimentally determined:

- The absorber configuration based on fan sheets showed better performance parameters than the droplets configuration. A significant reduction in the absorber size (up to 50%) is possible.
- The absorber performance has been characterized trough two parameters: the thermal transmission UA_A and the approach to equilibrium factor F_x. The influence of the controlling operating parameters (solution mass flow rate and recirculation ratio) on UA_A has been experimentally derived. Due to the influence of the overflow of refrigerant from evaporators on the absorber performance, it is difficult to observe a clear influence of controlled parameters on F_x. In spite of this, when RR is increased F_x seems to increase for both fan sheets and free falling droplets configurations.
- The UA_A has shown to be strongly dependent of recirculated mass flow rate. This way, the subcooling capacity of the absorber and for instance the absorption capacity, can be increased.

- Regarding single and two-phase heat transfer and pressure loss in plate heat exchangers:

Single and two-phase heat transfer and pressure drop have been studied in plate heat exchangers working in a single phase water-LiBr absorption system. The modified Wilson Plot method was used to find the correlation equations of Nusselt number for the particular operating conditions tested. The Fanning friction factor for single phase has been also obtained for the generator.

- Experimental results were compared to reported correlations in the literature. The agreement with prediction of previous works was discussed for the case of

correlations equations of Nusselt number and Fanning friction obtained for the operating conditions in the plate heat exchangers used in the facility here presented.

- For two-phase flow, the existence of a single phase zone in the entrance and a downstream two-phase zone was considered, as well as the important effect of pressure drop in the plate heat exchanger. Results showed the heat transfer coefficients, pressure drop, areas and temperature distribution corresponding to each zone. The influence of inlet temperature of the hot fluid, mass flux and solution heat exchanger efficiency on the two-phase heat transfer coefficients was discussed. It was verified that boiling heat transfer coefficients were in some cases higher than single heat transfer coefficients and that the single-phase pressure drop ΔP_{1ph} was significant, in some cases higher than two-phase pressure drop ΔP_{2ph}.

8.2. Contributions

A summary of the main contributions of this thesis is presented below.

- Extension of the characteristic equation model: Adapted for its application to an experimental single effect adiabatic absorption facility and special design with water-LiBr solution as working fluid.

- The effect of refrigerant overflow in the evaporators has been characterized as well as its influence on the cooling capacity.

- Experimental characterization of two adiabatic absorber configurations: drops and fan sheets. Configuration based on fan sheets showed better performance parameters that the droplets configuration, yielding a significant reduction in the size of the absorber (up to 50%). It is the first time that such configuration is applied to adiabatic absorbers in a built operational prototype.

- A study of heat transfer and pressure drop in plate heat exchangers operating in a single effect adiabatic absorption system has been carried out. In the case of two-phase calculation, the important effect of pressure drop in plate heat exchanger is considered. The results include film heat transfer coefficients and pressure drop, corresponding to single and two-phase zones in the plate heat exchanger.

- Analysis of the overall performance of the experimental facility and detailed components analysis, showing their influence in the absorption refrigeration facility of special design. Experimental results demonstrate the potential and operational flexibility of design, showing great potential in the preliminary sizing calculations.

8.3. Future Work

This study raises new challenges:

- Size reduction in other components, namely evaporator and condenser, not considered as critical beforehand. They would become critical due to the significant reductions in size obtained in the absorber.
- Deepening in the study of two-phase heat transfer of binary mixtures in order to determining the effects of different geometrical configurations and operating conditions on the flow boiling heat transfer process.
- Continue the experimental characterization of other absorber configurations included in the experimental facility: inverse jet flow, advanced sprays and fluid sheets.
- Approach to experimental techniques for the diagnosis of advanced two-phase flow (PIV and HRPIV) and participation in the preparation and implementation of relevant trials using these techniques.

BIBLIOGRAPHY

Albers J. Ziegler F., 2005. Improved control strategies for solar assisted cooling systems with absorption chillers using a thermosyphon generator. In: Proceedings of the International Solar Air Conditioning, October 16-17, Kloster Banz, Germany.

Aphornratana S., Sriveerakul T., 2007. Experimental studies of a single-effect absorption refrigerator using aqueous lithium–bromide: Effect of operating condition to system performance. Experimental Thermal and Fluid Science. 32 (2), 658-669.

Arun M. B., Maiya M. P., Srinivasa Murthy S., 2001.Performance comparison of double-effect parallel-flow and series flow water–lithium bromide absorption systems. Applied Thermal Engineering. 21(12), 1273-1279.

Arzoz D., Rodriguez P., Izquierdo M., 2005. Experimental study on the adiabatic absorption of water vapour into LiBr–H_2O solutions. Applied Thermal Engineering. 25, (5-6), 797-811.

Ayub, Z., 2003. Plate Heat Exchanger Literature Survey and New Heat Transfer and Pressure Drop Correlations for Refrigerant Evaporators. Heat Transfer Engineering, 24 (5), 3-16.

Asano H, Takenaka N, Terushige Fujii T., 2004. Flow characteristics of gas–liquid two-phase flow plate heat exchanger (Visualization and void fraction measurement by neutron radiography). Experimental Thermal and Fluid Science. 28 (223–230).

Asdrubali F., Grignaffini S., 2005. Experimental evaluation of the performances of a H_2O–LiBr absorption refrigerator under different service conditions. Int. J. Refrigeration. 28 (4), 489-497.

Bogaert R., Bölcs A., 1995. Global performance of a prototype brazed plate heat exchanger in a large Reynolds number range. Experimental Heat Transfer. 8, 293-311.

Bourouis M., Vallès M., Medrano M., Coronas A., 2005. Absorption of water vapour in the falling film of water–(LiBr + LiI + LiNO3 + LiCl) in a vertical tube at air-cooling thermal conditions. Int. J.Thermal Sciences. 44 (5), 491-498.

Burdukov A.P, Dorokhov A.R., Paniev G.A., 1989. Combined heat and mass transfer in absorption on droplets. Soviet J Appl Phys .3 (1), 39–45.

Castro J., Oliva A., Perez-Segarra Oliet C., 2008. Modelling of the heat exchangers of a small capacity, hot water driven, air-cooled H2O–LiBr absorption cooling machine. Int. J. Refrigeration. 31 (1), 75-86.

Cebeci, T., 1974. Laminar-free-convective heat transfer from the outer surface of a vertical slender circular cylinder. In: Proceedings of Fifth Int. Heat and mass transfer Conf. NCI, 4, pp 15-19.

Çengel Y., Boles M., 1995. Termodinámica. 2ª ed. McGrawHill, USA.

Chua H.T., Toh H. K., Malek A., Ng K. C., Srinivasan K.,2000. A general thermodynamic framework for understanding the behaviour of absorption. Int. J. Refrigeration. 23 (7), 491-507.

Chua H.T., Toh H. K., Malek A., Ng K. C., Srinivasan K.,2000. Improved thermodynamic property field of LiBr-H_2O solution. Int. J. Refrigeration. 23, 412-429.

Claesson, J., 2004. Thermal and Hydraulic Performance of Compact Brazed Plate Heat Exchangers Operating as Evaporators in Domestic Heat Pumps, Ph.D. thesis, KTH Energy Technology.

Cooper A., Usher J.D., 1983. Plate heat exchangers, in: Heat Exchanger Design Handbook, Hemisphere Publishing Corporation (Chapter 3.7).

Corberán J. M., Gonzálvez J., 2002. Two-phase heat transfer analysis of evaporators. Experimental Thermal and Fluid Science. 26 (2-4), 259–267-

Creus A., 1997. Instrumentación Industrial. 6th ed. Marcombo, España.

Donate M., Rodriguez L., De Lucas A. Rodríguez J., 2006. Thermodynamic evaluation of new absorbent mixtures of lithium bromide and organic salts for absorption refrigeration machines. Int. J. Refrigeration. 29 (1), 30-35.

Dong-Hyouck Han, Kyu-Jung Lee, Yoon-Ho Kim., 2003. Experiments on the characteristics of evaporation of R410A in brazed plate heat exchangers with different geometric configurations. Applied Thermal Engineering. 23 (10), 1209–1225.

Elperin T., Fominykh A., Orenbakh Z., 2007.Coupled heat and mass transfer during nonisothermal absorption by falling droplet with internal circulation. Int. J. Refrigeration. 30 (2), 274-281.

Fernández-Seara, J., Uhía F. J., Sieres J, Campo A., 2005. Experimental apparatus for measuring heat transfer coefficients by the Wilson plot method. Eur. J. Phys. 26, N1–N11.

Flamensbeck M., Summerer F., Riesch P., Ziegler F., Alefeld G., 1998. A cost effective absorption chiller with plate heat exchangers using water and hydroxides. Applied Thermal Engineering. 18 (6), 413-425.

Florides G. A., Kalogirou S. A., Tassou S. A.,L. C. Wrobel., 2003. Design and construction of a LiBr–water absorption machine. Energy Conversion and Management. 44 (15), 2483-2508.

García-Cascales J.R., Corberán-Salvador J.M., Vera-García F., Gonzálvez-Maciá J., 2007. Assessment of boiling and condensation heat transfer correlations in the modelling of plate heat exchangers. Int. J. Refrigeration. 30(6), 1029-1041.

Hewitt. Geoffrey F., 1998. Heat exchanger design handbook, Begell House Inc., publishers.

Grandgeorge S., Jallut C., Thonon B., 1998. Particulate fouling of corrugated plate heat exchangers. Global kinetic and equilibrium studies. Chemical Engineering Science. 53 (17), 3050-3071.

Hellmann H.M, Schweigler C., Ziegler F., 1998. A simple method for modelling the operating characteristics of absorption chillers. In: Proceedings of Thermodynamics heat and mass transfers of refrigeration machines and heat pumps seminar EUROTHERM Nº 59, France, 219-226.

Herold, Keith E., 1996. Absorption Chillers and Heat Pumps. CRC Press, USA.

Hsieh Y. Y., Lin T. F., 2003 Evaporation Heat Transfer and Pressure Drop of Refrigerant R-410A Flow in a Vertical Plate Heat Exchanger. Transactions of the ASME Journal of Heat Transfer. 125, 852-857.

Hsieh Y. Y., Lin T.F., 2002. Saturated flow boiling heat transfer and pressure drop of refrigerant R-410 A in a vertical plate heat exchanger. International Journal of Heat and Mass Transfer. 45 (5), 1033-1044.

Hsieh Y.Y., Chiang L.J., Lin T.F., 2002. Subcooled flow boiling heat transfer of R-134a and the associated bubble characteristics in a vertical plate heat exchanger. International Journal of Heat and Mass Transfer. 45 (9), 1791–1806.

Izquierdo M., 1998. Sistemas De Ciclos De Absorción Para Climatización Y Refrigeración.Curso. Universidad Carlos III De Madrid.

Izquierdo M., Lecuona A., Rodriguez P., 2004. Bomba De Calor De Absorción Agua-Aire De Alta Eficacia .Instalaciones Y Técnicas Del Confort. 159.

Izquierdo M., Lizarte R., Marcos J.D., Gutiérrez G., 2008. Air conditioning using an air-cooled single effect lithium bromide absorption chiller: Results of a trial

conducted in Madrid in August 2005. Applied Thermal Engineering. 28 (8-9), 1074-1081.

Jahnke A., Costa A., Ziegler F., Paris J., 2005. Experimental plan and statistical analysis of laboratory results for an absorption chiller. Int. Sorption Heat Pump Conf., ISHPC-05, Denver CO, USA.

Jokar A., Hosni M., Eckels S., 2006. Dimensional analysis on the evaporation and condensation of refrigerant R-134a in minichannel plate heat exchangers. Applied Thermal Engineering. 26.(17-18), 2287-2300.

Joudi K. A., Lafta A.H., 2001. Simulation of a simple absorption refrigeration system. Energy Conversion and Management. 42 (13), 1575-1605.

Kaita Y., 2001. Thermodynamic properties of lithium bromide–water solutions at high temperatures. . Int. J. Refrigeration. 24 (5), 374-390.

Kaynakli O., Horuz I., 2006. Comparison of parallel and counter flow coil absorber performance. International Communications in Heat and Mass Transfer. 33 (2), 211-223.

Karabelas A. J., Yiantsios S. G., Thonon B., Grillott J.M., 1997. Liquid-Side Fouling Of Heat Exchangers. An Integrated R & D Approach For Conventional And Novel Designs. Applied Thermal Engineering. 17 (8-10), 127-737.

Kaynakli O., Kilic M., 2007. Theoretical study on the effect of operating conditions on performance of absorption refrigeration system. Energy Conversion and Management. 48 (2), 599-607.

Kim D.S., Infante Ferreira C.A., 2006. A Gibbs energy equation for LiBr aqueous solutions. Int. J. Refrigeration. 29 (1), 36-46.

Kim Y., Joshi Y., Fedorov A., 2007. An absorption based miniature heat pump system for electronics cooling. Int. J. Refrigeration. 31 (1), 23-33.

Kohlenbach P. Ziegler F., 2008. A dynamic simulation model for transient absorption chiller performance. Part I: The model. Int. J. Refrigeration. 31 (2). 217-225.

Kohlenbach P. Ziegler F., 2008. A dynamic simulation model for transient absorption chiller performance. Part II: Numerical results and experimental verification. 31 (2). 226-233.

Kulankara S., Herold K. E, 2002. Surface tension of aqueous lithium bromide with heat/mass transfer enhancement additives: the effect of additive vapor transport. Int. J. Refrigeration. 25 (3), 383-389.

Kumar,H., 1984. The plate heat exchanger: construction and design. In: Proceedings First UK National Conference on Heat Transfer, University of Leeds, Inst. Chem. Symp. Series No. 86, pp. 1275–1288.

Kühn A., Ziegler F., Operational results of a 10 kW absorption chiller and adaptation to the characteristic equation. In: Proceedings of the International Conference Solar Air Conditioning, 6.-7. October 2005, Bad Staffelstein, Germany.

Lin J.H., Huang C.Y., Su C.C., 2007. Dimensional analysis for the heat transfer characteristics in the corrugated channels of plate heat exchangers. International Communications in Heat and Mass Transfer. 34 (3), 304-312.

Lloyd J. R., W. R. Moran., 1974.Natural Convection Adjacent to Horizontal Surfaces of various Platforms, ASME pp 74-WA/HT-66.

Longo G., Gasparella A., 2007. HFC-410A vaporisation inside a commercial brazed plate heat exchanger. Experimental Thermal and Fluid Science. 32 (1), 107-116.

Longo G., Gasparella A., 2007. Refrigerant R134a vaporisation heat transfer and pressure drop inside a small brazed plate heat exchanger. Int. J. Refrigeration., 30 (5), 821-830.

Longo G., Gasparella A., SartoriR., 2004. Experimental heat transfer coefficients during refrigerant vaporisation and condensation inside herringbone-type plate heat exchangers with enhanced surfaces. International Journal of Heat and Mass Transfer. 47 (19-20), 4125-4136.

Manglik R.M.., 1996. Plate heat exchangers for process industry applications: Enhanced thermal-hydraulic characteristics of chevron plates. Process, Enhanced and Multiphase Heat Transfer, Begell, 267-276.

Martinez P., Pinazo J., 2002. A method for design analysis of absorption machines. Int. J. Refrigeration. 25 (5), 634-639

Martinez P., Pinazo J., 2003. A method for obtaining performance correlations of absorption machines. Int. J.Thermal Sciences. 42 (4), 379-384.

Medrano M., Bourouis M. Coronas A., 2001. Double-lift absorption refrigeration cycles driven by low–temperature heat sources using organic fluid mixtures as working pairs. Applied Energy. 68 (2), 173-185.

Morioka M. Kiyota A. Ousaka T. Kobayashi I., 1992. Analysis of steam absorption by a subcooled droplet of aqueous solution of LiBr. JSME Int J Ser II 35 (3), 458–464.

Muley A, Manglik RM, Metwally HM., 1999. Enhanced heat transfer characteristics of viscous liquid flows in a chevron plate heat exchanger. Journal of heat transfer-transactions of the ASME 121 (4), 1011-1017.

Muley A., Manglik R. M, 1999. Experimental Study of turbulent Flow Heat Transfer and Pressure drop in a plate Heat Exchanger with Chevron Plates. Journal Of Heat Transfer-Transactions Of The Asme. 121 (1), 110-117.

Nakoryakov V.E., N.I. Grigoreva, 1977. Combined heat and mass transfer during absorption in droplets and films. Journal of Engineering Physics. 32 (3) (1977), 243 - 247.

Newman, A. 1931. The drying of porous solids: diffusion and surface emission equation. Transactions A.I.Ch.E., Vol. 27, pp. 203-220.

Palm B., Claesson J., 2006. Plate Heat Exchangers: Calculation Methods for Single and. Two-Phase Flow. Heat Transfer Engineering. 27(4), 88–98.

Paniev G.A., 1983. Absorption heat and mass transfer on droplets in a polydispersed spray. Heat Trans-Soviet Res. 15 (5), 62–72.

Park C.W., Jeong J. H., Kang Y.T., 2004. Energy consumption characteristics of an absorption chiller during the partial load operation. Int. J. Refrigeration. 27 (8),948-954.

Pátek J., Klomfar J., 2006. A computationally effective formulation of the thermodynamic properties of LiBr–H2O solutions from 273 to 500 K over full composition range. Int. J. Refrigeration. 29 (4), 566-578.

Pons M., Meunier F., Cacciola G., Critoph R. E., Groll M., Puigjaner L., Spinner B., Ziegler F., 1999. Thermodynamic based comparison of sorption systems for cooling and heat pumping: Comparaison des performances thermodynamique des systèmes de pompes à chaleur à sorption dans des applications de refroidissement et de chauffage. Int. J. Refrigeration. 22 (1), 5-17.

Rodríguez P.,Lecuona A., De Vega M, Izquierdo M, Martin E., 1999. Viabilidad energética, económica y ambiental de los sistemas de climatización por absorción en España. Montajes e Instalaciones 327, 73-79.

Ryan W.A., 1994. Water absorption in an adiabatic spray of aqueous lithium bromide solution. In: Proceedings of the international absorption heat pump conference, AES-vol. 31, New York: ASME; pp. 155–162.

Ryan W.A., Ruiz F., Wurm J., 1995. Model development and verification of spray absorption for gas driven cooling systems. In: Proceedings of the International Gas Research Conference, Cannes; pp. 1483–1493.

Saravanan M., Renganarayanan S., 2008. Experimental studies on R134a-DMAC hot water based vapour absorption refrigeration systems. Int. J. Thermal Sciences. 47 (2), 175-181.

Şencan A., Yakut K. Kalogirou S., 2006. Thermodynamic analysis of absorption systems using artificial neural network. Renewable Energy. 31 (1), 29-43.

Shah R.K., Kandlikar S., 1986. The influence of the number of thermal plates on plate heat exchanger performance. In: Current researches in heat and mass transfer, A compendium and a Festschrift for Professor Arcot Ramachandran, pp 267–88, Hemisphere, Washington, DC.

Shah R.K., 1990. Assesment of modified Wilson Plot tecniche for obtaining heat exchanger design data. Heat Transfer: Proc. 9th Int. Heat Transfer Conf. 5, 51–56.

Shiomi Y., Nakanishi S., Uehara T., 2004. Characteristics of two phase flow in a channel formed by chevron type plates. Experimental Thermal and Fluid Science. 28 (2-3), 231-235.

Soto V., Pinazo J., 2003. Validation of a model for the absorption process of H2O(vap) by a LiBr(aq) in a horizontal tube bundle, using a multi-factorial analysis. Int. J Heat and Mass Transfer. 46 (17), 3299-3312.

Soto V., Pinazo J., 2004. Multi-factorial study of the absorption process of H_2O(vap) by a LiBr(aq) in a horizontal tube bundle using 2-ethyl-1-hexanol as surfactant. Int. J. Heat and Mass Transfer. 47 (14-16), 3355-3373.

Stitou D., Spinner B., Satzger P., Ziegler F, 2000. Development and comparison of advanced cascading cycles coupling a solid/gas thermochemical process and a liquid/gas absorption process. Applied Thermal Engineering. 20 (14), 1237-1269.

Summerer F., Riesch P., Ziegler F., Alefeld G., 1997. Hydroxide absorption heat pumps with spray absorber. ASHRAE Technical Data Bulletin.12 (1), 50–57.

Taboas, F., 2006. Estudio del Proceso de Ebullición Forzada de da Mezcla Amoniaco/Agua en Intercambiadores de Placas Para Equipos de Refrigeración por Absorción. Ph.D. thesis, Universitat Rovira I Virgili.

Thonon B, Vidil R, Marvillet C., 1995. Recent Research And Developments In Plate Heat-Exchangers. Journal Of Enhanced Heat Transfer. 2 (1-2), 149-155.

Thonon B. Grandgeorge S. and Jallut C., 1999. Effect of Geometry and Flow Conditions on Particulate Fouling in Plate Heat Exchangers. Heat transfer engineering. 20 (3), 12-24.

Vallès M., Bourouis M., Boer D., Coronas A., 2003. Absorption of organic fluid mixtures in plate heat exchangers. Int. J.Thermal Sciences. 42 (1), 85-94.

Venegas B. M, 2001. Transferencia de masa y calor en gotas en procesos de absorción con Nitrato de Litio – Amoniaco: Nuevas Tecnologías. PhD thesis. Universidad Carlos III de Madrid.

Venegas M., Arzoz D., Rodriguez P., Izquierdo M., 2003. Heat and mass transfer in $LiNO_3$-NH_3 spray absorption system. International Communications in Heat and Mass Transfer.30 (6), 805-815.

Venegas M., Izquierdo M., Rodríguez P., Lecuona A., 2004. Heat and mass transfer during absorption of ammonia vapour by $LiNO_3$–NH_3 solution droplets. Int. J. Heat Mass Transfer. 47 (12-13), 2653-2667.

Venegas M., Rodríguez P., Lecuona A., Izquierdo M., 2005. Spray absorbers in absorption systems using lithium nitrate–ammonia solution. Int. J. Refrigeration. 28 (4), 554-564

Vlasogiannis P., Karagiannis G., Argyropoulos P. and Bontozoglou V., 2002. Air–water two-phase flow and heat transfer in a plate heat exchanger. International Journal Of Multiphase Flow 28 (5), 757-772.

Wang L., Chen G.M., Wang Q., Zhong M., 2007. Thermodynamic performance analysis of gas-fired air-cooled adiabatic absorption refrigeration systems. Applied Thermal Engineering. 27 (8-9), 1642-1652.

Warnakulasuriya F.S.K, 1998. Heat and mass transfer and water absorption properties of new absorbent droplets. PhD. Thesis. University of Illinois, Chicago.

Warnakulasuriya F.S.K., Worek W.M., 2006. Adiabatic water absorption properties of an aqueous absorbent at very low pressures in a spray absorber. Int. J. Heat Mass Transfer. 49 (9-10), 1592-1602.

Warnakulasuriya F.S.K., Worek W.M., 2008. Heat transfer and pressure drop properties of high viscous solutions in plate heat exchangers. International Journal of Heat and Mass Transfer. 51(1-2), 52-67.

Worek W., Ludovisi D., Meckler M., 2003. Enhancement of a double-effect absorption cooling system using a vapor recompression absorber. Energy. 28 (12),1151-1163.

Wu Y., Chen Y., Wu T., 2006.Experimental researches on characteristics of vapor–liquid equilibrium of NH3–H2O–LiBr system. Int. J. Refrigeration. 29 (2), 328-335.

Würfel R., Ostrowski N., 2004. Experimental investigations of heat transfer and pressure drop during the condensation process within plate heat exchangers of the herringbone-type. International Journal of Thermal Sciences. 43(1), 59-68.

Xie G., Sheng G., Kumar P., Li G.,2008. Absorber performance of a water/lithium-bromide absorption chiller. Applied Thermal Engineering. 28 (13), 1557-1562.

Kaita Y., 2002. Simulation results of triple-effect absorption cycles. Int. J. Refrigeration. 25 (7), 999-1007.

Yan Y.-Y., Lin T.-F., 1999. Evaporation heat transfer and pressure drop of refrigerant R-134a in a plate heat exchanger. Journal of Heat Transfer. Transactions of the ASME. 121, 118-127.

Yan Y.-Y., Lio H.-C, Lin T.-F., 1999. Condensation heat transfer and pressure drop of refrigerant R-134a in a plate heat exchanger. International Journal of Heat and Mass Transfer. 42 (6) 993-1006.

Yoon J., Kwon O., Moon C., Lee H., Bansal P., 2005. Heat and mass transfer characteristics of a helical absorber using LiBr and LiBr + LiI + LiNO3 + LiCl solutions. Int. J. Heat and Mass Transfer. 48 (10), 2102-2109.

Zhao Z., Zhou F., Zhang X., Li S., 2003. The thermodynamic performance of a new solution cycle in double absorption heat transformer using water/lithium bromide as the working fluids. Int. J. Refrigeration. 26 (3), 315-320.

.

APPENDIX A

Basics of Absorption cycles

In the following, a brief description of basic absorption cycles is given.

The components of a basic absorption system are: an absorber, a generator, a condenser, an evaporator, a solution heat exchanger or heat recuperator, expansion valves and a pump (Fig. A.1).

There are operational characteristics that differentiate the absorption systems with mechanical compression, although the end result is the same: chilled water for air conditioning or even for industrial cooling applications. First, absorption systems use a solution, whose concentration varies during the process instead of a substance of fixed chemical composition as in the case of mechanical compression (refrigerant). Moreover, for transporting the refrigerant from the evaporator to the condenser, four components are used, that perform the same function of a compressor: an absorber, a generator, a solution heat exchanger and a pump.

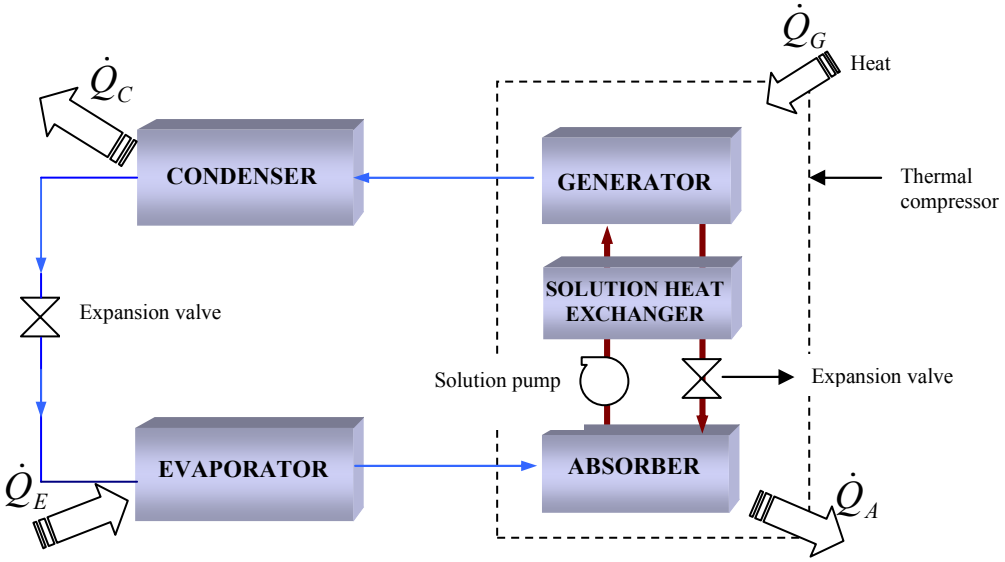

Fig. A.1. Basic components of an absorption cycle. Thick line: Solution. Thin line: Refrigerant

Refrigerants used in these systems are natural substances as water or ammonia, although organic compounds and mixtures of them have been used. The solution is

formed by two or more components. In the case of solutions of two components, these are known as **absorbent and refrigerant**, the later being volatile. The solutions most commonly used are water-ammonia (NH_3 refrigerant and H_2O absorbent) and water-lithium bromide (H_2O refrigerant and LiBr absorbent). The affinity of absorbent with respect to the refrigerant is a fundamental property in the performance of the cycle.

Operation:

The refrigerant leaves the evaporator and enters the absorber as vapour (Fig. A.1).There it is absorbed by the solution, producing a change in its concentration (weak to strong solution), producing heat that is evacuated. To restore the initial concentration of the solution, it is pumped to the generator to make it boil and remove the refrigerant from it. To fulfil this function, heat from an external source is provided to the generator as driving or activating heat. This source can come from a process that discard heat (exhaust gas engine, cogeneration processes, among others), using this energy instead of wasting or disposing of it to the environment. Fossil fuels also can be used, but in terms of profitability and environmental benefits, this is not the best option. Low-temperature solar energy can also be used for homes acclimatizing.

Once separated from the refrigerant, the concentrated solution goes back again to the absorber, passing previously through the solution heat exchanger in order to recuperate heat from strong solution in its path from the generator to the absorber. Then, it passes through an expansion valve in order to return to the pressure conditions of the absorber.

The refrigerant vapour, being separated in the generator, passes to the condenser and then returns to the evaporator as a liquid to complete its cycle.

As can be seen, in an absorption systems both the solution and refrigerant follow different cycles. Through the cycle that the refrigerant accomplishes within the set absorber - pump - generator, the same result is obtained as in the mechanical compression cycle when passing through the compressor. Therefore this set is called thermochemical compressor, noting that the source of energy used is heat, not electricity, except for consumption of the pump which is negligible compared to that of mechanical compression systems.

Advantages and disadvantages of absorption systems

Compared with mechanical compression machines, the absorption machine has the disadvantage of being less efficient in terms of energy, larger and heavier, making them less competitive. However, there are several reasons that drive their use and future development, among which include:

- The cost of electrical energy to drive mechanical compression systems is much higher (in the order of 3 to 4 times) than that required in an absorption system for obtaining the waste heat and to produce the same cooling capacity. In this case, the absorption machine performance would not be inconvenient because it would use free energy and ensures profitability.
- By using the waste heat from other processes, an absorption system utilizes thermal energy that would otherwise be expelled to the atmosphere. This contributes to a reduced use of conventional energy to activate the air conditioning or cooling equipment, more expensive and harmful to the environment.
- The refrigerant used in absorption systems (water or ammonia) does not contribute to the destruction of the ozone layer or the greenhouse effect, thus reducing the environmental impact is highest.
- It should be noted that an absorption machine should work at pressure lower than the atmospheric (when working with solutions BrLi - water) and therefore produces no emissions into the atmosphere caused by leaks. If, for any breakage, the substances used for operation are natural and do not produce harmful effects to the environment.
- The precautions to be taken in certain areas of operation and maintenance of the substances used are easily manageable thanks to technological advances in instrumentation and process control.
- As the function of the mechanical compressor is performed by several components in the case of absorption systems, the initial cost of a plant for the latter is higher than a mechanical compression equipment of the same cooling capacity. However, the cost may be favourable if we consider the above in terms of power consumption, compared with the use of waste heat.

Adiabatic absorption

As above mentioned, one of the main problems of commercial absorption cooling systems is the large size of their components, and among these the absorber is recognized as the most voluminous. This is a feature that reduces the competitiveness of these machines compared to the mechanical compression air conditioning. Because of this, there is currently a great interest in optimizing the processes of heat and mass transfer in the absorbers. Adiabatic absorption is being investigated as a way for improving compactness and efficiency. Principal aspects of the process are:

- The mass and heat transfer processes are divided in separated apparatus, thus probably optimized for a single purpose.
- The weak solution is dispersed in the form of droplets inside the absorber.
- The absorption heat is extracted downstream using a compact heat exchanger.
- Certain amount of weak solution must be continuously recirculated through the absorber and a small part of the solution leaving the absorber is sent to the generator.

In order to explain the previous aspects, the basics of adiabatic absorption are briefly described in the following.

Most of the conventional absorbers are based on falling film absorption. A bundle of tubes is covered with the free falling absorbing solution liquid film generated by dripping the sub-cooled solution over the outside of the pipes. The tubes are surrounded by the water vapour to be absorbed. Concurrently, the dilution heat is transferred from the liquid film through the pipe wall to an external cooling fluid which flow inside the pipe. An example of this type of absorber is shown on Fig. A.2.

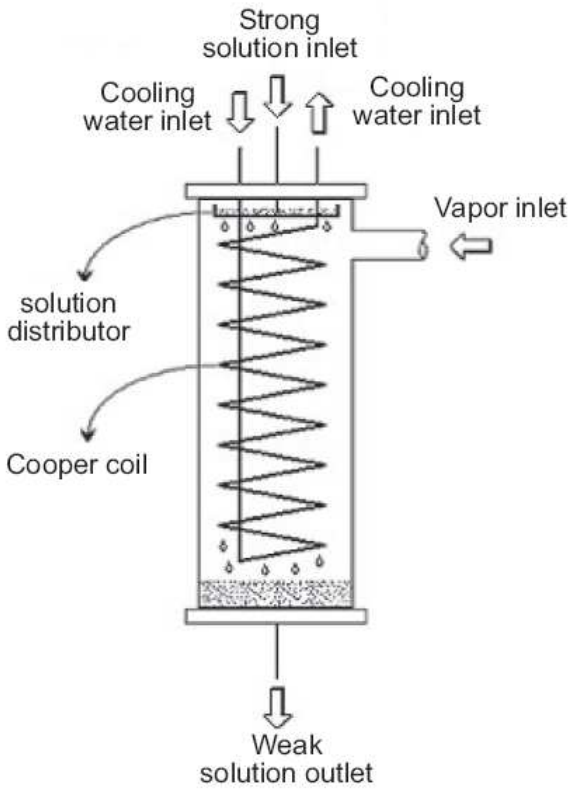

Fig. A.2 Schematic of coil absorber in counter current flow. Based on: Kaynakli and Horuz (2006).

In falling film absorption on vertical tubes, a homogeneous wetting of the entire surface of the tube is necessary so that the film is stable and continuous. This wetting will largely depend on the construction material of the pipes, the quality of finishing method of the tubes surface, mutual surface tension and the proper liquid distribution. In general, the film is very sensitive to instabilities, resulting in an incomplete wetting and consequently in a reduction of areas available for heat transfer and mass. The distribution of the solution at the entrance area is essential to avoid splashing or jets, which would destroy the liquid film. In addition to that the absorber becomes orientation sensitive, as its working relies on free falling.

The concept of adiabatic absorption is based on the fact that the rate of absorption of water vapour increases if three important factors also increases: the total absorption area of the salt solution, the penetration depth into the solution and the time that absorbing medium is in contact with vapour.

One way to accomplish these effects consists of introducing the solution in the form of droplets. Another way is to disperse the solution inside the absorber, introducing an array of nozzles spraying adequately the solution. The cooling tube bundle (used in

conventional absorbers) is taken out and the solution is cooled in an external high efficiency heat exchanger, with higher overall heat transfer coefficient (Fig. A.3). This can reduce size, weight and cost.

The main disadvantage of adiabatic absorption is that heating of the solution by the absorption heat causes absorption to stop (eventually reaching saturation) when only a fraction of vapour has been absorbed, typically in the order of one tenth. Subcooling is necessary to recover the potential of absorption. It is generally performed in a continuous way as a reciculation circuit. This way the almost saturated solution is cooled and injected again. Satisfactory absorption is generally reached using a recirculated flow rate in the order of ten times the flow rate through the absorber envelope. This makes the external heat exchanger larger.

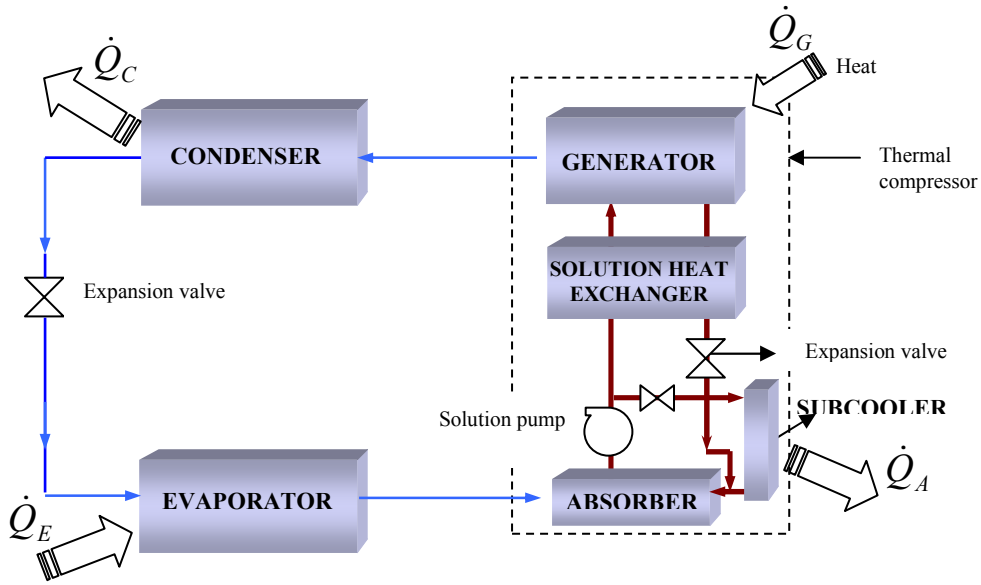

Figure A.3. Basic components of an Li-Br absorption cycle. Thick line: Solution. Thin line: Refrigerant

The reader in encouraged to look up Ryan (1994) for having a more extended summary about other important aspects on adiabatic absorption.

APPENDIX B

Calibration of Sensors and Uncertainty Analysis

Calibration consists of a set of operations that establish, under specified conditions, the relationship between the values of a magnitude indicated by an instrument or measurement system, and estimation of the corresponding real values of the magnitude, obtained by an external standart.

This appendix provides a description of the practical calibration for 30 T-type thermocouples, 8 flow meters and 4 pressure transducers, used for the measurement of the temperatures, flow rates and pressures of the fluids working in the simple effect absorption facility studied here. The results of uncertainty for the instruments and measured variables are also shown.

Calibration of Sensors

Calibration of Temperature sensors

Description of equipment used

For calibration of temperature sensors are used temperature bath (metal block calibrators, sand bath and liquid bath), ovens, potentiometer and Wheatstone bridge testers and universal testers (Creus, 1997).

In our case we use a liquid bath calibrator (Fig. B.1). It consists of a stainless steel tank filled with liquid with a stirrer incorporated, a submerged standard thermometer and temperature controller that acts on a set of resistance heaters. Various fluids are used depending on the working temperature: Trichlorethylene (from -80°C to ambient temperature), ethylene glycol and water (-20°C to ambient temperature), oil and silicone oil (from ambient temperature to 260ºC) and salt (220º C to 700ºC).

The thermocouples have been calibrated for a temperature range from 0°C to 100ºC, for which an oil calibrator has been used (Fig. B.1b).

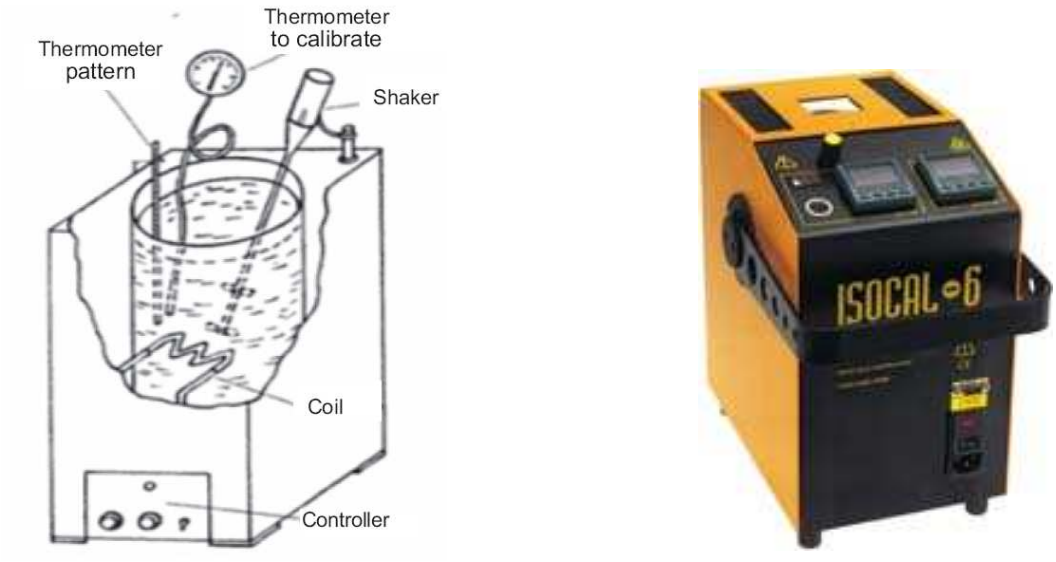

(a) (b)

Fig. B1. (a) Elements of a liquid bath calibrator. Source: Creus (1997) (b) Image of calibrator used.

Pattern features

The "Isotech Isocal calibrator" allows adjustment of stirring speed of the liquid, to optimize the viscosity of it as getting a very good uniformity. This is done by a wheel located on the front panel.

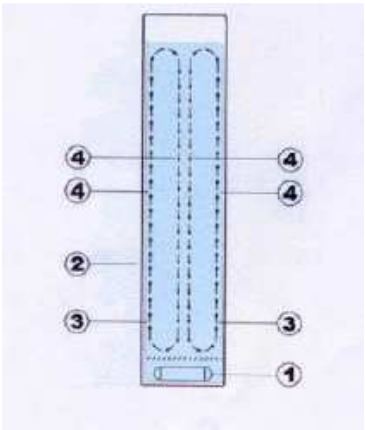

Fig. B2. Flow of stirred liquid

Fig. B2 shows the flow of liquid. The magnet in the bottom (1) circles exerting a centrifugal force on the fluid that surrounds it. Under this force the liquid moves towards the sides of the container (2) and is replaced by liquid from above (3). This action causes the fluid movement that is seen in Fig. B2 (4).

The front panel has two displays, one marked the desired temperature to calibrate, while the other allows observing the instant pattern temperature. The indicator of this calibrator has a resolution of 0.01º C.

The thermocouple calibration was conducted by comparing the measures with a platinum themoresistence, with uncertainty of ± 0.1° C.

Calibration procedure

The thermocouples have been introduced in groups of 4 inside the isothermal bath, according to the temperature range in which they will be used. The themoresistence pattern is introduced at the same time, selecting calibration points in increments of 20º C. After enough time, the bathroom reaches the isothermal conditions and the measurement of the thermocouples is stationary. This continues at least 20 minutes. The signal is collected by the datalogger. Since the speed of data acquisition is high, the data acquisition system takes many measurements during the calibration process and therefore this replication is considered. In this way, the calibration procedure aims to the metrological characterizing of the full measurement system. This procedure was repeated 5 times for each point of the measurement range selected. Besides this, a calibration for comparison was carried out for the thermocouples working in their specific loop, circulating the fluid without heating or cooling.

Calibration of flow sensors

As explained in Chapter 3, there are:

- 1 rotameter operating in the oil (hot) loop.
- 5 magnetic flowmeters operating in the chilled water loops, in the cooling water loops and in the route of the recirculated solution.
- 2 Coriolis type, operating in the solution loop, for measuring the concentrated and diluted solution streams.

Each flow meter was calibrated within his own loop using the working fluid specific of each one, and under its specific operating conditions. In order to do this we used a stopwatch to measure the filling time of a container, which was weighed before

and after the filling. Thus, an average value of mass flow rate was obtained to be compared with signals provided by the data acquisition system.

For all flow meters, five points of calibration were selected. Five measurements for each calibration point were taken. The circuits were opened in order to calibrate the instruments in their location within the machine, except the magnetic flowmeter used for recirculated solution measurements, which was calibrated by comparing the measure obtained in series with a Coriolis type flowmeter, previously calibrated with the same fluid.

It is noteworthy the complication of calibrating the rotameter inside the oil loop, with working temperatures up to 100ºC, which makes this fluid difficult to manage.

Calibration of pressure sensors

Each pressure sensor was calibrated by comparing its measure with a more accurate instrument, having both measurements recorded in the datalogger.

Estimation of the uncertainty of the instruments

Measurement uncertainty (often called in short "uncertainty") is a parameter that is an indicator of the comparative quality of the measurement, while allowing obtaining an approximate confidence interval for the true value of the measurand (magnitude to be measured). By taking into account in its calculation the contributions of the components of uncertainty due to both systematic and random errors, it allows a unified approach to study the relative importance of each of these contributions[1].

The measurement uncertainty associated with measurements is evaluated using one of the following methods: Type A or Type B.

- TYPE A UNCERTAINTY: method of evaluation of uncertainty by statistical analysis of observations (usually using the standard deviation) obtained in the course of the current measurement.

[1] Extracted from: Acerca de la incertidumbre de medición en los ensayos químico analíticos. Derrégibus, M.- Fuentes, J.

- TYPE B UNCERTAINTY: evaluation of uncertainty by using a different statistical analysis. In this case, the estimated uncertainty is based on other scientific knowledge.

Evaluation of type A uncertainty

In this case the repeatability of measurements is considered as uncertainty Type A.

The purpose of statistical analysis is to calculate an estimate of the value of the measurand and the confidence interval within which it is assumed that the measure is included. This analysis is carried out taking different measures in the experiment, i.e., repeating the experiment n times.

The random component can be estimated as

$$u_{a,1} = \frac{s}{\sqrt{n}} \qquad \text{(B.1)}$$

being:

s the standard deviation of repetition of the test

n the "replication", i.e. the number of times that the magnitude is measured under identical operating conditions.

This random estimation being applicable for n > 20.

The mean $\overline{x`}$ and standard deviation s`:

$$\overline{x`} = \frac{\sum_{i=1}^{n} x_i}{n} \qquad s` = \sqrt{\frac{\sum_{i=1}^{n} (x_i - \overline{x`})^2}{n}} \qquad \text{(B.1)}$$

These formulas result when the value of samples tends to infinity. If the number of samples is finite, the mean and standard deviation are as follows:

$$\overline{x} = \frac{\sum_{i=1}^{n} x_i}{n} \qquad s = \sqrt{\frac{\sum_{i=1}^{n} (x_i - \overline{x})^2}{n-1}} \qquad \text{(B.2)}$$

In our case, we will take into account the uncertainties due to the temperature standart. In the case of thermocouples, $u_{a,2} = \pm 0{,}1^{\circ} C$.

Evaluation of type B uncertainty

The systematic deviation of the measurement of instruments with regard to the standard at each calibration point is removed, using the **calibration function** specific for each calibrated instrument. In this way, it is obtained the correction between the measures of instrument and the standard used, taken from data of the calibration process.

Combined standard uncertainty

Once calculated the uncertainties due to the repeatability of the measures and the standard used, and having eliminated the difference between the measures of the instrument and the standard, the combined uncertainty for each calibration point is calculated as follows:

$$U_p = k_p \cdot \sqrt{u_{a,1}{}^2 + u_{a,2}{}^2} \qquad \text{(B.2)}$$

Where k_p is the coverage factor with confidence level p. Usually is used a 95% confidence level. In practice is often used $k_{0.95} \approx 2$.

The uncertainty of the measured data $u_{s,m}$ must be added to the calibration uncertainty of the sensor. For this, the deviation of each experimental point was calculated.

$$U_p = k_p \cdot \sqrt{u_{a,1}{}^2 + u_{a,2}{}^2 + u_{a,3}{}^2} \qquad \text{(B.3)}$$

Using the calibration functions for every sensor, systematic errors were reduced as far as possible. The random uncertainty U for an experimental result R, which is function of n independent parameters x_i, is estimated, according to the Gauss algorithm, as:

$$U = \sqrt{\sum_{i=1}^{n} \left(\frac{\partial f}{\partial x_i} \cdot U_{x_i} \right)^2} \;\; ; \; R = f(x_1, x_2, \ldots x_n) \qquad \text{(B.4)}$$

Results

The uncertainty of instruments is given in Chapter 3 (Table 3.5).

The uncertainty of measured variables is given in Table B.1.

Uncertainty results	**Uncertainty**
Generation power $\dot{Q}_G$	16%
Experimental cooling capacity $\dot{Q}_{E,\exp}$	24%
Calculated cooling capacity $\dot{Q}_{E,ref}$	32%
Subcooling power $\dot{Q}_s$	4,7%
Heat exchanged in the solution heat exchanger $\dot{Q}_{she}$	3,1%
Experimental Coefficient of Performance COP_{exp}	34%
Approach to equilibrium factor F_x	6%
Overall heat transfer coefficient (subcooler)	8,2%
Overall heat transfer coefficient (solution heat exchanger)	4,4%
Overall heat transfer coefficient (generator)	22%
Fanning friction factor f	2%

Table B.1. Uncertainty of measured variables.